Instituto de Física da

Universidade de São Paulo

Emaranhamento em variáveis contínuas, Morte Súbita, e Além

Tese de Livre-Docência

Marcelo Martinelli

São Paulo, 25 de abril de 2011.

Agradecimentos:

Meus profundos agradecimentos para

- Paulo Nussenzveig, o parceiro de primeira hora nesta empreitada, franqueando o acesso ao laboratório e disponibilizando toda a estrutura existente. Desde então, mantemos um franca colaboração, sócios no LMCAL, dividindo equipamentos, estudantes, ideias, bem como recursos, dores de cabeça, prazos finais,...
- Alessandro Villar e Katiúscia Nadyne Cassemiro, os primeiros estudantes que eu "quase" orientei. Aprendi muito com eles, creio ter ensinado algo, e espero tê-los como parceiros em empreitadas futuras.
- Paulo Valente, Luciano Soares da Cruz, José Aguirre Gómez e Daniel Felinto são amigos que me acompanharam desde o começo da jornada. Hoje, colegas em diferentes instituições, são mais do que colaboradores.
- Os amigos da UFF, Antônio Zelaquett Khoury, Kaled Dechoum e José Augusto Huguenin, os amigos da UFPE, José Tabosa, Sandra Viana, e Felinto, bem como Arturo Lezama e todo pessoal da Universidad de la República, em Montevidéu.
- Claude Fabre, que franqueou todos os segredos do OPO (até então conhecidos) quando era estudante, colaborou conosco quando era jovem docente, e agora é parceiro em novos e ousados projetos.
- Os valentes estudantes que me aceitaram como orientador, e sobreviveram para contar a história: Antônio Sales Coelho, Jônatas Eduardo César, Hélio Zhang He e Rodrigo Alves de Lima, bem como Felippe Alexandre Barbosa, igualmente envolvido. Eles são a vida do laboratório!
- Os outros valentes estudantes que estão tentando sobreviver para contar a história: Hans Marin Florez, Paula Sampaio Meirelles, Klara Theophilo, Igor Konieczniak, Rayssa Bruzaca, Flávio Campopiano Moraes. Que os feitos dos predecessores lhes inspirem!
- Alencar José de Faria, e Márcio Heráclyto, pós-doutorandos antigo e novo, cuja contribuição é simplesmente indispensável para o avanço da equipe.
- Os funcionários do IFUSP que ajudaram diretamente nos nossos projetos: Marcos, José Carlos, Wilson, Ângelo, "Periquito", Carlos, Eduardo, Celso Perego (FNC). E Luís Xavier de Souza, estagiário, braço direito e esquerdo na instrumentação (todo bom técnico eletrônico é ambidestro).
- As secretárias do grupo, Juliane Pagamice, e especialmente a Ednéia Alves de Rezende, cuja ajuda e incentivo foi indispensável para que este trabalho fosse redigido.

- E especialmente às mulheres de minha vida, Verônica, Isadora e Marina, sem as quais nada disto teria valido a pena!

Resumo

Estudamos o emaranhamento no regime de variáveis contínuas do campo eletromagnético, em especial envolvendo as quadraturas dos distintos modos do campo. Demonstramos a geração de feixes intensos (na faixa de mW), de frequências distintas (separadas por mais de uma oitava) e emaranhados pelo Oscilador Paramétrico Ótico, acima do seu limiar de oscilação. Mostramos que há emaranhamento entre os feixes sinal e complementar, produzidos por conversão paramétrica descendente, e entre estes e o campo de bombeio do oscilador, para uma cavidade triplamente ressonante.

Verificamos ainda que, para o regime de variáveis contínuas, a interação com o ambiente pode levar o sistema inicialmente emaranhado a um estado separável em tempos finitos, de forma não assintótica, algo semelhante à morte súbita de emaranhamento já verificado em variáveis discretas.

Discutimos, por fim, as perspectivas em informação quântica, visando uma aplicação imediata do emaranhamento multicor em teletransporte no espectro eletromagnético.

Abstract

We have studied the entanglement for continuous variables of the electromagnetic field, focusing on the quadratures of given modes of the field. We demonstrate the direct production of intense (mW range), entangled fields of different colors (covering more than one octave) using an Optical Parametric Oscillator in above threshold operation. We demonstrate bipartite entanglement between signal and idler modes, and tripartite entanglement of these with the pump field for a triply resonant OPO cavity.

We have also shown that the detrimental interaction with the environment can lead an initially entangled system into a separable state for finite interaction times, even for continuous variables. This effect is reminiscent of the sudden death of entanglement observed for discrete variables.

Finally, we present the possible uses of this entanglement in quantum information processing, with the immediate application of the multicolor entanglement in teleportation over the electromagnetic spectra.

Conteúdo

Capítulo 1

Introdução

Esta resenha de artigos, englobando minha produção desde minha admissão como docente na Universidade de São Paulo, em maio de 2004, vai necessariamente acompanhar a evolução do Oscilador Paramétrico Ótico ao longo da última década. A motivação para a escolha de uma resenha, no lugar de um texto mais autoral, é simples: quase tudo sobre o Oscilador Paramétrico Ótico já foi redigido, analisado e revisado ao longo das publicações nas quais estive envolvido em diferentes papéis. Tais trabalhos envolveram principalmente o Laboratório de Manipulação Coerente de Átomos e Luz (IF/USP), e incluem colaborações com o Groupe d´Optique Quantique do Laboratoire Kastler-Brossel (UPMC-Paris 6 e ENS/ França) e o Grupo de Óptica Quântica (IF/UFF). Apresentamos a seguir a sequência dos tópicos abordados. Ao final desta tese, há um apêndice, com o método de cálculo do ruído quântico no OPO, e outro sobre os critérios de emaranhamento em variáveis contínuas empregados neste trabalho.

Quando comecei este caminho, ainda como orientando, o OPO era de uma ferramenta de trabalho bem conhecida e amplamente utilizada em Ótica Quântica. Empregando a amplificação paramétrica através de uma não-linearidade de segunda ordem [1], e a realimentação em uma cavidade, é possível obter a oscilação, com o acoplamento entre um modo de bombeio, e dois modos convertidos. A este sistema podemos adicionar ainda campos de referência nos modos de frequência mais baixa, que podem ser amplificados ou "deamplificados", conforme a fase escolhida para os campos. Extremamente versátil, tinha um grande interesse em aplicações de Informação Quântica, conceito nascente à época, envolvendo a ideia de manipulação quântica da informação.

Faltavam poucos elementos do OPO, descrito na década de 80 por Margareth Reid e Peter Drummond [2, 3, 4], a serem demonstrados experimentalmente. Entre estes elementos, tínhamos a correlação quântica de fase entre os campos sinal e complementar em operação acima do limiar. Feito isto, mostrava-se que o OPO gera campos com correlações do tipo proposto por Einstein, Podolski e Rosen em 1935 [5] tanto abaixo do limiar [6] (vácuo emaranhado) quanto acima (feixes intensos emaranhados).

Como pós-doutorando, tive a oportunidade de me lançar a esta busca, com o então

estudante de doutorado Alessandro Villar em seu projeto de pesquisa, partindo do OPO construído em São Paulo durante meu próprio doutorado. A medida revelou-se mais complexa do que inicialmente esperado. Ainda que a aplicação da técnica de rotação de elipse ao problema do OPO, proposta pelo então supervisor Paulo Nussenzveig fosse exequível, algo estava faltando no problema. O desenvolvimento de novas implementações, de forma a vencer os desafios técnicos, permitiu por fim a realização da medida, resultando em uma publicação de grande impacto [7].

Porém, os dados, apesar de conclusivos quanto ao emaranhamento, não concordavam com a teoria. Torna-se necessário rever este modelo, e descobrir a real origem do efeito. Uma primeira tentativa fora feita, em conjunto com o grupo do IF/UFF, na qual testamos o limite das aproximações lineares nas equações de Langevin e na aproximação da função de Wigner do OPO como uma equação de Fokker-Planck. O resultado mostra a validade desta aproximação, e a consistência dela com um modelo mais completo do OPO. Fica então claro que há alguma outra fonte para este excesso de ruído. A modelagem inicial deste excesso de ruído e sua introdução na descrição do sistema levou a um bom acordo qualitativo para o problema, ao se observar apenas os feixes sinal e complementar [8]. Mas a questão da origem física deste ruído permaneceu em aberto.

Por outro lado, o estudo do acoplamento do campo de bombeio aos modos sinal e complementar indicou que ainda que tivéssemos uma descrição completa da matriz do OPO, e o seu comportamento para cada um dos modos envolvidos e suas correlações, havia na matriz espectral de covariâncias mais informação do que pensávamos a princípio. Os desenvolvimentos de aplicações do emaranhamento entre duas partículas levaram, naturalmente, à demanda por sistemas mais complexos, com o envolvimento de três partículas ou mais. No caso do OPO, a descrição aparentemente correta de Reid e Drummond guardava em si um efeito de emaranhamento que só viria a ser evidenciado em estudos mais recentes, realizados na década de 90 [9].

Em nossos estudos, observamos que a depleção do campo de bombeio, para a geração de pares de feixes nos modos sinal e complementar, associada à conservação de energia, levam à correlação entre estes três campos. Como consequência, o emaranhamento não era um problema bipartite, como fora então anunciado, mas sim tripartite. A discussão deste problema levou-nos de volta às equações, e durante o pós-doutorado, em colaboração com o prof. Claude Fabre, do Laboratoire Kastler-Brossel, conseguimos uma nova publicação, onde se demonstrava o emaranhamento tripartite no OPO acima do limiar [10].

Isto implica que além de termos dois feixes de cores distintas emaranhados, temos ainda um terceiro campo, correlacionado aos produtos da conversão paramétrica. Os feixes convertidos, por sua vez, não necessitam ter uma relação de frequência bem determinada entre si, além daquela dada pela conservação de energia. De fato, os feixes sinal e complementar tem uma difusão de fase completamente aleatória com relação ao feixe de bombeio. Mas nas medidas realizadas no referencial girante de cada campo, as flutuações quânticas estão por sua vez correlacionadas, e cobrem mais de uma oitava do espectro eletromagnético.

Após a descoberta teórica, torna-se necessária a medida deste efeito, tendo em vista

aplicações futuras. Esta tarefa coube a Katiúscia Nadyne Cassemiro, em sua tese de doutorado. Em dois artigos, ela demonstra a existência de correlações entre o campo de bombeio e os feixes sinal e complementar [12], mostrando correlações fortes de fase entre os três feixes, e correlações de intensidade entre bombeio e sinal, ou bombeio e complementar, que neste caso levam a uma nova relação de estados comprimidos do campo ("squeezing") [11]. No entanto, o emaranhamento tripartite não fora demonstrado ainda. Revela-se que nosso modelo anterior para o excesso de ruído [8] não reproduz nos cálculos a situação observada em laboratório.

A solução deste problema viria bem depois, na dissertação dos um dos meus primeiros estudantes de mestrado, após minha contratação no IFUSP. Nos mestrados de Jônatas da Silva César e Antônio Sales Coelho, foi possível testar uma hipótese nova: o espalhamento Brillouin de fótons do campo médio pelos fónons do cristal. O resultado das caracterizações rendeu um excelente acordo entre os parâmetros caracterizados, o modelo desenvolvido, e os resultados experimentais [13].

Será somente no final do mestrado de Antônio Sales Coelho e Felippe Barbosa da Silva que, diagnosticados os fónons como a fonte de ruído, é feito o resfriamento do cristal, que o leva finalmente a uma situação onde a geração de campos triplamente emaranhados é observada [14]. Aparentemente temos o OPO completamente caracterizado, colocando um ponto final na história e liberando-o para seu uso como ferramenta de trabalho.

No entanto, ao testar a linearidade da matriz de ruído do mesmo diante de atenuações dos campos, verificou-se que o emaranhamento podia ser eliminado para perdas finitas. O resultado, reminiscente da morte súbita do emaranhamento em sistemas de qubits [15, 16], foi uma surpresa. Partimos então para a busca dos elementos responsáveis por esta morte súbita de emaranhamento.

Neste caso, com a ajuda do Dr. Alencar José de Faria, em seu pós-doutorado junto ao grupo, os estudantes Felippe e Antônio, agora em seu doutorado, deram continuidade ao trabalho no caso mais simples: o emaranhamento bipartite. Foi demonstrada a condição suficiente para que ele seja robusto, e a divisão entre estados emaranhados robustos e sujeitos à morte súbita por perdas do meio. O resultado experimental e o trabalho teórico farão parte das teses destes estudantes, com defesa prevista para o próximo ano.

Estas medidas fecharam um longo ciclo, do qual partiu-se da teoria inicial do OPO, para a verificação experimental de elementos desta teoria. Neste processo, descobrimos características novas do OPO, à luz da Informação Quântica, como o emaranhamento tripartite, o que expande suas aplicações em protocolos de teletransporte. O sistema aponta ainda para fenômenos novos, como a morte súbita de emaranhamento. Isto não seria possível sem a solução do problema de excesso de ruído neste sistema.

Podemos então dizer que conhecemos quase tudo do OPO, finalmente. Pequenas perguntas permanecem a ser respondidas, mas desta vez não estão mais importunando as medidas: por que o ruído dos fónons cai tão rapidamente com a temperatura, e por que o limiar de oscilação é reduzido com uma variação de apenas 46 K? Enquanto avançamos neste sentido, vemos no OPO uma ferramenta poderosa para manipulação quântica de

informação, estendendo as possibilidades de teleportação para além da demonstração do princípio, visando uma aplicação prática das propriedades. Nosso objetivo agora é realizar o teletransporte de um estado para diferentes faixas do espectro eletromagnético, usando o emaranhamento multi-cor do OPO. Este projeto em curso envolve os estudantes de doutorado do grupo, e foi proposto à FAPESP. Esperamos os resultados para breve.

Capítulo 2

Emaranhamento Bipartite

O Oscilador Paramétrico Ótico foi uma das primeiras fontes de estados não-clássicos da luz, e uma das mais estudadas, desde a década de 80. O interesse inicial de tais estados, como os comprimidos, envolvia o estudo de propriedades fundamentais da mecânica quântica, empregando os recursos que a ótica tinha à disposição, oriundos da física de semicondutores, materiais, e estado sólido (fontes, detetores, cristais, etc.). Além disso, promessas de aplicação em telecomunicações, metrologia, medidas sensíveis de espectroscopia ou interferometria apontavam para a ligação da ótica quântica com aplicações em física.

É verdade que, logo no início, todas as questões sobre o OPO pareciam respondidas nos artigos de Reid e Drummond [2, 3, 4], onde se demonstrava que o OPO deveria gerar, abaixo do limiar, tanto estados de vácuo comprimido quanto campos emaranhados.

As medidas já haviam sido parcialmente feitas anteriormente para o vácuo comprimido [17]. Seguido do detalhamento teórico do processo de geração de feixes gêmeos [18], estes foram medidos com um OPO acima do limiar de oscilação [19]. Tais feixes apresentam correlações de intensidade melhores do que as que poderiam ser obtidas por uma fonte clássica, como um feixe coerente dividido em 2 partes iguais em intensidade média.

Nos artigos de M. Reid [20] ocorre ainda a demonstração que os campos produzidos pelo OPO violam um critério de emaranhamento baseado nas ideias de medidas propostas por Einstein, Podolski e Rosen [5]. Neste trabalho há a demonstração de geração dos campos sinal e complementar emaranhados no OPO, tanto abaixo e quanto acima do limiar. O emaranhamento abaixo do limiar foi observado em 1992 [6] para campos de mesma frequência. No entanto, a mesma observação do efeito acima do limiar de oscilação não fora feita desde sua previsão inicial.

A principal limitação para esta medida está no fato de que os feixes sinal e complementar gerados não apresentam necessariamente a mesma frequência de oscilação. Se assim fosse, o processo de medida seria semelhante ao sistema usado por Kimble nos seus dois artigos [17, 6]. O laser de bombeio, depois do dobramento, é por sua vez empregado

no bombeio do OPO. Uma amostra do feixe inicial é, no entanto, reservada para o uso como oscilador local no sistema de deteção dos campos de vácuo produzidos pelo OPO. O processo de conversão paramétrica ascendente, seguido pela conversão paramétrica descendente, vai resultar, de forma equivalente, à aplicação de um operador de compressão sobre um estado coerente de vácuo, ou sobre uma combinação de modos de vácuo no caso de geração de emaranhamento.

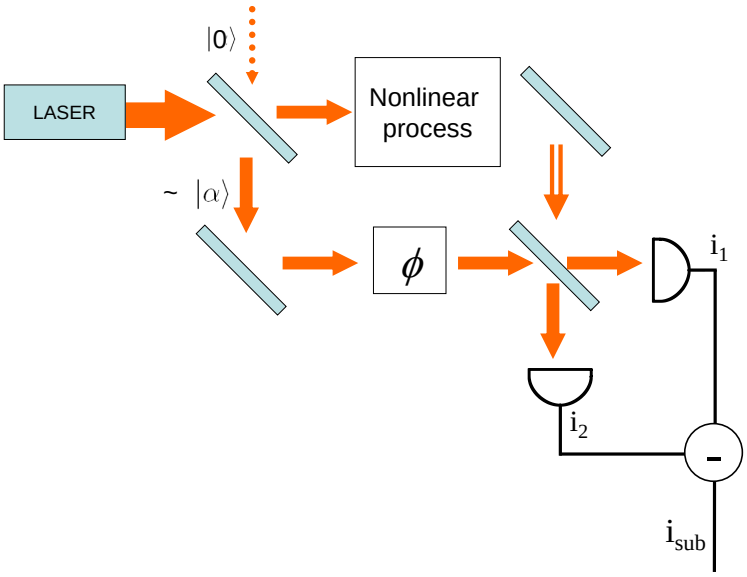

Figura 2.1: Medida do ruído com oscilador local. A saída do primeiro divisor de feixe fornece a referência aos processos de medida anteriores. Ela gera basicamente um estado de vácuo, deslocado pelo campo médio do laser. O processo não-linear pode acoplar ainda diversos modos do campo, e sua saída (ou saídas) são analisadas pela deteção homodina. O oscilador local é o próprio campo de referência, com um deslocamento de fase ϕ variável.

É curioso notar que, neste caso, além do modo degenerado, temos a geração de vácuo emaranhado em diferentes pares de modos do campo. Além dos modos degenerados, temos a geração simultânea de vácuo emaranhado entre modos com frequências ω_1 e ω_2, tal que a diferença $|\omega_1 - \omega_2| = 2\pi\, m\, FSR$, onde m é um inteiro positivo, e FSR é o intervalo espectral livre da cavidade do OPO. Uma medida deste comportamento fora feita ainda na década de 90 [21], e pode ser considerado um precursor do emaranhamento entre modos distintos do campo eletromagnético, apesar da pequena diferença envolvida (inferior a 1 GHz).

Estes campos, gerados aos pares, apresentam uma forte correlação na contagem de fótons, o que dá origem aos fótons gêmeos. No entanto, ainda que a medida de correlação de intensidade seja simples de ser feita, ela corresponde a apenas uma parte da caracterização do emaranhamento. Este implica na correlação simultânea de duas variáveis conjugadas. Neste caso, a variável conjugada à intensidade é a fase do campo, que fora medida nestes casos com a ajuda de osciladores locais para a investigação dos modos.

Já para o OPO acima do limiar de oscilação, há um problema. Dos modos m sujeitos à oscilação, aquele com o limiar mais baixo começa a oscilar, e irá fazer a depleção da potência de bombeio intracavidade, suprimindo a oscilação dos demais. Deve ocorrer ainda a geração de vácuo emaranhado nos outros modos, que pode eventualmente ser detectado, mas a potência do bombeio será convertida principalmente em luz nos modos sinal e complementar. As frequências dos campos não é necessariamente degenerada, requerendo, por um lado, um esforço extra para trazer o sistema à degenerescência.

Mas além do problema da degenerescência em frequência, há o problema da fase. A relação desta, entre os modos sinal e complementar, é indeterminada, graças ao processo difusivo. Retomando a descrição das equações de Langevin do OPO [22], vemos que um dos autovalores da matriz de arrasto é nulo, e que este irá levar a um processo de difusão na relação de fase. Isto está ligado também ao fato que a diferença de frequência entre sinal e complementar não está sujeita a nenhuma constante de evolução do sistema, contrariamente à soma das frequências dos três modos ou à diferença entre o número de fótons sinal e complementar (ligadas à conservação de energia). Fica a questão de como fazer a medida neste caso. Vários grupos, na década de 90, estavam envolvidos no travamento das fases dos modos convertidos do OPO, com técnicas de acoplamento ótico [23] ou travamento eletrônico [24]. Haveria alguma forma, no entanto, de fazer a medida no OPO livre?

2.1 Uma proposta de medida

A difusão de fase entre os modos sinal e complementar no OPO é semelhante à que ocorre em um laser: sua saída é tomada pelos experimentais como um estado coerente, para o arrepio de parte dos teóricos. Na realidade, a fase do laser sofre um processo difusivo bem conhecido, e dois lasers estabilizados na mesma referência de frequência vão sofrer um passeio aleatório em sua fase. Interferências serão observadas em tempos curtos, mas para tempos mais longos a integração vai destruir a correlação entre eles. Esta incoerência relativa pode ser deduzida pela largura de Schalow-Townes [25]. Esta difusão, no entanto, pode ser suprimida se os campos forem acoplados por injeção de parte de um dos lasers no outro. O feixe incidente irá atuar como uma referência de sinal, amplificado no meio após a injeção na cavidade, e irá estabilizar os dois campos. Se os lasers tiverem frequências distintas, pode se tomar o batimento deles, e estabilizá-lo em fase com uma referência na faixa de RF.

As ideias por trás destes dois métodos foram empregadas por dois grupos para estabilizar os seus OPOs e força-los a uma operação degenerada e travada em fase para os campos sinal e complementar. O grupo de Olivier Pfister empregou o batimento entre os campos para controlar cuidadosamente o índice de refração do cristal, atuando tanto na temperatura quanto com a aplicação de um campo externo [24]. Já o grupo de Claude Fabre empregou uma lâmina de quarto de onda dentro de uma cavidade, diante de um dos espelhos em uma cavidade linear. Uma parte do campo de cada um dos modos (sinal e complementar) de polarizações ortogonais, após passarem duas vezes pela lâmina de quarto de onda, sofrem uma pequena rotação de polarização. Como resultado, este giro

de polarização irá representar uma perda dos feixes antes de serem realimentados no amplificador. No entanto, se o cristal estiver em conversão próxima à degenerescência, este processo de realimentação poderá levar a um limiar mais baixo de oscilação no caso degenerado. O acoplamento entre os modos, por sua vez, irá levar ao travamento de fase [23].

Foi em 2002, pela época da livre-docência do meu colega de laboratório, prof. Paulo Nussenzveig, que lhe ocorreu a ideia de empregar a técnica de rotação de elipse, usada já em nosso laboratório para verificar o excesso de ruído em um laser de diodo [26]. Discutimos esta ideia rapidamente, e a técnica de medida nos pareceu viável. A principal questão que nos colocávamos era sobre a razão desta técnica de medida não ter sido empregada antes, sendo que já no artigo de Reid e Drummond [3] esta técnica, desenvolvida inicialmente por Levenson *et al.* [27], era apontada como uma forma de medir o emaranhamento.

A primeira restrição poderia ser a questão de como definir a fase entre dois campos de frequências distintas. Mas para isso vale lembrar aqui que as flutuações de fase, neste caso, estão ligadas à portadora do campo. Na nossa medida local, nos mantemos analisando as flutuações em torno desta frequência central, portanto nos mantemos em um referencial girante, acompanhando o valor médio da portadora dentro do intervalo de tempo de nossa medida. Se as portadoras tem frequências distintas, com flutuações de fase distintas variando a velocidade de fase relativas entre elas, pouco importa neste caso, posto que as medidas são feitas nos referencias girantes locais.

As primeiras medidas, no entanto, mostravam problemas em atingir o nível baixo de ruído, além de diversos problemas técnicos ligados à sua implementação, que podem ser vistos na dissertação de mestrado de Alessandro de Souza Villar [28]. Nas discussões, ocorreu-nos uma segunda limitação, lembrando da minha experiência anterior na medida da compressão de ruído no campo de bombeio [29]. Naquele caso, para mostrar a compressão de ruído, era necessário que o campo de entrada estivesse em um estado de mínima incerteza. No nosso caso, por melhor que fosse o laser empregado, ainda havia a possibilidade de que um excesso de ruído fosse afetar as medidas de correlação. Investigamos o efeito deste excesso de ruído no artigo mostrado a seguir. Vimos que os feixes gêmeos são robustos contra perdas, uma vez que o espaço de subtração dos campos se desacopla do campo de bombeio, porém a compressão de ruído na soma das fases é fortemente afetada, devido ao forte acoplamento com o ruído do campo de bombeio.

Além disso, mostramos como deve ser implementada a técnica de medida proposta, usando a rotação de elipse por cavidades de análise [30], e mostramos cálculos preliminares, levando em conta cavidades reais, incluindo o efeito de perdas nas mesmas. Este artigo [31] serviu de base teórica, preparando as medidas que seriam feitas posteriormente. A divulgação deste artigo envolvia um risco, o de anunciar a ideia (ou chamar a atenção para uma ideia antiga) e apontar para um problema possível no processo de medida, sabendo da elevada concorrência internacional. A medida, no entanto, tomaria ainda mais dois anos para ser realizada.

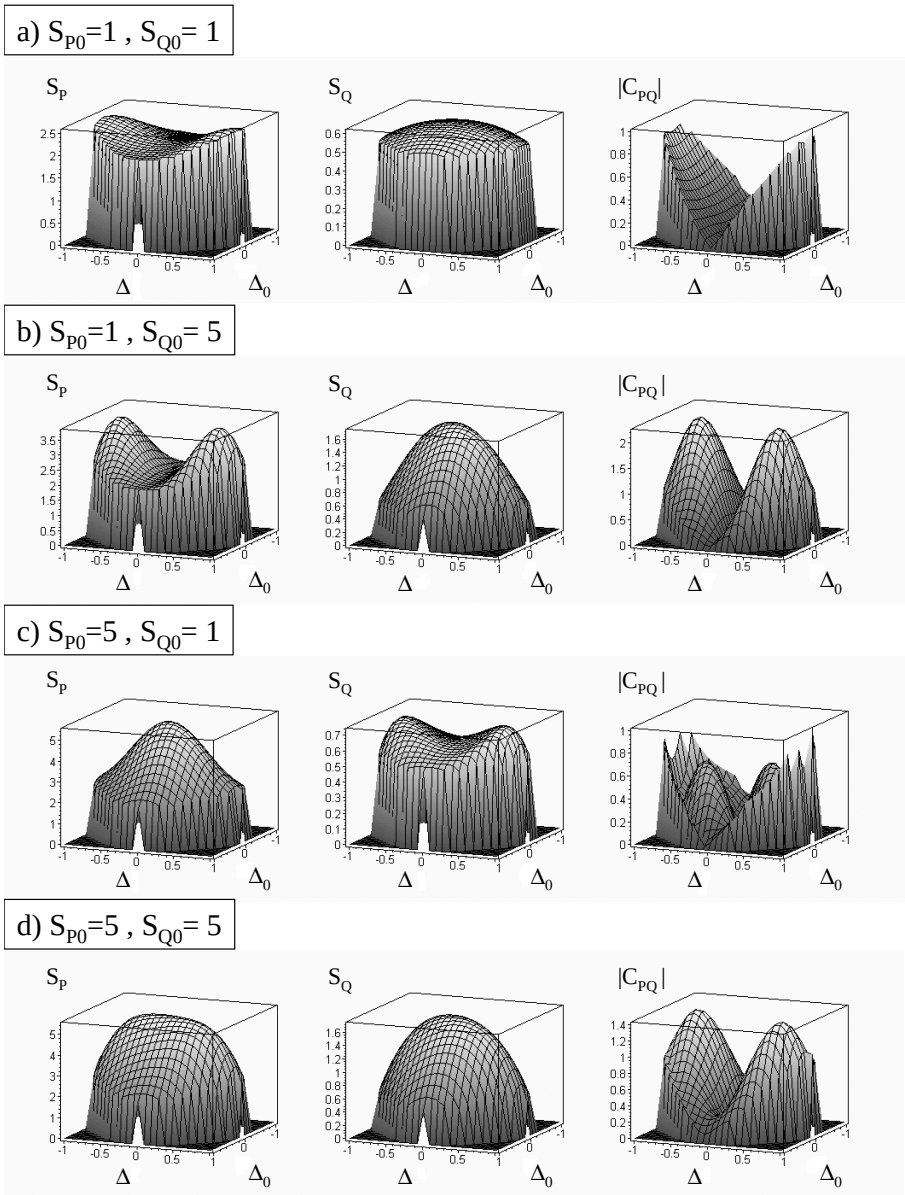

Figura 2.2: Vemos acima a dependência das variâncias de fase (S_Q) e amplitude (S_P) normalizadas pelo ruído quântico padrão, no subespaço da soma dos modos sinal e complementar em função da dessintonia do bombeio (Δ_0) e dos modos sinal e complementar (Δ) para diferentes níveis de excesso de ruído no campo de bombeio.

Available online at www.sciencedirect.com
SCIENCE DIRECT®
Optics Communications 242 (2004) 551–563
OPTICS COMMUNICATIONS
www.elsevier.com/locate/optcom

Testing the entanglement of intense beams produced by a non-degenerate optical parametric oscillator

A.S. Villar, M. Martinelli, P. Nussenzveig *

Instituto de Física – Universidade de São Paulo, P.O. Box 66318, CEP 05315-970 São Paulo-SP, Brazil

Received 6 May 2004; received in revised form 31 August 2004; accepted 1 September 2004

Abstract

We propose a direct measurement of the quadrature correlations of signal and idler beams in a non-degenerate optical parametric oscillator operating above threshold. We investigate the experimental limits where quantum correlations can be observed, fulfilling an inseparability criterion for defining them as intense entangled beams. The use of optical cavities to access quadrature noise in this situation is studied, and its advantages over homodyne detection are discussed. We also consider the application of this entanglement and the quadrature noise measurement technique to quantum cryptography.

PACS: 42.50.Dv; 42.50.Lc; 03.67.Mn; 03.67.Dd
Keywords: Entanglement; Optical parametric oscillator

1. Introduction

Entanglement of two states (e.g., a pair of light beams) is a purely quantum behavior, leading to non-locality, which is in the heart of the quantum information theory [1,2]. When the fields are in an entangled state, the non-classical behavior can be demonstrated by the violation of the Bell inequality [3,4]. For continuous variables, a Bell inequality is no longer directly applicable, but many authors have developed other relations that must be violated to show the inseparability of continuous variable systems [5], such as the proposal of Duan et al. [6], which we will refer to as the DGCZ criterion.

A well known example of entangled states are the twin photons produced by atomic fluorescence [7] or spontaneous parametric down-conversion [8,9]. For continuous variables, it has been demonstrated that squeezed states, combined in a beam splitter, can produce entangled states [10,11]. Experimentally, this source of entanglement has

* Corresponding author. Tel.: +55 11 309 16639; fax: +55 11 309 16832.
E-mail address: nussen@if.usp.br (P. Nussenzveig).

0030-4018/$ - see front matter
doi:10.1016/j.optcom.2004.09.006

already been produced by the combination of pulsed squeezed beams generated by the $\chi^{(3)}$ nonlinearity in optical fibers [12].

Optical parametric oscillators (OPO) or amplifiers (OPA) can be sources of entangled states. Sub-threshold OPO's are shown to produce an entangled pair of fields, either in frequency degenerate OPO's [13] and non-degenerate OPO's [14]. EPR-like beams have also been produced from the combination of the outputs of two degenerate sub-threshold OPO's and used for quantum teleportation [15].

On the other hand, it has already been predicted that the OPO would still produce entangled states above threshold, generating intense entangled beams that would satisfy the DGCZ entanglement criterion. But there are difficulties in performing this kind of measurement. The theory predicts that signal and idler beams will be intensity-correlated and phase-anti-correlated [16,17]. While it is easy to measure intensity correlations leading to sub-shot noise fluctuations in the difference of beam intensities [18], the measurement of phase quadrature fluctuations often requires the use of a local oscillator for an homodyne detection [19].

Typical OPO's will produce non-degenerate signal and idler beams with a frequency separation that is a multiple of the cavity free spectral range [20], but the usual configuration used for measuring quadrature fluctuations can be implemented only if signal and idler fields are frequency degenerate, like in the case of squeezed vacuum [21].

In this article, we investigate the possibility of measuring entanglement between intense signal and idler beams even in the non-degenerate situation, taking into account typical experimental conditions such as a noisy pump beam and a detuned OPO cavity. Our calculations for the OPO indicate that there is an experimentally accessible region of parameters where entanglement can happen. Although excess noise in the phase of the pump field can destroy the entanglement, its intensity noise has little effect.

In order to measure phase fluctuations of signal and idler, we propose a self-homodyne technique that uses external cavities to independently rotate the phase of the fields' fluctuations relative to their mean values [22], leading to a direct conversion of phase fluctuations into intensity fluctuations [23]. By summing or subtracting the measured signal and idler quadrature fluctuations, correlation or anti-correlation between their quadratures can be seen, and the DGCZ criterion can be applied. This implementation allows a generalized quadrature measurement and noise correlation even if the beams are not degenerate, thus overcoming the difficulties associated with homodyne detection in this system.

We finally consider using this implementation for quantum secure key distribution according to a recently proposed protocol [24]. This requires a stronger condition for the correlation between amplitudes and anti-correlation between phases: both of them must be squeezed. We show that this can be the case for the non-degenerate OPO, therefore enabling its use for quantum cryptography.

One direct advantage of this system is that intense beams are easier to manipulate than squeezed vacuum. The beams' mean intensities are another parameter to check any violation of the secure channel. Besides, the use of optical cavities to access quadrature noise has advantages over homodyne detection in this situation. By making Alice and Bob's measurements independent of local oscillators, difficulties like their production and distribution are eliminated, simplifying the experimental setup.

We begin by a brief description of the DGCZ criterion, and then we review the expected results for a type-II OPO above threshold, studying the effect of the pump noise and cavity detuning on entanglement. The conversion of phase noise into intensity noise by a lossy cavity is studied, and the experimental proposal is then described, showing that the use of cavities allows a local selection of the measured quadrature noise of the entangled beams, thus establishing a secure channel for quantum key distribution.

2. Entanglement criterion

As described in [6], a quantum state composed by two modes, 1 and 2, is said to be separable if its density matrix ρ can be described by a statistical mixture of the product of normalized states of the

systems 1 and 2 (ρ_{i1} and ρ_{i2}), $\rho = \sum_i p_i \rho_{i1} \otimes \rho_{i2}$ with positive probabilities p_i that satisfy $\sum_i p_i = 1$.

If the system is composed of two modes of the quantized electromagnetic field, we can define annihilation and creation operators for each mode, respectively a_j and $a_j^\dagger$ [25], where $j \in \{1, 2\}$ stands for the mode. These operators follow the usual commutation relation $[a_j, a_{j'}^\dagger] = \delta_{j,j'}$, and since they are not hermitian operators, the mean value will return a complex number that represents the complex field amplitude envelope. From these operators we can define a pair of hermitian operators, giving the quadratures of the field in the Fresnel representation:

$$\begin{aligned} q_j(t) &= \mathrm{i}[\mathrm{e}^{\mathrm{i}\varphi} a^\dagger(t) - \mathrm{e}^{-\mathrm{i}\varphi} a(t)], \\ p_j(t) &= [\mathrm{e}^{\mathrm{i}\varphi} a^\dagger(t) + \mathrm{e}^{-\mathrm{i}\varphi} a(t)], \end{aligned} \tag{1}$$

where the phase φ rotates the field in the plane of the Fresnel representation. We have then the commutation relation: $[p_j, q_{j'}] = 2\mathrm{i}\delta_{j,j'}$, that implies in the uncertainty relation: $\Delta^2 p_j \Delta^2 q_j \geqslant 1$. For a coherent state, $\Delta^2 p_j = \Delta^2 q_j = 1$, and for a squeezed state [25,26] we have, for instance, $\Delta^2 q_j > 1 > \Delta^2 p_j$. If we study two modes of the field, we can look for a vanishing commutator for a linear combination of the quadrature operators, that are called EPR-like operators of the system. As an example of a pair of EPR-like operators, we have

$$u = \frac{q_1 + q_2}{\sqrt{2}}, \quad v = \frac{p_1 - p_2}{\sqrt{2}}. \tag{2}$$

In this case, the variables u and v commute, and therefore they can be determined simultaneously with arbitrary precision.

Duan et al. [6] have shown that if a system composed of two modes is separable then there is a lower bound for the variances of the measurements of u and v:

$$\langle \Delta^2 u \rangle + \langle \Delta^2 v \rangle \geqslant 2. \tag{3}$$

Violation of this inequality is a sufficient condition for a quantum state to be considered inseparable, or, equivalently, for having an entanglement between modes 1 and 2. On the other hand, if we have gaussian states, it can be shown that violation of relation (3) is a sufficient and necessary condition for the inseparability of states.

Therefore one can verify the entanglement of two fields by measuring the variance of the sum of phase quadratures and subtraction of amplitude quadratures. We will now discuss the entanglement of the fields produced by a non-degenerate OPO, and study how its signature is affected by a noisy pump and a detuned cavity.

3. Entanglement of signal and idler fields

Strong intensity correlations between signal and idler beams produced in an above-threshold OPO have already been demonstrated with experimental data [18,27] that agrees with the usual treatment of the fields as classical values with stochastic fluctuations. This is equivalent to the quantum treatment using the density matrix, which is converted to a Wigner representation for the field values [28]. Similarly, there have been studies of phase anti-correlation between the output fields [29]. But, while intensity correlation is shown to be independent of cavity parameters like detuning and pump power and quite insensitive to pump noise, anti-correlation in phase fluctuations were predicted in only a very specific situation: zero cavity detuning and coherent pump [17], which is far from the usual situation observed in the laboratory.

We outline here a full treatment of the problem, showing that, although not completely independent of pump noise as intensity correlation is, phase anti-correlation can be obtained in normal experimental conditions, using the DGCZ criterion to demonstrate entanglement of a pair of macroscopic fields produced by an OPO above threshold.

Consider the complex field amplitudes, represented by the annihilation operators $\{a_0(t), a_1(t), a_2(t)\}$ for pump, signal and idler, respectively. Any field operator can be described in an equivalent way by its mean value and an operator for the field fluctuation taking the general form $a(t) = \alpha + \delta a(t)$, where $\alpha = \langle a(t) \rangle = |\alpha|\, \mathrm{e}^{\mathrm{i}\varphi}$. The intensity of each beam will be given by an average value and a real valued fluctuating term $I(t) = |\alpha|^2 + \alpha\delta a^\dagger(t) + \alpha^*\delta a(t)$, where terms of higher order in the fluctuation are neglected, since all fields are

assumed intense ($|\alpha|^2 \gg 1$). Therefore, the intensity will be given by $I(t) = |\alpha|^2 + |\alpha|\delta p(t)$, where $\delta p(t) = [e^{i\varphi}\delta a^\dagger(t) + e^{-i\varphi}\delta a(t)]$ is obtained from Eq. (1). The conjugate operator $\delta q(t)$ defines the phase quadrature fluctuation of the field.

In our procedure, we will begin with the Langevin equations obtained from the Wigner representation of the fields, presented in [28,30], and change it into the equivalent description of fields' quadrature fluctuations $\delta p(t)$, $\delta q(t)$. We will be searching for a DGCZ-like correlation between signal and idler fields, Eq. (3), obtained directly from the sum and subtraction of the fields' quadratures, $p_\pm(t) = [p_1(t) \pm p_2(t)]/\sqrt{2}$ and $q_\pm(t) = [q_1(t) \pm q_2(t)]/\sqrt{2}$.

Changing the density operator representation of the system into the Wigner representation of the fields as complex variables, we can obtain the Langevin equations of the fields, in the form

$$\tau \frac{d}{dt} P = -\mathbf{A}P + \mathbf{B}P_{in}, \tag{4}$$

where the vector of field fluctuations is $P = [\delta p_-(t), \delta q_-(t), \delta p_+(t), \delta q_+(t), \delta p_0(t), \delta q_0(t)]^T$. Here, τ is the cavity's round trip time, and the drift matrix $\mathbf{A}$ and the damping matrix $\mathbf{B}$ depend on cavity loss and detuning. The external fluctuations P_{in} are coupled to the OPO's cavity through the damping matrix. We will limit ourselves to the study of field fluctuations above oscillation threshold.

From the steady state values of the fields above threshold [20,28] we obtain the drift matrix

$$\mathbf{A} = \begin{bmatrix} 2\gamma & 0 & 0 & 0 & 0 & 0 \\ -2\gamma\Delta & 0 & 0 & 0 & 0 & 0 \\ 0 & 0 & 0 & 2\gamma\Delta & -\sqrt{2}\gamma\eta & \sqrt{2}\gamma\Delta\eta \\ 0 & 0 & 0 & 2\gamma & -2\gamma\Delta\eta & -2\gamma\eta \\ 0 & 0 & \sqrt{2}\gamma\eta & \sqrt{2}\gamma\Delta\eta & \gamma_0 & -\gamma_0\Delta_0 \\ 0 & 0 & -\sqrt{2}\gamma\Delta\eta & \sqrt{2}\gamma\eta & \gamma_0\Delta_0 & \gamma_0 \end{bmatrix} = \begin{bmatrix} \mathbf{A}_- & 0 \\ 0 & \mathbf{A}_+ \end{bmatrix}, \tag{5}$$

where the total cavity losses for pump (γ_0) and signal and idler fields (γ) are related to the coupling mirror transmissivity $T = 2\gamma$. If we have other spurious losses, they can be added to the mirror transmissivity when calculating the output fluctuations, but considering that only the field coming out through the coupling mirror will be detected, resulting in a linear degradation of the squeezing [19]. Δ and Δ_0 are the cavity detunings normalized by the internal loss ($\Delta = \varphi/\gamma$). The ratio η of the mean values of the signal (and idler) and pump fields (α, α_0) is given by

$$\eta = \frac{|\alpha|}{|\alpha_0|} = \sqrt{\frac{\gamma_0}{\gamma}} \left[\frac{\Delta\Delta_0 - 1 + \sqrt{\sigma - (\Delta + \Delta_0)^2}}{1 + \Delta^2} \right]^{1/2}, \tag{6}$$

where σ is the relative pump power, normalized to threshold power on resonance ($\Delta = \Delta_0 = 0$). Signal and idler detunings are equal as a condition for stable oscillation [20]. Phase matching in the non-linear crystal is implicit in the normalized pump power [20], and will change the threshold power of the OPO and the phase difference of signal and idler to the pump field. The small bistability region close to the oscillation threshold [28] is hardly seen in CW operation, and will not be considered in our calculations.

The incoming fluctuations P_{in}, coupled to the cavity through its input mirror, can be simply considered as vacuum fluctuations for the signal and idler fields, but not for the pump, where the pumping laser fluctuations must be taken into account. The phase difference between the intracavity fields and the incoming fields is considered in the coupling matrix $\mathbf{B}$,

$$\mathbf{B} = \begin{bmatrix} \mathbf{B}_- & 0 & 0 \\ 0 & \mathbf{B}_+ & 0 \\ 0 & 0 & \mathbf{B}_0 \end{bmatrix}, \tag{7}$$

with each submatrix $\mathbf{B}_j$ given by

$$\mathbf{B}_j = \sqrt{2\gamma_j} \begin{bmatrix} \cos(\varphi_j^{in} - \varphi_j) & -\sin(\varphi_j^{in} - \varphi_j) \\ \sin(\varphi_j^{in} - \varphi_j) & \cos(\varphi_j^{in} - \varphi_j) \end{bmatrix}. \tag{8}$$

The relationship between the phases of intracavity fields φ_j and incident fields φ_j^{in}, for pump, signal and idler modes can be reduced to a simple form if we consider the incoming pump field as a reference and set its phase to zero, $\varphi_0^{in} = 0$. The incoming vacuum fluctuations in the sum and subtraction of signal and idler modes can be arbitrarily set to be in phase with the intracavity fields.

Therefore, we will have for the linear combination of signal and idler beams $\varphi_+^{\text{in}} = \varphi_+$ and $\varphi_-^{\text{in}} = \varphi_-$. Finally, the phase of the intracavity pump mode is found to be

$$\begin{aligned} e^{2i\varphi_+} &= \frac{\sqrt{\sigma}}{\sqrt{\sigma - (\Delta + \Delta_0)^2} - i(\Delta + \Delta_0)}, \\ e^{i\varphi_0} &= \frac{1 - i\Delta}{\sqrt{1 + \Delta^2}} e^{2i\varphi_+}. \end{aligned} \tag{9}$$

To complete the treatment, and find the output field fluctuations, we need to combine the intracavity field transmitted through the coupling mirror with the incident field. Once again, we have to consider the phase relations between incoming field, intracavity field and output field to maintain our definitions of field quadratures p and q. The output field fluctuations vector will be $P_{\text{out}} = \mathbf{B}'P - \mathbf{B}''P_{\text{in}}$, where the phase rotated coupling matrices for reflection ($\mathbf{B}''$) and transmission ($\mathbf{B}'$) of the fields are similar to the one defined in Eq. (7), but with the submatrices given by

$$\begin{aligned} \mathbf{B}'_j &= \sqrt{2\gamma_j} \begin{bmatrix} \cos(\varphi_j - \varphi_j^{\text{out}}) & -\sin(\varphi_j - \varphi_j^{\text{out}}) \\ \sin(\varphi_j - \varphi_j^{\text{out}}) & \cos(\varphi_j - \varphi_j^{\text{out}}) \end{bmatrix}, \\ \mathbf{B}''_j &= \begin{bmatrix} \cos(\varphi_j^{\text{in}} - \varphi_j^{\text{out}}) & -\sin(\varphi_j^{\text{in}} - \varphi_j^{\text{out}}) \\ \sin(\varphi_j^{\text{in}} - \varphi_j^{\text{out}}) & \cos(\varphi_j^{\text{in}} - \varphi_j^{\text{out}}) \end{bmatrix}. \end{aligned} \tag{10}$$

From these equations defining the time evolution of the intracavity field and its coupling to the external modes, we can obtain the noise spectrum of each quadrature as a function of the cavity parameters, pump power, pump noise and analysis frequency.

In frequency domain, we have $\tilde{P}(\Omega) = \int P(t) e^{i\Omega t}\, dt$. The matrix of the output noise spectra $\mathbf{V}_{\text{out}} = \langle \tilde{P}_{\text{out}}(\Omega) \tilde{P}_{\text{out}}^{\text{T}}(-\Omega) \rangle$ is given by

$$\begin{aligned} \mathbf{V}_{\text{out}} = &\left[\mathbf{B}'(\mathbf{A} + i\Omega\mathbf{I})^{-1}\mathbf{B} - \mathbf{B}'' \right] \\ &\times \mathbf{V}_{\text{in}} \left[\mathbf{B}'(\mathbf{A} - i\Omega\mathbf{I})^{-1}\mathbf{B} - \mathbf{B}'' \right]^{\text{T}}, \end{aligned} \tag{11}$$

where $\mathbf{V}_{\text{in}} = \langle \tilde{P}_{\text{in}}(\Omega) \tilde{P}_{\text{in}}^{\text{T}}(-\Omega) \rangle$.

From the Langevin equations of the fields we can observe that those for the subtraction of the field quadratures are uncoupled from those for the sum of the quadratures and for the pump field. Therefore, we can independently obtain the noise spectra of the subtraction and the sum of the output fields. Considering the input field spectrum normalized to the vacuum fluctuations, we have for the subtraction of the amplitudes and phase quadratures [17]

$$\begin{aligned} S_{p-}(\Omega) &= \langle \delta p_{\text{out}-}(\Omega) \delta p_{\text{out}-}(-\Omega) \rangle \\ &= 1 - \frac{4\gamma^2}{4\gamma^2 + \tau^2\Omega^2}, \\ S_{q-}(\Omega) &= \langle \delta q_{\text{out}-}(\Omega) \delta q_{\text{out}-}(-\Omega) \rangle \\ &= \frac{1}{S_{p-}(\Omega)}. \end{aligned} \tag{12}$$

Therefore, the fluctuations of the subtraction of the outcoming fields are in a state of minimum uncertainty, and will show squeezing in the amplitude quadrature. Moreover, they are independent of pump or cavity parameters. For the sum of the fields' fluctuations, the result is not so simple, but can be obtained from Eq. (11), showing their dependence on cavity detuning, pump power and pump noise.

In what follows, we present results for the noise spectrum of the sum of fields quadratures (S_{p+}, S_{q+}), considering that the pump field can be either in a coherent state, or with excess noise either in amplitude or phase (considering that these fluctuations are uncorrelated). While the fluctuations of the difference of fields will depend only on the analysis frequency (Ω) and cavity bandwidth for signal and idler ($\delta\omega = 2\gamma/\tau$), the fluctuation of the sum will also depend on the normalized pump power σ, cavity bandwidth for the pump ($\delta\omega_0 = 2\gamma_0/\tau$), cavity detuning for the pump (Δ_0), signal and idler (Δ) and pump noise (S_{p0}, S_{q0}).

Consider a simple case: resonance ($\Delta = \Delta_0 = 0$) and a coherent pump ($S_{p0} = S_{q0} = 1$), operating at twice the threshold power ($\sigma = 2$), the cavity coupling mirror having a small transmissivity for signal and idler ($T = 2\gamma = 2\%$) and a large one for the pump ($T = 2\gamma = 10\%$). In Fig. 1, the normalized noise for each one of the quadratures of the difference of the field fluctuations are presented.

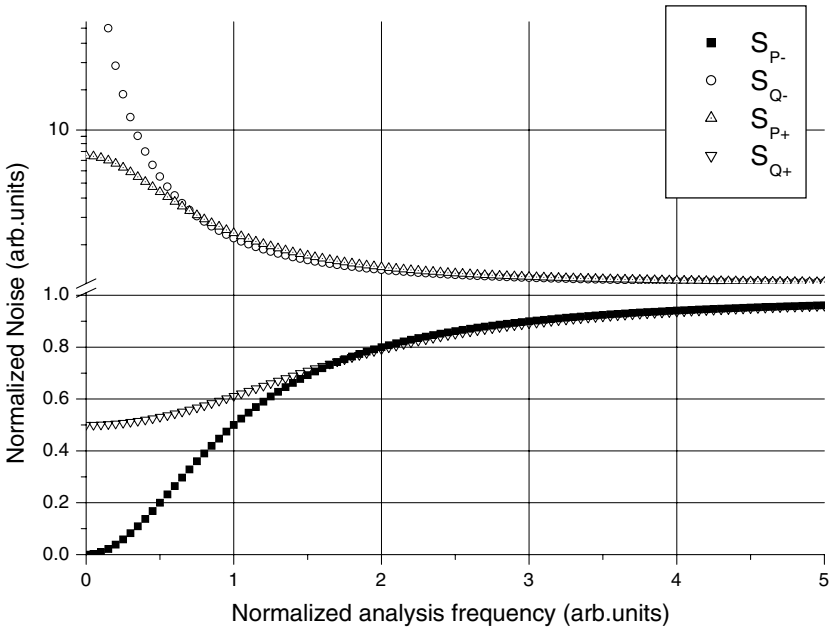

Fig. 1. Noise spectra of the fields correlations in an OPO, as a function of frequency. Analysis frequency normalized to the cavity bandwidth for the signal ($\delta\omega_1 = 2\gamma/\tau$). Parameters are $\gamma = 0.01$, $\gamma_0 = 0.05$, $\Delta = \Delta_0 = 0$, $\sigma = 2$.

As we can see, perfect intensity correlation between the fields can be obtained for a long integration time ($S_{p-} = 0$), and consequently the fluctuations of the conjugate variable (S_{q-}) diverge. This can be seen as a process of phase diffusion, already discussed in [17,31]. Energy conservation and phase matching imply that signal and idler phases are anti-correlated. Hence, the sum of phases is little affected by phase diffusion. The fluctuations in the sum of phases have a lower bound, as a function of analysis frequency, given by $S_{q+} = 0.5$. Lower values could be achieved as the threshold limit is approached ($\sigma \to 1$, $S_{q+} \to S_{p-}$), but the practical stability of the experimental setup is reduced. Of course, these values apply for a cavity without any spurious losses (the only loss is through the coupling mirror) and no losses in the detection process. But from these values we observe that an OPO can act as a source of entangled beams even with intense outputs, according to the DGCZ criterion, Eq. (3). Losses in the beam path and inside the cavity will linearly reduce the level of squeezing [19].

Perfect resonance and a pump laser with small noise are not the usual situation met in a laboratory. Squeezing in S_{p-} has been shown to be insensitive to these non-ideal laboratory conditions. As for the S_{q+} squeezing, we show that the effects of these imperfections are not so drastic, and entanglement can still be obtained in quite fair conditions of operation. In Fig. 2 we present the noise power and the absolute value of the correlation $C_{pq} = \langle \delta p_{\text{out}+}(\Omega)\delta q_{\text{out}+}(-\Omega)\rangle$ of the sum of the quadratures in typical measurement conditions ($\Omega = 2\gamma/\tau$, $\sigma = 2$), as a function of pump and signal detuning, for different pump noise conditions.

The non-zero values are the results for an oscillating OPO operating above threshold. In the first row, we see that although there is some dependence of noise power with detuning, it remains quite flat, with a minimum value of 2 for S_{p+} and a maximum of 0.5 for S_{q+}. Correlation between the quadratures occurs mainly in conditions of detuned cavity for the signal, being almost insensitive to pump detuning. As we will see, the C_{pq} correlation can mask the entanglement characterization of signal and idler fields, and its value should be taken into account when performing a measurement.

In the second row, we consider a pump laser with phase quadrature fluctuations, but shot noise limited intensity fluctuations. That is the typical

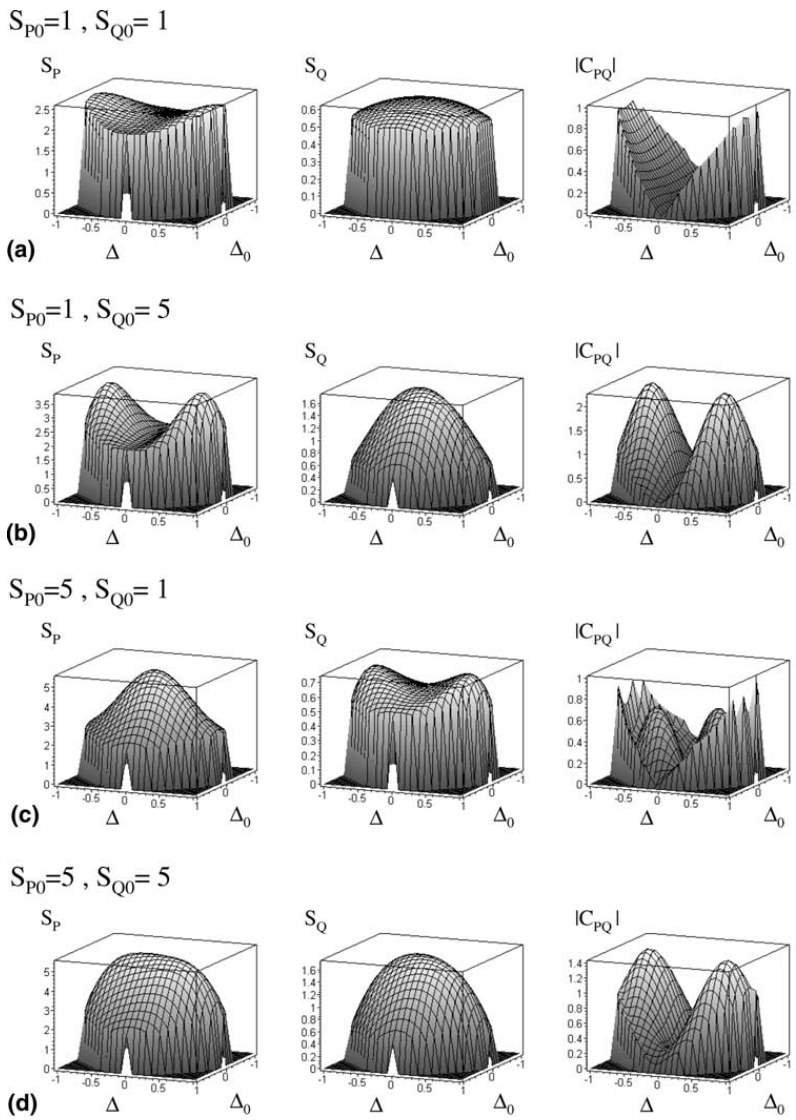

Fig. 2. Normalized noise of the field correlations in an OPO, as a function of the cavity detuning, for different pump noise conditions. S_P: noise of the sum of the amplitude quadratures p_+, S_Q: noise of the sum of the phase-related quadratures q_+, $|C_{pq}|$: absolute value of correlations between the sum of amplitude and phase-related fluctuations. Parameters are $\gamma = 0.01$, $\gamma_0 = 0.05$, $\Omega = 2\gamma/\tau$, $\sigma = 2$.

case of diode lasers [23]. We observe that the fluctuations can destroy the squeezing of S_{q+} at exact resonance; nevertheless, for detuned cavities close to the threshold limit, good squeezing is still achievable, and the DGCZ inequality is still violated. The third row shows a more convenient situation, where the pump has excess noise in amplitude fluctuations, but phase fluctuations are small. The effect in the S_q squeezing is small over the whole range of possible detuning values. Finally, with a noisy beam on both quadratures, the squeezing is much degraded, and the region where the DGCZ inequality is violated is really small, only very close to threshold.

We can conclude that, while the entanglement signature is quite stable under detuned cavity conditions, it is very sensitive to the phase noise of the pump. Therefore, to produce an entangled pair of intense beams in an OPO, we need a low noise pump. In the following section, we will describe how to make an independent measurement of the quadrature fluctuations of each field, allowing a

local measurement of the field quadratures that can be applied, for instance, to quantum communications.

4. Phase rotation of noise ellipse

We are interested in accessing the quadrature fluctuations of both signal and idler beams to measure correlation and anti-correlation. Measuring quadrature fluctuations usually requires the use of a local oscillator, but, regarding the difficulties this technique faces when applied to a non-degenerate OPO, the use of an optical cavity can be more interesting. As first showed by Galatola et al. [22], an optical cavity can project phase quadrature fluctuations into amplitude quadrature fluctuations, which is an easily measurable quantity, for some range of cavity detuning and analysis frequency.

In our case, the fields to be analyzed are the signal and idler fields produced by a type-II OPO: they can thus be separated by polarization and each one sent to its own analysis cavity. We treat the physical problem as schematized in Fig. 3. The field to be analyzed (input beam), signal or idler, is injected into a Fabry–Perot cavity, generating reflected and transmitted beams. In this process, owing to imperfections like a residual transmission in the output mirror of the cavity, vacuum leaks inside it and contributes to the noise of reflected and transmitted fields.

In what follows, we treat this problem explicitly relating the reflected beam quadrature fluctuations to the input beam ones, taking into account the input vacuum. All fields (input beam, input vacuum, reflected and transmitted beams) can be described as a stable mean value, with a well defined frequency ω_0, presenting small fluctuations in time with frequencies $\Omega \ll \omega_0$, so that their annihilation operators can be written in the general form

$$a(t) = \alpha(t) + \delta\tilde{a}(t) = [\alpha + \delta a(t)]\mathrm{e}^{-\mathrm{i}\omega_0 t}, \tag{13}$$

which have Fourier components

$$\begin{aligned} a(\omega) &= \int a(t)\mathrm{e}^{\mathrm{i}\omega t}\,\mathrm{d}t, \\ a^\dagger(\omega) &= \int a^\dagger(t)\mathrm{e}^{\mathrm{i}\omega t}\,\mathrm{d}t = [a(-\omega)]^\dagger \end{aligned} \tag{14}$$

(unless otherwise specified, integrals are made from $-\infty$ to ∞).

In the situation we are considering, the quantum equations relating reflected (a_{out}) and transmitted (b_{out}) beams to input beam (a_{in}) and input vacuum (b_{in}) have the same form as the classical ones. In frequency domain:

$$\begin{aligned} a_{\mathrm{out}}(\omega) &= r(\omega)a_{\mathrm{in}}(\omega) + t(\omega)b_{\mathrm{in}}(\omega), \\ b_{\mathrm{out}}(\omega) &= t(\omega)a_{\mathrm{in}}(\omega) - r'(\omega)b_{\mathrm{in}}(\omega), \end{aligned} \tag{15}$$

where $r(\omega)$, $t(\omega)$ are the reflection and transmission coefficients of a Fabry–Perot cavity for the input beam, and $r'(\omega)$ is the reflection coefficient for the input vacuum:

$$\begin{aligned} r(\omega) &= \frac{r_1 - r_2\exp[\mathrm{i}2\pi(\omega-\omega_{\mathrm{c}})/F_{\mathrm{sr}}]}{1 - r_1 r_2\exp[\mathrm{i}2\pi(\omega-\omega_{\mathrm{c}})/F_{\mathrm{sr}}]}; \\ t(\omega) &= \frac{t_1 t_2\exp[\mathrm{i}\pi(\omega-\omega_{\mathrm{c}})/F_{\mathrm{sr}}]}{1 - r_1 r_2\exp[\mathrm{i}2\pi(\omega-\omega_{\mathrm{c}})/F_{\mathrm{sr}}]}; \\ r'(\omega) &= \frac{r_2 - r_1\exp[\mathrm{i}2\pi(\omega-\omega_{\mathrm{c}})/F_{\mathrm{sr}}]}{1 - r_1 r_2\exp[\mathrm{i}2\pi(\omega-\omega_{\mathrm{c}})/F_{\mathrm{sr}}]}, \end{aligned} \tag{16}$$

with F_{sr} being the free spectral range of the cavity, ω_{c}, its resonance frequency, and r_1, r_2, t_1 and t_2, its mirrors' reflection and transmission coefficients for amplitudes.

As the vacuum mean value β_{in} is null, the average of these equations gives

Fig. 3. Physical situation being considered.

$$\alpha_{\text{out}} = r(\omega_0)\alpha_{\text{in}}, \qquad \beta_{\text{out}} = t(\omega_0)\alpha_{\text{in}}, \tag{17}$$

showing that the transmitted field mean value is rotated through the action of the cavity when compared to the input beam (i.e., it gains a phase). In order to assure the same quadrature is being compared in both input and output fields, this fact must be taken into account when defining the quadrature operators.

Therefore, we define, respectively, $p(t)$ and $q(t)$ as the input beam amplitude and phase quadratures, $x(t)$ and $y(t)$ as the input vacuum quadratures, $P(t)$ as the reflected field amplitude quadrature and $P'(t)$ as the transmitted field one, in the following way: if the input beam mean value is chosen real for simplicity ($\alpha_{\text{in}} = \alpha^*_{\text{in}}$), $r(\omega_0) = |\, r(\omega_0)\,|\, \mathrm{e}^{\mathrm{i}\phi_0}$ and $t(\omega_0) = |\, t(\omega_0)\,|\, \mathrm{e}^{\mathrm{i}\phi'_0}$, we have, in the interaction picture,

$$\begin{aligned}
p(t) &= a_{\text{in}}(t)\mathrm{e}^{\mathrm{i}\omega_0 t} + a^\dagger_{\text{in}}(t)\mathrm{e}^{-\mathrm{i}\omega_0 t};\\
q(t) &= -\mathrm{i}[a_{\text{in}}(t)\mathrm{e}^{\mathrm{i}\omega_0 t} - a^\dagger_{\text{in}}(t)\mathrm{e}^{-\mathrm{i}\omega_0 t}];\\
x(t) &= b_{\text{in}}(t)\mathrm{e}^{\mathrm{i}\omega_0 t} + b^\dagger_{\text{in}}(t)\mathrm{e}^{-\mathrm{i}\omega_0 t};\\
y(t) &= -\mathrm{i}[b_{\text{in}}(t)\mathrm{e}^{\mathrm{i}\omega_0 t} - b^\dagger_{\text{in}}(t)\mathrm{e}^{-\mathrm{i}\omega_0 t}];\\
P(t) &= \mathrm{e}^{-\mathrm{i}\phi_0} a_{\text{out}}(t)\mathrm{e}^{\mathrm{i}\omega_0 t} + \mathrm{e}^{\mathrm{i}\phi_0} a^\dagger_{\text{out}}(t)\mathrm{e}^{-\mathrm{i}\omega_0 t};\\
P'(t) &= \mathrm{e}^{-\mathrm{i}\phi'_0} b_{\text{out}}(t)\mathrm{e}^{\mathrm{i}\omega_0 t} + \mathrm{e}^{\mathrm{i}\phi'_0} b^\dagger_{\text{out}}(t)\mathrm{e}^{-\mathrm{i}\omega_0 t}.
\end{aligned} \tag{18}$$

In frequency domain, we define the Fourier transforms of these operators, so that their fluctuations can be written in terms of fluctuations of annihilation and creation operators in the interaction picture. For instance, we have for the transmitted field amplitude quadrature,

$$\begin{aligned}
P(\Omega) &= \int P(t)\mathrm{e}^{\mathrm{i}\Omega t}\,\mathrm{d}t \quad \Rightarrow \delta P(\Omega)\\
&= \mathrm{e}^{-\mathrm{i}\phi_0}\delta a_{\text{out}}(\Omega) + \mathrm{e}^{\mathrm{i}\phi_0}\delta a^\dagger_{\text{out}}(-\Omega),
\end{aligned} \tag{19}$$

where Ω is the analysis frequency.

For the annihilation operators' fluctuations, the first of Eq. (15) becomes

$$\delta\tilde{a}_{\text{out}}(\omega) = r(\omega)\delta\tilde{a}_{\text{in}}(\omega) + t(\omega)\delta\tilde{b}_{\text{in}}(\omega). \tag{20}$$

But, according to our definitions, $\delta a(\Omega) = \delta\tilde{a}(\Omega + \omega_0)$ and $\delta a^\dagger(\Omega) = \delta\tilde{a}^\dagger(\Omega - \omega_0)$, so that, using Eq. (20) in Eq. (18), it is possible to write $\delta P(\Omega)$ and $\delta P'(\Omega)$ in terms of $\delta a_{\text{in}}(\Omega)$, $\delta b_{\text{in}}(\Omega)$ and their adjoint operators. Using the first four equations of Eq. (18), we may express $\delta P(\Omega)$ in terms of input beam's quadratures fluctuations, obtaining

$$\begin{aligned}
\delta P(\Omega) = {} & g_1(\Omega)\delta p(\Omega) + \mathrm{i}g_2(\Omega)\delta q(\Omega)\\
& + g_3(\Omega)\delta x(\Omega) + \mathrm{i}g_4(\Omega)\delta y(\Omega),
\end{aligned} \tag{21}$$

with

$$\begin{aligned}
g_1(\Omega) &= \frac{1}{2}\left[\mathrm{e}^{-\mathrm{i}\phi_0} r(\omega_0 + \Omega) + \mathrm{e}^{\mathrm{i}\phi_0} r^*(\omega_0 - \Omega)\right],\\
g_2(\Omega) &= \frac{1}{2}\left[\mathrm{e}^{-\mathrm{i}\phi_0} r(\omega_0 + \Omega) - \mathrm{e}^{\mathrm{i}\phi_0} r^*(\omega_0 - \Omega)\right],\\
g_3(\Omega) &= \frac{1}{2}\left[\mathrm{e}^{-\mathrm{i}\phi_0} t(\omega_0 + \Omega) + \mathrm{e}^{\mathrm{i}\phi_0} t^*(\omega_0 - \Omega)\right],\\
g_4(\Omega) &= \frac{1}{2}\left[\mathrm{e}^{-\mathrm{i}\phi_0} t(\omega_0 + \Omega) - \mathrm{e}^{\mathrm{i}\phi_0} t^*(\omega_0 - \Omega)\right].
\end{aligned} \tag{22}$$

In Fig. 4, we present curves of the coefficients appearing in Eq. (21) for various analysis frequencies Ω as a function of analysis cavity detuning. In particular, we notice that it is only possible to completely rotate the noise ellipse (i.e., $|g_1(\Omega)|$ must go to zero for some value of Ω) when

$$\Omega \geqslant \sqrt{2}\,\delta\omega, \tag{23}$$

where $\delta\omega$ is the cavity bandwidth (FWHM), in agreement with [22]. Also noteworthy is the fact that, for common analysis frequencies Ω, the maximum of $|g_2(\Omega)|$ (and, consequently, the minimum of $|g_1(\Omega)|$) occurs approximately at the half maximum of the mean transmitted intensity. In the case of a lossy cavity, we can observe that, as the analysis frequency is increased, the vacuum contribution to the amplitude fluctuations, coupled by g_3 and g_4, will be reduced close to the cavity resonance. This is easily understood when one remembers that the noise term can be seen as a contribution of two sidebands of frequencies $\omega_0 \pm \Omega$. When Ω increases, these sidebands are farther detuned from resonance and therefore do not couple to the cavity field.

An analogous calculation reveals that the transmitted field amplitude fluctuations $\delta P'(\Omega)$ are related to the input fluctuations by a relation similar to Eq. (21). Unfortunately, a careful analysis shows that the noise ellipse is never completely

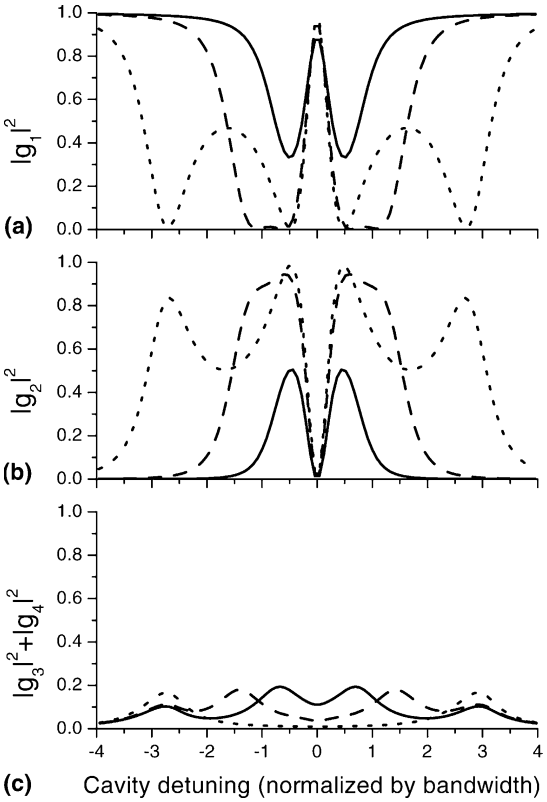

Fig. 4. These curves show the behaviour of the coefficients appearing in Eq. (21) as a function of cavity detuning (in units of cavity bandwidth). A finesse $F = 270$ is assumed. Continuous line: $\Omega = \delta\omega/\sqrt{2}$; dashed line: $\Omega = \sqrt{2}\,\delta\omega$; dotted line: $\Omega = 2\sqrt{2}\,\delta\omega$. (a) $|g_1(\Omega)|^2$, (b) $|g_2(\Omega)|^2$, (c) $|g_3(\Omega)|^2 + |g_4(\Omega)|^2$.

rotated in the transmitted beam, regardless of the analysis frequency or the cavity detuning.

The reflected beam's amplitude quadrature noise spectrum [32,33] $S_P(\Omega) = \langle \delta P(\Omega)\delta P^\dagger(\Omega')\rangle$ is given by

$$S_P(\Omega) = |g_1(\Omega)|^2 S_p(\Omega) + |g_2(\Omega)|^2 S_q(\Omega) + 2\mathrm{Im}\{g_1(\Omega)g_2^*(\Omega)C_{pq}(\Omega)\} + |g_3(\Omega)|^2 + |g_4(\Omega)|^2, \quad (24)$$

where $S_p(\Omega)$ and $S_q(\Omega)$ are the input beam p and q quadratures' noise spectra, and $C_{pq}(\Omega)$ is their correlations. $S_x(\Omega)$ and $S_y(\Omega)$ are normalized vacuum fluctuations, therefore equal to 1.

The correlation C_{pq} has the effect of making S_P asymmetric as a function of the analysis cavity detuning, for its coefficient in Eq. (24) is antisymmetric. Nevertheless, we will be interested in a cavity detuning for which $|g_1| \approx 0$ and, consequently, the effect of C_{pq} will be minimized.

5. Experimental setup

We propose the experimental setup as shown in Fig. 5. The two beams created in a type-II OPO, signal and idler, are separated by polarization using a polarizing beam splitter (PBS) just after

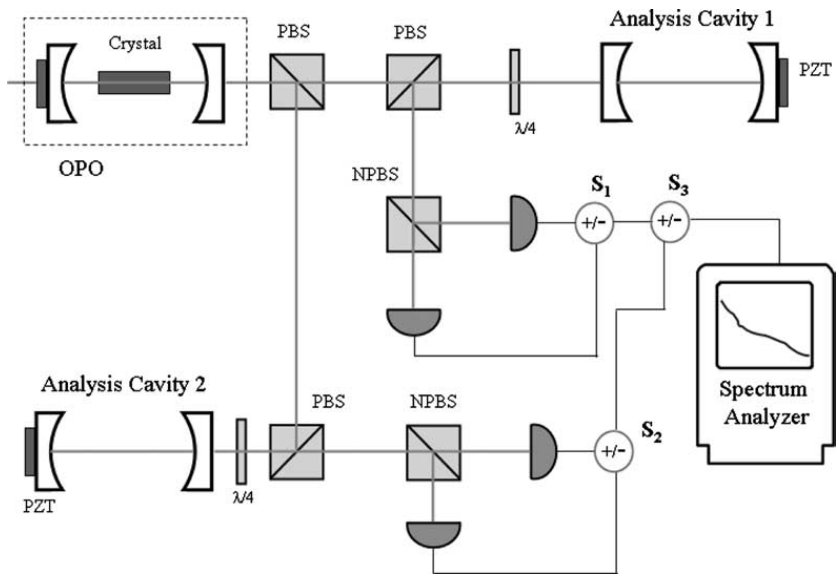

Fig. 5. Experimental setup.

they emerge from the OPO's cavity. Each beam passes through an optical circulator made by a quarter waveplate and a PBS. The field is reflected by a nearly confocal cavity after mode matching by a set of lenses (not shown). The reflected beams are sent to balanced detection setups, made by non-polarizing 50/50 beam splitters (NPBS) and two pairs of balanced photodetectors.

Each balanced detection has a sum/subtraction circuit (S_1 and S_2) for the measured photocurrents. A third circuit (S_3) is used to combine the resulting signals coming from the two detections. Shot noise is measured with S_1 and S_2 in subtraction position. Noise in each beam is measured with both S_1 and S_2 in sum position; these noises can then be summed or subtracted using S_3, where the photocurrent fluctuation will be $\delta P_{\pm}(\Omega) = \delta P_1(\Omega) \pm \delta P_2(\Omega)$, the combination of the signal and idler fluctuations after the transformation through the cavity reflection given by Eq. (21). The noise power is measured in a spectrum analyzer.

When the cavities are far away from resonance, the quadrature being measured is the amplitude. Correlation between amplitude quadrature fluctuations is one of the EPR variables of the pair and, for an OPO, it is well known to be squeezed. The other EPR variable is the anti-correlation between phase quadratures, obtained by a synchronous sweep of both cavities length while measuring the noise of the sum of the photocurrents, looking for a dip of the noise below the shot noise level. This measurement can also be made with stable cavities locked at the side of the transmission peak, making a direct measurement of the anti-correlation of the phase quadratures. Length fluctuations will add some information of the amplitude quadrature, reducing the squeezing level. As far as we can keep the cavity locked in the side of the peak, with usual techniques, this contribution can be neglected.

In order to characterize entanglement of signal and idler while the cavity length is swept, it is experimentally desirable that S_{P+} assumes squeezed values on both sides of cavity resonance, for detunings where $g_1(\Omega) \approx 0$. In this case, even if C_{PQ} causes asymmetries, the result can still be trusted.

Besides the stability of the cavities, it is important that the analysis cavities have very low spurious losses, reducing the amount of (uncorrelated) vacuum fluctuations added in the reflected fluctuations through the coefficients g_3 and g_4 in Eq. (21). The range of frequencies where entanglement can be characterized in this system has, as a lower bound, the bandwidth of the analysis cavity for a full ellipse rotation (according to Eq. (23)), and the diffusion of the phase difference, producing excess noise in the measurement, and as an upper bound, the OPO cavity bandwidth for signal and idler, that will determine the range of values where squeezing is still clearly measurable. With a careful project of the cavities, a range of tens of MHz can be achieved. Higher ranges can be implemented with very short OPO cavities, increasing its bandwidth.

6. Application to quantum cryptography

With the proposed setup, it is easy to imagine an implementation of the quantum communication protocol suggested in [24]. Alice and Bob have a cavity each one, and establish, through a classical channel, the analysis frequency they are going to look at and the synchronicity of the measurement (clock). A third part has the OPO, and can send each one of the entangled beams to Alice and Bob, that will perform, locally, a sequence of quadrature fluctuations measurements. Each one can choose randomly the quadrature to measure, storing the information, and Bob, for instance, sends the values of his photocurrent to Alice. Alice then compares the answers and checks whether they have chosen the same quadrature looking at the noise correlations that are below shot noise. Alice will return to Bob only the information of which events in the sequence were coincident. Establishing a binary relation of 0 and 1 to the quadratures, now Alice and Bob share a randomly generated key they can use to encrypt a message that is shared through the classical channel.

Any attack on the system can be noticed by a reduction in the squeezing level in the correlation measurement, or an increase in the error rate (bad quadrature choices of Alice and Bob), that should be around 50%. In this case, the output

beams of an OPO are in the order of a few mW, and can be easily detected. The mean values of the beams are also a tool to improve the quality of the detection, assuring a good mode matching to the analysis cavity, and an extra information on the possibility of an attack, which is an advantage over entanglement with squeezed vacuum.

Finally, using analysis cavities to access quadrature noise has some implementation advantages over homodyne detection schemes in quantum cryptography. Alice and Bob need a local oscillator, that has to be phase-locked to the incoming field, in order to perform the homodyne detection. If they are using entangled intense fields, either the OPO source has to send them the reference, or they will need to tap part of the entangled fields to seed their oscillators, degrading the entanglement characterization. For entangled squeezed vacuum, a distinct channel for sending the local oscillator is needed, making it sensitive to phase perturbations in the beam path.

On the other hand, analysis cavities allow each station to perform its measurement independently of the source. Any non-dispersive phase perturbation in the entangled beam path will affect simultaneously their mean values and their fluctuations, thus not disturbing the entanglement characterization. Besides, the experimental setup is simplified in comparison to the homodyne detection.

CW OPO's operating above threshold are therefore a reliable source of entangled fields, the communication bit rate being only limited by its cavity bandwidth. Frequency degeneracy of signal and idler beams is not an issue since a local self-homodyne technique is used in this implementation.

7. Conclusion

We propose a direct measurement of the entanglement of the intense beams produced by a non-degenerate type-II OPO operating above threshold, showing that entanglement is still preserved in typical experimental conditions, such as a detuned cavity and a noisy pump.

As entanglement is charaterized by the violation of the DCGZ inequality, a measurement of phase quadrature noise of signal and idler fields is needed. The use of analysis cavities to access phase noise allows a non-degenerate operation, and avoids some difficulties related to the use of local oscillators.

This setup can be used in secure key distribution through entanglement. Possible applications of this entanglement can also be expected in quantum teleportation and other implementations of quantum cryptography.

Acknowledgements

The authors wish to thank Coordenação de Aperfeiçoamento de Pessoal de Nível Superior (CAPES-BR), Conselho Nacional de Pesquisa (CNPq) and Fundação de Amparo à Pesquisa do Estado de São Paulo (FAPESP-BR) for funding.

References

[1] C.H. Bennett, Phys. Today 48 (1995) 24.
[2] D.P. DiVincenzo, Science 270 (1995) 255.
[3] J.S. Bell, Physics 1 (1965) 195.
[4] J.S. Bell, Speakable and Unspeakable in Quantum Mechanics, Cambridge University Press, Cambridge, UK, 1988.
[5] R. Simon, Phys. Rev. Lett. 84 (2000) 2726.
[6] Lu-Ming Duan, G. Giedke, J.I. Cirac, P. Zoller, Phys. Rev. Lett. 84 (2000) 2722.
[7] A. Aspect, J. Dalibard, G. Roger, Phys. Rev. Lett. 49 (1982) 1804.
[8] C.K. Hong, Z.Y. Ou, L. Mandel, Phys. Rev. Lett. 59 (1987) 2044.
[9] Y.H. Shih, C.O. Alley, Phys. Rev. Lett. 61 (1988) 2921.
[10] M.S. Kim, W. Son, V. Bužek, P.L. Knight, Phys. Rev. A 65 (2002) 032323.
[11] S. Scheel, D.-G. Welsch, Phys. Rev. A 64 (2001) 063811.
[12] Ch. Silberhorn, P.K. Lam, O. Weiß, F. König, N. Korolkova, G. Leuchs, Phys. Rev. Lett. 86 (2001) 4267.
[13] Z.Y. Ou, S.F. Pereira, H.J. Kimble, K.C. Peng, Phys. Rev. Lett. 68 (1992) 3663.
[14] C. Schori, J.L. Sørensen, E.S. Polzik, Phys. Rev. A 66 (2002) 033802.
[15] A. Furusawa, J.L. Sørensen, S.L. Braunstein, C.A. Fuchs, H.J. Kimble, E.S. Polzik, Science 282 (1998) 706.
[16] M.D. Reid, P.D. Drummond, Phys. Rev. Lett. 60 (1988) 2731.
[17] C. Fabre, E. Giacobino, A. Heidmann, S. Reynaud, J. Phys. France 50 (1989) 1209.
[18] A. Heidmann, R.J. Horowicz, S. Reynaud, E. Giacobino, C. Fabre, G. Camy, Phys. Rev. Lett. 59 (1987) 255.

[19] H.-A. Bachor, A Guide to Experiments in Quantum Optics, Weinheim – Federal Republic of Germany, Wiley-VCH, 1998.
[20] T. Debuisschert, A. Sizmann, E. Giacobino, C. Fabre, J. Opt. Soc. Am. B 10 (1993) 1668.
[21] L.A. Wu, H.J. Kimble, J.L. Hall, H.F. Wu, Phys. Rev. Lett. 57 (1986) 2520.
[22] P. Galatola, L.A. Lugiato, M.G. Porreca, P. Tombesi, G. Leuchs, Opt. Commun. 85 (1991) 95.
[23] T.C. Zhang, J.P. Poizat, P. Grelu, J.F. Roch, P. Grangier, F. Marin, A. Bramati, V. Jost, M.D. Levenson, E. Giacobino, Quantum Semiclass. Opt. 7 (1995) 601.
[24] Ch. Silberhorn, N. Korolkova, G. Leuchs, Phys. Rev. Lett. 88 (2002) 167902.
[25] D. Walls, G.J. Milburn, Quantum Optics, Springer-Verlag, Berlin, 1994.
[26] M.O. Scully, M.S. Zubairy, Quantum Optics, Cambridge University Press, Cambridge, UK, 1997.
[27] J. Mertz, T. Debuisschert, A. Heidmann, C. Fabre, E. Giacobino, Opt. Lett. 16 (1991) 1234.
[28] C. Fabre, E. Giacobino, A. Heidmann, L. Lugiato, S. Reynaud, M. Vadacchino, W. Kaige, Quantum Opt. 2 (1990) 159.
[29] Yun Zhang, Hai Wang, Xiaoying Li, Jietai Jing, Changde Xie, Kunchi Peng, Phys. Rev. A 62 (2000) 023813.
[30] M. Martinelli, C.L. Garrido Alzar, P.H. Souto Ribeiro, P. Nussenzveig, Braz. J. Phys. 31 (2001) 597.
[31] M.D. Reid, P.D. Drummond, Phys. Rev. A 40 (1989) 4493.
[32] M.J. Collet, C.W. Gardiner, Phys. Rev. A 30 (1984) 1386.
[33] M.J. Collet, D.F. Walls, Phys. Rev. A 32 (1985) 2887.

2.2 A realização da medida

A proposta feita tinha algumas limitações práticas, que podem ser notadas no próprio diagrama da montagem experimental proposta (fig. (5) no artigo anterior). Inicialmente, as montagens usavam cavidades lineares, onde o feixe refletido era recuperado por um circulador ótico composto de uma lâmina de quarto de onda e um cubo polarizador. Uma limitação óbvia está no fato deste sistema apresentar uma fuga importante de luz no retorno. Esta fuga, da ordem de 5%, representava uma perda na deteção mas, pior que isso, era uma fonte de instabilidade para o OPO, favorecendo o salto de modo.

Além disso, o antigo laser Nd:YAG dobrado (Lightwave LWE32-200), de potência nominal de 200 mW, sem saída no IR, começava a ter dificuldades em se manter neste nível de potência (caindo eventualmente para 150 mW). Esta baixa potência impedia o uso de uma cavidade de filtro, que implicava necessariamente em uma redução da potência disponível de saída, estando esta já tão escassa.

O cristal então empregado, um KTP da Crystal Laser (França), apresentava uma rápida degradação por "gray tracking" [32], limitando o tempo de uso e obrigando constantes deslocamentos transversais, limitando a confiabilidade das medidas iniciais e prevendo um tempo limitado de uso do sistema.

Por fim, o uso de montagens mecânicas comerciais implicava em uma elevada sensibilidade a ruídos ambientes, sejam vibrações mecânicas de baixa frequência (< 10 Hz), ou vibrações acústicas (> 10 Hz).

A solução envolveu diversas mudanças. A primeira foi a substituição do antigo laser por um laser da Innolight (Diabolo) com 800 mW de verde e 300 mW de IR. Esta saída revelou-se extremamente útil para o teste do sistema de deteção e o alinhamento de todas as cavidades de análise envolvidas.

Além disso, instalamos uma cavidade de filtragem, que não foi empregada nas nossas medidas preliminares. Com esta cavidade de filtro, reduzimos o laser a um estado coerente para frequências de análise acima de 15 MHz. Quanto à estabilidade mecânica, removemos todos os suportes mecânicos ("gimbals"), substituindo-os por montagens rígidas, tanto para o OPO quanto para as cavidades de filtro. Isto implicava em uma redução no grau de liberdade do delicado alinhamento das cavidades, que no entanto era suplantado pelo uso de espelhos no alinhamento dos campos acoplados à cavidade.

Realizamos ainda uma mudança estrutural nas cavidades de análise, que passaram a ser feitas em anel. Em que pese o astigmatismo induzido por esta configuração, a perda de acordo de modo espacial ("mode matching") era muito pequena, e a eficiência de acoplamento permanecia superior a 98%.

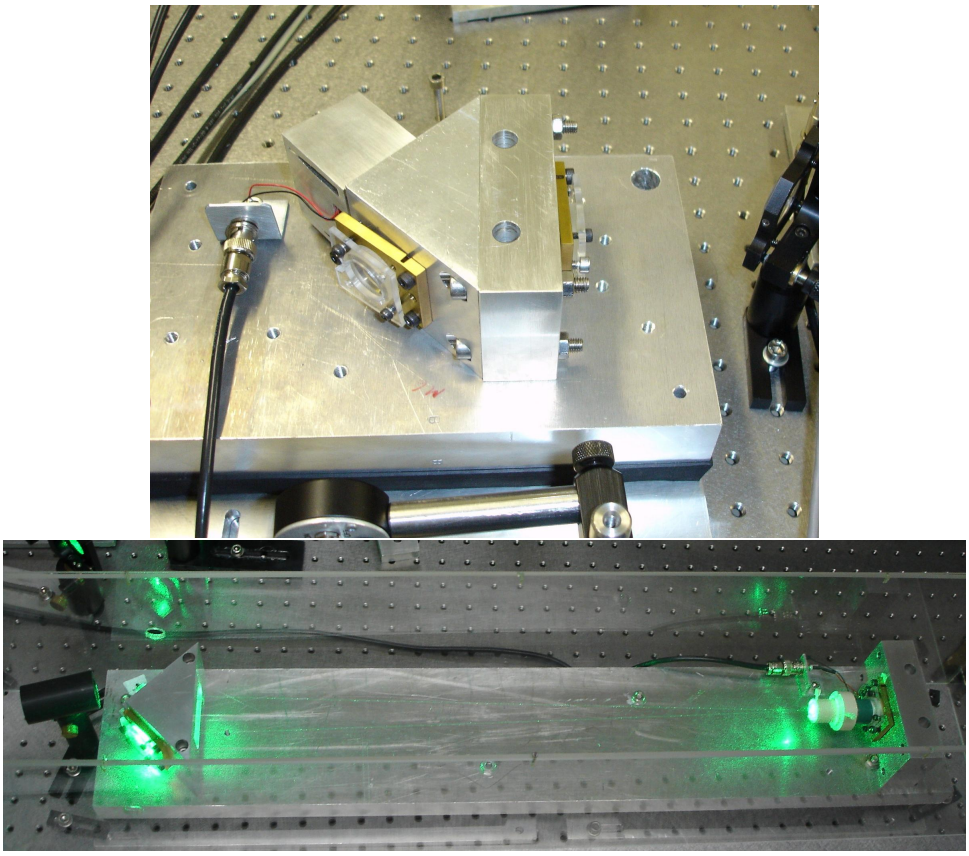

Figura 2.3: Montagem das cavidades de análise (acima) e filtro (abaixo).

As cavidades, feitas em alumínio, tinham a vantagem de empregar um material barato disponível no mercado interno, contrariamente às barras de Invar, importadas. Estas, por sua vez, além de limitarem o desenho da estrutura ao trabalho com barras cilíndricas, por conta da difícil usinagem, tem sua importação virtualmente impossível no nosso sistema atual [1]. Outra medida importante foi o fato destas ficarem montadas em unidades fechadas, reduzindo o acúmulo de poeira sobre a face dos espelhos. Quanto à dilatação térmica, esta revelou-se notável no processo de medida. No entanto, não impedia a realização da varredura simultânea das ressonâncias para dois campos, e a aquisição ocorria quanto os picos se apresentavam em coincidência. Já a cavidade de bombeio, de comprimento de cerca de 50 cm, permanecia estável por cerca de uma hora nos período de temperatura mais estável do dia (final da tarde, e alta madrugada).

[1] Caras demais para compra via cartão de crédito, pesadas demais para envio por courrier, baratas demais para que um fornecedor no meio dos Estados Unidos se disponha a todo o trâmite burocrático de uma importação regular pelas agências de fomento, enquanto ele pode vender com cartão para qualquer um na América do Norte.

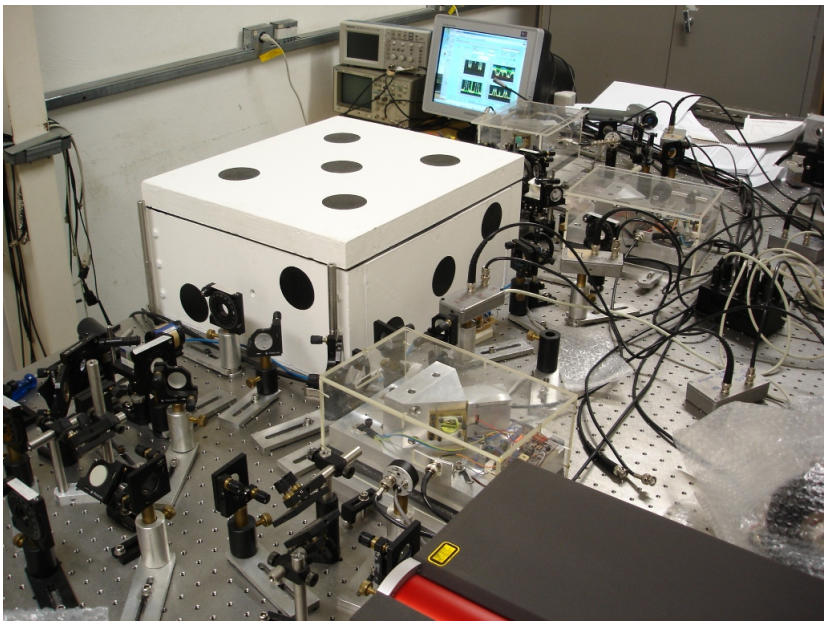

Figura 2.4: Montagem com o isolamento acústico instalado, mostrando ainda as cavidades de análise.

A medida tornou-se, portanto, possível. No entanto, as primeiras tentativas foram frustradas. Esperava-se que o sistema, com a filtragem empregada no bombeio, estivesse protegido de qualquer fonte de ruído do laser. As medidas mostravam imediatamente uma correlação de intensidade que correspondia a uma compressão de ruído de 50 %, mas para a fase, o nível de ruído permanecia muito alto, e a correlação insuficiente.

Notou-se, no entanto, que ao se aproximar do limiar de oscilação, a variância da soma das fase diminuía, consistente com o comportamento esperado pela teoria (ainda que o valor numérico estivesse em desacordo com ela). A solução foi se aproximar mais do limiar de oscilação. O problema é que se o OPO estava bem estável em sua operação com o bombeio 50 % acima do limiar de oscilação, manter o mesmo a meros 10 % tornava-se um desafio. Os ruídos acústicos do ambiente afetavam demais as medidas. A solução passou por construir um isolamento acústico de madeira com fibro-cimento, o que ajudou, sem dúvida, mas também por fazer as medidas quando o edifício estivesse vazio, e quando convencêssemos os vizinhos a desligarem os equipamentos de ar-condicionado desnecessários (aqueles não ligados a sistemas de informática).

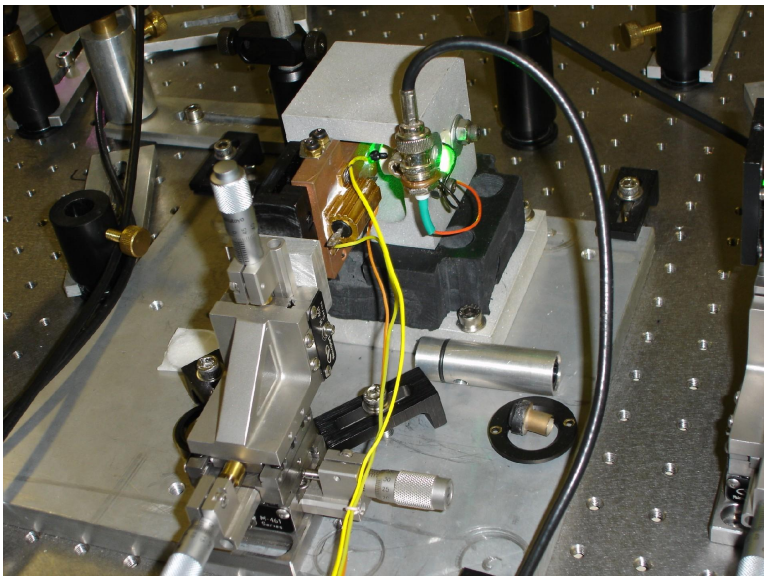

Figura 2.5: Detalhe da cavidade do OPO

As medidas forma feitas por Alessandro Villar, com a ajuda de Luciano Soares da Cruz e Katiúscia Nadyne Cassemiro. Após os primeiros resultados, obtivemos a violação do critério DGCZ para o emaranhamento bipartite, submetendo o artigo à publicação. No entanto, um dos "referees" não estava satisfeito se o critério EPR não fosse ainda violado. Fora mostrado anteriormente que este critério é falho, no sentido de que ele não demonstra o emaranhamento de diversos estados emaranhados [33]. Aceitamos porém o desafio, e repetimos o experimento ainda mais próximo ao limiar de oscilação, apenas 5% acima deste. O resultado aumentou a violação do critério DGCZ, e ficou compatível com o critério EPR.

Generation of Bright Two-Color Continuous Variable Entanglement

A. S. Villar, L. S. Cruz, K. N. Cassemiro, M. Martinelli, and P. Nussenzveig*

Instituto de Física, Universidade de São Paulo, Caixa Postal 66318, 05315-970 São Paulo, São Paulo, Brazil

(Received 16 June 2005; revised manuscript received 16 September 2005; published 9 December 2005)

We present the first measurement of squeezed-state entanglement between the twin beams produced in an optical parametric oscillator operating above threshold. In addition to the usual squeezing in the intensity difference between the twin beams, we have measured squeezing in the sum of phase quadratures. Our scheme enables us to measure such phase anticorrelations between fields of different frequencies. In the present measurements, wavelengths differ by ≈ 1 nm. Entanglement is demonstrated according to the Duan *et al.* criterion [Phys. Rev. Lett. **84**, 2722 (2000)] $\Delta^2\hat{p}_- + \Delta^2\hat{q}_+ = 1.41(2) < 2$. This experiment opens the way for new potential applications such as the transfer of quantum information between different parts of the electromagnetic spectrum.

DOI: 10.1103/PhysRevLett.95.243603 PACS numbers: 42.50.Dv, 03.67.Mn, 42.65.Yj

The field of quantum information has recently attracted great interest, owing to potential applications in information storage, communication, and computing [1]. Entanglement is viewed as a key resource for these applications, especially for quantum communication. A variety of physical systems presenting entanglement have been investigated both theoretically and experimentally. The vast majority of experiments concentrate on discrete variable systems, such as trapped ions [2], few photon electromagnetic fields in cavity QED [3], spontaneous parametric down-conversion [4], and nuclear magnetic resonance [5]. On the other hand, in recent experiments, continuous variable systems have been studied, including light beams [6–9] and atomic samples [10]. The number of such experiments, however, is still relatively small in comparison with discrete variable systems.

The first experimental demonstration of continuous variable entanglement used a continuous-wave (CW) optical parametric oscillator (OPO) operating below threshold [6]. The two squeezed vacuum outputs were shown to possess Einstein Podolsky Rosen (EPR) type correlations. Most recent experiments use a nonlinear interaction to produce squeezed fields, which are then combined in a beam splitter to generate entanglement [11]. Conversely, a beam splitter transformation can also be used to generate a squeezed beam from an entangled input [12]. In these experiments, it is mandatory to have fields of the same frequency.

In this Letter, we present the first (to our knowledge) measurement of continuous variable entanglement between bright fields of truly different frequencies. Even before the first experiment [6], it was predicted that the above-threshold OPO should produce entangled twin beams [13]. So far, this prediction had not yet been verified, owing to the difficulty of measuring phase properties of the twin beams. We have succeeded in measuring quantum anticorrelations between the phase quadratures of nondegenerate twin beams.

Bipartite continuous variable entanglement [14] can be tested according to a criterion established by Duan *et al.* [15] and also by Simon [16]. The criterion is based on the total variance of EPR-type operators. For operators $\hat{x}_i$ and $\hat{p}_i$ that obey position-momentum commutation relations, they consider the variances of combinations such as $\hat{x}_1 + \hat{x}_2$ and $\hat{p}_1$-$\hat{p}_2$. The quadratures of electromagnetic fields satisfy such commutation relations. We focus here on the so-called amplitude $\hat{p}$ and phase $\hat{q}$ field quadratures, defined by

$$\hat{a} = \frac{e^{i\phi}}{2}(\hat{p} + i\hat{q}), \tag{1}$$

where $\hat{a}$ is the field annihilation operator, ϕ is an arbitrary phase, and, for a macroscopic field with a well-defined mean amplitude, $\langle\hat{q}\rangle = 0$. In terms of these operators, inseparability (entanglement) is demonstrated by a violation of the inequality:

$$\Delta^2\left(\frac{\hat{p}_1 - \hat{p}_2}{\sqrt{2}}\right) + \Delta^2\left(\frac{\hat{q}_1 + \hat{q}_2}{\sqrt{2}}\right) \geq 2, \tag{2}$$

where the standard quantum level (SQL) is normalized to 1 for each combination of quadratures. In order to simplify notation, we refer to $(\hat{p}_1 \pm \hat{p}_2)/\sqrt{2}$ as $\hat{p}_\pm$ and to $(\hat{q}_1 \pm \hat{q}_2)/\sqrt{2}$ as $\hat{q}_\pm$. If both $\hat{p}_-$ and $\hat{q}_+$ are squeezed [$\Delta^2\hat{p}_- < 1$ and $\Delta^2\hat{q}_+ < 1$], inequality (2) is violated and we have squeezed-state entanglement.

It is easy to understand why entanglement is expected in the CW OPO operating above threshold. The OPO consists of a $\chi^{(2)}$ nonlinear crystal inside a resonant cavity, in which parametric down-conversion takes place. The cavity feeds back the down-converted fields, leading to stimulated parametric gain and hence to an oscillation threshold. Since the primary down-conversion process involves creating pairs of photons by annihilation of pump photons, one naturally expects strong correlations between the intensities of the twin beams: positive intensity fluctuations of one beam correspond to positive intensity fluctuations of the other beam. These correlations, however, are frequency dependent. For power spectrum analysis frequencies larger than

the OPO cavity bandwidth, correlations tend to disappear since, for times shorter than the cavity lifetime, a photon can exit the cavity while its "twin" still remains inside. Squeezing in the intensity difference was already observed back in 1987 [17]. On the other hand, energy conservation ($\omega_0 = \omega_1 + \omega_2$, where indices 0, 1, and 2 refer to pump, signal, and idler beams, respectively) and phase matching imply strong anticorrelations between phase fluctuations: positive phase fluctuations of one beam correspond to negative phase fluctuations of its "twin." This is exactly the situation discussed following (2): entanglement occurs if these (anti)correlations lead to fluctuations below the SQL. However, squeezing in the phase sum had not been measured to date.

The first prediction of entanglement in the above-threshold OPO was made by Reid and Drummond [13]. A recent detailed prediction, taking into account the effects of pump noise and cavity detunings for the three fields, for a triply resonant OPO, was presented in [18]. The basic difficulty in measuring (phase) quadrature fluctuations, in contrast with intensity fluctuations, is that the standard technique, homodyne detection, calls for a local oscillator having a well-defined phase relationship with the field to be measured. In the OPO, this is difficult to implement, since the frequencies of the twin beams are usually different, depending on the oscillating modes, and vary from one realization to the next. Hence, two local oscillators would be required: one for each beam. It would also be necessary to phase lock these fields to the twin beams.

One way to overcome this difficulty is to force the OPO to oscillate in a strictly frequency-degenerate situation. This is technically challenging and has been done by two groups, using different approaches [19,20]. Our strategy is to perform self-homodyne measurements, without the use of local oscillators, by a frequency-dependent reflection of each beam [21]. If one considers the field as a mean value at a carrier frequency with noise sidebands at some analysis frequency, a frequency-dependent reflectivity entails different phase shifts for the carrier and sidebands. Consequently, different quadrature fluctuations can be projected onto amplitude fluctuations (with respect to the phase of the mean field). A detailed description for a single field reflected off an optical cavity was given by Galatola *et al.* [22]. For an imperfect cavity, in which vacuum leaks from the outside through the mirrors, the reflected beam amplitude noise power spectrum $S_R(\Omega)$ can be written as [18]

$$S_R(\Omega) = |g_p|^2 S_p(\Omega) + |g_q|^2 S_q(\Omega) + |g_{vp}|^2 + |g_{vq}|^2, \tag{3}$$

where $S_p(\Omega)$ and $S_q(\Omega)$ are the incident beam amplitude and phase noise, respectively, and g_p, g_q, g_{vp}, and g_{vq} are coefficients that depend on cavity reflection and transmission coefficients through the relations:

$$\begin{aligned} g_p &= \frac{1}{2}\left[\frac{r^*(\Delta)}{|r(\Delta)|} r(\Delta+\Omega) + \frac{r(\Delta)}{|r(\Delta)|} r^*(\Delta-\Omega)\right], \\ g_q &= \frac{1}{2}\left[\frac{r^*(\Delta)}{|r(\Delta)|} r(\Delta+\Omega) - \frac{r(\Delta)}{|r(\Delta)|} r^*(\Delta-\Omega)\right], \\ g_{vp} &= \frac{1}{2}\left[\frac{t^*(\Delta)}{|t(\Delta)|} t(\Delta+\Omega) + \frac{t(\Delta)}{|t(\Delta)|} t^*(\Delta-\Omega)\right], \\ g_{vq} &= \frac{1}{2}\left[\frac{t^*(\Delta)}{|t(\Delta)|} t(\Delta+\Omega) - \frac{t(\Delta)}{|t(\Delta)|} t^*(\Delta-\Omega)\right]. \end{aligned} \tag{4}$$

Amplitude reflection $r(\Delta)$ and transmission $t(\Delta)$ coefficients can be simply written as

$$\begin{aligned} r(\Delta) &= \frac{r_1 - r_2 \exp(i\Delta/\delta\nu_{\rm ac})}{1 - r_1 r_2 \exp(i\Delta/\delta\nu_{\rm ac})}, \\ t(\Delta) &= \frac{t_1 t_2 \exp(i\Delta/\delta\nu_{\rm ac})}{1 - r_1 r_2 \exp(i\Delta/\delta\nu_{\rm ac})}, \end{aligned} \tag{5}$$

where Δ is the detuning between the incident field central frequency and the cavity resonance frequency, $\delta\nu_{\rm ac}$ is the cavity bandwidth (FWHM), and Ω is the analysis frequency. Cavity input mirror amplitude reflection and transmission coefficients are denoted by r_1 and t_1, while t_2 is defined so that all internal losses A obey the relation $t_2^2 = A = 1 - r_2^2$.

For analysis frequencies larger than $\sqrt{2}\delta\nu_{\rm ac}$, it is possible to completely convert incident phase fluctuations into amplitude fluctuations of the reflected beam. As a matter of fact, if this condition is satisfied, then, for $\Delta = \pm\delta\nu_{\rm ac}/2$, $|g_q|^2 \approx 1$ and incident phase fluctuations are projected onto amplitude fluctuations of the reflected beam. For $\Delta = 0$ and for $|\Delta| \gg \delta\nu_{\rm ac}$, then $|g_p|^2 \approx 1$ and we recover amplitude fluctuations. We use one analysis cavity for each beam and scan their frequencies synchronously. In this way, we are always measuring the same quadrature for each field, with respect to its mean value, regardless of the frequency difference between the fields.

Our experiment is performed with a triply resonant CW OPO operating above threshold [23]. The pump laser is an ultrastable diode-pumped frequency-doubled Nd:YAG source (Innolight Diabolo) at 532 nm, with a second output beam at 1064 nm, which we use for alignment purposes. The nonlinear crystal is a 12 mm long type-II High Gray Tracking Resistant Potassium Titanyl Phosphate (KTP) from Raicol. Crystal temperature is kept near 24 °C, with a stability of the order of 10 mK, by means of a peltier element. The cavity is a quasiconfocal linear Fabry-Perot cavity, with input mirror reflectivities equal to 89% at 532 nm and greater than 99.8% at 1064 nm. Output mirror reflectivities are greater than 99.8% at 532 nm and 95% at 1064 nm. The typical threshold power is 60 mW, and the OPO cavity bandwidth is $\delta\nu_{\rm OPO} = 53(3)$ MHz. Noise in the difference of signal and idler intensities has a stable value $\Delta^2\hat{p}_- = 0.59(1)$ registered by the photodetectors, or $-2.30(5)$ dB. According to [18], $\Delta^2\hat{q}_+$ is significantly

affected by pump excess phase noise. Our laser presented excess noise up to 25 MHz, which we had to filter by transmission through a ring cavity, with a bandwidth $\delta\nu_f = 2.3(1)$ MHz. In this way, the pump beam was shot-noise limited for frequencies above 15 MHz.

The experimental setup is sketched in Fig. 1. The pump beam at 532 nm is sent through the filter cavity and then mode matched to the OPO cavity. The orthogonally polarized twin beams produced, with powers of the order of a few milliwatts each, are separated by a polarizing beam splitter (PBS) cube and each directed to a tunable ring analysis cavity. For our working crystal temperature, wavelengths of signal and idler beams can differ by 0.8 to 0.9 nm. Analysis cavity bandwidths are $\delta\nu_{ac} = 14(1)$ MHz. The reflected field is detected by a high quantum efficiency [95(3)%] photodiode (Epitaxx ETX 300). The photocurrent is preamplified and the dc and high frequency (HF) components separated. The HF components are sent to a demodulating chain, where they are mixed with a sinusoidal reference at the analysis frequency $\Omega = 27$ MHz (with a filter bandwidth of 600 kHz). As the analysis cavities' resonances are swept over time, variances of each individual noise component, of their sum, and of their difference are calculated. The number N of points used, which is proportional to the acquisition time, is large enough to guarantee a well-defined variance and small enough to correspond to a very small change in cavities' detuning (this is equivalent to a low-pass filter of 1 kHz for the power spectrum).

Sum and difference noise spectra recorded as functions of the synchronous analysis cavity frequency scans are presented in Fig. 2. A scan over $\pm 3.2\delta\nu_{ac}$ is presented in Fig. 2(a). From the sum and difference spectra, one can easily notice that the quadrature being measured on each beam alternates between amplitude and phase. In particular, we recognize the amplitude quadrature behavior for detunings $|\Delta| \geq 3\delta\nu_{ac}$ (carrier frequency and noise sidebands unaffected by cavity resonance) and for $\Delta = 0$ (carrier frequency gains a π phase shift with respect to sidebands). One observes that $\Delta^2\hat{p}_-$ at $\Delta = 0$ does not recover the squeezing observed for $|\Delta| \geq 3\delta\nu_{ac}$, owing to a lack of experimental resolution (few data points are obtained at any particular detuning). Phase quadrature is measured for $|\Delta| = 0.5\delta\nu_{ac}$ (carrier frequency gains a $\pi/2$ phase shift with respect to sidebands) and, for the particular choice of analysis frequency we use, also at $|\Delta| = 1.8\delta\nu_{ac}$ (one sideband gains a π phase shift relative to carrier frequency and to the other sideband). For all other detunings we measure a linear combination of amplitude and phase quadratures. In Fig. 2(b), we present a scan with increased resolution, over only $\pm 1\delta\nu_{ac}$. Phase-sum squeezing is observed, with $\Delta^2\hat{q}_+ = 0.82(2)$. These spectra are individual scans and are representative of the best data obtained.

The solid curves in Figs. 2(a) and 2(b) are given by fits of Eq. (3) to the data. Apart from scale factors and curve central position, the relevant free parameters are the combined quadrature fluctuations $\Delta^2\hat{p}_+$, $\Delta^2\hat{p}_-$, $\Delta^2\hat{q}_+$, and $\Delta^2\hat{q}_-$. All other variables required in Eq. (3), such as

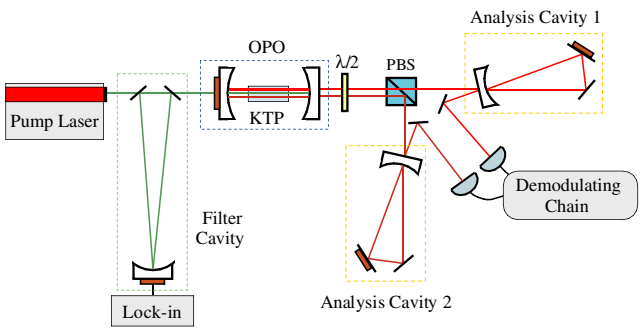

FIG. 1 (color online). Sketch of the experimental setup (details explained in the text).

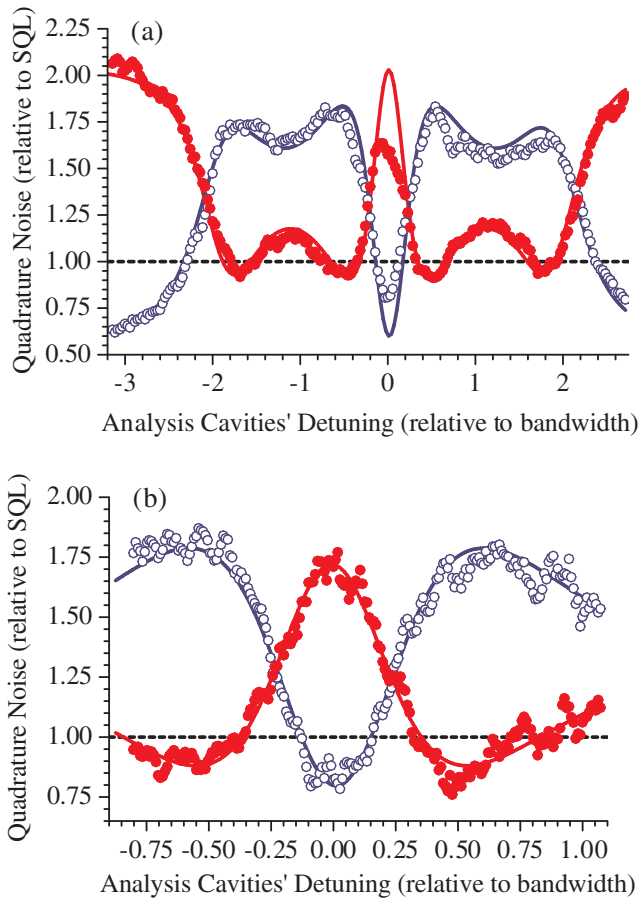

FIG. 2 (color online). Measurements of sum (full circles) and difference (open circles) of quadrature fluctuations as functions of analysis cavities' detunings. In (a) the detuning spans the range $\pm 3.2\delta\nu_{ac}$. In (b) an increased resolution scan is presented, in which we clearly observe $\Delta^2\hat{p}_- < 1$ for $\Delta = 0$ and $\Delta^2\hat{q}_+ < 1$ for $|\Delta| = 0.5\delta\nu_{ac}$, characterizing squeezed-state entanglement. The solid curves are given by fits of Eq. (3) to the data.

cavity bandwidth and analysis frequency, are independently measured and employed as constants in the fitting, which is done either for the sum or for the difference in each part of Fig. 2, with equally good results.

The phase noise is strongly dependent on pump power relative to threshold. At 1.5 times the threshold power, we observed large excess noise in the phase sum, as was also found in [20]. This excess noise is not predicted by the standard OPO linearized theory [13], and it is still not clear whether a full quantum theory [24] can account for it. Although the calculations in [18] are carried out with the linearized theory, they provided us with a useful indication: squeezing in the phase sum improves as the system approaches the threshold. Consistently with this indication, we could only observe phase-sum squeezing for pump powers less than 7% above threshold. The best data shown in Fig. 2 were obtained approximately 4% above threshold. In this situation, the OPO is very unstable, hindering the measurements.

In terms of the entanglement criterion of Eq. (2), using $\Delta^2\hat{q}_+ = 0.82(2)$, we obtain $\Delta^2\hat{p}_- + \Delta^2\hat{q}_+ = 1.41(2) < 2$, a clear violation of the inequality, characterizing, for the first time, entanglement between bright beams of truly different frequencies. Equation (2) is a necessary and sufficient separability condition for Gaussian states, which are predicted for the OPO and are consistent with our data. Another, more stringent, entanglement criterion is the so-called EPR criterion, which enables one to infer variances on one beam, as functions of variances on the other beam [13]. This criterion implies a violation of the inequality $\Delta^2\hat{p}_{\rm inf}\Delta^2\hat{q}_{\rm inf} \geq 1$, where

$$\Delta^2\hat{p}_{\rm inf} = \Delta^2\hat{p}_1\left(1 - \frac{\langle\delta\hat{p}_1\delta\hat{p}_2\rangle^2}{\Delta^2\hat{p}_1\Delta^2\hat{p}_2}\right), \tag{6}$$

with $\delta\hat{p}_i = \hat{p}_i - \langle\hat{p}_i\rangle$. An analogous relation holds for $\Delta^2\hat{q}_{\rm inf}$. Our measured data give the value $\Delta^2\hat{p}_{\rm inf}\Delta^2\hat{q}_{\rm inf} = 0.95(-3/+6)$, which is compatible with the violation of this second criterion as well. We have losses from the output of the OPO to the detectors. If the overall detection efficiency is η, the measured variances are related to the "true" variances (e.g., $\Delta^2\hat{p}'$) by $\Delta^2\hat{p} = \eta(\Delta^2\hat{p}' - 1) + 1$. For $\eta = 80(2)\%$, we obtain $\Delta^2\hat{p}'_- + \Delta^2\hat{q}'_+ = 1.26(4)$ and $\Delta^2\hat{p}'_{\rm inf}\Delta^2\hat{q}'_{\rm inf} = 0.77(-9/+11)$.

The entanglement generated in this system can be substantially improved. The intensity difference squeezing measured in [20] reached the impressive value of 9.7 dB, which would lead to even stronger violations of the above criteria. Furthermore, stable operation only a few percent above threshold is technically feasible, as shown in [19]. Hence, the above-threshold OPO can produce very high degrees of entanglement, at least comparable to the best results obtained below threshold [7,9].

In summary, we have demonstrated, for the first time, bright two-color squeezed-state continuous variable entanglement. Applications to quantum information, such as quantum key distribution [25] and quantum teleportation [26] with continuous variables, can easily be envisaged. Our measurement scheme has interesting properties for both. Quantum key distribution with squeezed-state entanglement usually requires sending the local oscillator, in addition to the entangled field, so as to enable homodyne measurements, a requirement that is not necessary in our case. Teleportation, on the other hand, has been restricted to fields of the same frequency. Two-color entanglement opens the way for distributing quantum information between different parts of the electromagnetic spectrum.

This work was funded by FAPESP, CAPES, and CNPq through Instituto do Milênio de Informação Quântica. We gratefully acknowledge very useful and stimulating discussions with Claude Fabre.

*Electronic address: nussen@if.usp.br

[1] M. A. Nielsen and I. L. Chuang, *Quantum Computation and Quantum Information* (Cambridge University Press, Cambridge, 2000).
[2] Q. A. Turchette *et al.*, Phys. Rev. Lett. **81**, 3631 (1998).
[3] E. Hagley *et al.*, Phys. Rev. Lett. **79**, 1 (1997).
[4] D. Bouwmeester *et al.*, Phys. Rev. Lett. **82**, 1345 (1999).
[5] N. Gershenfeld and I. L. Chuang, Science **275**, 350 (1997).
[6] Z. Y. Ou *et al.*, Phys. Rev. Lett. **68**, 3663 (1992).
[7] W. P. Bowen *et al.*, Phys. Rev. Lett. **90**, 043601 (2003).
[8] C. Schori, J. L. Sorensen, and E. S. Polzik, Phys. Rev. A **66**, 033802 (2002).
[9] X. Jia *et al.*, Phys. Rev. Lett. **93**, 250503 (2004).
[10] B. Julsgaard, A. Kozhekin, and E. S. Polzik, Nature (London) **413**, 400 (2001).
[11] Ch. Silberhorn *et al.*, Phys. Rev. Lett. **86**, 4267 (2001).
[12] Y. Zhang *et al.*, Phys. Rev. A **62**, 023813 (2000).
[13] M. D. Reid and P. D. Drummond, Phys. Rev. Lett. **60**, 2731 (1988); M. D. Reid and P. D. Drummond, Phys. Rev. A **40**, 4493 (1989).
[14] S. L. Braunstein and P. van Loock, Rev. Mod. Phys. **77**, 513 (2005).
[15] L.-M. Duan *et al.*, Phys. Rev. Lett. **84**, 2722 (2000).
[16] R. Simon, Phys. Rev. Lett. **84**, 2726 (2000).
[17] A. Heidmann *et al.*, Phys. Rev. Lett. **59**, 2555 (1987).
[18] A. S. Villar, M. Martinelli, and P. Nussenzveig, Opt. Commun. **242**, 551 (2004).
[19] S. Feng and O. Pfister, Phys. Rev. Lett. **92**, 203601 (2004).
[20] J. Laurat *et al.*, Opt. Lett. **30**, 1177 (2005).
[21] M. D. Levenson *et al.*, Phys. Rev. A **32**, 1550 (1985); R. M. Shelby *et al.*, Phys. Rev. Lett. **57**, 691 (1986).
[22] P. Galatola *et al.*, Opt. Commun. **85**, 95 (1991).
[23] M. Martinelli *et al.*, Braz. J. Phys. **31**, 597 (2001).
[24] P. D. Drummond, K. Dechoum, and S. Chaturvedi, Phys. Rev. A **65**, 033806 (2002).
[25] Ch. Silberhorn, N. Korolkova, and G. Leuchs, Phys. Rev. Lett. **88**, 167902 (2002).
[26] A. Furusawa *et al.*, Science **282**, 706 (1998).

A medida realizada pôs fim a uma busca de 18 anos, e tornou-se hoje uma referência obrigatória ao se falar de estados não-clássicos no OPO. Imediatamente após a divulgação dos resultados, recebemos as felicitações de Pfister e Fabre, concorrentes diretos, que conseguiram seus resultados pouco tempo depois [34, 35]. Além disso, descobrimos alguns meses mais tarde que o grupo de ótica quântica de Universidade de Shanxi conseguiu realizar uma medida semelhante, usando interferômetros Mach-Zender no lugar das cavidades Fabry-Perot [36].

A demonstração de emaranhamento bipartite entre feixes intensos, de frequências distintas, abre caminho para aplicações em teletransporte [37], e criptografia com variáveis contínuas [38]. Poderia ser o começo, então, de aplicações do sistema desenvolvido. No entanto, incomodava nele, para aplicações diretas, o emaranhamento tão próximo do limiar de oscilação. Por que esta limitação, não prevista em teoria? Passamos a este problema nos nossos próximos estudos.

Capítulo 3

Excesso de Ruído no OPO

Diante das discrepâncias entre o ruído esperado nos experimentos de emaranhamento bipartite contra a teoria, que até então teve um grande sucesso em medidas abaixo do limiar e na geração de feixes gêmeos, decidimos investigar a razão deste problema. Uma primeira hipótese fora alguma limitação na nossa capacidade de filtrar o ruído do bombeio. O problema seria externo ao OPO, e isto seria consistente com o que fora calculado anteriormente [31]. No entanto, como podemos ver no artigo a seguir (figura (3)), investigamos com cuidado o comportamento do feixe de bombeio, e verificamos que na frequência de análise o nível de ruído estava já bem baixo, indistinguível do ruído quântico padrão.

Resolvemos investigar o problema com mais cuidado, e divulgamos os resultados em um artigo no J. Opt. Soc. Am. B [8]. Neste artigo, mais longo, investigamos algumas hipóteses para o OPO, mudando inicialmente a cavidade para uma semi-monolítica (com um dos espelhos depositado na face do cristal) de forma a reduzir as perdas por reflexão nas interfaces ar/cristal. Além disso, o cristal usado, um KTP da Litton, apresenta uma absorção mais baixa, e uma menor sensibilidade ao "gray tracking". As investigações não foram conclusivas, mas permitiram descartar algumas hipóteses.

Inicialmente, consideramos a possibilidade de haver alguma limitação na teoria. O modelo usualmente empregado para a descrição do OPO, como podemos ver no apêndice, envolve a aproximação markoviana para obter a descrição da equação mestra, o descarte de termos de ordem cúbica na equação de evolução da representação de quase-probabilidade, e a linearização na equação de Langevin. Destas aproximações, a primeira é bem razoável, mas as duas seguintes poderiam envolver o descarte de propriedades importantes do OPO. Na análise subsequente da equação de Langevin, obtém-se um processo difusivo no espaço da subtração dos campos, o que leva a uma divergência para a variância do ruído da soma das fases para uma frequência de análise nula. Poderia esta divergência invalidar a aproximação linear que levou a esta equação? Por outro lado, a representação de Wigner descarta explicitamente os termos de derivada terceira, ausentes em outras representações. Seria este termo relevante em nosso caso?

Para resolver tais questões, contamos com a ajuda do Grupo de Óptica Quântica do IF/UFF, que vinha trabalhando com OPOs. O prof. Kaled Dechoum vem trabalhando especificamente no tema [39] em colaboração com o prof. Antônio Zelaquett Khoury [40], lidando com as simulações teóricas do sistema dentro da representação P-positiva. Nesta versão da representação P de Glauber-Sudarshan, o uso de um espaço dobrado de variáveis elimina o problema das singularidades da solução em representação P, ainda que a um custo de aumento do espaço de fases. As equações de Langevin não-lineares permitem o cálculo numérico da evolução temporal, das correlações entre instantes diferentes, e sua subsequente transformada de Fourier para cálculo do espectro de ruído. Paralelamente, foi feito o cálculo dentro da linearização destas equações. A comparação dos resultados da equação explícita com os calculados numericamente revelou uma excelente coincidência (discrepâncias inferiores a 10^{-3}, limitado pela resolução no cálculo numérico).

Esta concordância mostrou que a linearização é válida na situação usual de trabalho, com não-linearidades pequenas (ganho da ordem de 1% no cristal por passagem) e fora da transição do regime no limiar. Divergências, correlações de terceira ordem, perturbações, são esperadas próximo ao limiar de oscilação, mas para potências de bombeio diferindo do limiar por menos de 1%. Isto torna a observação de tais efeitos impraticável pelas técnicas atuais. Eles são muito sutis, ocorrendo em condições de operação insustentáveis.

A concordância da teoria linearizada implica em buscar a fonte de ruído em algum outro lugar. Por outro lado, o campo de bombeio é bem comportado, e seu ruído está limitado ao estado coerente (após medida nas duas quadraturas). Discutindo com o prof. Khoury, foi levantada a hipótese do ruído percebido ter origem intracavidade [41]. Decidimos neste caso investigar o ruído de saída no modo do bombeio. Os trabalhos anteriores envolvendo compressão de ruído [29] davam a impressão que este seria baixo. No entanto, ao verificar o mesmo com uma deteção balanceada (sensível, portanto, apenas às flutuações de intensidade), notamos um excesso de ruído. Espantados com o resultado, resolvemos fazer a medida abaixo do limiar de oscilação. O ruído no feixe refletido estava lá ainda (figura (4) do artigo, reproduzida a seguir). Note que neste caso, estávamos abaixo do limiar de oscilação, de forma que o ruído não poderia ser gerado pelo acoplamento não-linear do processo paramétrico. Na varredura lenta, a absorção do verde pelo OPO leva a uma biestabilidade de origem térmica. Portanto, temos o caso extremo de uma lorenztiana deformada, com um alongamento na parte com dessintonia negativa, e uma variação abrupta para dessintonia positiva, visível na curva da intensidade refletida. O que se observa é que, para a dessintonia de meia largua de banda, temos um pico no ruído, que cai rapidamente ao nos aproximarmos da dessintonia nula. Isto é compatível com um excesso de ruído de fase, e algum excesso de ruído de amplitude. Notamos ainda que este ruído variava linearmente conforme a potência de bombeio adicionada.

Este ruído de fase e amplitude proporcional à potência de bombeio, observado no modo de bombeio, não era previsto na teoria do OPO, porém podia ser facilmente modelado por um ruído constante, levando em consideração que, acima do limiar de oscilação, a potência intracavidade é constante. Este ruído fora adicionado ao bombeio no modelo desenvolvido em [31], e o resultado apresentou um bom acordo com os resultados experimentais.

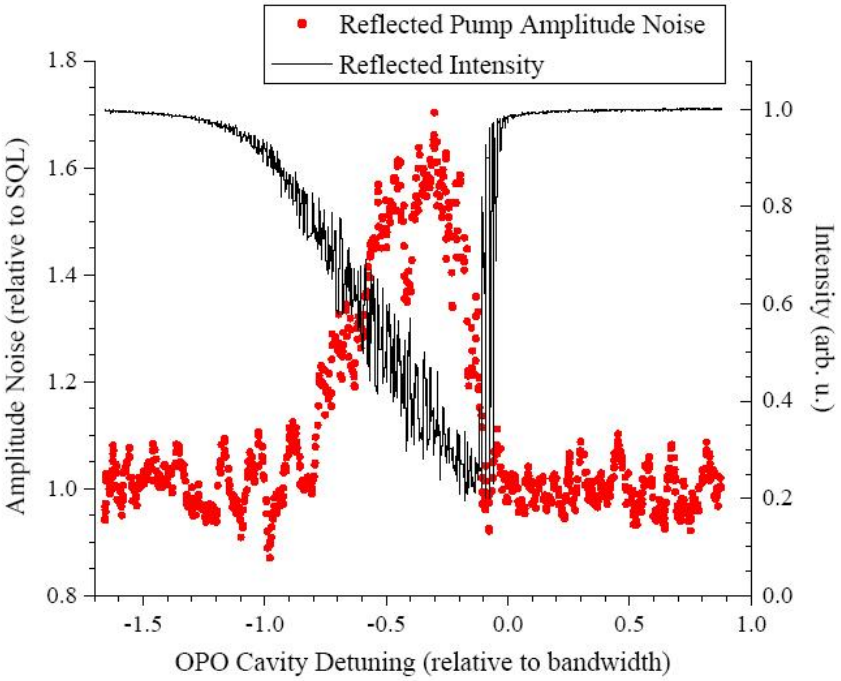

Figura 3.1: Excesso de ruído no campo de bombeio, abaixo do limiar de oscilação. Vemos o valor médio do campo refletido pela cavidade do OPO (reflected intensity), e sua variância (em unidades de "shot noise").

Conseguimos então uma das maiores violações da desigualdade de Duan [42] à época. Apesar de contentes com o resultado, saímos do trabalho com uma grande incógnita. Descobrimos que o ruído era gerado dentro do OPO, pelo cristal, por um processo independente do processo paramétrico. Mas não tínhamos ideia da origem deste. Outro dado importante: este excesso de ruído parecia afetar mais a fase do que a amplitude do campo intracavidade. Nossa hipótese era de que havia algo afetando o índice de refração, e isto dependia da intensidade do campo intracavidade. Uma modulação de terceira ordem, um efeito Kerr no meio? Sabe-se que tal processo gera uma compressão de ruído de intensidade, e um aumento de ruído de fase [27], que seria compatível com o efeito observado.

Estas questões, abertas em 2005, tomariam ainda mais quatro anos para serem resolvidas.

Entanglement in the above-threshold optical parametric oscillator

Alessandro S. Villar and Katiúscia N. Cassemiro

Instituto de Física, Universidade de São Paulo, Caixa Postal 66318, 05315-970 São Paulo, São Paulo, Brazil

Kaled Dechoum and Antonio Z. Khoury

Instituto de Física da Universidade Federal Fluminense, Boa Viagem, 24210-340, Niterói, Rio de Janeiro, Brazil

Marcelo Martinelli and Paulo Nussenzveig

Instituto de Física, Universidade de São Paulo, Caixa Postal 66318, 05315-970 São Paulo, São Paulo, Brazil

Received May 12, 2006; accepted June 27, 2006;
posted September 5, 2006 (Doc. ID 70938); published January 26, 2007

We investigate entanglement in the above-threshold optical parametric oscillator, both theoretically and experimentally, and discuss its potential applications to quantum information. The fluctuations measured in the subtraction of signal and idler amplitude quadratures are $\Delta^2\hat{p}_-=0.50(1)$, or $-3.01(9)$ dB, and in the sum of phase quadratures they are $\Delta^2\hat{q}_+=0.73(1)$, or $-1.37(6)$ dB. A detailed experimental study of the noise behavior as a function of pump power is presented, and the discrepancies with theory are discussed. © 2007 Optical Society of America

OCIS codes: 270.0270, 270.6570, 190.4970.

1. INTRODUCTION

The optical parametric oscillator (OPO) has been studied since the 1960s.[1,2] In the 1980s it was already recognized as an important tool in quantum optics for the generation of squeezed states of light.[3,4] It was also recognized as a suitable system for the demonstration of continuous variable (CV) entanglement in 1988 by Reid and Drummond[5] who considered the above-threshold operation. In the early 1990s, CV entanglement was indeed demonstrated for the first time in an OPO, although operating below threshold.[6] The OPO has since been used in several applications in CV quantum information.[7–11] Entanglement in the above-threshold OPO, on the other hand, remained an experimental challenge until 2005, when it was first observed by Villar *et al.*,[12] and subsequently by two other groups.[13,14]

Bipartite CV entanglement can be demonstrated by a violation of the following inequality, obtained independently by Duan *et al.*[15] and Simon:[16]

$$\Delta^2\hat{p}_- + \Delta^2\hat{q}_+ \geq 2, \tag{1}$$

where $\hat{p}_-=(\hat{p}_1-\hat{p}_2)/\sqrt{2}$ and $\hat{q}_+=(\hat{q}_1+\hat{q}_2)/\sqrt{2}$ are Einstein–Podolsky–Rosen (EPR) -type operators constructed by combining operators of each subsystem. We chose $\hat{p}_j$ and $\hat{q}_j, j\in\{0,1,2\}$, as the amplitude and phase quadrature operators of the pump, signal, and idler fields, respectively, which obey the commutation relations $[\hat{p}_j,\hat{q}_k]=2i\delta_{jk}$. Any separable system must satisfy Eq. (1); a violation is an unequivocal signature of entanglement.

Entanglement between the intense signal and idler beams generated by an above-threshold OPO can be physically understood as a consequence of energy conservation in the parametric process. On one hand, pump photons are converted into pairs of signal and idler photons, leading to strong intensity correlations; on the other hand, the sum of the frequencies of signal and idler photons is fixed to the value of pump frequency, leading to phase anticorrelations. The difficulty of measuring phase fluctuations was largely responsible for the long time between the prediction and the first observation of entanglement in the above-threshold OPO. The technique we used to measure phase fluctuations consists of reflecting each field off an empty optical cavity, as explained in Ref. 17.

The value of Eq. (1) obtained in the first demonstration of entanglement was 1.41(2), with squeezing observed in both EPR-type operators, $\Delta^2\hat{p}_-=0.59(1)$ and $\Delta^2\hat{q}_+=0.82(2)$.[12] Nevertheless, such a result could be achieved only very close to threshold, otherwise the phase sum $\Delta^2\hat{q}_+$ would present excess noise, increasing with pump power relative to the threshold $\sigma=P_0/P_{\text{th}}$. This strange behavior, also observed by other groups,[18] is not predicted by the standard linearized OPO theory for a shot-noise limited pump beam. According to this model, entanglement should exist for all values of σ, although the degree of entanglement should decrease for increasing σ. This presented an additional complication for the first demonstration of entanglement in the above-threshold OPO.

In this paper we present new improved results of entanglement in the above-threshold OPO, together with a theoretical and experimental study of this unexpected excess phase sum noise. The paper is organized as follows. We begin by describing the linearized model for the OPO and its predictions for a shot-noise limited pump beam.

This model includes losses and also allows for nonvanishing detunings of pump, signal, and idler modes with respect to the OPO cavity. We then present a full-quantum treatment, neglecting losses and for zero detunings. Even after eliminating the linearization approximation, the theory does not predict the observed excess noise. The experiment is described next, and we present the measurements of the sum and difference of the quadrature fluctuations as a function of σ. As we will see, the excess noise in the phase sum can be related to pump noise generated inside the OPO cavity. Finally we present our current best measurement of two-color squeezed-state entanglement. We conclude by mentioning applications of this entanglement in quantum information.

2. THEORETICAL DESCRIPTION OF THE OPTICAL PARAMETRIC OSCILLATOR

The OPO consists of three modes of the electromagnetic field coupled by a nonlinear crystal, which is held inside an optical cavity. The OPO is driven by an incident pump field at frequency ω_0. Following the usual terminology, the downconverted fields are called the signal and the idler of frequencies ω_1 and ω_2, where, by energy conservation $\omega_0 = \omega_1 + \omega_2$. Here we will treat the case of a cavity that is triply resonant for ω_0, ω_1, and ω_2. Each field is damped via the cavity output mirror, thereby interacting with reservoir fields. The effective second-order nonlinearity of the crystal is represented by the constant χ.

Reid and Drummond investigated the correlations in the nondegenerate OPO (NOPO) both above[19] and below threshold.[20] In the above-threshold case, they studied the effects of phase diffusion in the signal and idler modes, beginning with the positive P-representation equations of motion for the interacting fields.[21,22] Changing to intensity and phase variables, they were able to show that output quadratures could be chosen that exhibited fluctuations below the coherent state level and also EPR-type correlations. In the below-threshold case, a standard linearized calculation was sufficient to obtain similar correlations. In the limit of a rapidly decaying pump mode, Kheruntsyan and Petrosyan were able to calculate the exact steady-state Wigner function for the NOPO, showing clearly the threshold behavior and the phase diffusion above this level of pumping.[23] We begin by describing the linearized model, and then proceed to calculate the noise spectra beyond linearization.

A. Linearized Model

The equations describing the evolution of signal, idler, and pump amplitudes, α_j, inside the triply resonant OPO cavity are given below.[17] They are obtained by writing the density operator equation of motion in the Wigner representation, and then searching for a set of equivalent Langevin equations,

$$\tau\frac{\mathrm{d}}{\mathrm{d}t}\alpha_0 = -\gamma_0'(1-i\Delta_0)\alpha_0 - 2\chi^*\alpha_1\alpha_2 + \sqrt{2\gamma_0}\alpha_0^{\mathrm{in}} + \sqrt{2\mu_0}\delta v_0,$$

$$\tau\frac{\mathrm{d}}{\mathrm{d}t}\alpha_1 = -\gamma'(1-i\Delta)\alpha_1 + 2\chi\alpha_0\alpha_2^* + \sqrt{2\gamma}\delta u_1 + \sqrt{2\mu}\delta v_1,$$

$$\tau\frac{\mathrm{d}}{\mathrm{d}t}\alpha_2 = -\gamma'(1-i\Delta)\alpha_2 + 2\chi\alpha_0\alpha_1^* + \sqrt{2\gamma}\delta u_2 + \sqrt{2\mu}\delta v_2, \tag{2}$$

where γ and γ_0 are half the transmissions of the mirrors, γ' and γ_0' are the total intracavity losses, $\mu = \gamma' - \gamma$ and $\mu_0 = \gamma_0' - \gamma_0$ are the spurious intracavity losses, Δ and Δ_0 are the detunings of the OPO cavity relative to the central frequencies of the fields, and τ is the cavity roundtrip time. We have considered here that $\gamma_1 = \gamma_2 = \gamma$ and $\gamma_1' = \gamma_2' = \gamma'$. The parameter χ is the effective second-order nonlinearity. The terms δu_j and δv_j are vacuum fluctuations associated to the losses from transmissions from the mirrors and from spurious sources, respectively. In the case of the intracavity pump mode, the fluctuations that come from the mirror transmission are attributable to the quantum fluctuations of the input pump laser beam, $\delta\alpha_0^{\mathrm{in}} = \delta p_0^{\mathrm{in}} + i\delta q_0^{\mathrm{in}}$.

Linearization consists in writing $\alpha_j(t) = e^{i\phi_j}(p_j + \delta p_j(t) + i\delta q_j(t))$ and ignoring terms that involve products of fluctuations in the equations. Here $\langle\alpha_j\rangle = p_j e^{i\phi_j}$ is each field's mean amplitude, with $p_1 = p_2 \equiv p$ for equal overall intracavity losses in the signal and the idler, $\delta p_j(t)$ is the amplitude fluctuation, and $\delta q_j(t)$ is the phase fluctuation. Taking the average of the resulting equations gives us information on the mean values of the fields. We may then separate the fluctuating part in the real and imaginary contributions to obtain the equations of evolution for the quadratures of the fields. Defining $\delta q_\pm = (\delta q_1 \pm \delta q_2)/\sqrt{2}$ and $\delta p_\pm = (\delta p_1 \pm \delta p_2)/\sqrt{2}$ as the normalized sum–subtraction of the signal and the idler amplitude and phase quadratures, we write the above equations in terms of the EPR variables:

$$\tau\frac{\mathrm{d}}{\mathrm{d}t}\delta p_- = -2\gamma'\delta p_- + \sqrt{2\gamma}\delta u_{p_-} + \sqrt{2\mu}\delta v_{p_-},$$

$$\tau\frac{\mathrm{d}}{\mathrm{d}t}\delta q_- = 2\Delta\gamma'\delta p_- + \sqrt{2\gamma}\delta u_{q_-} + \sqrt{2\mu}\delta v_{q_-},$$

$$\tau\frac{\mathrm{d}}{\mathrm{d}t}\delta p_+ = -2\Delta\gamma'\delta q_+ + \sqrt{2}\gamma'\beta\delta p_0 + \sqrt{2}\Delta\gamma'\beta\delta q_0 + \sqrt{2\gamma}\delta u_{p_+} + \sqrt{2\mu}\delta v_{p_+},$$

$$\tau\frac{\mathrm{d}}{\mathrm{d}t}\delta q_+ = -2\gamma'\delta q_+ - \sqrt{2}\Delta\gamma'\beta\delta p_0 + \sqrt{2}\gamma'\beta\delta q_0 + \sqrt{2\gamma}\delta u_{q_+} + \sqrt{2\mu}\delta v_{q_+},$$

$$\tau\frac{\mathrm{d}}{\mathrm{d}t}\delta p_0 = -\sqrt{2}\gamma'\beta\delta p_+ + \sqrt{2}\Delta\gamma'\beta\delta q_+ - \gamma_0'\delta p_0 - \Delta_0\gamma_0'\delta q_0 + \sqrt{2\gamma_0}\delta p_0^{in} + \sqrt{2\mu_0}\delta v_{p_0},$$

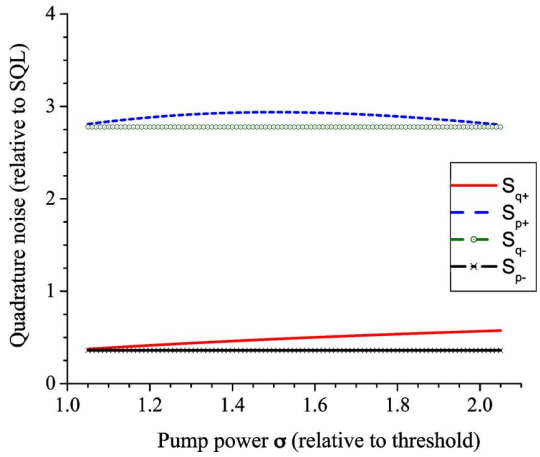

Fig. 1. (Color online) Prediction of the linearized theory for fluctuation in the sum–subtraction of field quadratures as a function of σ for a shot-noise limited pump beam. Solid line, S_{q_+}; dashed curve, S_{p_+}; line with crosses, S_{p_-}; line with circles, S_{q_-}.

$$\tau\frac{\mathrm{d}}{\mathrm{d}t}\delta q_0 = -\sqrt{2}\Delta\gamma'\beta\delta p_+ - \sqrt{2}\gamma'\beta\delta q_+ + \Delta_0\gamma_0'\delta p_0 - \gamma_0'\delta q_0 + \sqrt{2\gamma_0}\delta q_0^{in} + \sqrt{2\mu_0}\delta v_{q_0}, \tag{3}$$

where $\beta = p/p_0$ is the ratio between the intracavity amplitudes of the downconverted and the pump fields. The noise spectra of the transmitted fields are calculated by solving the above equations in Fourier space. We define $S_{p\pm}$ and $S_{q\pm}$ as the noise spectra of the operators $\hat{p}_\pm$ and $\hat{q}_\pm$, respectively.

It is clear from Eq. (3) that the quadrature subtraction subspace decouples from the others, so that S_{q_-} and S_{p_-} depend only on the ratio of losses through the output cavity mirror to the total intracavity losses and on the analysis frequency Ω. These fluctuations do not depend on pump power, and are in a minimum uncertainty state, $S_{p_-}\times S_{q_-}=1$, if $\gamma=\gamma'$.

On the other hand, the sum of the quadratures and pump field subspaces are connected. This directly implies that excess noise in the pump beam degrades signal–idler entanglement, and can even destroy it.[17] The behavior of the twin beams' fluctuations as functions of pump power relative to threshold σ, for a shot-noise limited pump, is presented in Fig. 1. The maximum squeezing of S_{q+} occurs at threshold, and approaches shot noise for higher pump powers.

This behavior changes in the presence of excess noise in the pump. In that case, both S_{q+} and S_{p+} increase from their values at threshold. In particular, S_{q+} goes from squeezing to excess noise. The point where it crosses the shot noise value depends solely on the amount of excess phase noise present in the pump beam. For this reason, it was necessary to filter the pump field in the experiment, in order to observe entanglement.

B. Noise Spectra beyond the Linearized Model

We present here a comparison between the linearized approach to the quantum noise in the OPO and the numerical integration of the quantum stochastic equations in the positive P representation. This will help us to eliminate the linearization procedure as the reason for the discrepancy between the theoretical prediction of squeezing and the experimentally observed excess phase noise for $\sigma > 1.2$. We shall follow the procedure used in Ref. 24.

Although exact Heisenberg equations of motion can be found for this system, it is, at the very least, extremely difficult to solve nonlinear operator equations. Therefore we develop stochastic equations of motion in the positive P representation, which in principle give access to any normally ordered operator expectation values we may wish to calculate. To find the appropriate equations, we proceed via the master and Fokker–Planck equations. Using the standard techniques for elimination of the baths,[25] we find the zero-temperature master equation for the reduced density operator. The master equation may be mapped onto a Fokker–Planck equation[26] for the positive-P pseudoprobability distribution.

The cavity damping rates at each frequency are $\gamma^D = 2\gamma/\tau$, with $\gamma_1=\gamma_2=\gamma$. We further define $\gamma_r=\gamma_0/\gamma$. To apply the perturbation theory, we introduce a normalized coupling constant

$$g = \frac{\chi}{\gamma^D\sqrt{2\gamma_r}}, \tag{4}$$

which will be a power expansion parameter. Moreover, it will be useful to work with the scaled quadratures

$$\begin{aligned} x_0 &= g\sqrt{2\gamma_r}p_0, & q_0 &= g\sqrt{2\gamma_r}q_0,\\ x_+ &= gp_+, & y_+ &= gq_+,\\ x_- &= gp_-, & y_- &= gq_-, \end{aligned} \tag{5}$$

to render the stochastic equations amenable to perturbation. The stochastic equations for the scaled EPR variables become

$$\begin{aligned}
\frac{\mathrm{d}x_0}{\mathrm{d}T} &= -\gamma_r\left[x_0 - 2\sqrt{\sigma} + \frac{1}{2}(x_+^2 - x_-^2 - y_+^2 + y_-^2)\right],\\
\frac{\mathrm{d}y_0}{\mathrm{d}T} &= -\gamma_r[y_0 + x_+y_+ - x_-y_-],\\
\frac{\mathrm{d}x_-}{\mathrm{d}T} &= -x_- - \frac{1}{2}[x_0x_- + y_0y_-] + \frac{g}{\sqrt{2}}[\sqrt{x_0+iy_0}\xi_- + \sqrt{x_0-iy_0}\xi_-^+],\\
\frac{\mathrm{d}y_+}{\mathrm{d}T} &= -y_+ + \frac{1}{2}[y_0x_+ - x_0y_+] - i\frac{g}{\sqrt{2}}[\sqrt{x_0+iy_0}\xi_+ - \sqrt{x_0-iy_0}\xi_+^+],\\
\frac{\mathrm{d}x_+}{\mathrm{d}T} &= -x_+ + \frac{1}{2}[x_0x_+ + y_0y_+] + \frac{g}{\sqrt{2}}[\sqrt{x_0+iy_0}\xi_+ + \sqrt{x_0-iy_0}\xi_+^+],\\
\frac{\mathrm{d}y_-}{\mathrm{d}T} &= -y_- + \frac{1}{2}[x_0y_- - y_0x_-] - i\frac{g}{\sqrt{2}}[\sqrt{x_0+iy_0}\xi_- - \sqrt{x_0-iy_0}\xi_-^+],
\end{aligned} \tag{6}$$

where $T=\gamma^D t$ is time in units of the cavity lifetime for the downconverted fields. The functions $\xi_\pm(T)$ and $\xi_\pm^+(T)$ are independent Langevin forces with the following nonvanishing correlation functions:

$$\langle \xi_+(T)\xi_+(T')\rangle = \langle \xi_+^+(T)\xi_+^+(T')\rangle = \delta(T-T'),$$

$$\langle \xi_-(T)\xi_-(T')\rangle = \langle \xi_-^+(T)\xi_-^+(T'T)\rangle = -\delta(T-T'). \quad (7)$$

We notice the symmetry properties of the stochastic Eqs. (6). In fact, it is easy to verify that the equations of motion are unchanged by the transformation $x_- \leftrightarrow y_+$ and $x_+ \leftrightarrow -y_-$. Of course, all noise terms appearing in Eqs. (6) are statistically equivalent. Therefore these equations should not change the symmetries of the initial values chosen for x_+ and y_-.

To provide a comparison between the linearized model and the full stochastic integration, we will use a perturbation expansion of the positive P representation of the dynamical equations. This allows us to include quantum effects in a systematic fashion.[27] We first introduce a formal perturbation expansion in powers of the parameter g:

$$x_k = \sum_{n=0}^{\infty} g^n x_k^{(n)},$$

$$y_k = \sum_{n=0}^{\infty} g^n y_k^{(n)}. \quad (8)$$

The series expansion written in this way has the property that the zeroth-order term corresponds to the classical field of order 1 in the unscaled quadrature, while the first-order term is related to quantum fluctuations of order g, and the higher-order terms correspond to the nonlinear corrections to the quantum fluctuations of order g^2 and greater. The stochastic equations are then solved by the technique of matching powers of g in the corresponding time evolution equations.

The steady-state solutions x_{js} of the zeroth order give the operation point of the OPO and describe its macroscopic behavior. For a triply resonant operation, the expressions for the steady state are quite simple:

$$x_{0s} = 2,$$

$$x_{+s} = 2(\sqrt{\sigma}-1)^{1/2},$$

$$x_{-s} = 0,$$

$$y_{0s} = y_{+s} = y_{-s} = 0. \quad (9)$$

The first-order equations are often used to predict squeezing in a linearized fluctuation analysis. They are nonclassical in the sense that they can describe states without a positive-definite Glauber–Sudarshan P distribution,[28,29] but correspond to a simple form of linear fluctuation that has a Gaussian quasi-probability distribution. A full quantum description of the OPO dynamics can be obtained by a numerical integration of the stochastic Eqs. (6), and can be compared to analytical expressions obtained from the linearized approach. Taking the first-order terms and using the steady-state solutions given by Eqs. (9), we can write the following equations for the linear quantum fluctuations:

$$\frac{dx_0^{(1)}}{dT} = -\gamma_r[x_0^{(1)} + 2(\sqrt{\sigma}-1)^{1/2}x_+^{(1)}],$$

$$\frac{dy_0^{(1)}}{dT} = -\gamma_r[y_0^{(1)} + 2(\sqrt{\sigma}-1)^{1/2}y_+^{(1)}],$$

$$\frac{dx_+^{(1)}}{dT} = -(\sqrt{\sigma}-1)^{1/2}x_0^{(1)} + (\xi_+ + \xi_+^+),$$

$$\frac{dx_-^{(1)}}{dT} = -2x_-^{(1)} + (\xi_- + \xi^+),$$

$$\frac{dy_+^{(1)}}{dT} = -2y_+^{(1)} + (\sqrt{\sigma}-1)^{1/2}y_0^{(1)} - i(\xi_+ - \xi_+^+),$$

$$\frac{dy_-^{(1)}}{dT} = -i(\xi_- - \xi_-^+). \quad (10)$$

The linear coupled stochastic equations obtained agree with Eqs. (3), for zero detunings and no spurious losses. From them we may readily calculate the steady-state averages of the first-order corrections and use them to compute the linearized fluctuations. Notice that under the linear approximation y_- becomes a purely diffusive variable (phase diffusion).

In an experimental situation, the noise spectra outside the cavity are generally the quantities of interest. Therefore we will proceed to analyze the problem in frequency space, via a Fourier decomposition of the fields. The first-order stochastic equations may be rewritten in the frequency domain so that we may calculate the spectra of the squeezed and antisqueezed field quadratures.

The solutions for the noise of the squeezed operators, $\hat{p}_-$ and $\hat{q}_+$, are

$$S_{p_-}(\Omega') = 1 - \frac{1}{\Omega'^2+1}, \quad (11)$$

$$S_{q+}(\Omega') = 1 - \frac{(4\Omega'^2+\gamma_r^2)^2}{\Omega'^2[4\Omega'^2+\gamma_r^2-2\gamma_r(\sqrt{\sigma}-1)]^2+[4\Omega'^2+\gamma_r^2\sqrt{\sigma}]^2}, \quad (12)$$

where $\Omega' = \Omega/\gamma^D$ is the analysis frequency in units of the cavity bandwidth.

Under the limits of the linearized approach, the results of the noise spectra are independent of the phase space representation employed. Therefore these results coincide with the usual ones obtained with the Wigner representation.

The spectra given by Eqs. (11) and (12) can now be compared with those found via a stochastic integration of the full equations of motion (6) in the positive P representation. The nonlinear spectra are calculated by Fourier transform of the stochastic integration, which must be performed numerically. A somewhat subtle point arises

here: the nonlinear Eqs. (6) have more than one possible steady-state solution. Thus for a fair comparison with the linearized spectra, it is necessary to choose the same steady state. By doing this, we verified that both predictions, in the above-threshold OPO, agree within a good numerical precision. Therefore we conclude that possible limitations of the linearized model for dealing with the OPO dynamics under phase diffusion do not account for the experimentally observed excess noise of $\hat{q}_+$.

3. EXPERIMENT

Our system is a triply resonant type-II OPO operating above threshold. The experimental setup is depicted in Fig. 2. The pump beam is a diode-pumped doubled Nd:YAG laser (Innolight Diabolo) with 900 mW output power at 532 nm. A secondary output at 1064 nm is used for alignment purposes. Since the pump beam presents excess noise for frequencies as high as 20 MHz, a filter cavity is necessary. Our filter cavity has a bandwidth of 2.4 MHz and assures that the pump laser is shot-noise limited for analysis frequencies higher than 15 MHz (see Fig. 3). We measured the laser phase noise by reflecting the beam off an empty cavity, in the same way we measure the phase noise of the downconverted beams. The phase noise equals the intensity noise, except at a frequency of 12 MHz, where there is very big phase noise, owing to a frequency modulation inside the Diabolo laser for stabilization purposes. This excess noise saturates our electronics and prevents measurements for analysis frequencies close to 12 MHz and also to its second harmonic, 24 MHz, as can be seen in Fig. 3. The OPO cavity is a linear semimonolithic cavity composed of a flat input mirror, directly deposited on one face of the nonlinear crystal, with 93% reflectivity at 532 nm and high reflectivity (>99.8%) at 1064 nm, and a spherical output mirror (50 mm curvature radius) with high reflectivity at 532 nm (>99.8%) and 96% reflectivity at 1064 nm. The nonlinear crystal is a 10 mm long potassium titanyl phosphate (KTP) from Litton. The threshold power is 12 mW.

The signal and the idler beams are separated by a polarizing beam splitter (PBS) and sent to detection, which consists of a ring cavity and a photodetector (Epitaxx ETX 300) for each beam. The overall detection efficiency is $\eta = 80(2)\%$. Both analysis cavities have bandwidths of 14 MHz, allowing for a complete conversion of phase to amplitude noise for analysis frequencies higher than 20 MHz. The measurements are taken at an analysis frequency equal to 27 MHz. To access the same quadrature

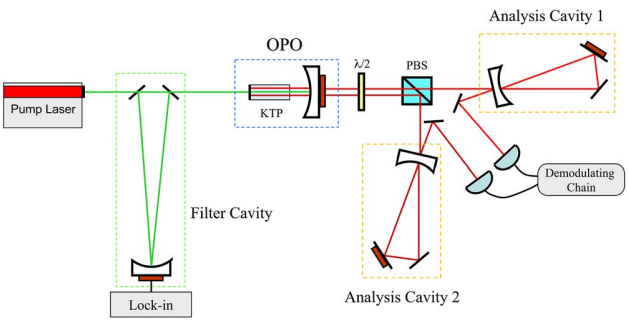

Fig. 2. (Color online) Sketch of the experimental setup.

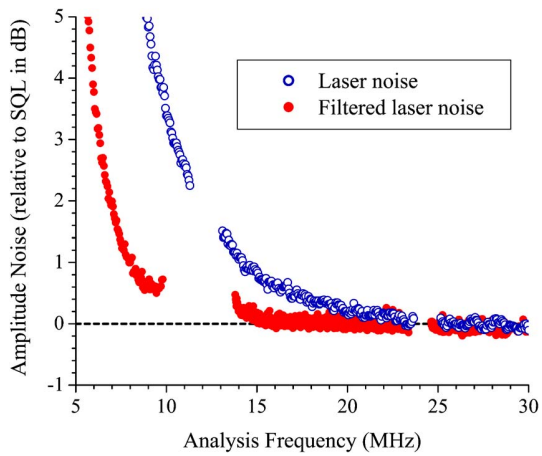

Fig. 3. (Color online) Measurement of the pump noise as a function of the analysis frequency. Open circles, unfiltered laser noise; full circles, laser noise at the output of the filter cavity. In view of the large excess noise at 12 MHz and its second harmonic, we suppressed those frequencies from the data.

for both beams, the two cavities must be detuned by the same amount at the same time. By scanning the detunings synchronously, we can measure all quadratures of the twin beams. In particular, we can easily select the amplitude (off resonance) or phase (detuning equal to one-half the bandwidth) quadratures.[30]

The data acquisition is carried out by a demodulating chain, which mixes the photocurrents from each detector with a sinusoidal electronic reference at the analysis frequency and filters the resulting low-frequency signal. The demodulated photocurrent fluctuations are sampled at 600 kHz repetition rate by an analog-to-digital (A/D) card connected to a personal computer. The variances of these fluctuations are then computed taking groups of 1000 points, resulting in something proportional to the power spectrum of the photocurrents at the analysis frequency. At the end, measured variances are normalized to the shot noise standard quantum level (SQL).

A. Fluctuations as a Function of σ

The input pump field is guaranteed to be shot-noise limited for frequencies above 15 MHz after being transmitted through the filter cavity. Even before being filtered, the pump field is shot-noise limited above 25 MHz, as shown in Fig. 3. Nevertheless, we observed excess noise in the sum of the phases of the signal and the idler beams, preventing the violation of the inequality given in Eq. (1) except for pump powers very close to threshold.[12]

As seen in Section 2 from the theoretical description of the OPO, excess noise in the pump beam would generate excess noise in the phase sum of the twin beams. Yet how could that be the case if we carefully measured the input pump to be shot-noise limited? By following this single lead, it is natural to examine the noise properties of the pump beam reflected from the OPO cavity. This was done by scanning the OPO cavity for crystal temperatures such that there was no parametric oscillation (triple resonance depends sharply on crystal temperature and can easily be avoided). Since the incident beam is shot-noise limited, could there be excess noise generated inside the cavity

containing the KTP crystal? We did indeed find excess noise in the reflected pump's amplitude (Fig. 4) and phase quadratures. The maximum values, for $\sigma=1$, were $S_{p0}^{\mathrm{R}}=1.8(1)$ and $S_{q0}^{\mathrm{R}}=4.5(3)$.

At present, we can still not claim to fully understand the origin of this excess noise. We verified, of course, that no such noise is generated in an empty cavity (which would also invalidate the measurements we perform with the analysis cavities for the twin beams). We also checked whether this effect depended on χ and would thus be directly related to the parametric process. For a polarization of the incident beam orthogonal to the usual polarization, phase matching cannot be fulfilled, and no downconversion can occur. The noise in the reflected beam did not show any significant dependence on the incident polarization. It does, however, increase for increasing power of the incident beam. We can speculate that this can be a result of photon absorption by the crystal at 532 nm (which is at the origin of the thermal bistability observed in Fig. 4), with a subsequent relaxation by spontaneous emission or nonradiative processes. This, may give rise to an intensity-dependent refractive index, yielding phase and amplitude modulation at 532 nm. We are currently investigating these possibilities.

As a first approximation, in order to see whether this would account for the behavior of $\Delta^2\hat{p}_-,\Delta^2\hat{q}_-,\Delta^2\hat{p}_+$, and $\Delta^2\hat{q}_+$, as a function of σ, we simply added excess noise to the input pump beam in the linearized OPO theory. In Fig. 5 we compare the results from the model, with incident $S_{p0}=1.5$ and $S_{q0}=5.5$, to the measured data. The signal and idler powers varied from 0.4 up to 5.5 mW each during the experiment, corresponding to pump powers between 13 and 26 mW, or $1.06<\sigma<2.2$. As expected, noises corresponding to the subtraction subspace, $\Delta^2\hat{p}_-$ and $\Delta^2\hat{q}_-$, are independent of pump power. But $\Delta^2\hat{q}_+$ is very sensitive to σ, as is $\Delta^2\hat{p}_+$ to a lesser degree. The agreement with the theoretical model is surprisingly good. This is a strong indication that the intracavity pump excess noise is the main responsible for the excess noise in $\Delta^2\hat{q}_+$.

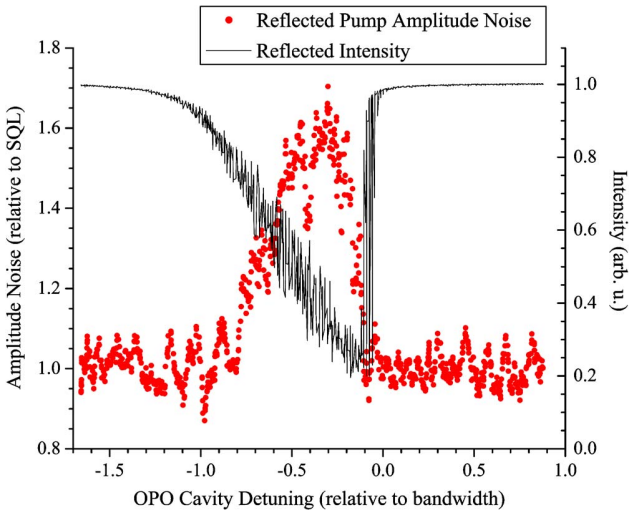

Fig. 4. (Color online) Intensity noise of the reflected pump beam, as a function of the detuning of the OPO cavity. The excess noise observed is peaked for Δ_0, close to one-half the OPO cavity bandwidth. The asymmetry in the mean-field signal is attributable to the thermal bistability. The analysis frequency is 27 MHz. Circles, reflected pump noise; full curve, reflected average intensity.

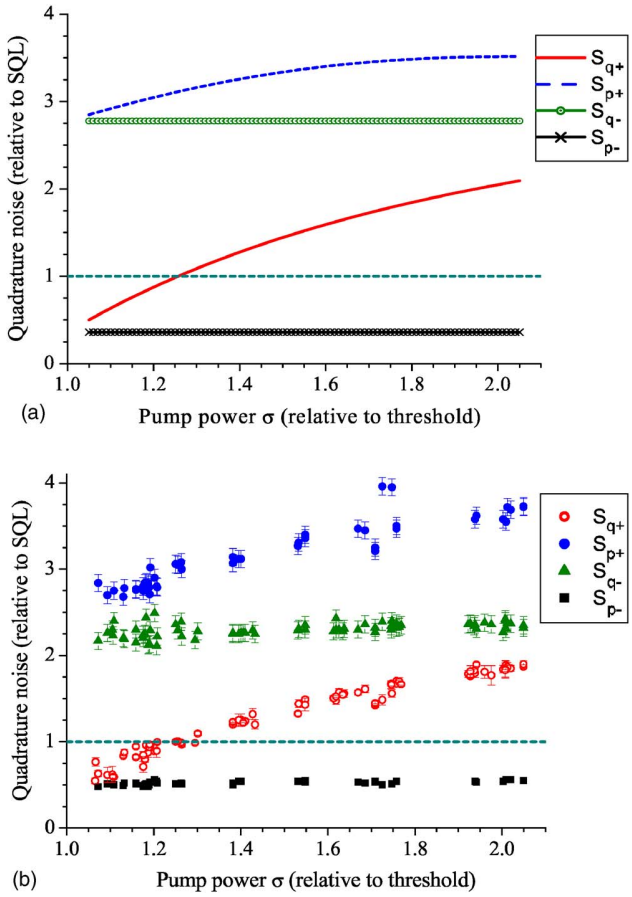

Fig. 5. (Color online) Noise behavior as a function of σ. (a) Predictions of the linearized model for an input pump beam with $S_{p_0}=1.5$ and $S_{q0}=5.5$; dashed curve, S_{p_+}; solid line with open circles, S_{q_-}, solid curve, S_{q_+}; solid line with crosses, S_{p_-}; SQL =1.0 is indicated by a dashed line. (b) Experimental result for σ ranging from 1.06 to 2.2. Full circles, S_{p_+}; triangles, S_{q_-}; open circles, S_{q_+}; squares, S_{p_-}; SQL=1.0 is indicated by a dashed line.

B. Two-Color Entanglement

The sum of the phase noise is squeezed very close to threshold, and the squeezing is degraded with increasing pump power. $\Delta^2\hat{q}_+$ crosses the shot-noise level approximately at $\sigma=1.20$, from squeezing to antisqueezing, although only below $\sigma=1.15$ can squeezing be observed with certainty.

Figure 6 shows the recorded noise in sum and subtraction of the photocurrent fluctuations of the signal and the idler beams as functions of the detuning of the analysis cavities for $\sigma=1.06$. Off-resonance, quantum correlations are observed in the subtraction of amplitudes, $\Delta^2\hat{p}_-=0.50(1)$, or $-3.01(9)$ dB. For detuning of analysis cavities equal to one-half the bandwidth, squeezing is present in the sum of phases, $\Delta^2\hat{q}_+=0.73(1)$, or $-1.37(6)$ dB. The Duan *et al.* and Simon criteria [Eq. (1)], are clearly violated:

$$\Delta^2\hat{p}_- + \Delta^2\hat{q}_+ = 1.23(2) < 2, \tag{13}$$

attesting to the entanglement. This value, together with the one reported by Jing *et al.*,[14] is the lowest achieved for

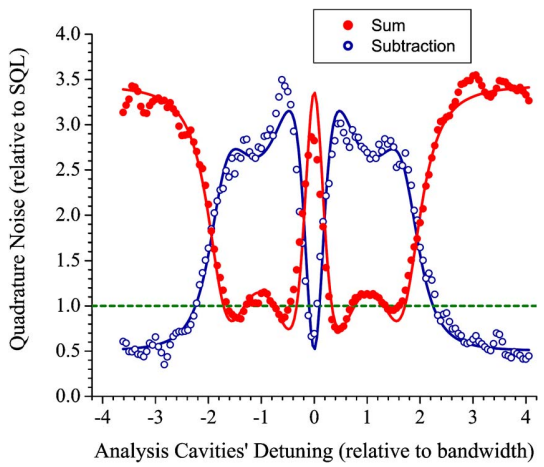

Fig. 6. Sum (full circles) and difference (open circles) of the quadrature noise measured as a function of the detuning of the analysis cavities. Squeezed-state entanglement can be directly observed, with $\Delta^2\hat{p}_-=0.50(1)$, or $-3.01(9)$ dB, and $\Delta^2\hat{q}_+=0.73(1)$, or $-1.37(6)$ dB.

twin beams produced by an above-threshold OPO.

We also point out that, in this experiment, the twin beams have very different frequencies (the wavelengths differ by ≈ 1 nm), an unusual situation. Such two-color entanglement can be very interesting for the transfer of quantum information between different parts of the electromagnetic spectrum.

4. CONCLUSION

We presented a theoretical and experimental investigation of phase noise and entanglement in the above-threshold OPO. Excess noise in the phase sum of the twin beams was measured as a function of pump power relative to threshold, and we found that it decreases as pump power is lowered. We finally discovered that excess pump noise is generated inside the OPO cavity containing the nonlinear crystal, even for a shot-noise limited pump beam and without parametric oscillation. The ultimate physical origin of this phenomenon still requires further investigation. Another important question to address is how one can eliminate this effect. Su *et al.*[13] were able to observe entanglement for σ of the order of 2. The difference between their setup and others is a lower cavity finesse for the pump field. If the assumption of an intensity-dependent index of refraction is correct, this makes sense. For a lower finesse, the phase shifts accumulated inside the cavity should be smaller, hence the excess noise generated should also be smaller.

In spite of these unexpected phenomena, two-color entanglement was measured in the above-threshold OPO. There are interesting avenues to pursue for applications in quantum information. First of all, we should mention that the strongest squeezing measured to date, -9.7 dB, was generated in an above-threshold OPO.[18] Thus, entanglement in the above-threshold OPO may be the strongest ever achieved for continuous variables. The bright twin beams can have very different frequencies, and one can envisage CV quantum teleportation[10] to transfer quantum information from one frequency to another (in other words, to tune quantum information). For example, this system could be used to communicate quantum information between quantum memories or quantum computers based on hardware that has different resonance frequencies. Finally, a quantum key distribution protocol proposed by Silberhorn *et al.*[31] can be readily implemented with the advantage that the measurement with analysis cavities does not require sending a local oscillator together with the quantum channel to the distant receiver.

The above-threshold OPO, which was the first system proposed to observe CV entanglement, has finally been added to the optical quantum information toolbox. We expect new and exciting applications to come in the near future.

ACKNOWLEDGMENTS

This work was supported by Fundação de Amparo à Pesquisa do Estado de São Paulo, Coordenação de Aperfeiçoamento de Pessoal de Nível Superior, and Conselho Nacional de Desenvolvimento Científico e Technológica through the Instituto do Milênio de Informação Quântica. We thank C. Fabre and T. Coudreau for lending us the nonlinear crystal.

The corresponding author P. Nussenzveig can be reached by e-mail at nussen@if.usp.br.

REFERENCES

1. R. H. Kingston, "Parametric amplification and oscillation of optical frequencies," Proc. IRE **50**, 472–474 (1962).
2. R. Graham and H. Haken, "The quantum fluctuations of the optical parametric oscillator," Z. Phys. **210**, 276–302 (1968).
3. L.-A. Wu, H. J. Kimble, J. L. Hall, and H. Wu, "Generation of squeezed states by parametric down conversion," Phys. Rev. Lett. **57**, 2520–2523 (1986).
4. A. Heidmann, R. J. Horowicz, S. Reynaud, E. Giacobino, C. Fabre, and G. Camy, "Observation of quantum noise reduction on twin laser beams," Phys. Rev. Lett. **59**, 2555–2557 (1987).
5. M. D. Reid and P. D. Drummond, "Quantum correlations of phase in nondegenerate parametric oscillation," Phys. Rev. Lett. **60**, 2731–2733 (1988).
6. Z. Y. Ou, S. F. Pereira, H. J. Kimble, and K. C. Peng, "Realization of the Einstein–Podolsky–Rosen paradox for continuous variables," Phys. Rev. Lett. **68**, 3663–3666 (1992).
7. S. L. Braunstein and P. van Loock, "Quantum information with continuous variables," Rev. Mod. Phys. **77**, 513–577 (2005).
8. W. P. Bowen, R. Schnabel, P. K. Lam, and T. C. Ralph, "Experimental investigation of criteria for continuous variable entanglement," Phys. Rev. Lett. **90**, 043601 (2003).
9. C. Schori, J. L. Sorensen, and E. S. Polzik, "Narrow-band frequency tunable light source of continuous quadrature entanglement," Phys. Rev. A **66**, 033802 (2002).
10. A. Furusawa, J. L. Sorensen, S. L. Braunstein, C. A. Fuchs, H. J. Kimble, and E. S. Polzik, "Unconditional quantum teleportation," Science **282**, 706–709 (1998).
11. X. J. Jia, X. L. Su, Q. Pan, J. G. Gao, C. D. Xie, and K. C. Peng, "Experimental demonstration of unconditional entanglement swapping for continuous variables," Phys. Rev. Lett. **93**, 250503 (2004).
12. A. S. Villar, L. S. Cruz, K. N. Cassemiro, M. Martinelli, and P. Nussenzveig, "Generation of bright two-color continuous variable entanglement," Phys. Rev. Lett. **95**, 243603 (2005).

13. X. L. Su, A. Tan, X. J. Jia, Q. Pan, C. D. Xie, and K. C. Peng, "Experimental demonstration of quantum entanglement between frequency-nondegenerate optical twin beams," Opt. Lett. **31**, 1133–1135 (2006).
14. J. Jing, S. Feng, R. Bloomer, and O. Pfister, "Experimental continuous-variable entanglement of phase-locked bright optical beams," arXiv.org archive, e-Print quant-ph/0604134 http://arxiv.org/abs/quantph/0604134.
15. L. M. Duan, G. Giedke, J. I. Cirac, and P. Zoller, "Inseparability criterion for continuous variable systems," Phys. Rev. Lett. **84**, 2722–2725 (2000).
16. R. Simon, "Peres–Horodecki separability criterion for continuous variable systems," Phys. Rev. Lett. **84**, 2726–2729 (2000).
17. A. S. Villar, M. Martinelli, and P. Nussenzveig, "Testing the entanglement of intense beams produced by a nondegenerate optical parametric oscillator," Opt. Commun. **242**, 551–563 (2004).
18. J. Laurat, L. Longchambon, C. Fabre, and T. Coudreau, "Experimental investigation of amplitude and phase quantum correlations in a type II optical parametric oscillator above threshold: from nondegenerate to degenerate operation," Opt. Lett. **30**, 1177–1179 (2005).
19. M. D. Reid and P. D. Drummond, "Correlations in nondegenerate parametric oscillation—squeezing in the presence of phase diffusion," Phys. Rev. A **40**, 4493–4506 (1989).
20. P. D. Drummond and M. D. Reid, "Correlations in nondegenerate parametric oscillation. 2. Below threshold results," Phys. Rev. A **41**, 3930–3949 (1990).
21. S. Chaturvedi, P. D. Drummond, and D. F. Walls, "2 photon absorption with coherent and partially coherent driving fields," J. Phys. A **10**, L187–L192 (1977).
22. P. D. Drummond and C. W. Gardiner, "Generalized *P*-representations in quantum optics," J. Phys. A **13**, 2353–2368 (1980).
23. K. V. Kheruntsyan and K. G. Petrosyan, "Exact steady-state Wigner function for a nondegenerate parametric oscillator," Phys. Rev. A **62**, 015801 (2000).
24. B. Coutinho dos Santos, K. Dechoum, A. Z. Khoury, L. F. da Silva, and M. K. Olsen, "Quantum analysis of the nondegenerate optical parametric oscillator with injected signal," Phys. Rev. A **72**, 033820 (2005).
25. H. J. Carmichael, *Statistical Methods in Quantum Optics 1: Master Equations and Fokker–Planck Equations* (Springer, 1999).
26. C. W. Gardiner, *Quantum Noise* (Springer-Verlag, 1991).
27. K. Dechoum, P. D. Drummond, S. Chaturvedi, and M. D. Reid, "Critical fluctuations and entanglement in the nondegenerate parametric oscillator," Phys. Rev. A **70**, 053807 (2004).
28. R. J. Glauber, "Coherent and incoherent states of the radiation field," Phys. Rev. **131**, 2766–2788 (1963).
29. E. C. G. Sudarshan, "Equivalence of semiclassical and quantum mechanical descriptions of statistical light beams," Phys. Rev. Lett. **10**, 277–279 (1963).
30. P. Galatola, L. A. Lugiato, M. G. Porreca, P. Tombesi, and G. Leuchs, "System control by variation of the squeezing phase," Opt. Commun. **85**, 95–103 (1991).
31. Ch. Silberhorn, N. Korolkova, and G. Leuchs, "Quantum key distribution with bright entangled beams," Phys. Rev. Lett. **88**, 167902 (2002).

3.1 Fónons como fonte

A resposta às questões vieram junto com as tentativas de medida de emaranhamento tripartite, tema do próximo capítulo. Era claro que o excesso de ruído comprometia a medida das correlações quânticas entre os campos. Todas as medidas feitas posteriormente, observando o ruído do bombeio refletido juntamente com os feixes gerados, não aceitavam nem mesmo o modelo proposto no artigo anterior [11]. Diversos grupos estavam igualmente envolvidos no problema, modelando o excesso de ruído do campo e comparando-o com o resultado observado experimentalmente [43].

Foi durante o mestrado dos meus dois primeiros estudantes, Jônatas Eduardo César e Antônio Coelho, que surgiu uma ideia. Não havia notificações de não-linearidades importantes em terceira ordem no KTP, que justificassem a ideia de modulação de fase. Consideramos que o problema fosse intrínseco ao KTP, de forma que a solução para a medida do emaranhamento tripartite poderia passar pela troca do cristal. Testes com outros cristais, como o $LiNbO_3$; mostraram que também nestes sistemas havia excesso de ruído presente no modo de bombeio, tão grande ou maior que o observado no KTP.

A hipótese do ruído vir de algum processo ligado à conversão paramétrica era descartada por sua presença abaixo do limiar de oscilação. Havia a remota possibilidade de que o processo de geração de vácuo comprimido ou vácuo emaranhado nestas condições poderia levar a este excesso de ruído, situação improvável devido à depleção praticamente nula do campo de bombeio. No entanto, os testes realizados permitiam descartar esta hipótese. A condição de conservação de momento em conversão paramétrica descendente ocorre para o bombeio com polarização paralela ao plano dos eixos cristalográficos xy, gerando um campo na mesma polarização (complementar) e um campo em polarização ortogonal, paralela ao eixo z (sinal). Ao repetirmos a medida do ruído refletido com polarização de bombeio paralela ao eixo z, impedíamos a conversão paramétrica por não satisfazer a condição de acordo de fase. Nesta situação, o ruído era semelhante ao observado para a o bombeio na polarização de bombeio.

Na reunião em 2005, na qual o estudante de doutorado Alessandro Villar fora comigo em visita ao prof. Antônio Zelaquett Khoury (IF/UFF), fora apontado um artigo onde é incluída, *ad hoc*, uma fonte de ruído de fase, associada a uma flutuação de comprimento de cavidade [41]. Isto nunca havia ocorrido antes, em cavidades vazias, mas apenas com o cristal inserido. Havia portanto um efeito intrínseco ao cristal, isto é claro. Mas uma flutuação de comprimento de cavidade seria originária de uma modulação do índice de refração do cristal. Por outro lado, esta modulação de índice de refração deveria estar presente em todos os modos ressonantes. Com esta ideia, injetamos um campo no IR (1064 nm), paralelo à polarização sinal, na ausência de bombeio intracavidade, fora de uma condição de acordo de fase (ajustado pela temperatura), suprimindo assim a geração de segundo harmônico, e analisamos o ruído de saída. O excesso de ruído, medido com o auxílio de uma cavidade de análise, estava lá. Idêntico resultado foi obtido para o modo complementar.

A conclusão é que o ruído de modulação de fase estava presente em todos os mo-

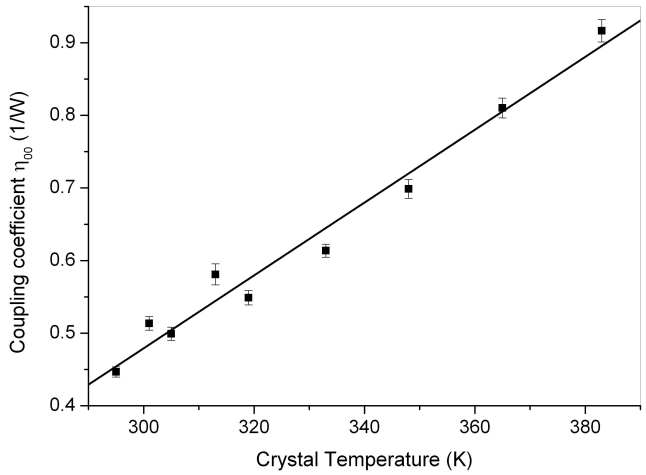

Figura 3.2: Medida preliminar da dependência do ruído com a temperatura.

dos, e era sempre proporcional à intensidade (figura 3 do artigo seguinte). Portanto, esperávamos que a caracterização do ruído pudesse justificar a resposta obtida com os campos da cavidade. Efetivamente, o ruído parametrizado pode ser adicionado ao modelo do OPO, caracterizado, e o resultado apresenta uma excelente concordância com as variâncias medidas.

Mas qual a origem do mesmo? A resposta saiu da ideia que a modulação do índice de refração, responsável pela flutuação de fase, é aleatória. Esta modulação poderia estar ligada a uma flutuação aleatória de densidade no cristal. Ou seja, a um deslocamento dos íons na rede cristalina - fónons, portanto. Este fónons serão responsáveis por um espalhamento Brillouin, alterando levemente a frequência do campo espalhado. O fóton da portadora central espalhado pelo fónons irá ter uma frequência deslocada, contribuindo para a banda lateral à portadora central. Isto irá gerar um excesso de ruído, que se somará ao ruído normal do OPO (seção II do artigo seguinte).

A hipótese do ruído vindo dos fónons implica na dependência do ruído com a temperatura. Medimos o ruído adicionado e sua dependência com a temperatura do cristal, e notamos um aumento linear do ruído com o aquecimento (figura 3.2). A surpresa fora ter este aumento mais rápido do que seria esperado com uma resposta simplesmente proporcional à temperatura, o que nos favorecia, e permitia baixar rapidamente o ruído com o resfriamento. Será este controle de temperatura a chave para a medida do emaranhamento tripartite, que veremos no próximo capítulo.

Uma questão curiosa se colocava. Nas equações do OPO, o ganho paramétrico aparece acoplado sempre à amplitude do campo, e portanto à intensidade local do mesmo. Portanto, uma forma de reduzir o limiar de oscilação é trabalhar com campos mais focalizados, com comprimento de Rayleigh mais próximos do limite de Boyd-Kleinman [44]. Diante da nossa fonte de ruído, qual seria a melhor estratégia para lidar com o campo intracavidade, esperando minimizar o efeito do mesmo?

Se pensarmos nas flutuações do índice de refração como centros de espalhamento

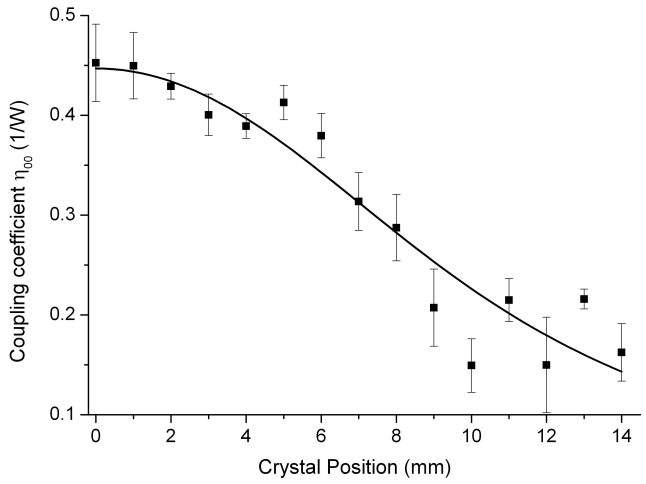

Figura 3.3: Estudo da dependência do ruído com a posição do cristal, implicando em uma dependência daquele com a intensidade.

espalhados aleatoriamente no cristal com uma certa densidade, é de se esperar que, com um tamanho de feixe menor, para a mesma intensidade, teremos um espalhamento menor. Como neste caso reduziríamos a potência de limiar, reduziríamos igualmente o número de fótons espalhados, e portanto o excesso de ruído na cavidade. Neste caso, trabalhar com um feixe menor seria uma técnica de redução do ruído. No entanto, há uma contrapartida: um campo com uma cintura de feixe menor implica em um recobrimento maior da luz espalhada com o modo da cavidade, que passa a ter um ângulo sólido maior. Este efeito compensa o anterior, e portanto o ruído está ligado à intensidade do campo, mais do que à potência total intracavidade (eq. (18) do artigo). Esta teoria é válida deste que o termo de acoplamento possa ser descrito por um modelo de fónons pontuais (com comprimento de coerência tendendo a zero). Se o meio tiver ressonâncias específicas para os fónons, advindas de um tamanho menor do meio paramétrico, por exemplo, podemos eventualmente esperar que certas faixas do espectro sejam inibidas, e se tornem mais favoráveis à realização de experimentos. Isto torna interessante a possibilidade de usar guias de onda como meio de ganho, para tentar controlar estas fontes de ruído. A dependência do ruído com a intensidade foi verificada através do uso de uma cavidade de tamanho fixo, para a qual deslocamos o cristal longitudinalmente e verificamos o excesso de ruído gerado em função da posição. Efetivamente, neste caso temos uma variação da intensidade sobre o cristal. O resultado, apresentado na figura 3.3, apresentou um excelente acordo com o modelo.

Um ponto importante observado neste artigo é que as flutuações de fase adicionadas a cada modo não são perfeitamente correlacionadas. Se assim fosse, as correlações de fase poderiam se anular em algumas medidas, e o excesso de ruído seria menos danoso nas correlações entre os campos de bombeio e sinal, ou bombeio e complementar. Teríamos então conseguido obter o emaranhamento tripartite antes, nas medidas descritas nos trabalhos do próximo capítulo.

Extra phase noise from thermal fluctuations in nonlinear optical crystals

J. E. S. César,[1] A. S. Coelho,[1] K. N. Cassemiro,[2] A. S. Villar,[3] M. Lassen,[4] P. Nussenzveig,[1] and M. Martinelli[1]
[1]*Instituto de Física, Universidade de São Paulo, Caixa Postal 66318, 05315-970 São Paulo, SP, Brazil*
[2]*Max Planck Junior Research Group, Günther Scharowskystr. 1/Bau 24, 91058 Erlangen, Germany*
[3]*Max Planck Institute for the Science of Light, University of Erlangen-Nuremberg, Staudtstr. 7/B2, 91058 Erlangen, Germany*
[4]*Department of Physics, Technical University of Denmark, Fysikvej, 2800 Kgs. Lyngby, Denmark*
(Received 25 March 2009; published 11 June 2009)

We show theoretically and experimentally that scattered light by thermal phonons inside a second-order nonlinear crystal is the source of additional phase noise observed in optical parametric oscillators. This additional phase noise reduces the quantum correlations and has hitherto hindered the direct production of multipartite entanglement in a single nonlinear optical system. We cooled the nonlinear crystal and observed a reduction in the extra noise. Our treatment of this noise can be successfully applied to different systems in the literature.

DOI: 10.1103/PhysRevA.79.063816 PACS number(s): 42.50.Lc, 42.50.Dv, 03.67.Mn

I. INTRODUCTION

In quantum information, processes with continuous variables have attracted growing attention, involving the manipulation of states of light and atoms. Examples are the unconditional quantum teleportation of states of the electromagnetic field [1] and teleportation and storage of quantum information between light and atoms [2]. Many of these experiments involved nonclassical states of the electromagnetic field, either squeezed or N-partite entangled state, generally obtained from the combination of squeezed states in a set of beam splitters [3]. Quadrature squeezed states of the electromagnetic field attracted renewed interest, after the initial promises of ultrasensitive spectroscopy and noiseless communication channels, predicted in the late 1980s.

A source of nonclassical states is nonlinear crystals inside optical cavities. This was the case for the first generation of squeezing in parametric down conversion [4], soon followed by the observation of quantum correlations between separate fields [5] and production of entangled states [6] in an optical parametric oscillator (OPO), and squeezing in second-harmonic generation (SHG) [7]. At the heart of this process is the parametric coupling of three fields, used for twin photon generation, but with the enhancement and the mode selection given by a resonant cavity. Early studies [8] theoretically demonstrated that a nonlinear crystal inside a cavity would produce squeezing in different modes and entanglement between pairs of modes.

Despite this long list of successful implementations showing excellent agreement with the theory, the measurement of other nonclassical fundamental characteristic features remained elusive. Phase quadrature squeezing of the pump field in the above-threshold OPO [9] presented an unexplained excess noise that could not be accounted for by any known source in the system. Furthermore, the first measurements of noise correlations between the phases of signal and idler beams in OPO's above threshold resulted in great excess noise where squeezing was expected [10]. The first measurement of this quantum correlation, demonstrating entanglement of signal and idler beams [11], was limited to operation very close to threshold. An increase in the pump power rapidly degraded the quantum phase correlations. This was one of the main reasons why signal and idler entanglement remained unobserved for almost 20 years after its prediction [8]. Measurements performed later by other groups [12,13] confirmed this excess noise, and many attempts where made to explain its origin [14–16]. The same kind of problems was observed in the coupling of infrared and green fields in a degenerate OPO and SHG [17]. Moreover, the direct production of three-mode entanglement was also predicted [18], but the first experimental implementations could not overcome this unknown source of extra phase noise [19].

Here, we make a detailed treatment of this extra noise in the OPO and experimentally verify its predictions. The model is described in Sec. II, and the expected behavior for an OPO is then presented. A full characterization of this noise in the three modes of an optical cavity encompassing a nonlinear crystal is given in Sec. III. This complete description of the noise presents good agreement with the experimental observations of the covariance matrix, measured for the OPO described in Ref. [19] (Sec. IV). We show that this additional noise is consistent with a model of incoherent (thermal) phonon noise. Random density fluctuations are induced and, via the change in the refractive index, entail phase fluctuations as described in Sec. V. We also apply our model to other results reported in the literature, with good agreement. Finally, we conclude by a discussion on proposals for reducing or eliminating this noise in experiments for the production of squeezed or entangled state involving phase quadratures.

II. MODEL FOR THE INTRODUCED PHASE NOISE

In the present study, we will consider that the crystal, although homogeneous, can have small fluctuations in its permittivity. The refractive index fluctuates owing to local-density fluctuations associated with acoustic phonons inside the crystal. This density change results in Stokes and Brillouin light scattering [20] with frequency shifts in the scattered light. In the present case, we will be interested in the fraction of the scattering that is coupled into the cavity

modes, with small shifts in the frequency (within the cavity bandwidth).

If we consider that the constitutive relation between the displacement vector $\vec{D}$ and the electric field $\vec{E}$ includes a random local fluctuation in permittivity $\delta\varepsilon$,

$$\vec{D} = \varepsilon\vec{E} + \delta\varepsilon(z,t)\vec{E}, \tag{1}$$

we have, from the Maxwell equations,

$$\nabla \times \vec{E} = -\frac{\partial}{\partial t}\vec{B}, \quad \nabla \times \vec{H} = \frac{\partial}{\partial t}\vec{D}. \tag{2}$$

The resulting wave equation coupling this fluctuation to the propagating field is thus given by

$$\nabla^2\vec{E} = \mu_0\varepsilon\frac{\partial^2}{\partial t^2}\vec{E} + \mu_0\frac{\partial^2}{\partial t^2}(\delta\varepsilon\vec{E}). \tag{3}$$

In the present case, we will be interested in a single frequency, of a given polarization, referring to a mode j of the optical cavity. We can thus separate a slowly varying amplitude of the field A_j from the fast oscillating part,

$$E_j(\vec{r},t) = \mathrm{Re}[A_j(\vec{r},t)\exp(in_jk_jz - i\omega_jt)], \tag{4}$$

with $k_j=\omega_j/c$, where c is the speed of light in vacuum and $n_j=\sqrt{\varepsilon_j/\varepsilon_0}$ is the refractive index. The amplitude includes both the mean value $\bar{A}_j$ and the fluctuations induced by the permittivity,

$$A_j(\vec{r},t) = \bar{A}_j(\vec{r}) + \delta A_j(\vec{r},t). \tag{5}$$

Since we are dealing with the resonant modes in a cavity, the solutions of the wave equation can be limited to the paraxial approximation. The amplitude of the field will satisfy the paraxial wave equation [21], so $\bar{A}_j(\vec{r})=\alpha_ju_j^{(h)}(\vec{r})$, where the transverse mode (h) for the longitudinal mode j can be described in the Hermite or the Laguerre-Gauss basis by the function $u_j^{(h)}(\vec{r})$. The mode amplitude α_j is treated as a constant, an approximation which is valid in the case that field depletion is small.

The wave equation for the fluctuating part can then be solved, in the paraxial approximation, considering a slowly varying envelope for the field fluctuation. Examining the contribution of scattering at the sideband of the carrier, we have, in the frequency domain,

$$\delta A_j(\vec{r},\Omega) = i\frac{n_jk_j}{2\varepsilon_j}\alpha_ju_j^{(h)}(\vec{r})\,\delta\varepsilon_j(\vec{r},\Omega)\,\delta z \tag{6}$$

for a given position of the wave front. Note that this contribution occurs in quadrature with the local field mean amplitude $\alpha_ju_j^{(h)}(\vec{r})$.

The total contribution of the fluctuation for a given field mode, $\delta\alpha_j(z,\Omega)$, can be evaluated using the orthogonality of the basis states $(\int u_j^{(h)}(\vec{r})u_j^{(g)*}(\vec{r})dxdy=\delta_{hg})$. Performing the transverse integration of the fluctuating part of Eq. (5), with the weight factor $u_j^{(h)*}(\vec{r})$ accounting for the coupling of the scattered field into the cavity mode, we have

$$\delta\alpha_j(z,\Omega) = \int \delta A_j(\vec{r},\Omega)u_j^{(h)*}(\vec{r})dxdy. \tag{7}$$

Finally, the total contribution of the fluctuation will include the integration over the crystal length. The resulting added noise will be a fluctuation term, named δQ_j, to be added in the stochastic treatment of the quantum fluctuations inside the cavity. This term is in quadrature with the amplitude α_j of the field. Thus, it can be described as an additional phase noise for an intense mean field,

$$\begin{aligned}\delta Q_j(\Omega) &= -i\int \delta\alpha_j(z,\Omega)dz \\ &= \frac{n_jk_j}{2\varepsilon_j}\alpha_j\int |u_j^{(h)}(\vec{r})|^2\delta\varepsilon_j(\vec{r},\Omega)dxdydz.\end{aligned} \tag{8}$$

As we can see, the random fluctuation in the crystal permittivity will not produce any significant contribution to the amplitude quadrature. The resulting change in the refractive index will only produce phase fluctuations that couple to the resonant cavity mode, within the cavity bandwidth, resulting in an additional source of noise. This noise will be particularly important for experiments in quantum optics, as we observe in the next section, when we add this term to the treatment of quantum fluctuations in the OPO.

A. Excess noise in the OPO

Most of the systems involving second-order nonlinearities inside a cavity can be described by the evolution of the three coupled fields. Let us define our amplitude and phase quadrature operators from the creation operator of the field $\hat{a}=e^{i\theta}(\hat{p}+i\hat{q})$, where the arbitrary phase θ is chosen such that $\langle\hat{q}\rangle=0$. With this choice of θ, quadrature $\hat{p}$ is associated with the amplitude and $\hat{q}$ is associated with the phase in the case of an intense field. In a linearized description of the fields, with $\delta\hat{a}=\hat{a}-\langle\hat{a}\rangle$, field fluctuations are given by the vector

$$\vec{X} = [\delta\hat{p}_0, \delta\hat{q}_0, \delta\hat{p}_1, \delta\hat{q}_1, \delta\hat{p}_2, \delta\hat{q}_2]^T. \tag{9}$$

The operators can be replaced with c numbers using the master equation for the density operator and a quasiprobability representation of the field, such as the Wigner distribution, to obtain a Fokker-Planck equation [22] and its equivalent description by Langevin equations. In this linearized approach, equations for the evolution of field fluctuations inside a cavity are described by the following Langevin equation:

$$\tau\frac{\partial}{\partial t}\vec{X} = \boldsymbol{M_A}\vec{X} + \boldsymbol{M_\gamma}\vec{X}_1^{in} + \boldsymbol{M_\mu}\vec{X}_2^{in} + \vec{Q}, \tag{10}$$

where τ is the round trip time of the wave inside this cavity. The drift matrix $\boldsymbol{M_A}$ describes the evolution of the field fluctuations in a round trip, including attenuation, parametric amplification, and phase shifts. The next two terms couple the input field fluctuations to the cavity through the input coupler (IC) $(\boldsymbol{M_\gamma})$ and the spurious losses $(\boldsymbol{M_\mu})$ and are associated with the diffusion in a Langevin process. This coupling is described by the diagonal matrices

$$\boldsymbol{M_\gamma} = \mathrm{diag}[\sqrt{2\gamma_0}, \sqrt{2\gamma_0}, \sqrt{2\gamma_1}, \sqrt{2\gamma_1}, \sqrt{2\gamma_2}, \sqrt{2\gamma_2}],$$

$$\boldsymbol{M}_{\boldsymbol{\mu}} = \mathrm{diag}[\sqrt{2\mu_0}, \sqrt{2\mu_0}, \sqrt{2\mu_1}, \sqrt{2\mu_1}, \sqrt{2\mu_2}, \sqrt{2\mu_2}], \quad (11)$$

connecting the input fields $\vec{X}_1^{in}$ and vacuum fluctuations $\vec{X}_2^{in}$ through the input ports. In this description, spurious losses in each mode j are given by $2\mu_j$, and the mirror transmission is given by $T_j = 2\gamma_j$.

The excess phase noise coming from the phonons in the crystal is given by the additional contribution to the phase fluctuations [Eq. (8)]. This stochastic fluctuation will be present in the three relevant cavity modes, described by the vector

$$\vec{Q} = [0, \delta Q_0, 0, \delta Q_1, 0, \delta Q_2]^T. \quad (12)$$

In the frequency domain, Eq. (10) can be described by $i\Omega\vec{X} = \boldsymbol{M}_{\boldsymbol{A}}\vec{X} + \boldsymbol{M}_{\boldsymbol{\gamma}}\vec{X}_1^{in} + \boldsymbol{M}_{\boldsymbol{\mu}}\vec{X}_2^{in} + \vec{Q}$, and the intracavity fluctuations will then be given by

$$\vec{X}(\Omega) = [i\Omega\boldsymbol{I} - \boldsymbol{M}_{\boldsymbol{A}}]^{-1}(\boldsymbol{M}_{\boldsymbol{\gamma}}\vec{X}_1^{in} + \boldsymbol{M}_{\boldsymbol{\mu}}\vec{X}_2^{in} + \vec{Q}). \quad (13)$$

Using the input-output formalism [23] we have the fluctuations of the output port of the cavity given by the reflection of the input added to the transmitted internal fluctuation: $\vec{X}^{out}(\Omega) = \boldsymbol{M}_{\boldsymbol{\gamma}}\vec{X}(\Omega) - \vec{X}_1^{in}$. In this case we can easily calculate the covariance matrix of the output field $\boldsymbol{V} = \vec{X}^{out}(\Omega)[\vec{X}^{out}(-\Omega)]^T$, resulting in

$$\boldsymbol{V} = \boldsymbol{I} + \boldsymbol{V}_{pure} + \boldsymbol{V}_{loss} + \boldsymbol{V}_{phase}. \quad (14)$$

The identity matrix $\boldsymbol{I}$ is associated with the standard quantum level (SQL) of noise, characteristic of coherent states (including vacuum). The next term

$$\boldsymbol{V}_{pure} = \boldsymbol{M}_{\boldsymbol{\gamma}}[i\Omega\boldsymbol{I} - \boldsymbol{M}_{\boldsymbol{A}}]^{-1}\boldsymbol{M}_{\boldsymbol{\gamma}}\boldsymbol{M}_{\boldsymbol{\gamma}}\{[-i\Omega\boldsymbol{I} - \boldsymbol{M}_{\boldsymbol{A}}]^{-1}\}^T\boldsymbol{M}_{\boldsymbol{\gamma}} - \boldsymbol{M}_{\boldsymbol{\gamma}}([i\Omega\boldsymbol{I} - \boldsymbol{M}_{\boldsymbol{A}}]^{-1} + \{[-i\Omega\boldsymbol{I} - \boldsymbol{M}_{\boldsymbol{A}}]^{-1}\}^T)\boldsymbol{M}_{\boldsymbol{\gamma}} \quad (15)$$

stands for the squeezing and the quantum correlation leading to entanglement in this system. For unitary intracavity operations, the resulting state will be pure and $\det[\boldsymbol{I} + \boldsymbol{V}_{pure}] = 1$ [24]. There is also a noise term owing to the input fluctuations through the spurious losses, uncorrelated with the reflected fluctuations through the input port, degrading the level of squeezing and/or entanglement and state purity as well,

$$\boldsymbol{V}_{loss} = \boldsymbol{M}_{\boldsymbol{\gamma}}[i\Omega\boldsymbol{I} - \boldsymbol{M}_{\boldsymbol{A}}]^{-1}\boldsymbol{M}_{\boldsymbol{\mu}}\boldsymbol{M}_{\boldsymbol{\mu}}\{[-i\Omega\boldsymbol{I} - \boldsymbol{M}_{\boldsymbol{A}}]^{-1}\}^T\boldsymbol{M}_{\boldsymbol{\gamma}}. \quad (16)$$

Finally, the internal added noise will depend on the covariance matrix for the additional phase fluctuations $\boldsymbol{V}_{\boldsymbol{Q}}(\Omega) = \vec{Q}(\Omega)\vec{Q}^T(-\Omega)$, affected by the cavity interaction and the nonlinear coupling given by the drift matrix $\boldsymbol{M}_{\boldsymbol{A}}$,

$$\boldsymbol{V}_{phase} = \boldsymbol{M}_{\boldsymbol{\gamma}}[i\Omega\boldsymbol{I} - \boldsymbol{M}_{\boldsymbol{A}}]^{-1}\boldsymbol{V}_{\boldsymbol{Q}}(\Omega)\{[-i\Omega\boldsymbol{I} - \boldsymbol{M}_{\boldsymbol{A}}]^{-1}\}^T\boldsymbol{M}_{\boldsymbol{\gamma}}. \quad (17)$$

A detailed evaluation of the terms in the covariance matrix $\boldsymbol{V}_{\boldsymbol{Q}}$ will be given in Sec. V. For the moment, considering the fluctuation term presented in Eq. (8), we expect that the covariance terms of this extra noise are given by

$$\langle \delta Q_j(\Omega)\delta Q_k(-\Omega)\rangle = \frac{n_j k_j n_k k_k}{4\varepsilon_j\varepsilon_k}\sigma_{jk}\alpha_j\alpha_k = \eta_{jk}\sqrt{P_j P_k}. \quad (18)$$

The noise coupling term η_{jk} depends on the wavelength through k_j and k_k and on the evaluation of the double integration coming from the product of Eq. (8) for two different modes, resulting in σ_{jk}. Here we have used the fact that the intracavity amplitude of the field α_j is proportional to the square root of the intracavity power P_j.

From this simple model, a wide variety of experiments involving two or three fields coupled by nonlinear effects can be studied, implying in different forms of matrix $\boldsymbol{M}_{\boldsymbol{A}}$ in Eq. (10). In the case that signal and idler modes are degenerate, as in a degenerate OPO, seeded optical parametric amplifier (OPA), subthreshold OPO, and SHG, the problem can be reduced to the evaluation of a matrix of size 4×4. In the case of a cavity without nonlinear interaction, the drift matrix is reduced to $\boldsymbol{M}_{\boldsymbol{A}} = -(\boldsymbol{M}_{\boldsymbol{\gamma}}^2 + \boldsymbol{M}_{\boldsymbol{\mu}}^2)/2$. For a nondegenerate unseeded OPO above threshold, with balanced losses for the signal and idler modes ($\gamma_1 = \gamma_2 = \gamma$ and $\mu_1 = \mu_2 = \mu$), the drift matrix has a simple form in the case of exact resonance (zero detuning) [25],

$$\boldsymbol{M}_{\boldsymbol{A}} = \begin{bmatrix} -\gamma_0' & 0 & -\gamma'\beta & 0 & -\gamma'\beta & 0 \\ 0 & -\gamma_0' & 0 & -\gamma'\beta & 0 & -\gamma'\beta \\ \gamma'\beta & 0 & -\gamma' & 0 & \gamma' & 0 \\ 0 & \gamma'\beta & 0 & -\gamma' & 0 & -\gamma' \\ \gamma'\beta & 0 & \gamma' & 0 & -\gamma' & 0 \\ 0 & \gamma'\beta & 0 & -\gamma' & 0 & -\gamma' \end{bmatrix}, \quad (19)$$

with the coefficient β being given by the ratio of the amplitude for signal and idler fields α by the pump field amplitude α_0,

$$\beta = \frac{\alpha}{\alpha_0} = \sqrt{\frac{\gamma_0}{\gamma}}\sqrt{\sqrt{\frac{P_{in}}{P_{th}}} - 1}, \quad (20)$$

where P_{in} is the input power of the pump beam and P_{th} is the oscillation threshold. $2\gamma_0' = 2(\gamma_0 + \mu_0)$ and $2\gamma' = 2(\gamma + \mu)$ are the sum of round trip losses. Before we apply this model to the OPO described in Ref. [19], we will characterize the coupling terms η_{jk} of Eq. (18), describing the dependence of the noise matrix $\boldsymbol{V}_{\boldsymbol{Q}}$ with the intracavity power for each mode. This can be done by injection of a classical coherent field in each mode of the cavity involved in the parametric oscillation and studying the dependence of the phase noise of the output field with the intracavity power (proportional to the incident power).

III. EXPERIMENTAL CHARACTERIZATION OF THE EXCESS NOISE

We investigated the spurious excess noise using the experimental system as described in [19], reproduced here in Fig. 1. The cavity is pumped by the second harmonic of a Nd:yttrium aluminum garnet (YAG) laser (Innolight Diabolo), filtered with a mode cleaning cavity to ensure that

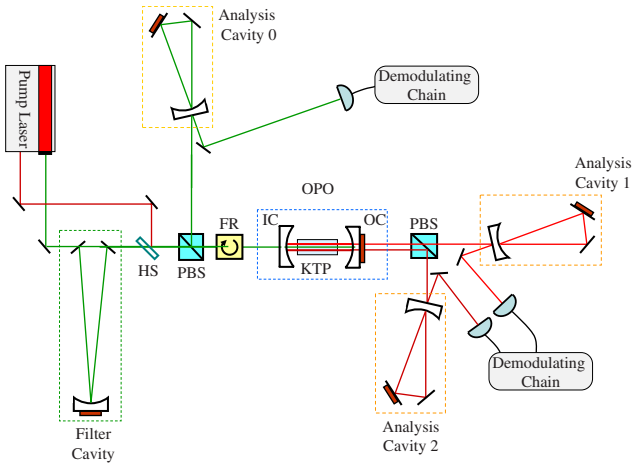

FIG. 1. (Color online) Setup for the experiment. Pump laser: Innolight Diabolo, HS: harmonic separator and combiner, and PBS: polarizing beam splitter. Filtering cavity, analysis cavities, and OPO as described in the text.

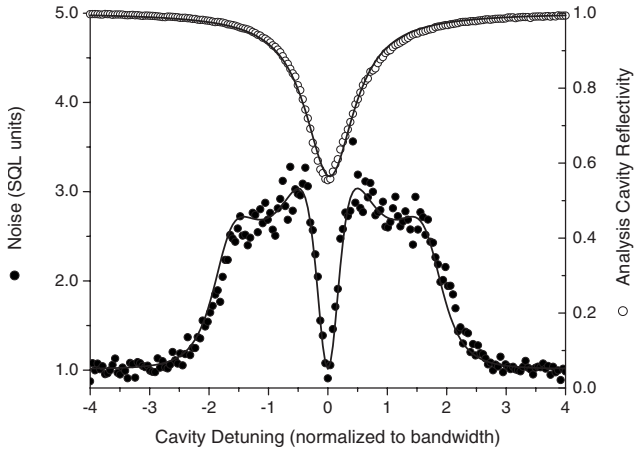

FIG. 2. Measurement of phase noise using the reflection off an empty cavity. The intensity noise of the reflected beam is normalized to the shot-noise level and fitted according to [25], returning the phase and amplitude variances. The reflectivity of the cavity is fitted by a Lorentzian.

pump fluctuations are reduced to the SQL for frequencies above 20 MHz. The filter cavity bandwidth is 2.3 MHz, and its transmission is 55% for the carrier frequency. The filtered pump beam is then injected in the OPO, with adjustable power, through the IC with a reflectivity of 70% for the pump field (532 nm). The reflected pumped field is recovered from the Faraday rotator (FR). The infrared output coupler (OC) has a reflectivity of 96% at ≈ 1064 nm. Both mirrors are deposited on concave substrates with a curvature radius of 50 mm. The crystal is a bulk high gray-tracking resistant potassium titanyl phosphate (HGTR-KTP, by Raicol Crystals) cut for type-II phase matching, with length $\ell = 12$ mm, and antireflective coating for both wavelengths. The average free spectral range for the three modes is 5.1(1) GHz. The cavity finesses for pump, signal, and idler modes (the latter defined as the mode with the same polarization as the pump) are, respectively, 16, 135, and 115. The overall detection efficiencies are 87% for the infrared beams and 65% for the pump, accounting for detector efficiencies and losses in the beam paths. An infrared beam could be injected in the OPO cavity using a harmonic beam splitter (HS). Its polarization could be adjusted with a half-wave plate (not shown) to match each mode of the cavity with the birefringent crystal inserted.

In this setup, the initial study of the excess noise produced inside the cavity was done by the injection of an intense field in each one of the modes involved in the OPO. In all the measurements presented here, care was taken to avoid phase matching for the relevant parametric processes of up and down conversions. The absence of stimulated parametric conversion was assured by keeping the pump beam below the OPO threshold. For the infrared injection, second-harmonic generation is avoided by careful temperature tuning of the crystal. All measurements were made keeping the OPO at exact resonance by a simple dither-and-lock technique applied to the cavity length using a piezo actuator on the input coupler. Mode 0 (which corresponds to the pump mode in the OPO) is investigated by the injection of the 532 nm beam, polarized in the xy plane (referring to crystallographic axes), through the input coupler for the pump mode. The noise and the total power of the reflected field are then measured. Mode 1 (signal mode) is investigated by the injection of the 1064 nm beam through the input coupler, which has a very small transmittance at this wavelength ($<0.2\%$), with polarization parallel to the z axis of the crystal. Mode 2 (idler mode) is investigated with light at the same frequency, with polarization parallel to the xy plane. In both cases, the noise properties of the transmitted light are analyzed.

Phase noise measurements were performed using the ellipse rotation method described in [26,27], with the help of analysis cavities. Cavities 1 and 2 (for the transmitted infrared beams) have bandwidths of 14(1) MHz, and cavity 0 (for the reflected pump) has a bandwidth of 12(1) MHz. This ensures a full rotation of the noise ellipse [25] for the chosen analysis frequency of 21 MHz. Mode matching of the beams to the analysis cavities was better than 95%.

An example of such a measurement is presented in Fig. 2, where the intensity noise of the beam reflected by the cavity is fitted according to [25], returning the values of the variance of amplitude and phase quadrature noises. Noise was measured using a demodulating chain and an analog-to-digital (A/D) converter, and each measured correlation value was an average of 1000 points, acquired with a bandwidth of 600 kHz. SQL calibration was obtained by the measurement of the variance of a coherent field at different intensities, showing a linear dependence with the beam power. Linearity is verified with great precision, such that the shot-noise level is determined within 0.5% [28].

The covariance terms $\Delta^2 Q_k(\Omega)$ from the matrix $\boldsymbol{V_Q}$ and their dependence on the intracavity power are obtained from the excess noise measured from the reflected beam (532 nm) or from the transmitted beam (1064 nm), applying the model of Eq. (14) with the drift matrix $\boldsymbol{M_A}$ for uncoupled fields. The measured variance for amplitude and phase quadratures of mode 0 is shown in Fig. 3 (left) for different values of the

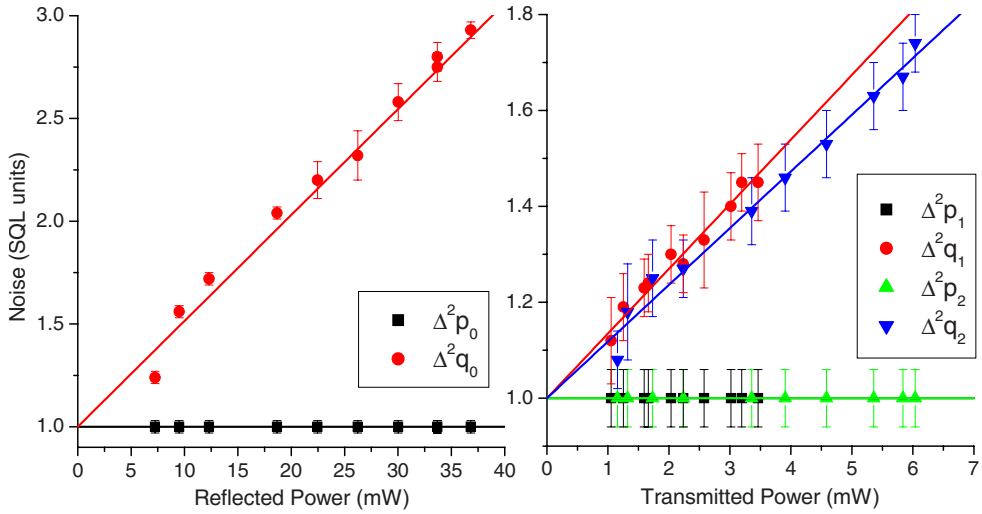

FIG. 3. (Color online) Measured variances for each mode of the field, as a function of the output power. Left: reflected light from the cavity for mode 0 (532 nm). Right: transmitted light for modes 1 and 2 (1064 nm).

reflected power. Amplitude fluctuations remain at the shot-noise level and the phase quadrature presents an excess noise which varies linearly with the power, consistent with the results observed in [14]. Similar results were obtained for modes 1 and 2 (Fig. 3, right). The small transmission of the input coupler provided a strong attenuation of the ir beam, and the measured results for the cavity transmission without the crystal revealed that the noise level of both quadratures for the transmitted beam were reduced to the standard quantum level. Thus, any excess noise at this wavelength is provided by the crystal and occurs only for the phase quadrature, as expected.

The results agree well with the description of a linear dependence of the internal noise with the light power (from Eq. (18), $\Delta^2 Q_j = \eta_{jj} P_j$). Using the measured mirror coupling and losses for this cavity, the noise coupling terms η_{jj} relating the added noise to internal circulating power are

$$\eta_{00} = 0.53 \text{ per Watt}, \quad \eta_{11} = 0.15 \text{ per Watt},$$

$$\eta_{22} = 0.14 \text{ per Watt}. \tag{21}$$

Uncertainties of these values are mainly due to their local dependence with the point of the crystal where the beam is injected. Lateral displacements of the crystal resulted in changes on the order of 20%. The first point to notice is the ratio of the coupling constant to the wavelength. We have $\eta_{11} \simeq \eta_{22}$, and $\eta_{00}/\eta_{11} = 3.7(5)$, in good agreement with the dependence expected from Eq. (18).

After the characterization of the diagonal terms in the covariance $\boldsymbol{V}_Q$, we studied the cross correlation terms using simultaneous injection of two modes. The crystal temperature is carefully tuned in order to obtain cavity double resonance, while keeping the third mode far from resonance, thereby avoiding system oscillation owing to the injection of a seed in the parametric process.

As a result, the curves plotted in Fig. 4 show that the correlation depends on the square root of the power of each beam. Similar results were obtained for the noise correlation between modes 0 and 2 and modes 1 and 2. From the fitting of these curves we can evaluate the following noise coupling terms:

$$\eta_{01} = 0.14 \text{ per Watt}, \quad \eta_{02} = 0.15 \text{ per Watt},$$

$$\eta_{12} = 0.087. \text{ per Watt} \tag{22}$$

Although the uncertainties are somewhat high (about 20%), the confidence band ensures that correlations are not perfect ($\eta_{jk} < \sqrt{\eta_{jj}\eta_{kk}}$), differently from the treatment in Ref. [17].

We conclude that the generated phase quadrature noise depends linearly on the intracavity power, as described in Ref. [29], but that the noises of different beams are not perfectly correlated. Moreover, amplitude fluctuations remain uncoupled from this additional noise source. After this characterization, we independently measured all the parameters involved in the evaluation of the covariance matrix of the OPO presented in Eq. (14). Now we compare the results obtained from the model, after the parameters' evaluation, with the experimental results.

IV. NOISE IN THE ABOVE-THRESHOLD OPO

In order to study the noise properties in the OPO, we removed the injected infrared field and increased the power of the green beam, pumping the OPO above threshold. We measured the covariance terms for many different values of input power, ranging from 1 to 1.7 times the threshold power of 70 mW. In the following, we present the experimental data obtained, with its uncertainties, and the expected values from our model. We also include the theoretical predictions in the absence of the additional phonon noise.

According to the model, covariance matrix terms for the amplitude quadratures are unaffected by this additional phase noise, and the results do not change by its inclusion. The results in this case are shown in Fig. 5 for the amplitude variances and for the amplitude correlations. The plots are obtained from the model using measured detection efficiency

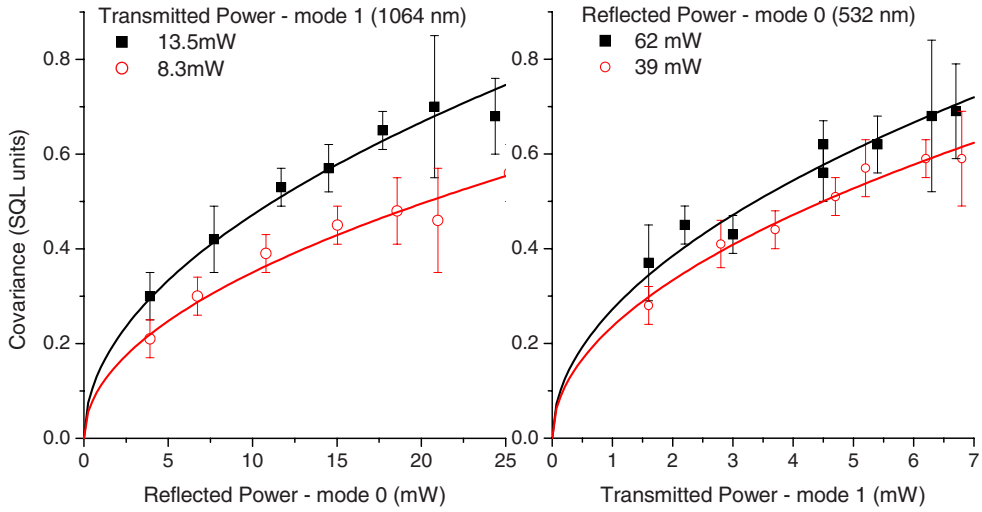

FIG. 4. (Color online) Left: covariance of phase quadratures of modes 0 and 1 (orthogonally polarized modes) as a function of the reflected power for different transmitted powers of mode 1. Right: the same but varying power of mode 1 for two different values of power in mode 0.

and cavity parameters, without any free parameters. Good agreement is observed, although the amplitude fluctuations of the signal mode are slightly smaller than expected. Noise covariances involving two fields are in very good agreement with the theory.

For the phase quadrature, the fluctuations of the refractive index scatter light from the carrier (the mean-field amplitude) into the sidebands at 21 MHz. The resulting noise in the output combines the contributions from the parametric process and from this additional noise term. Our results are presented in Fig. 6 for the covariances of the phase quadrature fluctuations. The curves are obtained from the values of cavity parameters and from the measured noise terms given in Eqs. (21) and (22) applied to Eq. (14). Good agreement is obtained for the variances of signal and idler (Fig. 6, left). As for the pump, the measured noise level was smaller than expected, but its dependence with the pump power presents good qualitative agreement. The results are, nevertheless, much closer to the presented model with extra noise than to the OPO model without additional noise (open symbols in the plot), which predicts squeezing for the pump and a nearly constant noise for signal and idler. The agreement for the cross covariance terms is even better (Fig. 6, right), with a very good agreement for the correlations of pump with signal and idler, and a qualitative agreement for signal and idler correlation. The expected values without additional noise fail to describe the observed results. The unbalance of signal and idler correlations with the pump mode can be understood in view of the simplified model for the drift matrix $\boldsymbol{M_A}$, where balanced losses for these modes are used. The good qualitative agreement for these results could be improved by fitting the curves using the noise coupling η_{jk} as an adjustable parameter.

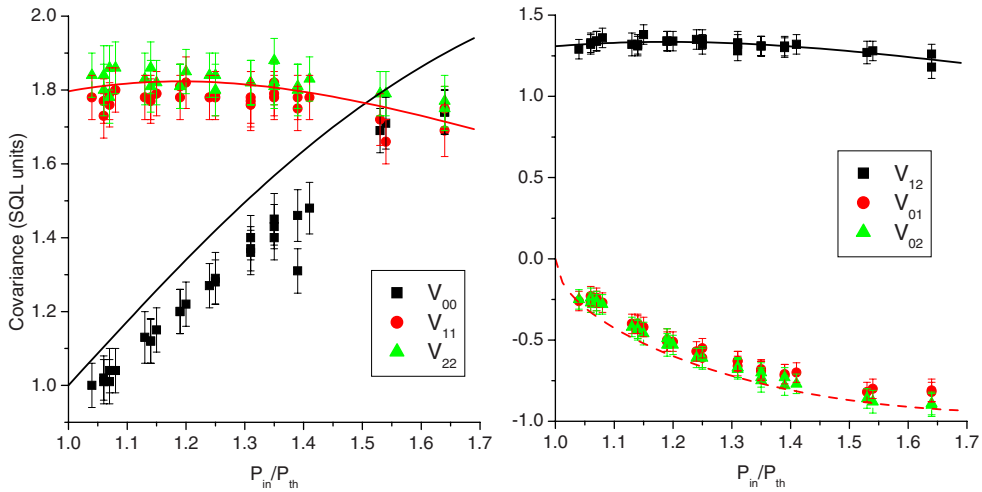

FIG. 5. (Color online) Covariance terms of the amplitude quadratures in the OPO operating above threshold, as a function of the pump power (normalized to threshold). The lines are obtained from the model, without any fitting. Left: variance for pump (0), signal (1), and idler (2). Right: covariances involving pairs of fields.

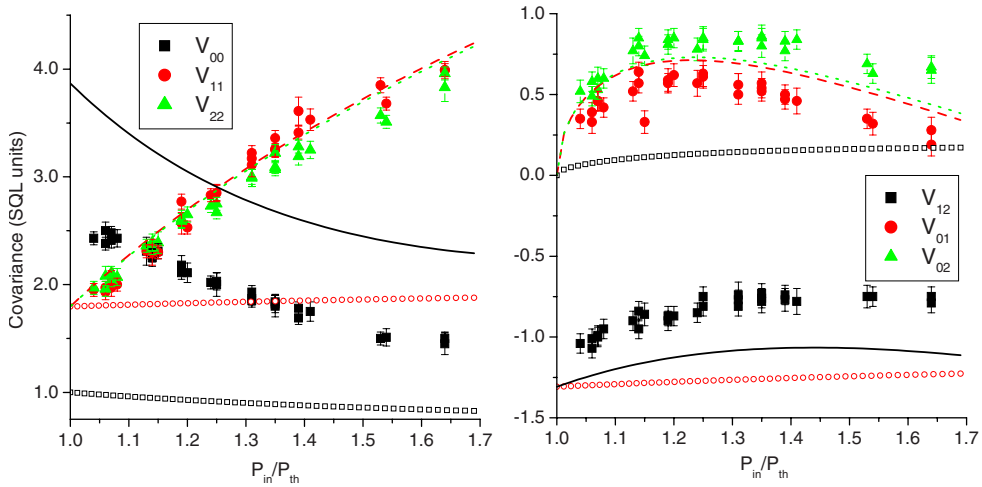

FIG. 6. (Color online) Covariance of the phase quadratures in the OPO operating above threshold, as a function of the pump power (normalized to threshold). The lines are obtained from the model, without any fitting. Open symbols refer to the model, without additional noise. Left: variance for pump (0), signal (1), and idler (2). Right: covariances involving pairs of fields.

Thus, the model allows us to consistently explain the previously unexpected OPO measurements reported in [19]. Correlations among all three fields are now accounted for and we can explain why the predicted pump-signal-idler tripartite entanglement was not observed for these levels of additional noise. Two challenges remain: how can we ascertain that the physical origin of the noise is related to phonons in the crystal and how can we control and reduce it to achieve tripartite entanglement. This is discussed in the following section, where we present a detailed theory for the phonon noise in the crystal and verify experimental signatures of its predictions. Then, we also apply our model to other systems described in the literature, where the same kind of phase quadrature noise behavior was reported.

V. PHONON NOISE COUPLING

In order to develop a model that relates the crystal vibration to the phase fluctuations of the fields in their propagation through the crystal, we have to consider the modulation of the permittivity by the local displacement of each part of the crystal. This displacement is represented by a field of local dislocations $\vec{u}(\vec{r})$, where $\vec{r}$ is a position in the crystal. Displacements involving an overall crystal displacement or rotation do not contribute to any change in the crystal energy [30,31] and therefore cannot affect the dielectric constant. The important quantity, in this case, is the strain

$$S_{lm} = \frac{1}{2}\left[\frac{\partial u_m(\vec{r})}{\partial x_l} + \frac{\partial u_l(\vec{r})}{\partial x_m}\right] \tag{23}$$

that is a six-element vector (with $lm=[xx,yy,zz,yz,xz,xy]$). The strain vector $\vec{S}$ is coupled to the fluctuations of the dielectric tensor $\delta\boldsymbol{\varepsilon}$ by a rank 4 photoelastic tensor [32],

$$\delta\varepsilon_{id} = -\frac{\varepsilon_i\varepsilon_d}{\varepsilon_0}\sum_{lm} p_{idlm}S_{lm}. \tag{24}$$

In the present case, looking for the contribution of the strain to the propagating field, we can restrict this study to the polarization term that is collinear with the electric field and limit the problem to the case $i=j$. We will therefore keep the short notation $\delta\varepsilon_i=\delta\varepsilon_{ii}$ used in Eq. (6).

In order to evaluate the correlation of the phase fluctuations, we can apply Eq. (24) to Eq. (8), obtaining

$$\begin{aligned}\langle\delta Q_j(\Omega)\delta Q_k(-\Omega)\rangle &= k_jk_k\frac{n_j^3n_k^3}{4}\alpha_j\alpha_k\int |u_j(\vec{r})|^2|u_k(\vec{r}')|^2 \\ &\quad\times\sum_{(lm),(np)} p_{jjlm}p_{kknp}\langle S_{lm}(\vec{r},\Omega)S_{np}(\vec{r}',-\Omega)\rangle d\vec{r}d\vec{r}'.\end{aligned} \tag{25}$$

The integration involves a convolution of the intensity profile of each field by the correlation of the noisy strain vector, implying in an accurate knowledge of this correlation. Nevertheless, further understanding of the scattering process can be obtained if we consider some specific conditions of operation and some assumptions involving this correlation term.

For the case where the beam waist inside the crystal is larger than the coherence length l_c of the acoustic waves of thermal origin, we can approximate the correlation by a delta function,

$$\langle S_{lm}(\vec{r},\Omega)S_{np}(\vec{r}',-\Omega)\rangle = S_{lm}^2(\Omega)\delta_{lm,np}\delta(\vec{r}-\vec{r}')l_c^3, \tag{26}$$

where $S_{lm}(\Omega)$ is the root-mean-square (rms) value of the strain fluctuation at a given frequency Ω. In this case, integration of the amplitude envelope of the field in the paraxial approximation is simplified. For fundamental Gaussian modes of waist $w_j(z)$, integration over the crystal volume gives an effective waist for the field w_{jk},

$$\int |u_j(\vec{r})|^2 |u_k(\vec{r})|^2 d\vec{r} = \int \frac{2}{\pi} \frac{1}{w_j^2(z) + w_k^2(z)} dz = \frac{\ell}{\pi w_{jk}^2}. \tag{27}$$

The noise coupling coefficient is inversely proportional to the (effective) area of the beam inside the crystal. Considering that the noise is also proportional to the power, the integration implies in an averaging of the intensity over the crystal volume. The resulting noise is thus proportional to the intensity of the field inside the crystal.

Finally, the product of the photoelectric tensor will result in a coupling term

$$c_{jk}(\Omega) = \sum_{lm} p_{jjlm} p_{kklm} S_{lm}^2(\Omega) \tag{28}$$

obtained by the scalar product of two vectors of six dimensions. If the vectors are not collinear in this six-dimensional space, we expect to have $c_{jk} < \sqrt{c_{jj} c_{kk}}$. Strain fluctuations will therefore couple differently to each field, resulting in imperfect correlation of the additional phase noise.

Expressing the amplitudes $\alpha_j = \sqrt{P_j/(h\nu_j)}$ in such a way that $|\alpha_j|^2$ is the photon flux per second in the wave front of the mode, we have

$$\langle \delta Q_j(\Omega) \delta Q_k(-\Omega) \rangle = k_j k_k \frac{n_j^3 n_k^3}{4hc} l_c^3 c_{jk}(\Omega) \left(\frac{\ell \sqrt{\lambda_j \lambda_k}}{\pi w_{jk}^2} \right) \sqrt{P_j P_k}$$
$$= \eta_{jk} \sqrt{P_j P_k}. \tag{29}$$

Some important conclusions can be inferred. Wavelength dependence of the noise coupling η_{jk} is restricted to the wavevector modulus k_j. The term in parentheses is equivalent to the ratio of the crystal length to the effective Rayleigh length of the cavity [32]. The cavity geometry determines the beam waist as well, resulting in a noise that is proportional to the intensity. The evaluation of c_{jk} also explains the reason for having $\eta_{jk} < \sqrt{\eta_{jj} \eta_{kk}}$, leading to the expected imperfect noise correlations for the phonon noise contribution to each field: $\langle \delta Q_j(\Omega) \delta Q_k(-\Omega) \rangle < \sqrt{\Delta^2 Q_j(\Omega) \Delta^2 Q_k(\Omega)}$.

As for the coupling c_{jk}, its direct evaluation is rather cumbersome, but we can use the fact that the acoustic energy density per unit volume V is related to the strain field as $E/V = \rho v_s^2 S^2/2$ [32], where the crystal density is ρ and v_s is the speed of sound. To the first approximation, acoustic phonons can be considered to follow the Bose-Einstein distribution [31] and at temperature T their mean energy is

$$E = \sum_s h\Omega_s \left[\frac{1}{\exp[h\Omega_s/(k_B T)] - 1} + \frac{1}{2} \right], \tag{30}$$

where different modes s imply in different wave vectors and transverse or longitudinal component. For a given frequency $\Omega \ll k_B T/h$, the dependence of the energy density on the temperature is linear. The coupling term c_{jk} should have a linear behavior with temperature.

Very few parameters involved in the value of η_{jk} in Eq. (29) can be controlled, in an attempt to reduce the contribution of this noise in quantum optics experiments. Finding crystals with smaller refractive index and photoelastic effects, while maintaining high optical nonlinearities, is not a trivial task. On the other hand, cavity parameters (changing the field's spatial profile) and crystal temperature can be changed in order to reduce the extra noise.

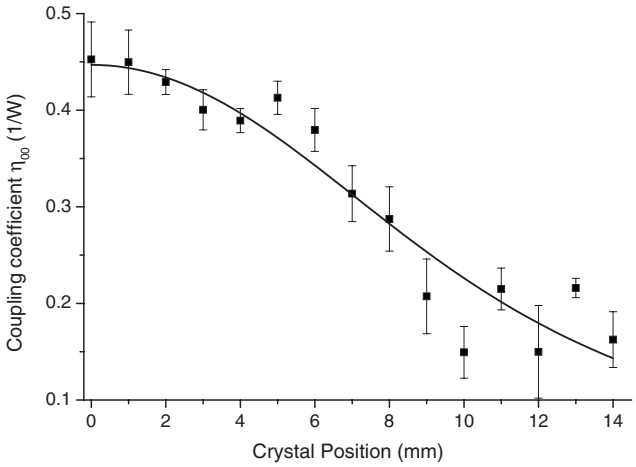

FIG. 7. Noise coupling term η_{00} as a function of the position of the crystal inside the cavity. Solid line is a fit to Eq. (31).

A. Intensity dependence

In order to make the study of the noise dependence on the effective beam waist inside the crystal, we replaced the OPO cavity with a nearly concentric cavity comprising two spherical mirrors of curvature radius $R = 25$ cm, separated by 62.6 mm, resulting in a beam waist of $w_0 = 27.8$ μm. The resulting Rayleigh length was $z_0' = n\pi w_0^2/\lambda = 8.13(10)$ mm, where $n = 1.788$ is the refractive index for mode 0 (532 nm, polarized in the xy plane). Input coupler transmittance is $T = 2\gamma = 12.0\%$ and internal losses amount to $2\mu = 3.3\%$. We measured the noise coupling for different crystal positions, obtaining different values for the effective waist w_{00}. For different positions z of the crystal relative to the position of the cavity waist, we expect to have, from Eq. (27),

$$\frac{\ell\lambda}{\pi w_{00}^2(z)} = n \left\{ \arctan\left(\frac{2z + \ell}{2z_0'} \right) - \arctan\left(\frac{2z - \ell}{2z_0'} \right) \right\}, \tag{31}$$

resulting in the term in parentheses in Eq. (29). As we can see, this term depends only on the cavity geometry (that determines the Rayleigh length), on the crystal length ℓ, and on the refractive index. The results for the evaluation of the noise coupling at different positions inside the cavity are presented in Fig. 7. The value of η_{00} is fitted to Eq. (31) with an overall multiplicative factor as the single adjustable parameter, providing good agreement with the theory.

Therefore, the reduction in the waist inside the crystal increases the noise coupling. On the other hand, it will also reduce the threshold power. Both effects tend to compensate each other. According to Eq. (29), the noise level depends on the intensity, as does the parametric amplification [33]. For this reason, changes in the cavity geometry are not expected to significantly affect the contribution of the phonon noise, even though the threshold power is reduced.

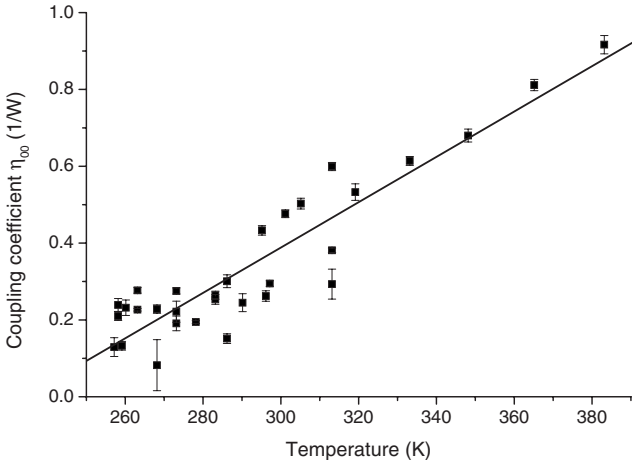

FIG. 8. Temperature dependence of the noise coupling. Data points for temperatures above 300 K were obtained in a single experimental run. For lower temperatures, data points were obtained on different days, leading to the increased dispersion observed. Nevertheless, a clear trend is observed.

B. Temperature dependence

In order to analyze the temperature dependence of the noise coupling constant η_{00}, we returned to the original OPO cavity configuration and controlled the crystal temperature, heating it above room temperature. As discussed, noise power is expected to be proportional to the temperature. Indeed, as can be seen in Fig. 8, the results in the range from 257 to 383 K can be adjusted by a linear fit with $\eta_{00}(T) = [5.92(46)\times 10^{-3}T\ [\mathrm{K}] - 1.38(13)]$ per Watt. This monotonic increase in noise with temperature agrees qualitatively with the naive model of the phonon noise, although the slope of the curve does not match the parameters in Eqs. (29) and (30). Furthermore, it can be extrapolated to zero for a finite temperature. This discrepancy can be explained by the fact that the simplified model does not account for the temperature dependence of the photoelastic tensor, the crystal density, or the speed of sound, and a more complex behavior is expected. Nevertheless, this result shows consistently that cooling the crystal reduces the phonon noise. On the other hand, nonlinear crystals such as $LiNbO_3$, where phase matching is obtained by heating the crystal above 370 K, should give an increased contribution from this noise.

VI. APPLICATION TO OTHER EXPERIMENTS

The additional phase noise treated here has been observed in different OPOs by several research groups. In a first attempt to understand its origin [14], we observed excess phase noise in the reflected pump beam, which grew linearly with the incoming pump power below threshold. Since the intracavity pump power above threshold remains constant, this extra noise was initially modeled as a constant noise, similar to what would be expected from a noisy input pump [25].

Peng *et al.* [15] investigated the effect of pump excess noise in the phase correlation between signal and idler fields as well. Afterward, they included in their model a gain for the pump phase noise [16] and applied this model to the analysis of previous results obtained from different groups. In those models, the noise source remained in the pump, while signal and idler were coupled to this noise source only through the parametric process. As such, perfectly correlated classical noise between signal, idler, and pump beams would be created, in contradiction to the observed discrepancies [19]. The observation of tripartite entanglement, for instance, would have been easier.

Another model for this excess noise was recently proposed and applied to the study of bipartite entanglement between the fundamental and the second harmonic in parametric conversion [17]. The phase noise introduced is proportional to the field amplitude, and it is presented as guided acoustic wave Brillouin scattering (GAWBS) [29]. In this case, crystal absorption would be the origin of this extra noise term.

Our model relies on the intrinsic fluctuations of thermal origin in the refractive index, which scatter photons from the carrier into the noise sidebands. Here we extend our model to other experiments. In what follows, based on the cavity parameters (losses, threshold power, free spectral range, and detection efficiency) and the measured results of entanglement or squeezing, we calculate the values of the noise coupling terms η_{jk}. In order to simplify the number of free parameters, we assumed that all the noise couplings scale according to the values independently obtained in our experiment [Eqs. (21) and (22)]. Therefore we kept $\eta_{11}=\eta_{22}=\eta_{00}/4$, $\eta_{01}=\eta_{02}=0.27\eta_{00}$, and $\eta_{12}=0.16\eta_{00}$ and evaluated the value of η_{00} using the model of Eq. (14).

Previous measurements of bipartite entanglement in our laboratory employed another OPO cavity used in Refs. [14,28]. Noise in these systems could be correctly fitted with $\eta_{00}=0.72$ per Watt. In the first demonstration of bipartite entanglement in the above-threshold OPO [11], a value $\eta_{00}=0.64$ per Watt accounts for the difference of 0.21 units of SQL between the measured quadrature noise and the expected value from the theory without additional noise.

Extending this analysis to other measurements, we carried out the analysis for the frequency-degenerate OPO studied in Ref. [10]. In their case, the expected value for the phase quadrature correlation would give a noise level of 47% of the SQL. Instead, they measured excess noise of twice the SQL. A noise coupling $\eta_{00}=1.16$ per Watt would explain their results.

Other experiments presented unaccounted sources of excess noise. For instance, in a cascaded $\chi^{(3)}$ process [9], pump squeezing reached only 6% (pump noise equal to 94% of SQL) in the phase quadrature that could be explained with $\eta_{00}=0.24$ per Watt. This is a reasonable value, considering here that they used a periodically poled lithium niobate (PPLN) crystal pumped at 1.064 μm, which is half the wavelength of the other experiments.

Recently, entanglement between fundamental and second harmonic in process of up or down conversion in a cavity was demonstrated. From the work of Ref. [17], using a degenerate OPO and SHG with injection at both wavelengths, we could calculate the relation of the constants η_{kk} using the given value for the parameter ξ_k, obtaining values of $\eta_{00}=0.77$ per Watt and $\eta_{11}=0.19$ per Watt.

All those experiments, involving different crystals, wavelengths, and configurations, returned values for the noise coupling of the same magnitude of the results obtained in the present paper. Other experiments with the OPO, such as twin beam generation, involved only amplitude quadratures. Thus, they were free from this excess noise source. The reported values of squeezing matched the expected results once the technical problems were taken in account. The fact that amplitude noise is uncoupled from the fluctuation in the refractive index due to phonons inside the crystal is a good reason why they were observed long before phase quadrature squeezing and entanglement.

On the other hand, the experiment of squeezing in SHG [7] was performed with a scanning cavity that presented squeezing at exact resonance but with very high excess noise for nonzero detuning. In this case, amplitude and phase noise are coupled in the drift matrix, and the excess phase noise owing to the additional phonon noise, expected to be present in that case, was coupled to the amplitude.

For experiments with the OPO below threshold, the pump field acts as a classical field, driving the parametric process, and therefore the noise remains uncoupled. Since these experiments have negligible intracavity power for the generated vacuum modes, the scattering of the central carrier can be neglected. Nevertheless, it may still act as an extra loss source and may need to be considered when attempting to obtain very high levels of squeezing.

Not all the other experiments considered could be successfully analyzed by our model. Exceptions, resulting in smaller values for the noise coupling η were observed. In a letter by Peng *et al.* [12], the difference of 10% of SQL between theory and measurement could be explained by a value of $\eta_{00}=0.68\times10^{-2}$ per Watt, which is much smaller than the value obtained in the present paper. Another communication by Pfister *et al.* [13] would yield $\eta_{00}=0.84\times10^{-1}$ per Watt for the difference of 14.2% of the SQL in the phase correlation. In both cases an (almost) open cavity for the pump mode (very low cavity finesse) was employed. This invalidates the assumption of small losses for the pump mode used in the present model.

VII. CONCLUSION

We analyzed the unexpected phase noise observed in optical parametric oscillators and developed a model that agrees well with the experimental results. The origin of the noise was determined to be the random fluctuations of the refractive index (or the crystal permittivity) induced by thermal phonons within the crystal. This fluctuation scatters light from the mean field into the noise sidebands, acting as an additional noise source in quantum optics measurements.

The noise source was characterized for a cavity with a KTP crystal, and the observed results agree well with the model regarding the noise dependence with power, cavity geometry, wavelength, and temperature dependence. The latter is the strongest evidence of the role played by the phonons. We applied the noise model to the OPO and observed good agreement with the experiment.

Other systems reported in the literature were analyzed, and the model consistently succeeded in explaining discrepancies between the theory without extra noise and the observed results. The additional noise value we have inferred for most of the experiments was on the same order of magnitude of the noise we measured in the present paper. This indicates that such an effect may have to be considered in designing other quantum optical systems with nonlinear crystals inside cavities.

Our recent research has been driven by a quest for three-color tripartite pump-signal-idler entanglement in the above-threshold OPO [18,19]. Previous attempts were frustrated by the presence of this extra noise source of then unknown physical origin. Following the results presented here, by lowering the crystal temperature, we finally succeeded in experimentally observing the direct generation of tripartite entanglement [34], producing three entangled fields of different colors. We expect interesting applications in quantum information for this unusual light source.

ACKNOWLEDGMENTS

We acknowledge partial support from Conselho Nacional de Desenvolvimento Científico e Tecnológico (CNPq), Coordenação de Aperfeiçoamento de Pessoal de Nível Superior (CAPES), and Deutscher Akademischer Austausch Dienst (DAAD). M.L. acknowledges support from the Alexander von Humboldt Foundation.

[1] A. Furusawa, J. L. Sørensen, S. L. Braunstein, C. A. Fuchs, H. J. Kimble, and E. S. Polzik, Science **282**, 706 (1998).
[2] Jacob F. Sherson, Hanna Krauter, Rasmus K. Olsson, Brian Julsgaard, Klemens Hammerer, Ignacio Cirac, and Eugene S. Polzik, Nature (London) **443**, 557 (2006).
[3] S. L. Braunstein and P. van Loock, Rev. Mod. Phys. **77**, 513 (2005).
[4] L. A. Wu, H. J. Kimble, J. L. Hall, and H. F. Wu, Phys. Rev. Lett. **57**, 2520 (1986).
[5] A. Heidmann, R. J. Horowicz, S. Reynaud, E. Giacobino, C. Fabre, and G. Camy, Phys. Rev. Lett. **59**, 2555 (1987).
[6] Z. Y. Ou, S. F. Pereira, H. J. Kimble, and K. C. Peng, Phys. Rev. Lett. **68**, 3663 (1992).
[7] A. Sizmann, R. J. Horowicz, G. Wagner, and G. Leuchs, Opt. Commun. **80**, 138 (1990).
[8] M. D. Reid and P. D. Drummond, Phys. Rev. Lett. **60**, 2731 (1988); Phys. Rev. A **40**, 4493 (1989).
[9] K. S. Zhang, T. Coudreau, M. Martinelli, A. Maitre, and C. Fabre, Phys. Rev. A **64**, 033815 (2001).
[10] J. Laurat, T. Coudreau, L. Longchambon, and C. Fabre, Opt. Lett. **30**, 1177 (2005).
[11] A. S. Villar, L. S. Cruz, K. N. Cassemiro, M. Martinelli, and P. Nussenzveig, Phys. Rev. Lett. **95**, 243603 (2005).
[12] X. L. Su, A. H. Tan, X. J. Jia, Q. Pan, C. D. Xie, and K. C.

Peng, Opt. Lett. **31**, 1133 (2006).
[13] Jietai Jing, Sheng Feng, Russell Bloomer, and Olivier Pfister, Phys. Rev. A **74**, 041804(R) (2006).
[14] A. S. Villar, K. N. Cassemiro, K. Dechoum, A. Z. Khoury, M. Martinelli, and P. Nussenzveig, J. Opt. Soc. Am. B **24**, 249 (2007).
[15] Dong Wang, Yana Shang, Zhihui Yan, Wenzhe Wang, Xiaojun Jia, Changde Xie, and Kunchi Peng, EPL **82**, 24003 (2008).
[16] Dong Wang, Yana Shang, Xiaojun Jia, Changde Xie, and Kunchi Peng, J. Phys. B **41**, 035502 (2008).
[17] Nicolai B. Grosse, Syed Assad, Moritz Mehmet, Roman Schnabel, Thomas Symul, and Ping Koy Lam, Phys. Rev. Lett. **100**, 243601 (2008).
[18] A. S. Villar, M. Martinelli, C. Fabre, and P. Nussenzveig, Phys. Rev. Lett. **97**, 140504 (2006).
[19] K. N. Cassemiro, A. S. Villar, M. Martinelli, and P. Nussenzveig, Opt. Express **15**, 18236 (2007).
[20] Robert W. Boyd, *Nonlinear Optics* (Academic Press, Inc., San Diego, 1992).
[21] H. Kogelnik and T. Li, Appl. Opt. **5**, 1550 (1966).
[22] D. F. Walls and G. J. Milburn, *Quantum Optics* (Springer, New York, 2008).
[23] M. J. Collett and C. W. Gardiner, Phys. Rev. A **30**, 1386 (1984).
[24] G. Adesso, A. Serafini, and F. Illuminati, Open Syst. Inf. Dyn. **12**, 189 (2005).
[25] A. S. Villar, M. Martinelli, and P. Nussenzveig, Opt. Commun. **242**, 551 (2004).
[26] P. Galatola, L. A. Lugiato, M. G. Porreca, P. Tombesi, and G. Leuchs, Opt. Commun. **85**, 95 (1991).
[27] A. S. Villar, Am. J. Phys. **76**, 922 (2008).
[28] K. N. Cassemiro, A. S. Villar, P. Valente, M. Martinelli, and P. Nussenzveig, Opt. Lett. **32**, 695 (2007).
[29] K. Goda, K. McKenzie, E. E. Mikhailov, P. K. Lam, D. E. McClelland, and N. Mavalvala, Phys. Rev. A **72**, 043819 (2005).
[30] N. W. Ashcroft and N. D. Mermin, *Solid State Physics* (Saunders College, Philadelphia, 1976).
[31] C. Kittel, *Introduction to Solid State Physics* (John Wiley & Sons, New York, 1953).
[32] A. Yariv, *Quantum Electronics*, 3rd ed. (John Wiley & Sons, New York, 1989).
[33] T. Debuisschert, A. Sizmann, E. Giacobino, and C. Fabre, J. Opt. Soc. Am. B **10**, 1668 (1993).
[34] A. S. Coelho, F. A. S. Barbosa, K. N. Cassemiro, A. S. Villar, M. Martinelli, and P. Nussenzveig (unpublished).

O modelo apresentado não só ajustou bem nossos dados, como conseguiu, com sucesso, ajustar diversas medidas anteriores. Em relação ao modelo proposto na demonstração de emaranhamento entre o bombeio e o sub-harmônico [45], e sua hipótese de espalhamento Brillouin por ondas acústicas guiadas (GAWBS) [46], conseguimos obter uma descrição detalhada do comportamento do ruído, e mostrar sua dependência com a temperatura. Contrariamente ao que fora apresentado naquele artigo, não há o acoplamento de flutuações de temperatura, induzidas por flutuações de intensidade. Tampouco havia o acoplamento de flutuações de intensidade em variação do índice de refração por efeito Kerr. Há o espalhamento de fótons da portadora central do campo para as bandas laterais, adicionando ruído ao sistema que, de outra forma, seria idealmente puro, na ausência de perdas espúrias.

Como resultado, conseguimos enfim controlar o ruído no OPO, e mostrar que ele era o grande responsável pelas limitações observadas acima do limiar de oscilação, quando a resposta do sistema abaixo do limiar de oscilação concorda muito bem com a teoria. Além disso, mostramos que este ruído está ausente na correlação de intensidade, o que explica a excelente concordância das medidas de feixes gêmeos observada desde as primeiras medidas. Uma vez com este controle adquirido, temos a possibilidade de estudar o emaranhamento entre os três campos do OPO, tema do nosso próximo capítulo.

Capítulo 4

Emaranhamento Tripartite

Os questionamentos iniciais sobre o acoplamento do ruído do bombeio ao ruído dos modos sinal e complementar levantaram uma outra suspeita, como fora proposto pelo meu colega, Paulo Nussenzveig. Se há um acoplamento de ruído do bombeio ao sinal e complementar, e se estes não estão mais em um estado puro acima do limiar de oscilação, mesmo no caso teórico de um OPO perfeito, houve uma perda de informação no subsistema dos feixes convertidos. Para onde foi esta informação, se o processo todo é, a princípio, unitário?

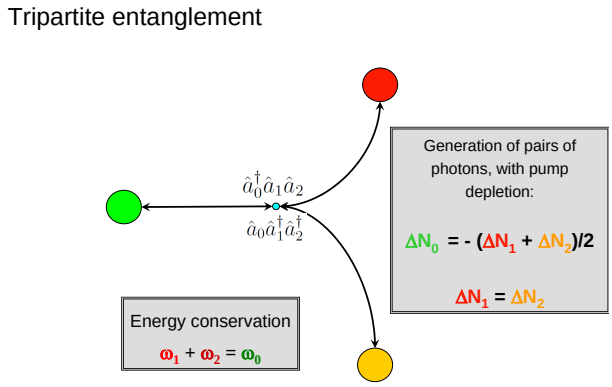

Figura 4.1: A hamiltoniana de interação leva à troca de fótons entre os campos, conservando energia no processo não-ressonante, no qual o cristal atua apenas como um mediador entre os campos.

Esta questão apontou para a existência de informação compartilhada entre o bombeio, sinal e complementar. Ou seja, existem correlações esperadas entre os três campos. De um lado, dada a conservação de energia, e a consequente relação entre as frequências ω_0, ω_1 e ω_2, é de se esperar que mais do que simplesmente a correlação entre as fases dos campos sinal e complementar, haja também a correlação destas com a fase de bombeio. Por outro lado, o fato de termos uma depleção no campo de bombeio intracavidade leva

à ideia de uma correlação entre as intensidades deste, com as intensidades dos modos sinal e complementar.

Para entender como ocorre o emaranhamento, podemos pensar na hamiltoniana do OPO como envolvendo as hamiltonianas de três cavidades independentes, em comprimentos de ondas distintos, acopladas por um hamiltoniano de interação

Esta hamiltoniana de interação implica na aniquilação de um fóton no bombeio para a criação de um fóton no modo sinal, e outro no complementar. O processo inverso, por sua vez, pode ocorrer também. A conservação de energia implica em uma relação estrita para as frequências dos campos.

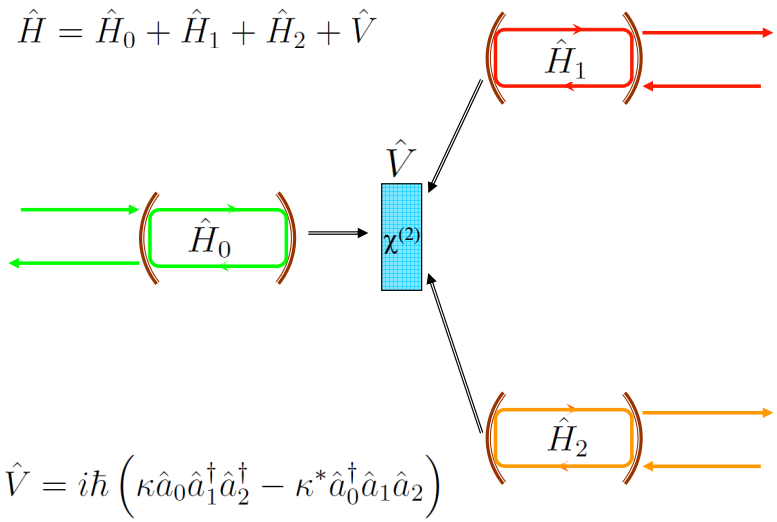

Figura 4.2: Emaranhamento no OPO: a interação $\hat{V}$ acopla as hamiltonianas $\hat{H}_i$ de três modos do campo de cavidades que seriam de outra forma independentes, envolvendo perdas pelo espelho de acoplamento, campo de alimentação intracavidade, e reflexão pelos espelhos.

Para descobrir como podemos colocar este emaranhamento em evidência, retornamos às equações do OPO na descrição linearizada e verificamos que, na operação acima do limiar, o sistema apresenta correlações entre os modos convertidos e o modo de bombeio, e ainda que estas correlações sejam mais fracas do que as que ocorrem entre sinal e complementar, elas são suficientes para caracterizar o emaranhamento tripartite.

Em colaboração com o prof. Claude Fabre, durante sua visita dentro de um acordo CAPES/COFECUB, estudamos este comportamento e verificamos que o OPO, para algumas frequências de análise e algums condições de potência de bombeio, viola as desigualdades de van Loock e Furusawa [9]. Podemos construir três inequações a partir da descrição do operador densidade de um estado separável. A violação de apenas duas destas inequações, como podem ser vistas no apêndice, são uma demonstração suficiente do emaranhamento entre os três campos.

Como se pode ver na primeira figura do artigo seguinte, a violação de uma inequação que toma a desigualdade de Duan [42], e sobre ela adiciona informação da fase de bombeio, é claramente a mais forte. Isto é claro ao lembrar que o emaranhamento entre os campos sinal e complementar já era satisfeito, e verificado pelo critério de Duan, impedindo que o subsistema possa ser descrito por um operador densidade densidade da forma

$$\rho_{12} = \sum_i p_i \rho_1^{(i)} \otimes \rho_2^{(i)}, \tag{4.1}$$

portanto, como a matriz ρ_{12} é obtida tirando o traço sobre o bombeio, fica evidente que não é possível descrever a matriz total como

$$\rho = \sum_i p_i \rho_1^{(i)} \otimes \rho_{02}^{(i)}, \qquad \text{ou} \tag{4.2}$$

$$\rho = \sum_i p_i \rho_2^{(i)} \otimes \rho_{01}^{(i)}. \tag{4.3}$$

O que verifica-se é que a adição de informação da fase do bombeio aumenta a violação, um sinal da correlação deste com os modos sinal e complementar, verificado na inequação (3) do artigo.

$$S_1 = \Delta^2 (\hat{p}_1 - \hat{p}_2) + \Delta^2 (\hat{q}_1 + \hat{q}_2 - \alpha_0 \hat{q}_0) \geq 4 \tag{4.4}$$

onde o parâmetro α_0 pode ser variado à vontade, de forma a minimizar o lado esquerdo da inequação acima, o que implica no cálculo de uma variância inferida para $\hat{q}_1 + \hat{q}_2$, baseado na correlação desta grandeza com $\hat{q}_0$ e na variância destas duas[1].

É necessário ainda testar a hipótese de que o sistema possa ser descrito por um operador densidade do tipo

$$\rho = \sum_i p_i \rho_0^{(i)} \otimes \rho_{12}^{(i)}. \tag{4.5}$$

Ou seja, neste caso as correlações entre bombeio e sinal, ou bombeio de complementar, poderiam igualmente ser descritas como tendo origem clássica, representada por uma mistura estatística com pesos p_i. Neste caso, a violação de uma das inequações abaixo seria suficiente para descartar as três possibilidades de separabilidade no sistema.

$$S_2 = \Delta^2 (\hat{p}_0 + \hat{p}_1) + \Delta^2 (\hat{q}_1 - \hat{q}_0 + \alpha_2 \hat{q}_2) \geq 4, \tag{4.6}$$

$$S_3 = \Delta^2 (\hat{p}_0 + \hat{p}_2) + \Delta^2 (\hat{q}_2 - \hat{q}_0 + \alpha_1 \hat{q}_1) \geq 4. \tag{4.7}$$

Como os campos sinal e complementar são simétricos, na teoria as variâncias corrigidas S_2 e S_3 são idênticas

O que notamos neste caso é que, exceto para uma região extremamente próxima da potência de bombeio (figura 4.3) a violação é verificada. Isto nos dá um testemunho de emaranhamento confiável, com uma violação máxima a cerca de 60% acima do limiar de oscilação. A perda deste testemunho perto do limiar pode ser compreendida pelo fato de que, neste caso, a depleção do campo de bombeio é menor, e o acoplamento deste com os campos sinal e complementar é mais fraco

[1] Para maiores detalhes no cálculo, veja o apêndice

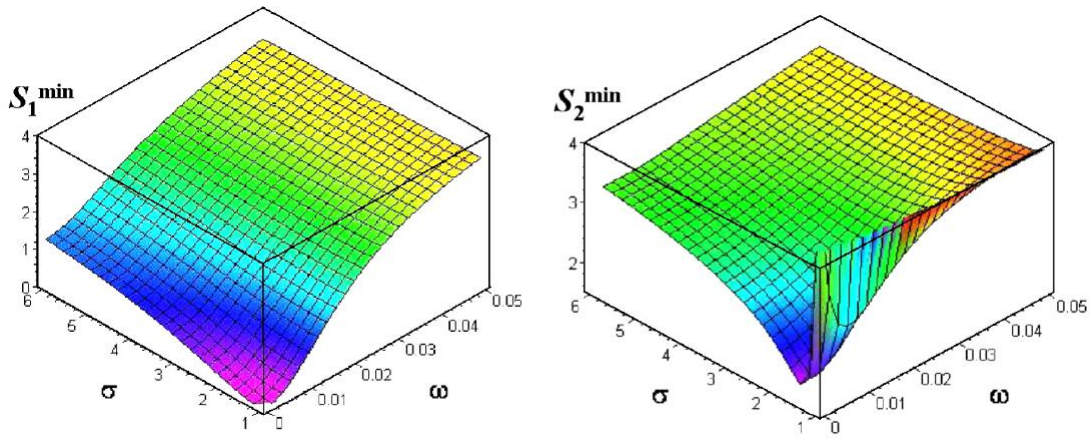

Figura 4.3: Medidas esperadas das testemunhas de emaranhamento em função da potência de bombeio σ (normalizada pelo limiar de oscilação) e da frequência de análise ω (multiplicada pelo tempo de voo intracavidade.

Este resultado, quando de sua submissão, gerou reações opostas entre os "referees". Um deles coloca que a teoria do OPO já era conhecida deste o final dos anos 80, o que é fato. Porém, em sua opinião, não haveria nada de novo no trabalho pelo fato de usarmos uma teoria "antiga". O segundo "referee", no entanto, tem uma reação justamente oposta: do seu ponto de vista, tomando as equações conhecidas deste a década de 80, demonstramos algo que havia passado desapercebido desde então. O emaranhamento tripartite, e as implicações de termos três campos emaranhados, com suas aplicações às implementações de informação quântica, só seriam evidenciadas posteriormente. Diversas propostas de geração de emaranhamento entre três campos haviam sido feitas até então, porém sempre em configurações mais complexas usando a interferência de campos comprimidos [47, 48]. Já para gerar campos emaranhados de cores distintas, os esquemas pediam diversos campos de bombeio e múltiplas não-linearidades, levando a operações de soma e subtração de frequências [49]. O que mostramos foi a forma mais simples de gerar emaranhamento tripartite, com a vantagem de usar um único OPO, com um único termos não-linear de acoplamento, permitindo obter na saída três modos de cores distintas com emaranhamento.

Direct Production of Tripartite Pump-Signal-Idler Entanglement in the Above-Threshold Optical Parametric Oscillator

A. S. Villar,[1] M. Martinelli,[1] C. Fabre,[2] and P. Nussenzveig[1,*]

[1]*Instituto de Física, Universidade de São Paulo, Caixa Postal 66318, 05315-970 São Paulo, SP, Brazil*

[2]*Laboratoire Kastler Brossel, Case 74, Université Pierre et Marie Curie-Paris 6, 4 Place Jussieu, 75252 Paris Cedex 05, France*

(Received 10 March 2006; published 6 October 2006)

We calculate the quantum correlations existing among the three output fields (pump, signal, and idler) of a triply resonant nondegenerate optical parametric oscillator operating above threshold. By applying the standard criteria [P. van Loock and A. Furusawa, Phys. Rev. A **67**, 052315 (2003)], we show that strong tripartite continuous-variable entanglement is present in this well-known and simple system. Furthermore, since the entanglement is generated directly from a nonlinear process, the three entangled fields can have very different frequencies, opening the way for multicolored quantum information networks.

DOI: 10.1103/PhysRevLett.97.140504 PACS numbers: 03.67.Mn, 03.65.Ud, 03.67.Hk, 42.50.Dv

Entanglement, which is probably the strangest of all quantum phenomena, is considered the most important resource for future quantum information technology. Recent experiments on quantum computing, storage, and communication of information utilize different "quantum hardware," such as atom clouds [1], quantum dots [2], and trapped ions [3], all with different resonance frequencies. These systems will probably be used in nodes of quantum networks, implying the necessity of devising ways to address them without loss of quantum information. For networks with several nodes, multipartite entangled light beams will be important to carry out such tasks.

Most of the current realizations of entangled light beams are implemented by combining squeezed beams on beam splitters [4–9]. The beam splitter transformation is linear and does not lead to entangled beams of different frequencies. In order to produce multicolored entangled beams it is important to generate them directly from a nonlinear process. In the case of bipartite two-color entanglement, this has been done very recently, in the above-threshold optical parametric oscillator (OPO) [10–12].

The OPO is the best known and most widely used source of entangled continuous variables for quantum information purposes [13]. Nevertheless, focus thus far has been on the down-converted beams it produces, usually overlooking quantum properties of the pump beam. Recent proposals for direct generation of tripartite entanglement use so-called cascaded nonlinearities, combining down-conversion and sum or subtraction frequency generation [14], which are not present in standard OPOs. In this Letter, we theoretically demonstrate that the standard triply resonant above-threshold OPO naturally produces pump-signal-idler tripartite entanglement. We show that the down-converted and the pump fields' noises violate inequalities which are sufficient for witnessing entanglement [13]. We believe this to be the simplest and most practical proposal of a multicolored multipartite entanglement source to date.

For tripartite systems with subsystems (k, m, n), if the state is partially separable, the density operator can be written in the form of a statistical mixture of reduced density operators $\hat{\rho}_{i,km}$ and $\hat{\rho}_{i,n}$:

$$\hat{\rho} = \sum_i \eta_i \hat{\rho}_{i,km} \otimes \hat{\rho}_{i,n}, \tag{1}$$

with weights $\eta_i \geq 0$ satisfying $\sum_i \eta_i = 1$. A necessary condition for separability of two subsystems was demonstrated by Duan *et al.* [15], in the form of an inequality: if it is violated, there is bipartite entanglement. This criterion is easily checked experimentally by measuring second order moments of combinations of operators acting on each of the subsystems.

The inequality presented in Ref. [15] for the variances of two combinations of positions and momenta $(\hat{x}_j, \hat{p}_j)$ of subsystems $j = \{1, 2\}$ can be readily extended to a combination of three subsystems [16]. If we define two commuting operators $\hat{u} = h_1\hat{x}_1 + h_2\hat{x}_2 + h_3\hat{x}_3$ and $\hat{v} = g_1\hat{p}_1 + g_2\hat{p}_2 + g_3\hat{p}_3$, where the h_i and g_i are arbitrary real parameters, for a (partially) separable state written in the form of Eq. (1), inequalities of the form:

$$\langle \Delta^2 \hat{u} \rangle + \langle \Delta^2 \hat{v} \rangle \geq 2(|h_n g_n| + |h_k g_k + h_m g_m|), \tag{2}$$

with different permutations of the subsystems (k, m, n), must hold. Therefore, violations of the inequalities corresponding to the three possible permutations suffice to demonstrate tripartite entanglement.

For electromagnetic fields, position and momentum operators can be replaced by the field amplitude and phase quadrature operators, defined as functions of the creation and annihilation operators as $\hat{p}_j(t) = [e^{i\varphi_j}\hat{a}_j^\dagger(t) + e^{-i\varphi_j}\hat{a}_j(t)]$ and $\hat{q}_j(t) = i[e^{i\varphi_j}\hat{a}_j^\dagger(t) - e^{-i\varphi_j}\hat{a}_j(t)]$, where the phase φ_j of each mode is chosen from its mean value in order to have $\langle \hat{q}_j \rangle = 0$. In this case, $\hat{p}$ represents the amplitude fluctuations of the field, and $\hat{q}$ is related to the phase fluctuations. From the commutation relation

$[\hat{a}_j, \hat{a}_{j'}^\dagger] = \delta_{jj'}$, it follows that $[\hat{p}_j, \hat{q}_{j'}] = 2i\delta_{jj'}$. In the present situation, we look for violations of the following inequalities:

$$S_1 = \langle \Delta^2(\hat{p}_1 - \hat{p}_2)\rangle + \langle \Delta^2(\hat{q}_1 + \hat{q}_2 - \alpha_0\hat{q}_0)\rangle \geq 4, \quad (3)$$

$$S_2 = \langle \Delta^2(\hat{p}_0 + \hat{p}_1)\rangle + \langle \Delta^2(\hat{q}_1 + \alpha_2\hat{q}_2 - \hat{q}_0)\rangle \geq 4, \quad (4)$$

$$S_3 = \langle \Delta^2(\hat{p}_0 + \hat{p}_2)\rangle + \langle \Delta^2(\alpha_1\hat{q}_1 + \hat{q}_2 - \hat{q}_0)\rangle \geq 4, \quad (5)$$

with an optimized choice of the free parameters α_i, in order to show that all three modes are entangled, i.e., that the state of the full system is not even partially separable.

The tripartite entangled fields are directly produced by a triply resonant nondegenerate OPO, composed of a $\chi^{(2)}$ nonlinear crystal placed inside an optical cavity (a full description of field mean values and tuning characteristics can be found in Ref. [17]). The OPO is a well-known source of nonclassical states of the electromagnetic field, both above and below the oscillation threshold. In this system, a pump photon of frequency ω_0 is down-converted into a pair of signal and idler twin photons of frequencies ω_1 and ω_2. These fields exit the cavity and can be easily separated by color (pump) and polarization (signal and idler) in the case of type-II phase matching. Below threshold, signal and idler modes are in an entangled state with zero mean values for the electric field [18]. Above threshold, the parametric coupling leads to both intensity coupling between the three modes (this is the well-known pump depletion effect: a pump photon is destroyed each time a couple of twin and idler photons is created) and to phase coherence between them: the sum of the signal and idler field phases is locked to the pump phase as a consequence of energy conservation ($\omega_1 + \omega_2 = \omega_0$). This leads to both intensity and phase correlations between the three modes that extend to the quantum regime, and eventually culminate in tripartite entanglement as we show below. So far, physicists' interest has been concentrated on the signal and idler quantum correlations [19] or on the pump squeezing [20]. The full three-mode system has indeed genuine quantum properties [21], which are partly lost when one traces out the pump mode, although the signal and idler modes remain of course entangled [10].

Quantum fluctuations of the system are calculated as usual [22]: we start from the evolution equations of the operators of the three modes ($\hat{a}_0$, $\hat{a}_1$, $\hat{a}_2$) inside the OPO cavity. We write the field operators as the sum of their mean values and a fluctuation term and, assuming that the fluctuations are small compared to the mean fields, which is true everywhere except very close to threshold, we linearize these equations around the classical mean values [17]. One obtains in this way six linear Langevin equations that enable us to calculate the evolution of the real and imaginary parts of the intracavity fluctuations of the three fields. If we assume that the cavity transmission factor and the extra-losses are the same for the signal and idler modes, the evolution equations can be decoupled into two independent sets [22]: two equations for the signal and idler difference, and four equations coupling the sum of the signal and idler fluctuations to the pump fluctuations. Using the input-output relation on the coupling mirror, one obtains the output field fluctuations in Fourier domain, $\delta\vec{p}(\Omega) = [\delta\hat{p}_0(\Omega), \delta\hat{q}_0(\Omega), \delta\hat{p}_1(\Omega), \delta\hat{q}_1(\Omega), \delta\hat{p}_2(\Omega), \delta\hat{q}_2(\Omega)]^T$, as a function of the input field fluctuations. This enables us to determine the full 6×6 three-mode covariance matrix, $C = \langle \delta\vec{p}(\Omega)\delta\vec{p}(-\Omega)^T\rangle$, of the pump, signal and idler output modes, and the variance of any combination of these modes. The full treatment is described in Ref. [23].

From the calculated covariances, we derive the optimized values of the parameters α_i which minimize the quantities S_1, S_2 and S_3 of Eqs. (3)–(5) as functions of the covariance matrix elements for the output field, and calculate the corresponding minimum value for these three quantities. We take typical experimental conditions: cavity coupling mirror transmittance for pump $T_0 = 10\%$ and signal and idler beams $T = 2\%$, and exact cavity resonance for the three modes. We can now study the dependence of S_1, S_2, and S_3 with the normalized pump power σ (power normalized to the oscillation threshold on resonance) and with the analysis frequency ω (normalized to the inverse of the cavity round trip time τ).

In Fig. 1, we display the minimized value of S_1. As can be seen, $S_1^{\min}$ is smaller than 4 in all the presented range of parameters, which establishes the inseparability of the signal and idler modes. Let us stress that the resulting violation, with the optimization of the variance, is much stronger than that observed by tracing out the pump mode and looking only at signal and idler modes under the Duan *et al.* criterion [23]. In the present case, the measurement of pump phase increases the knowledge that one can obtain about the idler beam phase from the measurement of the signal phase. Nevertheless, the state can still be partially separable if the other two inequalities [Eqs. (4) and (5)] are not violated. The interchangeability of the roles of signal and idler makes evident that $S_2 = S_3$. The common mini-

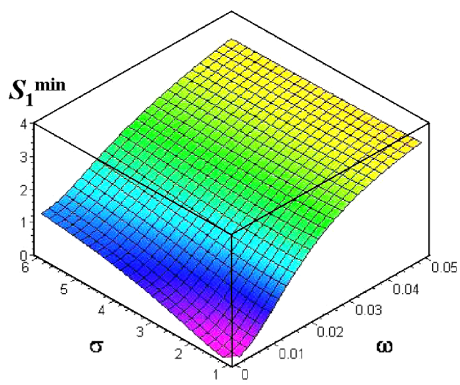

FIG. 1 (color online). Optimized sum of variances, $S_1^{\min}$, for Eq. (3): σ = pump power relative to threshold, ω = analysis frequency, in units of $1/\tau$.

mized value of this quantity is shown in Fig. 2. We observe that it is also below 4, implying inseparability for a broad range of values of analysis frequency and pump power, even though the violation is not as strong as for $S_1^{\min}$ (Fig. 1). Correlations between the twin beams tend to be stronger than those between one of the twins and the pump, since the pump is not generated inside the cavity. $S_2^{\min} = S_3^{\min}$ is everywhere larger than $\simeq 1.7$, a value obtained for $\sigma \simeq 1.6$. For this value of σ, all three fields have approximately the same intensities, which is in general the best situation for observing correlations.

Another method to characterize the amount of entanglement in a system is to study the eigenvalues of its covariance matrix: they provide information about the maximum squeezing that can be obtained from the different modes by unitary transformations and about the maximum bipartite entanglement that can be extracted from these modes [24]. In our case, the minimum eigenvalue is given by the variance of $\hat{p}_1 - \hat{p}_2$. The next lower eigenvalue is related to the combination of phases in the form $(\hat{q}_1 + \hat{q}_2 - \beta\hat{q}_0)$, where β is a real number. Both values can be strongly squeezed, at the expense of excess noise for the variances of their conjugate variables.

From these two smallest eigenvalues λ_1, λ_2 we calculate the logarithmic negativity $E_N = \max[0, -\log_2(\lambda_1\lambda_2)/2]$ [25,26]. This is a computable measure of the degree of bipartite entanglement of a system, and it is especially useful owing to its immediate extension to entangled mixed states. We calculate here the difference, E_N^{diff}, between the logarithmic negativities for the full system and for just the signal and idler modes, tracing out the pump. This difference is positive for the full range of parameters displayed in Fig. 3, with maximum values obtained for low analysis frequencies ($\omega < 0.02/\tau$). It is clear that quantum information is present in all three modes and one only recovers a fraction of it when restricting measurements to signal and idler beams.

The tripartite pump-signal-idler entanglement in the OPO can be observed in a broad range of frequencies and pump power. The correlation is, as expected, stronger for analysis frequencies below the cavity bandwidth T/τ for the signal and idler modes, and for pump powers close to threshold, although it does not depend so much on this last parameter. Calculations from the covariance matrix show that there is a small dependence of S_1 and S_2 on the cavity detunings, which is important because the locking of the OPO is typically done with some small detuning for pump and down-converted modes. If we consider the presence of spurious losses inside the cavity, there is a linear increase of the value of S_1 with these losses, much in the way observed for the intensity correlation of twin beams emitted from the OPO. As for S_2, inseparability no longer occurs for lower analysis frequencies, but still holds for a wide range of the parameters σ and ω.

In conclusion, we have demonstrated that the standard nondegenerate optical parametric oscillator directly yields tripartite entangled light beams when operating above threshold. Above-threshold OPOs have produced the highest level of intensity quantum correlations to date [27]. Figure 1 shows that they can also produce a very low bound for the combined phases quantum fluctuations. Thus, the magnitudes of expected quantum correlations are among the best achievable at present. The experimental realization of this system is much simpler than the proposals based on combined nonlinearities [28], especially considering the high degree of experimental control achieved over the OPO. We also note that the above-threshold OPO entanglement renders it a possible device for such tasks as a tripartite teleportation network [8]. Moreover, it allows distribution of quantum information through three modes of very different frequencies, a topic that is attracting growing attention [10,29,30]. This is of practical interest, since high efficiency photodetectors are only available in limited ranges of the electromagnetic spectrum. Frequency-tunable quantum information will also be very useful for light-matter interfaces in quantum networks.

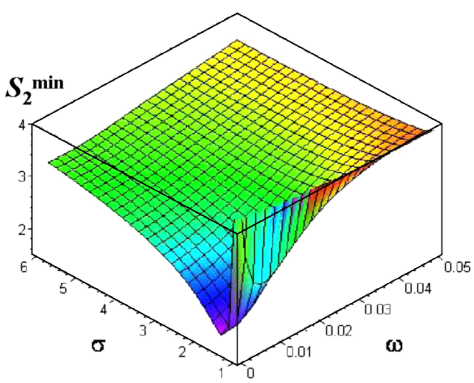

FIG. 2 (color online). Optimized sum of variances, $S_2^{\min} = S_3^{\min}$, for Eqs. (4) and (5): σ = pump power relative to threshold, ω = analysis frequency, in units of $1/\tau$.

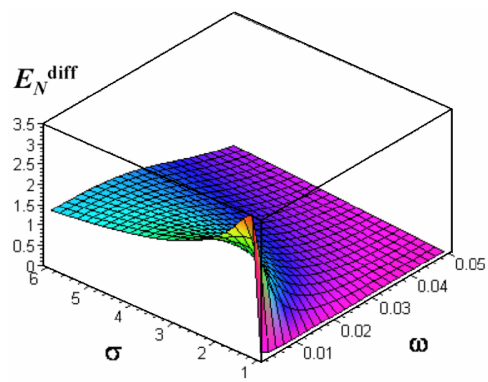

FIG. 3 (color online). Difference between logarithmic negativities, E_N^{diff}, for the full three modes and for only signal and idler modes. σ = pump power relative to threshold, ω = analysis frequency, in units of $1/\tau$.

We thank János Bergou for discussions and encouragement. Laboratoire Kastler-Brossel, of the Ecole Normale Supérieure and the Université Pierre et Marie Curie, is associated with the CNRS (UMR 8552). This work was supported by the program CAPES-COFECUB and the Brazilian agencies FAPESP and CNPq (Instituto do Milênio de Informação Quântica).

*Electronic address: nussen@if.usp.br

[1] C. W. Chou, H. de Riedmatten, D. Felinto, S. V. Polyakov, S. J. van Enk, and H. J. Kimble, Nature (London) **438**, 828 (2005); T. Chanelière, D. N. Matsukevich, S. D. Jenkins, S.-Y. Lan, T. A. B. Kennedy, and A. Kuzmich, Nature (London) **438**, 833 (2005); M. D. Eisaman, A. André, F. Massou, M. Fleischhauer, A. S. Zibrov, and M. D. Lukin, Nature (London) **438**, 837 (2005).

[2] M. Atatüre, J. Dreiser, A. Badolato, A. Högele, K. Karrai, and A. Imamoglu, Science **312**, 551 (2006).

[3] D. Leibfried, E. Knill, S. Seidelin, J. Britton, R. B. Blakestad, J. Chiaverini, D. B. Hume, W. M. Itano, J. D. Jost, C. Langer, R. Ozeri, R. Reichle, and D. J. Wineland, Nature (London) **438**, 639 (2005); H. Häffner, W. Hänsel, C. F. Roos, J. Benhelm, D. Chek-al-kar, M. Chwalla, T. Körber, U. D. Rapol, M. Riebe, P. O. Schmidt, C. Becher, O. Gühne, W. Dür, and R. Blatt, Nature (London) **438**, 643 (2005).

[4] A. Furusawa, J. L. Sørensen, S. L. Braunstein, C. A. Fuchs, H. J. Kimble, and E. S. Polzik, Science **282**, 706 (1998).

[5] Ch. Silberhorn, P. K. Lam, O. Weiss, F. König, N. Korolkova, and G. Leuchs, Phys. Rev. Lett. **86**, 4267 (2001).

[6] P. van Loock and S. L. Braunstein, Phys. Rev. Lett. **84**, 3482 (2000).

[7] T. Aoki, N. Takei, H. Yonezawa, K. Wakui, T. Hiraoka, A. Furusawa, and P. van Loock, Phys. Rev. Lett. **91**, 080404 (2003).

[8] H. Yonezawa, T. Aoki, and A. Furusawa, Nature (London) **431**, 430 (2004).

[9] J. Jing, J. Zhang, Ying Yan, F. Zhao, C. Xie, and K. Peng, Phys. Rev. Lett. **90**, 167903 (2003).

[10] A. S. Villar, L. S. Cruz, K. N. Cassemiro, M. Martinelli, and P. Nussenzveig, Phys. Rev. Lett. **95**, 243603 (2005).

[11] X. L. Su, A. Tan, X. J. Jia, Q. Pan, C. D. Xie, and K. C. Peng, Opt. Lett. **31**, 1133 (2006).

[12] J. Jing, S. Feng, R. Bloomer, and O. Pfister, quant-ph/0604134.

[13] S. L. Braunstein and P. van Loock, Rev. Mod. Phys. **77**, 513 (2005).

[14] A. Ferraro, M. G. A. Paris, M. Bondani, A. Allevi, E. Puddu, and A. Andreoni, J. Opt. Soc. Am. B **21**, 1241 (2004); O. Pfister, S. Feng, G. Jennings, R. Pooser, and D. Xie, Phys. Rev. A **70**, 020302(R) (2004); A. S. Bradley, M. K. Olsen, O. Pfister, and R. C. Pooser, Phys. Rev. A **72**, 053805 (2005).

[15] Lu-Ming Duan, G. Giedke, J. I. Cirac, and P. Zoller, Phys. Rev. Lett. **84**, 2722 (2000).

[16] P. van Loock and A. Furusawa, Phys. Rev. A **67**, 052315 (2003).

[17] T. Debuisschert, A. Sizmann, E. Giacobino, and C. Fabre, J. Opt. Soc. Am. B **10**, 1668 (1993).

[18] Z. Y. Ou, S. F. Pereira, H. J. Kimble, and K. C. Peng, Phys. Rev. Lett. **68**, 3663 (1992).

[19] A. Heidmann, R. J. Horowicz, S. Reynaud, E. Giacobino, C. Fabre, and G. Camy, Phys. Rev. Lett. **59**, 2555 (1987).

[20] K. Kasai, Gao Jiangrui, and C. Fabre, Europhys. Lett. **40**, 25 (1997).

[21] P. D. Drummond and P. Kinsler, Quantum Semiclass. Opt. **7**, 727 (1995).

[22] C. Fabre, E. Giacobino, A. Heidmann, L. Lugiato, S. Reynaud, M. Vadacchino, and Wang Kaige, Quantum Opt. **2**, 159 (1990).

[23] A. S. Villar, M. Martinelli, and P. Nussenzveig, Opt. Commun. **242**, 551 (2004).

[24] G. Adesso, A. Serafini, and F. Illuminati, Phys. Rev. A **70**, 022318 (2004).

[25] G. Vidal and R. F. Werner, Phys. Rev. A **65**, 032314 (2002).

[26] M. M. Wolf, J. Eisert, and M. B. Plenio, Phys. Rev. Lett. **90**, 047904 (2003).

[27] J. Laurat, T. Coudreau, L. Longchambon, and C. Fabre, Opt. Lett. **30**, 1177 (2005).

[28] It should be noted, however, that such proposals may lead to even higher orders of entanglement, if the pump mode is taken into account.

[29] S. Tanzilli, W. Tittel, M. Halder, O. Alibart, P. Baldi, N. Gisin, and H. Zbinden, Nature (London) **437**, 116 (2005).

[30] N. B. Grosse, W. P. Bowen, K. McKenzie, and P. K. Lam, Phys. Rev. Lett. **96**, 063601 (2006).

4.1 As primeiras tentativas

Depois da proposta teórica, fica evidente que o próximo passo era a realização da medida em si. Esta tarefa ficou a cargo de uma estudante de doutorado, Katiúscia Nadine Cassemiro, que já estava envolvida nas medidas de emaranhamento bipartite, e portanto estava bem familiarizada com o sistema.

Como de hábito, a medida parecia fácil, uma vez que tínhamos enfrentado a maioria dos problemas conhecidos no caso bipartite. A princípio, bastaria montar uma cavidade de análise extra para medir o feixe refletido pelo OPO. Infelizmente, o primeiro espelho de acoplamento que empregamos tinha uma transmissão muito baixa, e perdas excessivas. Com isto, a cavidade não operava a contento, e não chegava a fazer o giro de elipse.

O melhor que foi possível fazer, nesta primeira etapa, foi usar o OPO estudado na ref. [8], e tomar o feixe de bombeio refletido por sua cavidade, fazendo uma medida direta da intensidade, enquanto aguardávamos os novos espelhos para a cavidade de análise do bombeio. A escolha deste OPO não fora fortuita: o mesmo tinha uma ressonância estreita para a cavidade de bombeio, e pela teoria deveria dar um acoplamento mais balanceado entre os três modos.

Além disso, ainda que esperássemos correlações entre a soma das quadraturas fase dos modos sinal e complementar com a fase do campo de bombeio, e não com a intensidade, o fato do OPO ter uma cavidade estreita em frequência para o bombeio permitia trabalhar levemente fora da ressonância exata para este modo, e assim usar a própria cavidade do OPO para converter fase em amplitude. Como os modos sinal e complementar são travados pela eletrônica na ressonância exata podemos jogar com a temperatura do cristal (estabilizada na faixa de 10 mK), e controlar a dessintonia no modo de bombeio. Com isso, a flutuação da quadratura amplitude p_0 se acopla a da quadratura fase q_0. O resultado é a existência de correlações entre as fases dos modos sinal e complementar e a amplitude do bombeio refletido.

Na figura 3 do artigo, notamos que o OPO, sem a informação adicional do bombeio, mostra emaranhamento bipartite apenas para potências até 15% acima do limiar de oscilação. Com a adição da informação do bombeio, podemos estender a faixa até 30% acima do limiar. Esta foi a primeira demonstração de correlação quântica entre três campos de cores distintas, cobrindo mais de uma oitava do espectro eletromagnético. Isto poderia ser útil para a realização de teletransporte no sistema bipartite, posto que a informação do bombeio pode ser empregada para reforçar a correlação verificada, e garantir sucesso no processo de teletransporte, o que não seria possível usando apenas dois feixes. Isto seria muito semelhante à montagem de uma rede quântica, como fora proposto por Furusawa [47]. No entanto, o emaranhamento tripartite pedia mais do que isso, e por seu caráter amplo em frequência torna-se um sistema mais interessante para aplicações de teletransporte.

Experimental observation of three-color optical quantum correlations

Katiúscia N. Cassemiro, Alessandro S. Villar, Paulo Valente, Marcelo Martinelli, and Paulo Nussenzveig

Instituto de Física, Universidade de São Paulo, Caixa Postal 66318, 05315-970 São Paulo, São Paulo, Brazil

Received October 23, 2006; revised December 6, 2006; accepted December 13, 2006;
posted December 14, 2006 (Doc. ID 76384); published February 15, 2007

Quantum correlations among bright pump, signal, and idler beams produced by an optical parametric oscillator, all with different frequencies, are experimentally demonstrated. We show that the degree of entanglement between signal and idler fields is improved by using information on pump fluctuations. To our knowledge this is the first observation of three-color optical quantum correlations. © 2007 Optical Society of America

OCIS codes: 270.0270, 270.6570, 190.4970.

Quantum correlations are a signature of nonclassical light generation. The optical parametric oscillator (OPO) is the best known and most widely used source of such correlations. Squeezing in the intensity difference of the twin beams that the OPO produces above threshold[1] (signal and idler) yielded the record value for squeezing of −9.7 dB.[2] Bipartite continuous variable entanglement in this system, which requires the observation of phase anticorrelations as well, although predicted in 1988,[3] was demonstrated only very recently.[4–6] The parametric process involves three fields, yet the pump field is typically treated as a classical quantity. As an exception, quantum properties of the pump were first measured by Kasai *et al.*[7] This raises a natural question: are there quantum correlations among all three fields? An affirmative answer was recently given by Villar *et al.*,[8] who investigated the problem theoretically. Here, we provide what we believe to be the first experimental affirmative answer by observing triple correlations among quadratures of pump, signal, and idler fields.

Beyond the demonstration of nonclassical light features, one should notice that all three fields have different frequencies. Interest in quantum frequency conversion developed in the early 1990s[9,10] and opens perspectives for the interaction of light with physical systems having different resonance frequencies. The above-threshold OPO produces, in general, nondegenerate twin beams, and the pump beam has approximately twice their frequencies. Three-color quantum correlations increase the number of physical systems that can be simultaneously investigated. Correlations with the pump can also be used to enhance the bipartite entanglement between the twin beams, as we show below.

Quantum correlations should exist between the phase quadrature of the pump field and the sum of phase quadratures of the signal and idler fields as a direct consequence of phase matching, $\vec{k}_0=\vec{k}_1+\vec{k}_2$, and of energy conservation, $\omega_0=\omega_1+\omega_2$. These conditions imply that phase fluctuations are related following $\delta\phi_0=\delta\phi_1+\delta\phi_2$. This qualitative argument is confirmed by detailed theoretical predictions.[3,8] Indices $j\in\{0,1,2\}$ refer to pump, signal, and idler fields, respectively. The quadratures are defined through the field annihilation operators $\hat{a}_j=\exp(i\phi_j)(\hat{p}_j+i\hat{q}_j)$, where ϕ_j is chosen so that $\langle\hat{q}_j\rangle=0$. When the OPO is detuned from exact triple resonance, this phase–phase correlation, $C_{\hat{q}_0\hat{q}_+}=\langle\delta\hat{q}_0\delta\hat{q}_+\rangle$, is partially transferred to an amplitude–phase correlation, $C_{\hat{p}_0\hat{q}_+}=\langle\delta\hat{p}_0\delta\hat{q}_+\rangle$, owing to phase noise to amplitude noise conversion[11] inside the OPO cavity $[\hat{q}_+\equiv(\hat{q}_1+\hat{q}_2)/\sqrt{2}]$. Our experiment is designed to measure joint fluctuations of a combination of $\hat{q}_+$ and $\hat{p}_0$ and compare them with the shot-noise level, which defines the standard quantum limit (SQL). This will enable us to improve the bipartite entanglement of the twin beams.

Twin beam entanglement is proved by violation of an inequality derived by Duan *et al.*[12] and Simon.[13] Van Loock and Furusawa[14] generalized it to include a third field:

$$\Delta^2\hat{p}_- + \Delta^2(\hat{q}_+ - \alpha_0\hat{p}_0) \geqslant 2, \qquad \alpha_0 = \frac{C_{\hat{p}_0\hat{q}_+}}{\Delta^2\hat{p}_0}. \tag{1}$$

Here α_0 is a parameter chosen to minimize the left-hand side of the expression above and $\hat{p}_-\equiv(\hat{p}_1-\hat{p}_2)/\sqrt{2}$. Each term $\Delta^2\hat{p}_-$ and $\Delta^2(\hat{q}_+-\alpha_0\hat{p}_0)$ is normalized to the SQL. Our attention will be focused on the corrected phase sum noise (second term above), which can be rewritten as

$$\Delta^2\hat{q}'_+ \equiv \Delta^2\hat{q}_+ - \beta_0; \qquad \beta_0 = \frac{C^2_{\hat{p}_0\hat{q}_+}}{\Delta^2\hat{p}_0}. \tag{2}$$

If $\Delta^2\hat{q}'_+<1$ and $\beta_0\neq 0$, there is a quantum correlation between $\hat{p}_0$ and $\hat{q}_+$.

The experimental setup is sketched in Fig. 1. The triply resonant type II OPO is pumped by a frequency-doubled diode-pumped Nd:YAG laser (Innolight Diabolo) at 532 nm. This laser is first transmitted through a filter cavity (bandwidth of 2.4 MHz) prior to injection into the OPO, which removes all classical noise for analysis frequencies above 15 MHz. It is important to have a shot-noise-limited pump, since excess pump phase noise is converted to

0146-9592/07/060695-3/$15.00

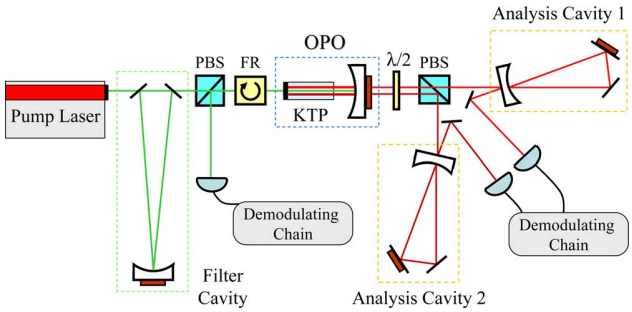

Fig. 1. (Color online) Sketch of the experimental setup. PBS, polarizing beam splitter; FR, Faraday rotator; λ/2, half-wave plate.

excess noise in $\hat{q}_+$, thus hindering twin beam entanglement.[15] The nonlinear crystal is a 10 mm long potassium titanyl phosphate from Litton. The OPO cavity input mirror is flat, directly coated on one crystal surface, with 97% reflection at 532 nm and high reflectivity ($R>99.8\%$) at 1064 nm. The other crystal surface is antireflection coated for both wavelengths ($R<3\%$ at 532 nm and $R<0.25\%$ at 1064 nm). The spherical output mirror is a high reflector for 532 nm ($R>99.8\%$) and a partial reflector for 1064 nm, $R=96\%$, with a curvature radius of 25 mm. The OPO cavity bandwidth for 1064 nm is 50 MHz, and the threshold power is 12 mW. Orthogonally polarized signal and idler beams are separated by a polarizing beam splitter. To measure their quadrature noise, each beam is reflected off an analysis optical cavity that converts phase noise to amplitude noise as a function of its detuning.[16–18] The twin beams are finally detected on high-quantum-efficiency (>93%) photodiodes (Epitaxx ETX300). Both analysis cavities have bandwidths of 14(1) MHz. Overall detection efficiency is $\eta=80\%$. The signal and idler optical frequencies differ by approximately 0.35 THz, corresponding to $\Delta\lambda=1.3$ nm in wavelength. Photocurrents are recorded as a function of time as both cavities are synchronously scanned. At the same time, amplitude fluctuations of the reflected pump beam (extracted by means of a polarizing beam splitter and a Faraday rotator) are recorded by another photodetector (EG&G FND100, quantum efficiency 60%), with an overall detection efficiency of $\eta_0=45\%$ (we are currently working to improve this value by using higher-quantum-efficiency photodiodes). Noise power spectra are obtained by direct demodulation of the photocurrents. Each photocurrent is electronically mixed with the same sinusoidal reference at the analysis frequency $\nu=27$ MHz, and the low-frequency beat signal is sampled at a 600 kHz repetition rate by an analog-to-digital card connected to a computer. Variances of these fluctuations are then calculated by taking groups of 1000 points and are finally normalized to the SQL. The shot-noise level is measured independently, either by using light at 1064 nm directly emitted from the Diabolo laser or by mixing the OPO's twin beams. Ten different values of average intensity are used for this, and linearity is checked with great precision. For each intensity, 60 averages of 10,000 acquisition points are made, allowing for an error in the shot-noise level below 0.5%.

Typical noise spectra of sum and difference of twin beam quadratures are presented in Fig. 2, as functions of the analysis cavities' detuning relative to their bandwidth, Δ. Phase noise $\Delta^2\hat{q}_\pm$ is measured for $\Delta=0.5$ and also (partially) for $\Delta\cong1.4$. Far off ($|\Delta|\geqslant2.5$) and on exact resonance ($\Delta=0$), the amplitude noise $\Delta^2\hat{p}_\pm$ is measured. The squeezed difference of amplitude quadratures, $\Delta^2\hat{p}_-=0.53(2)$, and the shot-noise-limited sum of phase quadratures, $\Delta^2\hat{q}_+=0.99(2)$, suffice to demonstrate bipartite entanglement, since $\Delta^2\hat{p}_-+\Delta^2\hat{q}_+=1.52(3)<2$.

Quantum correlations between pump and downconverted fields are demonstrated in the solid curve. It shows that $\Delta^2\hat{q}_+$ can be reduced by using information from the pump beam amplitude. When corrected by $\beta_0=0.13(3)$, the shot-noise-limited sum of phases $\Delta^2\hat{q}_+$ becomes squeezed: $\Delta^2\hat{q}'_+=0.86(2)$. The generalized criterion of Eq. (1) assumes the improved value $\Delta^2\hat{p}_-+\Delta^2\hat{q}'_+=1.39(3)<2$.

The behaviors of β_0, $\Delta^2\hat{q}_+$, and $\Delta^2\hat{q}'_+$ are presented in Fig. 3 as functions of pump power relative to threshold, σ. Each experimental point was taken from curves similar to those of Fig. 2. The solid curves were calculated from the standard linearized OPO theory.[15] As described in Ref. 19, the theory has to be corrected to include extra noise that is acquired by the intracavity pump field and that is not related to the parametric process. We model this by simply adding noise to the input pump field. This noise depends on the OPO cavity detuning for the pump field.[19] Since in our present experiment we do not have precise control or knowledge of OPO cavity detunings for the pump, Δ'_0, and the downconverted fields, Δ' (all normalized to the OPO cavity bandwidth for the twin beams), these are used as free pa-

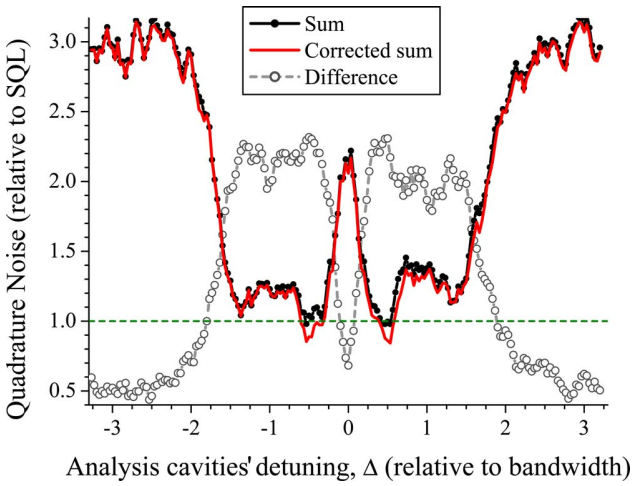

Fig. 2. (Color online) Noise spectra at 27 MHz as a function of the analysis cavities' detuning. Black curve with circles, sum of twin beam quadratures; gray curve with open circles, difference of twin beam quadratures; red curve, sum of twin beam quadratures corrected by correlations with the pump amplitude. Dashed green line, shot-noise level (error bars in the shot-noise level measurement are less than 0.5%). $\sigma=1.34$.

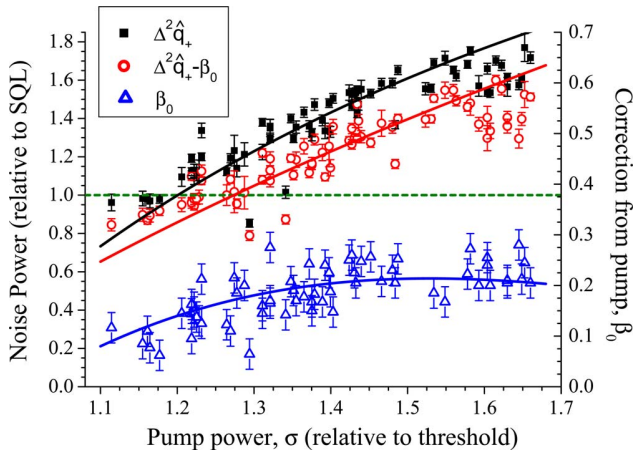

Fig. 3. (Color online) Behavior of $\Delta^2\hat{q}_+$ with and without correction owing to correlations with the pump amplitude as a function of σ. Black squares, $\Delta^2\hat{q}_+$; red circles, $\Delta^2\hat{q}'_+ - \beta_0$; blue triangles, β_0. The solid curves correspond to the physical model with pump detuning and excess noise as free parameters.

rameters to fit the data of Fig. 3. Furthermore, the excess phase noise added to the input pump, $S^{\text{in}}_{q_0}$, which is deduced from independent measurements of the reflected pump beam for $\Delta'_0=0$ and $\sigma\approx 1$ ($S^{\text{in}}_{q_0} \approx 23$), also has to be adjusted for the nonzero detunings.

We verify that $\Delta^2\hat{q}_+$ is squeezed close to threshold and its noise increases as the pump power is increased, crossing the shot-noise value at $\sigma\cong 1.2$. Its behavior was studied in detail in Ref. 19. The correction term β_0 is always nonzero, varying from $\beta_0 \approx 0.10$ to $\beta_0\approx 0.23$ for increasing σ. This is in agreement with the theoretical prediction of Ref. 8, since the degree of triple correlations should be maximum close to $\sigma=1.5$, where all fields have approximately the same intensity. In particular, for $\sigma\leqslant 1.3$, the correlation between $\hat{p}_0$ and $\hat{q}_+$ reveals or increases the squeezing value in $\Delta^2\hat{q}'_+$, attesting its quantum nature. Better control of the detunings[6] would probably decrease the scattering of the data points. The theoretical model is in good agreement with the experiment. The parameters that best fit the data are $\Delta'_0 = 0.2$, $\Delta'=0.26$, and $S_{q_0}=15$. From these results, we can surmise that, for $\Delta'_0=\Delta'=0$, $\hat{q}_0$ and $\hat{q}_+$ should be strongly correlated.

In summary, twin beam entanglement produced by an above-threshold OPO can be improved by using the quantum correlations with the pump beam demonstrated here. To our knowledge, this is the first experimental demonstration of three-color quantum correlations. They can be used, for instance, to increase the fidelity of quantum information distribution. The measurement of triple optical quantum correlations is a necessary first step en route to the observation of three-color entanglement in the above-threshold OPO.

This work was supported by the Fundação de Amparo à Pesquisa do Estado de São Paulo and the Conselho Nacional de Desenvolvimento Científico e Tecnológico (through Instituto do Milênio de Informação Quântica). P. Nussenzveig's e-mail address is nussen@if.usp.br.

References

1. A. Heidmann, R. J. Horowicz, S. Reynaud, E. Giacobino, C. Fabre, and G. Camy, Phys. Rev. Lett. **59**, 2555 (1987).
2. J. Laurat, L. Longchambon, C. Fabre, and T. Coudreau, Opt. Lett. **30**, 1177 (2005).
3. M. D. Reid and P. D. Drummond, Phys. Rev. Lett. **60**, 2731 (1988).
4. A. S. Villar, L. S. Cruz, K. N. Cassemiro, M. Martinelli, and P. Nussenzveig, Phys. Rev. Lett. **95**, 243603 (2005).
5. X. L. Su, A. Tan, X. J. Jia, Q. Pan, C. D. Xie, and K. C. Peng, Opt. Lett. **31**, 1133 (2006).
6. J. Jing, S. Feng, R. Bloomer, and O. Pfister, Phys. Rev. A **74**, 041804(R) (2006).
7. K. Kasai, J. G. Gao, and C. Fabre, Europhys. Lett. **40**, 25 (1997).
8. A. S. Villar, M. Martinelli, C. Fabre, and P. Nussenzveig, Phys. Rev. Lett. **97**, 140504 (2006).
9. J. Huang and P. Kumar, Phys. Rev. Lett. **68**, 2153 (1992).
10. P. Kumar, Opt. Lett. **15**, 1476 (1990).
11. T. Yabuzaki, T. Mitsui, and U. Tanaka, Phys. Rev. Lett. **67**, 2453 (1991).
12. L. M. Duan, G. Giedke, J. I. Cirac, and P. Zoller, Phys. Rev. Lett. **84**, 2722 (2000).
13. R. Simon, Phys. Rev. Lett. **84**, 2726 (2000).
14. P. van Loock and A. Furusawa, Phys. Rev. A **67**, 052315 (2003).
15. A. S. Villar, M. Martinelli, and P. Nussenzveig, Opt. Commun. **242**, 551 (2004).
16. M. D. Levenson, R. M. Shelby, A. Aspect, M. D. Reid, and D. F. Walls, Phys. Rev. A **32**, 1550 (1985).
17. R. M. Shelby, M. D. Levenson, S. H. Perlmutter, R. G. DeVoe, and D. F. Walls, Phys. Rev. Lett. **57**, 691 (1986).
18. P. Galatola, L. A. Lugiato, M. G. Porreca, P. Tombesi, and G. Leuchs, Opt. Commun. **85**, 95 (1991).
19. A. S. Villar, K. N. Cassemiro, K. Dechoum, A. Z. Khoury, M. Martinelli, and P. Nussenzveig, J. Opt. Soc. Am. B **24**, 249 (2007).

Depois de superarmos as limitações da medida do campo de bombeio, com a aquisição de novos espelhos para a cavidade de análise, refletimos mais sobre o caráter da nossa medida, e as discrepâncias observadas entre a teoria e o experimento, investigadas no artigo [8]. Verificamos que os resultados experimentais se aproximavam mais das medidas nas quais a cavidade de bombeio apresenta perdas de acoplamento mais elevadas [34, 36], enquanto que cavidades mais fechadas tornavam-se mais suscetíveis ao excesso de ruído presento no bombeio [7, 35].

Na nossa hipótese de excesso de ruído de bombeio com origem no cristal, o uso de cavidades mais fechadas leva a um efeito importante de realimentação das flutuações de fase adicionadas, enquanto resultados de emaranhamento pareciam mais bem sucedidos com cavidades de bombeio mais abertas. Optamos então por uma nova cavidade do OPO, e uma cavidade de análise para o feixe de bombeio com espelhos de qualidade e características comparáveis às empregadas para os modos no infravermelho (sinal e complementar).

Para nosso espanto, as tentativas realizadas ao longo de oito meses se mostraram infrutíferas. Como podemos ver no artigo a seguir, retornamos à cavidade da ref. [7], empregada na verificação do emaranhamento bipartite. Buscando aumentar as correlações, fizemos as medidas a 21 MHz, avançando dentro da largura de banda da cavidade. Trocamos os detetores do verde por outos de eficiência mais alta (94 %), favorecendo a medida do sinal e reduzindo o ruído de vácuo adicionado à medida.

Ainda que a violação da desigualdade (4.4) fosse observada (fig. 4.4), com uma violação consistente na variância inferida da soma das fases dos modos sinal e complementar, nenhuma das desigualdades (4.6) ou (4.7) era violada, atingindo no máximo o limite quântico padrão tanto para a amplitude quanto para a fase.

Apesar do insucesso, aprendemos muito neste trabalho. Primeiro, que nosso modelo apresentado na ref. [8] era insuficiente, como pode ser visto na fig. 4.5. Neste caso, observa-se um bom ajuste do excesso de ruído de fase para a variância do modo de bombeio ($\Delta^2\hat{q}_0$). Porém, para descrever o excesso de ruído na soma das fases ($\Delta^2\hat{q}_+$), precisamos adicionar um excesso de ruído duas vezes maior, o qual, no entanto, falha ao descrever o resultado do cálculo da variância inferida ($\Delta^2\hat{q}'_+$).

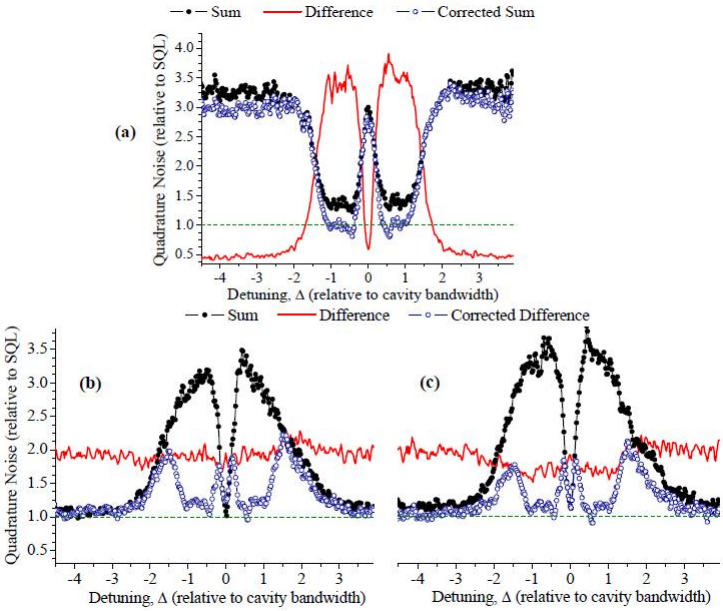

Figura 4.4: Medidas das testemunhas de emaranhamento: a) S_1 (eq. 4.4), a) S_2 (eq. 4.6), a) S_3 (eq. 4.7)

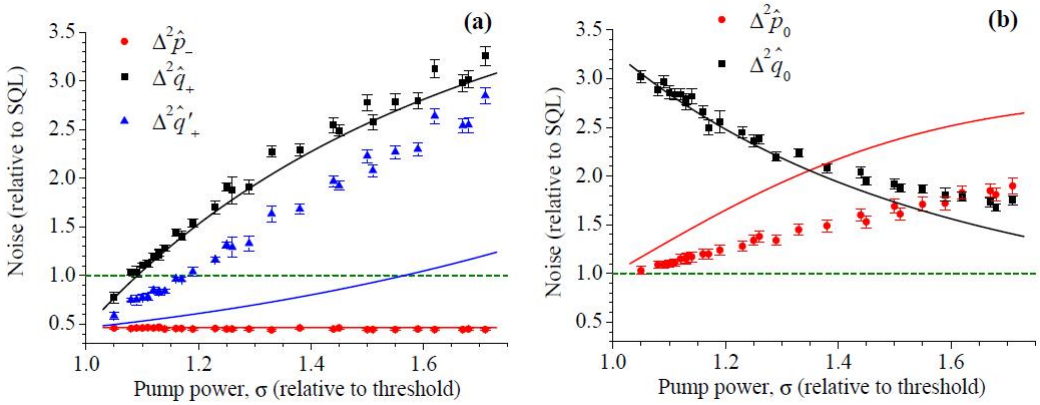

Figura 4.5: a) Medida das contribuições do ruído da diferença das intensidades e da variância inferida da soma das fases dos feixes sinal e complementar. As curvas consideram um excesso de ruído no bombeio de 14 unidades do ruído quântico padrão (SQL). b) Variância do campo de bombeio. O melhor acordo foi obtido com ruído adicional de bombeio de 6 SQL.

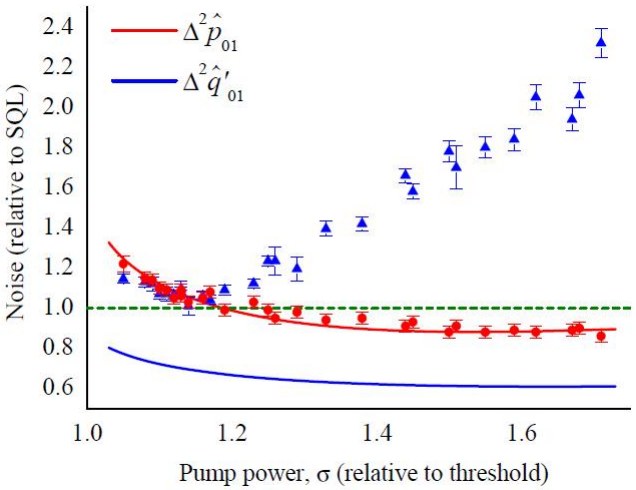

Figura 4.6: Observação de correlações quânticas entre as intensidades dos campos bombeio e sinal.

Nem todas as notícias foram ruins, no entanto. Na figura 4.6 vemos que pelo menos na soma das flutuações de amplitude dos modos sinal e bombeio temos uma correlação quântica, com a obtenção de compressão de ruído neste sinal. A resposta é condizente com o modelo teórico, como fora a variância da diferença de amplitudes entre sinal e complementar. Portanto, a parte da amplitude do OPO parecia funcionar a contento. E ainda que a variância de van Loock e Furusawa não fosse violada, ela chegava muito perto disso.

Os resultados foram divulgados, na espera de novas ideias, novas discussões, que solucionassem o emaranhamento perdido. O problema foi atacado de duas maneiras. Nas medidas, para a obtenção dos resultados, foi feita a primeira caracterização completa da matriz espectral de ruído do OPO, para uma dada frequência de análise. Sabíamos que a violação das desigualdades de van Loock era uma condição suficiente para o emaranhamento, mas não necessária. A otimização dos pesos dos campos dava margem para grandes incertezas sobre os melhores valores. Haveria alguma forma melhor de testar o emaranhamento? Haveria um critério necessário e suficiente para variáveis contínuas?

Por outro lado, como lidar com o ruído? Por que o OPO insistia em não concordar com a teoria? O que lhe faltava, se o modelo de ruído no bombeio não era suficiente para justificar o comportamento do sistema?

The quest for three-color entanglement: experimental investigation of new multipartite quantum correlations

K. N. Cassemiro,[1] A. S. Villar,[1,2] M. Martinelli,[1] and P. Nussenzveig[1*]

[1]*Instituto de Física, Universidade de São Paulo, Caixa Postal 66318, São Paulo, SP, Brazil, 05315-970*
[2]*Current address: Institute for Quantum Optics and Quantum Information of the Austrian Academy of Sciences, and Institut für Experimentalphysik, Universität Innsbruck, Technikerstr. 25/4, 6020 Innsbruck, Austria*
[*]*Corresponding author: nussen@if.usp.br*

Abstract: We experimentally investigate quadrature correlations between pump, signal, and idler fields in an above-threshold optical parametric oscillator. We observe new quantum correlations among the pump and signal or idler beams, as well as among the pump and a combined quadrature of signal and idler beams. A further investigation of unforeseen classical noise observed in this system is presented, which hinders the observation of the recently predicted tripartite entanglement. In spite of this noise, current results approach the limit required to demonstrate three-color entanglement.

OCIS codes: (270.0270) Quantum optics; (270.6570) Squeezed states; (190.4970) Parametric oscillators and amplifiers

References and links

1. A. Heidmann, R. J. Horowicz, S. Reynaud, E. Giacobino, C. Fabre, and G. Camy, "Observation of Quantum Noise Reduction on Twin Laser Beams," Phys. Rev. Lett. **59,** 2555–2557 (1987).
2. J. Laurat, L. Longchambon, C. Fabre, and T. Coudreau, "Experimental investigation of amplitude and phase quantum correlations in a type II optical parametric oscillator above threshold: from nondegenerate to degenerate operation," Opt. Lett. **30,** 1177–1179 (2005).
3. M. D. Reid and P. D. Drummond, "Quantum correlations of phase in nondegenerate parametric oscillation," Phys. Rev. Lett. **60,** 2731–2733 (1988)
4. Z. Y. Ou, S. F. Pereira, H. J. Kimble, and K. C. Peng, "Realization of the Einstein-Podolsky-Rosen Paradox for Continuous Variables," Phys. Rev. Lett. **68,** 3663–3666 (1992).
5. A. Furusawa, J. L. Sørensen, S. L. Braunstein, C. A. Fuchs, H. J. Kimble, and E. S. Polzik, "Unconditional Quantum Teleportation," Science **282,** 706–709 (1998).
6. X. Li, Q. Pan, J. Jing, J. Zhang, C. Xie, and K. Peng, "Quantum Dense Coding Exploiting a Bright Einstein-Podolsky-Rosen Beam," Phys. Rev. Lett. **88,** 047904 (2002).
7. H. Yonezawa, T. Aoki, and A. Furusawa, "Demonstration of a quantum teleportation network for continuous variables," Nature **431,** 430–433 (2004).
8. A. S. Villar, L. S. Cruz, K. N. Cassemiro, M. Martinelli, and P. Nussenzveig, "Generation of Bright Two-Color Continuous Variable Entanglement," Phys. Rev. Lett. **95,** 243603 (2005).
9. X. L. Su, A. Tan, X. J. Jia, Q. Pan, C. D. Xie, and K. C. Peng, "Experimental demonstration of quantum entanglement between frequency-nondegenerate optical twin beams," Opt. Lett. **31,** 1133–1135 (2006).
10. J. Jing, S. Feng, R. Bloomer, and O. Pfister, "Experimental continuous-variable entanglement of phase-locked bright optical beams," Phys. Rev. A **74,** 041804(R) (2006).
11. A. S. Villar, K. N. Cassemiro, K. Dechoum, A. Z. Khoury, M. Martinelli, and P. Nussenzveig, "Entanglement in the above-threshold optical parametric oscillator," J. Opt. Soc. Am. B **24,** 249–256 (2007).
12. K. Kasai, G. Jiangrui, and C. Fabre, "Observation of squeezing using cascaded nonlinearity," Europhys. Lett. **40,** 25–30 (1997).

13. A. S. Villar, M. Martinelli, C. Fabre, and P. Nussenzveig, "Direct Production of Tripartite Pump-Signal-Idler Entanglement in the Above-Threshold OPO," Phys. Rev. Lett. **97,** 140504 (2006).
14. K. N. Cassemiro, A. S. Villar, P. Valente, M. Martinelli, and P. Nussenzveig, "Experimental observation of three-color optical quantum correlations," Opt. Lett. **32,** 695–697 (2007).
15. P. van Loock and A. Furusawa, "Detecting genuine multipartite continuous-variable entanglement," Phys. Rev. A **67,** 052315 (2003).
16. P. Hyllus and J. Eisert, "Optimal entanglement witnesses for continuous-variable systems," New J. Phys. **8**, 51 (2006).
17. S. J. van Enk, N. Lütkenhaus, and H. J. Kimble, "Experimental procedures for entanglement verification," Phys. Rev. A **75**, 052318 (2007).
18. L. M. Duan, G. Giedke, J. I. Cirac, and P. Zoller, "Inseparability Criterion for Continuous Variable Systems," Phys. Rev. Lett. **84,** 2722–2725 (2000).
19. R. Simon, "Peres-Horodecki Separability Criterion for Continuous Variable Systems," Phys. Rev. Lett. **84,** 2726–2729 (2000).
20. B. Willke, N. Uehara, E. K. Gustafson, R. L. Byer, P. J. King, S. U. Seel, and R. L. Savage, "Spatial and temporal filtering of a 10-W Nd:YAG laser with a Fabry-Perot ring-cavity premode cleaner," Opt. Lett. **23,** 1704–1706 (1998).
21. A.S. Villar, M. Martinelli, and P. Nussenzveig, "Testing the entanglement of intense beams produced by a non-degenerate optical parametric oscillator," Opt. Commun. **242,** 551-563 (2004).
22. P. Galatola, L. A. Lugiato, M. G. Porreca, P. Tombesi, and G. Leuchs, "System control by variation of the squeezing phase," Opt. Commun. **85,** 95–103 (1991).
23. D. Wang, Y. Shang, X. J. Jia, C. D. Xie, and K. C. Peng, "Dependence of quantum correlations of twin beams on pump finesse of optical parametric oscillator," http://arxiv.org/abs/0709.4520.

1. Introduction

The optical parametric oscillator (OPO) is a very well-known source of non-classical light. Quantum correlations between the intensities of the downconverted beams, signal and idler, were first measured already in 1987 [1]. Because of the high degree of correlation attainable between these two bright light fields, they were called, in the above-threshold operation, *twin beams*. In fact, squeezing in the intensity difference reached the impressive value of -9.7 dB [2]. As was first recognized by Reid and Drummond in 1988, the quantum correlations are not restricted to intensity but also extend to their phases: the OPO produces twin beams in an *Einstein-Podolsky-Rosen* (EPR) state [3]. EPR-type entanglement was obtained a few years later in the OPO, but only when operating below threshold [4]. Since then, this system has been used in many applications in continuous-variable quantum information [5–7].

The measurement of entanglement in the above-threshold OPO would take 17 years to be realized [8–10], in part because of technical difficulties to perform phase measurements on bright beams that usually have different frequencies. Another important reason was the presence of an unexpected excess noise generated in the intracavity pump field by the non-linear crystal, which was transferred to the sum of downconverted phases during the parametric process, as was discovered by Villar *et al.* [11]. As a consequence, squeezing in this observable could only be found very close to the oscillation threshold [8]. This strange feature, unaccounted for by the theoretical model, went unnoticed until recently, when phase measurements were performed above threshold. We present here a further study of the fields' quadrature noises as functions of pump power to show that the standard theoretical model for the OPO can not account for the observed features. Even the *ad hoc* model presented in ref. [11] reveals itself to be insufficient. These noise features warrant investigation in themselves, which will have to go beyond the present work.

Another "surprise" was to be encountered in this thoroughly studied system. Although quadrature squeezing of the reflected pump beam was experimentally observed in 1997 [12], little attention was paid to quantum properties of the pump field. In many theoretical approaches, the pump was treated as a classical quantity. A very recent investigation of the quantum properties of the full three-mode system, by Villar *et al.*, revealed that all three fields should be

entangled [13]. This seems to be the simplest system predicted to directly generate tripartite continuous-variable entanglement. It also appears to be a distinctive feature of above-threshold operation, in contrast to the widely-used OPO below threshold. The first observation of a triple quantum correlation was recently reported by *Cassemiro et al.*, who observed squeezing in the combination of the sum of twins' phases with the reflected pump amplitude, for a detuned OPO [14]. This result was a good indication that phase–phase correlations should be present for a resonant OPO, as theoretically predicted [13].

Here we present the first direct observation of such triple quantum phase correlations. For higher pump powers, we show as well that the amplitude of the reflected pump beam is quantum-mechanically correlated to each of the twin's amplitudes. To our knowledge, this is the most comprehensive experimental characterization of the above-threshold OPO to date. As for the tripartite entanglement, owing to the spurious excess phase noise introduced by the non-linear crystal in the intracavity pump field [11], the quantum correlations observed do not suffice.

The quest for bright multicolor entangled beams will be rewarded by providing an interesting tool for quantum information networks, since they can concomitantly interact with physical systems otherwise incompatible. We describe below our latest experimental advancements in this direction.

2. Tripartite entanglement

The existence of direct tripartite pump-signal-idler entanglement can be physically understood as a consequence of energy conservation. The parametric process imposes for the frequencies of these fields the relation $\nu_0=\nu_1+\nu_2$ (indices 0, 1, and 2 refer to pump, signal, and idler fields, respectively). Phase fluctuations, regarded as small frequency fluctuations, are therefore connected: $\delta\varphi_0=\delta\varphi_1+\delta\varphi_2$. This leads to strong quantum correlations among the phase fluctuations of the three fields. On the other hand, the creation of a pair of signal and idler photons inside the OPO cavity only occurs upon annihilation of a pump photon. In triply resonant cavities, as we consider here, pump depletion above threshold is a well-known effect. Correlations between the amplitudes of the pump and twin beams are thus created.

In order to demonstrate multipartite entanglement, there exist different criteria [15–17]. We note that a general classification of multipartite entanglement for continuous-variable states is still an open problem. As in most recent experiments, we test our system for full inseparability [15]: none of the three modes can be described separately from the other two. We denote the electromagnetic field's amplitude and phase quadratures as $\hat{p}_j = \exp(-i\varphi_j)\hat{a}_j + \exp(i\varphi_j)\hat{a}_j^\dagger$ and $\hat{q}_j = -i[\exp(-i\varphi_j)\hat{a}_j - \exp(i\varphi_j)\hat{a}_j^\dagger]$, respectively, where $j \in \{0,1,2\}$. The fields' annihilation and creation operators are denoted $\hat{a}_j$ and $\hat{a}_j^\dagger$, satisfying $[\hat{a}_j, \hat{a}_{j'}^\dagger] = \delta_{j,j'}$, $j' \in \{0,1,2\}$, and φ_j are the fields' mean phases. Tripartite entanglement among three fields can be witnessed by violation of the following inequalities [13, 15]:

$$V_0 = \Delta^2\left(\frac{\hat{p}_1-\hat{p}_2}{\sqrt{2}}\right) + \Delta^2\left(\frac{\hat{q}_1+\hat{q}_2}{\sqrt{2}} - \alpha_0\hat{q}_0\right) \geq 2, \quad (1)$$

$$V_1 = \Delta^2\left(\frac{\hat{p}_0+\hat{p}_1}{\sqrt{2}}\right) + \Delta^2\left(\frac{\hat{q}_1-\hat{q}_0}{\sqrt{2}} + \alpha_2\hat{q}_2\right) \geq 2, \quad (2)$$

$$V_2 = \Delta^2\left(\frac{\hat{p}_0+\hat{p}_2}{\sqrt{2}}\right) + \Delta^2\left(\frac{\hat{q}_2-\hat{q}_0}{\sqrt{2}} + \alpha_1\hat{q}_1\right) \geq 2, \quad (3)$$

where α_j are numbers that minimize V_j. These are generalizations for tripartite systems of a criterion for bipartite systems derived independently by Duan *et al.* and Simon [18, 19]. In fact,

if one makes $\alpha_j = 0$, the bipartite criterion is recovered. Violation of at least two inequalities entails full three-mode inseparability [15]. In our case, one has $V_1 = V_2$ according to the model, since signal and idler beams play the same role in the OPO equations, differing only by polarization for type-II conversion, and by optical frequency. In the experiment, these two inequalities differ slightly owing to imperfections, such as unbalanced losses for signal and idler intracavity modes.

The first inequality contains well-known correlations. Its first term, $\Delta^2\hat{p}_-$ [where $\hat{p}_- = (\hat{p}_1 - \hat{p}_2)/\sqrt{2}$] corresponds to the amplitude correlation between the twin beams. The second one, $\Delta^2\hat{q}'_+$ [where $\hat{q}'_+ = (\hat{q}_1 + \hat{q}_2)/\sqrt{2} - \alpha_0\hat{q}_0$], can be written as the difference of $\Delta^2\hat{q}_+$ [where $\hat{q}_+ = (\hat{q}_1 + \hat{q}_2)/\sqrt{2}$], which involves the twins' phase anti-correlations, and a correction term β_0 given by their phase correlation with the pump,

$$\Delta^2\hat{q}'_+ = \Delta^2\hat{q}_+ - \beta_0\,, \qquad \beta_0 = \frac{(C_{\hat{q}_0\hat{q}_1} + C_{\hat{q}_0\hat{q}_2})^2}{2\Delta^2\hat{q}_0}, \tag{4}$$

where $C_{\hat{q}_j\hat{q}_{j'}} = \langle\delta\hat{q}_j\delta\hat{q}_{j'}\rangle$, $j' \neq j$. Notice that $\beta_0 \geq 0$. If $\Delta^2\hat{q}'_+ < 0$ and $\beta_0 \neq 0$, there is a quantum correlation between all three fields. The inequality corresponding to V_0 is violated even in the absence of the correction term, since signal and idler are entangled [8]. The correlation to the pump, signaled by β_0, strengthens this entanglement and increases the region of parameters where violation occurs [14].

Here, we present an extended experimental investigation of this system, by measuring in addition the quadrature noises appearing in the second and third inequalities. To simplify notation, we named the terms appearing in V_1 and V_2 as

$$\Delta^2\hat{p}_{0j} = \Delta^2\left(\frac{\hat{p}_0 + \hat{p}_j}{\sqrt{2}}\right), \tag{5}$$

$$\Delta^2\hat{q}'_{0j} = \Delta^2\left(\frac{\hat{q}_j - \hat{q}_0}{\sqrt{2}} + \alpha_j\hat{q}_j\right). \tag{6}$$

Following Eq. (4), we write

$$\Delta^2\hat{q}'_{0j} = \Delta^2\hat{q}_{0j} - \beta_{j'}, \qquad \beta_{j'} = \frac{(C_{\hat{q}_0\hat{q}_{j'}} - C_{\hat{q}_j\hat{q}_{j'}})^2}{2\Delta^2\hat{q}_{j'}}, \tag{7}$$

where $\hat{q}_{0j} = (\hat{q}_j - \hat{q}_0)/\sqrt{2}$ and $j' \neq j$. In this case, $\hat{q}_{0j}$ is the composite noise of the pump and one of the twin beams, and $\beta_{j'}$ is a correction term directly dependent on their correlations with the remaining beam.

3. Experimental set-up and system characteristics

The optical parametric oscillator comprises a non-linear $\chi^{(2)}$ crystal disposed inside a linear Fabry-Perot cavity. The coupling mirror for the pump beam is a partial reflector at 532 nm (reflectivity R =69.4%) and a high reflector (R >99.8%) at 1064 nm; the coupling mirror for the twin beams has reflectivities which are equal to 96.0% at 1064 nm and greater than 99.8% at 532 nm. The crystal is a 12 mm long type-II High Gray Tracking Resistant Potassium Titanyl Phosphate (KTP) from Raicol Crystals Ltd. The crystal temperature is kept constant by a peltier element near 25 °C, with a stability of the order of tens of mK. Its losses are approximately 3% at 532nm and less than 1% at 1064nm. Typical threshold power is about 75 mW, and the OPO cavity bandwidth is $\delta\nu_{opo}$=45(2) MHz. A frequency doubled diode-pumped Nd:YAG source (Innolight Diabolo) at 532 nm is used to pump the OPO. This laser is 'filtered' by a mode-cleaning cavity [20] (bandwidth of 2.4 MHz) prior to injection in the OPO, in order to

remove all classical noise which could hinder the entanglement for analysis frequencies above 15 MHz [11, 21].

Phase fluctuations are measured through a self-homodyne technique using optical cavities [21, 22]. An optical cavity adds a frequency-dependent phase to the field it reflects, as a function of the detuning between the incident beam carrier frequency and the cavity resonance frequency. Scanning the cavity resonance (e.g. with a piezo-electric device to change its length) results in different dephasings between the carrier and noise sidebands for each cavity detuning. In the Fresnel plane this can be qualitatively visualized as a rotation of the noise ellipse with respect to the mean field. As a result, the intensity fluctuations of the beam reflected by the cavity can correspond to fluctuations of any desired quadrature of the incident beam. It can be shown that the incident phase quadrature is totally converted into the reflected amplitude quadrature when the analysis frequency Ω is higher than $\sqrt{2}$ times the cavity bandwidth $\delta\nu$ [21, 22]. The cavity-carrier detunings Δ (relative to the cavity bandwidth) for which it occurs are $\Delta \approx \pm 0.5$ and $\Delta \approx \pm\Omega/\delta\nu$.

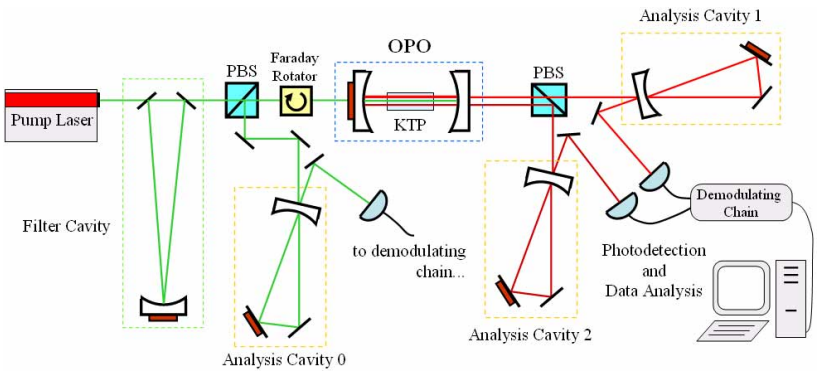

Fig. 1. Sketch of the experimental setup. PBS: polarizing beam splitter.

A sketch of the experimental set-up is presented in Fig. 1. There are three analysis cavities in the apparatus, with the following bandwidths: $\delta\nu_0$=11.5(6) MHz, $\delta\nu_1$=14.5(1) MHz and $\delta\nu_2$=13.6(2) MHz, where the indices correspond to the beam analyzed in each one. In order to measure the pump beam reflected by the OPO we use a Faraday Rotator and a polarizing beam splitter (PBS). The infrared beams are detected with high quantum efficiency (93%) photodiodes (Epitaxx ETX300), resulting in an overall detection efficiency of $\eta = 87(3)\%$. Another photodetector is used for the pump beam (Hamamatsu S5973-02, quantum efficiency of 94%), with an overall detection efficiency of $\eta_0 = 74(3)\%$.

The photocurrent high frequency component (HF) is sent to a demodulation chain, where it is mixed with a sinusoidal reference at the desired analysis frequency ($\Omega = 21$ MHz), within a 600 kHz bandwidth. Analysis frequency is chosen to have the smallest value (since the quantum correlations increase for decreasing frequency) such that the analysis cavity can still completely rotate the beams' noise ellipses. The resulting low frequency beat note is acquired at a rate of 600 kHz by an analog-to-digital (A/D) card connected to a computer. Variances of each individual noise component are then calculated taking a group of 1000 acquisition points. Finally, the noise power is normalized to the standard quantum limit (SQL), previously calibrated [14].

4. Measurement results

Our measurements were performed with the OPO cavity closely resonant to all three fields. We estimate that the OPO cavity detunings were smaller than 0.05 relative to its bandwidth

for twin beams. In this situation, amplitude and phase quadratures decouple [21]. All analysis cavities were synchronously scanned, such that the same quadrature (amplitude, phase, or a linear combination of them) was acquired simultaneously for the three beams at each time.

In our experimental investigation towards tripartite entanglement, we obtain data as presented in Fig. 2. It shows the noise of the sum (full circles + line) and the difference (full line) of each pair of beams' quadrature fluctuations as functions of the analysis cavities' detunings Δ relative to their bandwidths (set to be equal during the experiment). The calibrated shot noise level is given by the dashed line. Fig. 2(a) shows signal-idler combined noises, Fig. 2(b) considers signal-pump beams, and Fig. 2(c) depicts idler-pump noises. All curves show the expected noise ellipse rotation: amplitude quadrature noises are measured for large detunings ($|\Delta| \gtrsim 3$) and exactly on resonance ($\Delta = 0$), while phase quadrature noises appear for detunings half-bandwidth off-resonance ($\Delta \approx \pm 0.5$).

A third curve in each Fig. (open circles + line) shows the effect of including information about the third beam. They are obtained by subtracting the correction term from the sum curve, in the case of Fig. 2(a), or from the difference curve, in the cases of Figs. 2(b)-(c). The relevant regions in the corrected curves are located at $\Delta \approx \pm 0.5$, corresponding to phase measurements [(a) $\Delta^2\hat{q}'_+$, (b) $\Delta^2\hat{q}'_{01}$ and (c) $\Delta^2\hat{q}'_{02}$]. All the curves presented in Fig. 2 come from a single measurement where all three fields' noises were recorded at the same time.

We begin our analysis by Fig. 2(a), devoted to signal-idler correlations and to the noise correction by the pump beam. The well-known squeezing in $\hat{p}_-$ is seen for large detunings in the difference curve, with noise value $\Delta^2\hat{p}_- = 0.46(1)$. The sum curve at $\Delta = \pm 0.5$ gives the noise in $\hat{q}_+$, equal to $\Delta^2\hat{q}_+ = 1.28(3)$. Although no squeezing is observed in $\hat{q}_+$ in this situation (pump power relative to threshold $\sigma = P/P_{th} = 1.14$), entanglement is present, since $\Delta^2\hat{p}_- + \Delta^2\hat{q}_+ = 1.73(6) < 2$, violating the Duan *et al.* inequality [18]. However, squeezing can be obtained in the three-field composite observable $\hat{q}'_+$, with the value $\Delta^2\hat{q}'_+ = 0.84(3)$, according to the corrected sum curve at $\Delta = \pm 0.5$. This is the first direct observation of a quantum correlation among the phases of pump, signal, and idler. Ineq. (1) then provides the expected violation of the first tripartite entanglement inequality, $V_0 = \Delta^2\hat{p}_- + \Delta^2\hat{q}'_+ = 1.29(5) < 2$.

Figs. 2(b) and (c) present pump-twin correlations, and their difference noise corrected by the remaining twin. These two are very similar, as expected. The first term appearing in Ineq. (2) is measured in the sum curve of Fig. 2(b). It is shot noise limited, $\Delta^2\hat{p}_{01} = 1.03(3)$, as expected by the theoretical model, for this pump power. The difference of their phases $\Delta^2\hat{q}_{01}$ presents excess noise, which is reduced by the correction term β_2. The corrected difference phase noise $\hat{q}'_{01}$, however, is not squeezed as expected, but shot noise limited as well, $\Delta^2\hat{q}'_{01} = 1.01(4)$. This saturates Ineq. (2), $V_1 = \Delta^2\hat{p}_{01} + \Delta^2\hat{q}'_{01} = 2.04(11) \approx 2$. A similar result holds for Fig. 2(c). In this case, $\hat{p}_{02}$ presents a small amount of excess noise, $\Delta^2\hat{p}_{02} = 1.12(2)$, and $\hat{q}'_{02}$ is shot noise limited, $\Delta^2\hat{q}'_{01} = 0.97(3)$, resulting in $V_2 = \Delta^2\hat{p}_{02} + \Delta^2\hat{q}'_{02} = 2.09(7) > 2$ for Ineq. (3).

4.1. Unexpected noise features

Contrary to our expectations [13], we could not observe squeezing in $\Delta^2\hat{q}'_{01}$ or in $\Delta^2\hat{q}'_{02}$. We performed several measurements similar to those presented in Fig. 2 and recorded the values of noises for various pump powers. Each set of curves taken in one measurement scan, as the ones presented in Fig. 2, gives seven quantities of interest: $\Delta^2\hat{p}_-$, $\Delta^2\hat{q}_+$, $\Delta^2\hat{p}_0$, $\Delta^2\hat{q}_0$, $\Delta^2\hat{q}'_+$, $\Delta^2\hat{p}_{01}$, and $\Delta^2\hat{q}'_{01}$. Part of the results are presented in Fig. 3, where quadrature noises or their combinations are plotted as functions of pump power relative to threshold, σ.

In Fig. 3(a), the behaviors of terms belonging to Ineq. (1) are presented. The only noise curve that behaves in agreement with the theoretical model is $\Delta^2\hat{p}_-$ (red circles). It's constant value is quantitatively compatible with what we expect from the other independently measured

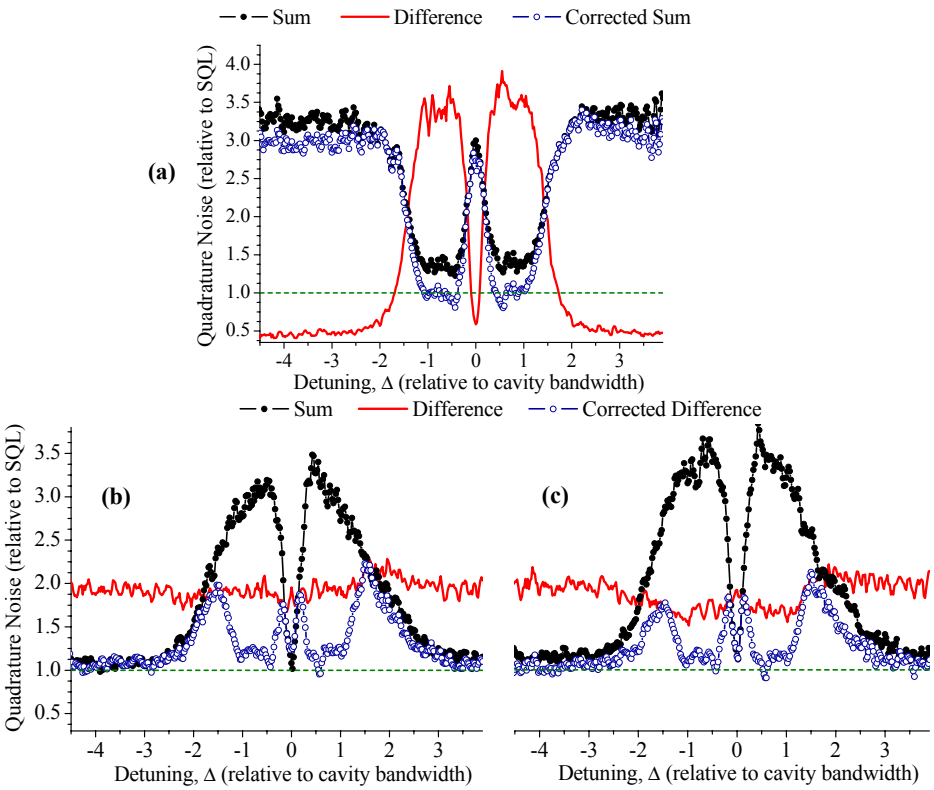

Fig. 2. Noise measurements of the terms appearing in the tripartite entanglement criteria of Ineqs. (1)–(3) (pump power relative to threshold $\sigma = P/P_{th} = 1.14$). As functions of cavity detuning Δ, black full circles + line curves correspond to the noises in the sum of quadratures of two beams, solid red line to their difference, and blue open circles + line to a corrected noise, in which information from the remaining beam is included. Amplitude quadratures are measured at large cavity detuning $|\Delta| \gtrsim 3$ and at $\Delta = 0$; phase quadratures are measured at $\Delta = \pm 0.5$. (a) The considered pair of beams is signal and idler, and the corrected *sum* curve includes the term β_0 coming from correlations with the pump beam; (b) signal–pump beams and *difference* correction using idler; (c) idler–pump beams and *difference* correction using signal. The corrected sum in (a) presents the first direct observation of a quantum correlation among the phases of pump, signal, and idler: the noise is 26% below the SQL.

OPO parameters (mirror transmissions, total intracavity loss, OPO bandwidth, and detection efficiency [21]), $\Delta^2 \hat{p}_- = 0.46(1)$. Model prediction is the red solid line.

Noise in the sum of twins' phases $\Delta^2 \hat{q}_+$ (black squares) shows squeezing only very close to the oscillation threshold ($\sigma \leq 1.1$) and excess noise otherwise. The usual theoretical model predicts that it should be squeezed for all values of σ tested, reaching shot noise only for $\sigma \gg 1$, if the incident pump beam is shot noise limited. The pump beam at the output of the filter cavity was verified to fulfill this requirement [11]. Yet, as we reported previously, excess noise is introduced in the intracavity pump beam by interaction within the non-linear crystal [11,14]. This was observed in the pump beam reflected from the OPO cavity, even when no parametric oscillation took place. The data presented in those papers was successfully modeled by introducing extra noise in the input pump beam. As we speculated in [11], this could be due to a non-linear

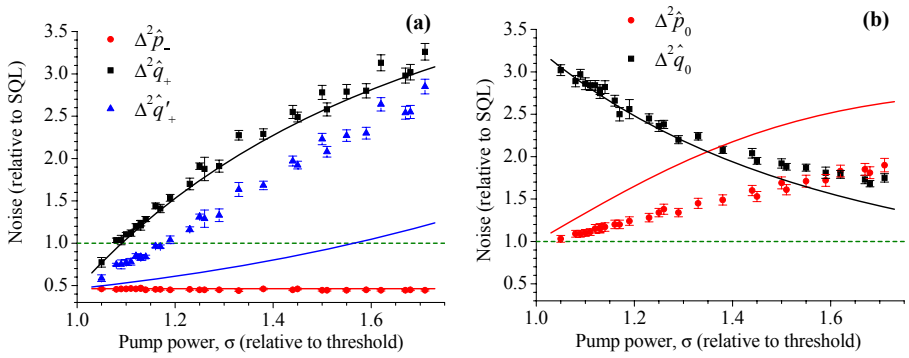

Fig. 3. Noise behaviors as functions of pump power σ. (a) Terms appearing in Ineq (1): the well-known squeezing in the subtraction of twins' intensity fluctuations $\Delta^2\hat{p}_-$ is shown in the red circles, noise of twins' sum of phase fluctuations $\Delta^2\hat{q}_+$ are the black squares and the phase noise corrected by information from the pump $\Delta^2\hat{q}'_+$ are the blue triangles. (b) Amplitude (red circles) and phase (black squares) noise of the pump beam reflected by the OPO cavity. Solid lines are tentative fits to the *ad hoc* model explained in the text. Predictions differ from the usual ones only for the phase quadratures. Theoretical curves have the same colors as the experimental curve to which they relate.

refractive index effect, which would generate excess phase noise. The quasi-resonant cavity would then partially convert it into amplitude noise. In order to circumvent this effect, we decided to lower the pump finesse, which would minimize accumulated spurious phase shifts (the authors of ref. [9] claim this to be the main difference between their system, in which they do not observe this extra phase noise, and others). The OPO cavity finesse for the pump beam here is much lower than in our previous experiments. This modification entailed a lower reflected pump excess phase noise and completely suppressed the reflected pump amplitude noise but, alas, the mystery is far from solved, as described below.

In Fig. 3(b), we present measurements of the reflected pump amplitude and phase quadratures during oscillation, respectively shown as red circles and black squares, as functions of σ. We could not account simultaneously for the data of Figs. 3 (a) and (b). We tried to mimic the spurious excess noise effect by introducing *incident* pump phase noise $\Delta^2\hat{q}_0^{in}$ in the equations, as an *ad hoc* free parameter. Two different values of this parameter are needed in order to obtain the (already poor) agreement observed in Figs. 3 (a) and (b). In order to obtain the black solid curve in Fig. 3 (a), we used the value $\Delta\hat{q}_{0T}^{in} = 14$; in order to do the same in Fig. 3 (b), we used $\Delta\hat{q}_{0P}^{in} = 6$. The reflected pump phase noise is lower than would be needed to account for the twins' excess phase noise. Furthermore, the reflected pump amplitude noise is even lower than expected by the linear model with *no* extra noise (already taking into account the finite detection efficiency). We also tried to fit our data to a recently proposed model [23] for this excess noise, but did not obtain good agreement.

Next, we observe a correlation between the pump and twins' phase quadratures. In spite of its novel manifest quantum nature, we do not find agreement with the model. The blue solid line in Fig. 3 (a), was obtained by using $\Delta^2\hat{q}_{0T}^{in} = 14$. Since we are investigating a correlation between pump and twins' quadratures, and we could not find a single parameter to account for pump and twins separately, the poor agreement is not surprising.

The noise features of the reflected pump phase quadrature are indeed more complicated than could be modeled by a single parameter. We measured this phase noise as a function of the analysis frequency, for pump powers close to threshold and two different incident polariza-

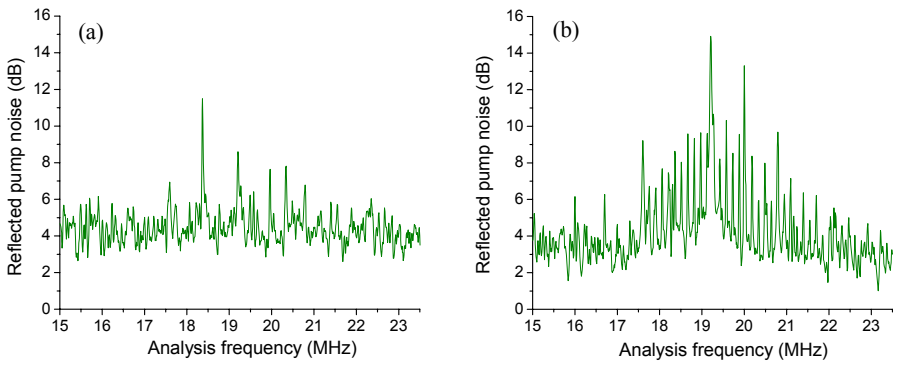

Fig. 4. Reflected pump phase noise, as a function of the analysis frequency. Pump power is close to threshold, but temperature is tuned to avoid triple resonance. In (a), the pump polarization is such that the phase matching conditions are fulfilled, whereas in (b) the orthogonal polarization is used. Measurements are normalized to the shot noise level (0 dB level).

tions.In this measurement, the analysis cavity for the pump beam is locked to a detuning $\Delta = 0.5$ and the photocurrents are analyzed by means of a spectrum analyzer (Resolution Bandwidth, RBW = 10 kHz, Video Bandwidth, VBW = 100 Hz). The phase matching conditions for the parametric process are only fulfilled for one of these polarizations. We observed a rich spectrum, presented in Fig. 4, with evenly spaced peaks [spacing approximately 150(10) kHz] of up to 15 dB of excess noise, on top of a broad ~ 4 dB excess noise plateau. The peak structure is more pronounced for the "wrong" polarization, for which phase matching is not fulfilled [Fig. 4 (b)]. At present, we cannot explain these noise features. Further investigation is needed, in order to reveal the physical mechanism behind such rich structure.

4.2. New quantum correlations

In spite of these unknown noise features, we could still check our experimental results against the tripartite criteria of Ineqs. (1) – (3). We have already shown violation of Ineq. (1). Owing to the similarity between the twin beams, Ineqs. (2) and (3) should be equivalent, but we obtained better results for Ineq. (2), as explained above. Our experimental results, as a function of σ, are presented in Fig. 5. A new quantum correlation, among the amplitudes of the pump and the signal beams (manifest in $\Delta^2\hat{p}_{01}$, red circles), is observed for the first time in the above-threshold OPO. We obtain squeezing for higher values of pump power, $\Delta^2\hat{p}_{01} \approx 0.88$. Since it only involves amplitude quadratures, good agreement with the theoretical model (full red line) is obtained (no excess noise is input in the model). The sum of this term with $\Delta^2\hat{q}'_{01}$ (phase difference between pump and signal phases, corrected by idler phase noise) corresponds to the left hand side in Ineq. (2). Data for $\Delta^2\hat{q}'_{01}$ are presented as blue triangles in Fig. 5. The solid blue line corresponds to the theoretical model with no extra noise (adding extra noise does not provide good agreement). For $\sigma \approx 1.15$, we approach the classical limit of Ineq. (2), with the lowest value given by V_1=2.04(11).

Even by including spurious excess noise in the model, we would expect lower noise values for $\Delta^2\hat{q}'_{01}$, leading to the predicted tripartite entanglement. Although we observed two new quantum correlations among the pump and the twin beams, tripartite entanglement still remains to be demonstrated. Our results suggest that further modifications to the setup may suffice. Technical improvements, such as a reduction of intracavity spurious losses and of detection losses, entail better squeezing and better detection efficiency.

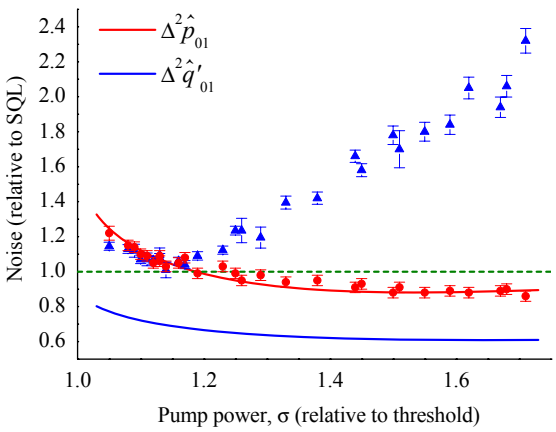

Fig. 5. Behaviors of the noise terms appearing in Ineq (2) as functions of pump power σ. The red circles correspond to the first term in the inequality and the blue triangles to the second one. The former presents the observation of amplitude quantum correlations between one of the twin beams and the reflected pump beam: there is $\approx 12\%$ of squeezing for higher σ values. The solid lines are the predictions of the model explained in the text, without added noise. Theoretical curves have the same color as the experimental symbol to which they relate.

The ability to measure any given quadrature of each field and their combinations, together with the broad range of pump powers relative to threshold that we can access, allow for complete characterizations of the OPO's noise properties. In the near future, we expect to determine the excess noise source, to circumvent it, and reliably generate tripartite entanglement.

5. Conclusion

We presented a new and thorough investigation of quadrature noise of pump, signal, and idler fields in the above-threshold OPO. Although the OPO theory is well established, an important part of it had never been tested above the oscillation threshold. We revealed an unnoticed extra noise in the system and have further characterized several of its features. It seems safe to say that only phase noise is generated in the intracavity crystal. The amplitude noise observed in previous experiments was due to phase-to-amplitude conversion by the quasi-resonant cavity. This effective refractive index should be frequency dependent. Thus, by changing the pump frequency, it may be possible to minimize it. All this is still insufficient to pin down the ultimate physical origin of this noise. More research is needed to solve this intriguing puzzle.

Notwithstanding the unwelcome extra noise, we could demonstrate new quantum correlations among pump and twin beams. The predicted quantum correlation among the phase quadratures, which is a direct consequence of energy conservation, was observed for the first time. When operating further above threshold, pump depletion becomes more evident as we observe the quantum correlation between the pump and each twin's amplitudes. By combining these results, we approached the limit for demonstrating tripartite entanglement: V_0=1.29(5), V_1=2.04(11), and V_2=2.09(7), where a violation corresponds to $V_j < 2$. Hopefully, by improving the squeezing and the detection efficiencies, we will beat this limit. As mentioned above, we should also test other tripartite entanglement criteria, to rule out every possible form of partially separable states or their mixtures [16].

The approach to directly generate multipartite entanglement, when compared to its genera-

tion by means of individual squeezers and linear optics, has the potential advantage of entangling fields of different colors. This advantage is exploited in our setup and we expect it to be the starting point for multicolor quantum networks.

Acknowledgments

We thank Dr. Peter van Loock for fruitful discussions. This work was supported by Fundação de Amparo à Pesquisa do Estado de São Paulo (FAPESP), Conselho Nacional de Desenvolvimento Científico e Tecnológico (CNPq), through *Instituto do Milênio de Informação Quântica*, and Coordenação de Aperfeiçoamento de Pessoal de Nível Superior (CAPES).

4.2 Tripartite afinal!

Como vimos no capítulo anterior, o modelo do OPO era incompleto. É curioso notar que um dos grandes trunfos da ótica quântica realizada na faixa do visível e do infravermelho próximo é que a densidade de fótons da radiação de corpo negro na faixa de energia de 1 *ev* é baixa o suficiente para ser ignorada em todos os procedimentos experimentais. No entanto, o espalhamento Brillouin leva ao acoplamento entre os fótons e os fónons da rede, produzindo o excesso de ruído observado em [13], graças à interação do meio de conversão paramétrica. Na hamiltoniana, falta portanto um termo de acoplamento, em contato com um reservatório térmico, o qual precisamos agora controlar.

Antônio Sales Coelho, durante seu mestrado [50] e o início do seu doutorado, montou um sistema que permitia a refrigeração do cristal, mantendo-o em vácuo de bomba mecânica para evitar a condensação. Usando um fluxo de água gelada na base de cobre, e um peltier para refrigerar o cristal, atingimos -23°C. Esta variação de temperatura foi suficiente para reduzir o excesso de ruído na fase dos termos de variância (fig. 4.7). Note que a correlação de fase se mantém aproximadamente a mesma que fora observada na figura (4.8), bem como os termos da matriz de covariância ligados à amplitude. O ruído de fónons, no entanto, ainda está presente.

Paralelamente aos esforços para controlar o excesso de ruído no OPO, investigamos critérios mais seletivos para verificar o emaranhamento entre os campos. Ao longo do seu doutorado, Katiúscia havia investigado um outro critério, descrito por R. Simon [51], traduzindo para variáveis contínuas o critério de positividade sob transposição parcial de A. Peres [52]. A vantagem deste critério é que sua violação, para estados gaussianos, não é apenas condição suficiente para emaranhamento, mas também necessária. Podíamos aplicar então a transposição parcial a cada um dos modos, e descartar as três diferentes formas de escrever a matriz densidade mostradas nas equações (4.1 - 4.3). Ela havia feito o teste para o OPO descrito no artigo anterior, mas a violação era inferior à incerteza da testemunha de emaranhamento.

Seriam necessários mais dois anos para conseguir vencer este limite. Uma primeira questão que surge, na desigualdade de van Loock e Furusawa, é a presença de diversos parâmetros de ajuste. Escolhemos sempre alguns deles iguais a um (em módulo), outros nulos, e otimizamos o parâmetro restante. A violação nos garante emaranhamento, porém o inverso não implica em separabilidade, devido à indeterminação dos parâmetros. A solução, neste caso, é obter o máximo de informação possível, realizando a medida de *todos* os elementos da matriz de covariância, e buscar algum critério otimizado que pudesse dizer se estes estados estavam emaranhados. Descobrimos que o critério Simon-PPT [51] satisfazia esta condição. Mais que isso, se os estados fossem gaussianos, o resultado é uma testemunha indiscutível de emaranhamento ou separabilidade.

No artigo a seguir, vemos que após o resfriamento conseguimos satisfazer tanto o critério de van Loock e Furusawa quanto o critério Simon-PPT para emaranhamento. Esta é a conclusão de uma busca que, em nossos laboratórios, começou em 2003, e ao final da qual, acreditávamos saber tudo sobre o OPO. Descobrimos uma fonte insuspeita

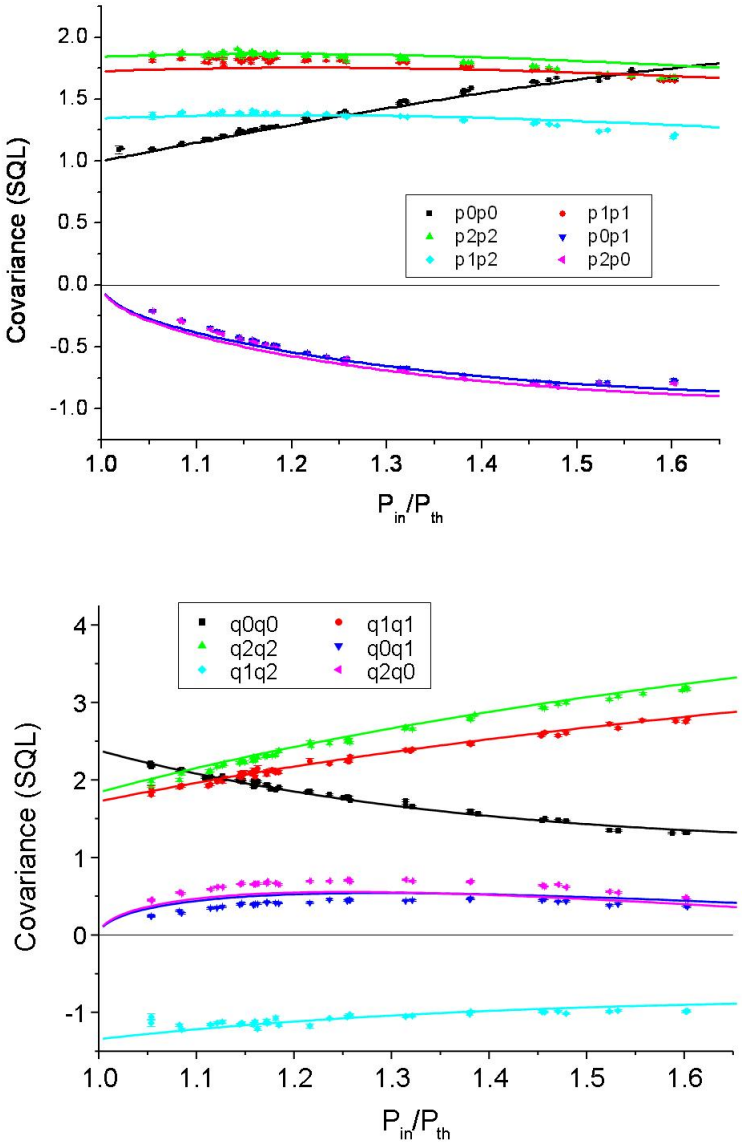

Figura 4.7: Valores dos termos da matriz de ruído do OPO, em função da potência de bombeio, a -23°C.

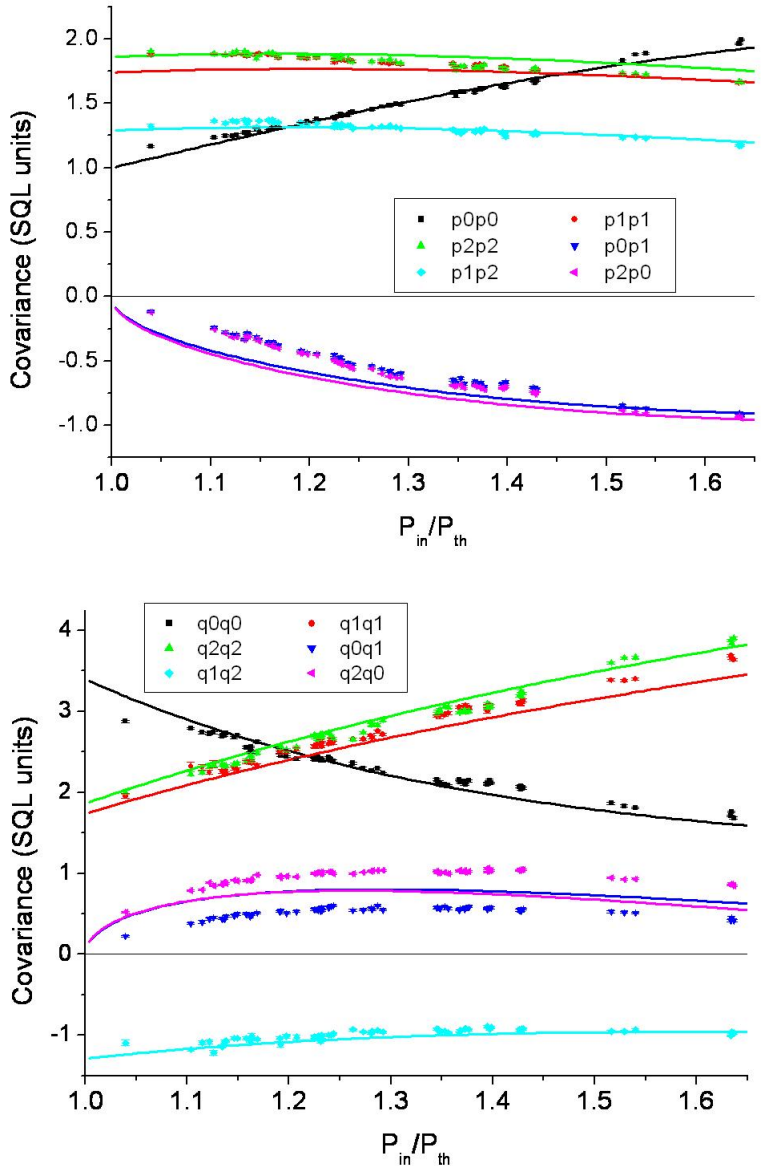

Figura 4.8: Valores dos termos da matriz de ruído do OPO, em função da potência de bombeio, a $23°C$.

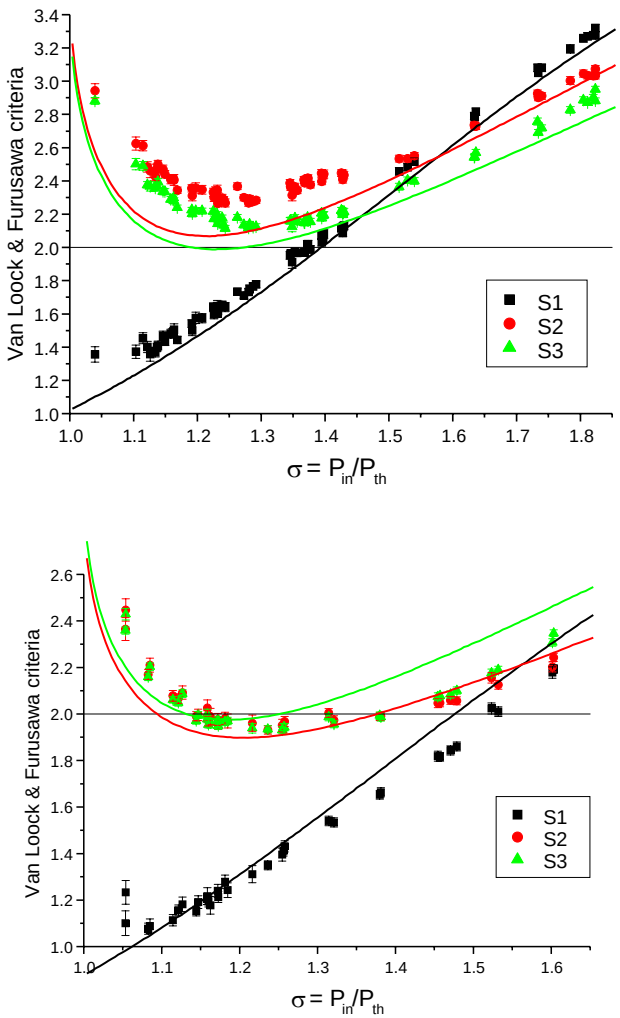

Figura 4.9: Critérios de van Loock e Furusawa, calculados a partir dos termos de matriz de covariância: acima, usando os valores presentes no gráfico 4.8, medidos a 23 $°C$; abaixo, calculados a partir dos termos de matriz de covariância presentes no gráfico 4.7, medidos a -23 $°C$.

de excesso de ruído, e conseguimos controlá-la. Alguns poucos detalhes técnicos nos escapavam ainda. Por quê o limiar de oscilação caiu em cerca de 14 % com a variação de temperatura observada? E por quê o ruído de fónons cai tão rapidamente, de forma que basta uma variação de 46 K a partir da temperatura ambiente (16% apenas) para obter o emaranhamento?

Mas havíamos obtido a matriz de ruído completa, e demonstramos que podemos gerar emaranhamento entre três campos distintos, com cores diferentes, diretamente a partir da conversão paramétrica de segunda ordem, o mesmo sistema empregado para geração de estados comprimidos desde 1986.

15. A. R. W. Schröder *et al.*, *Cell* **110**, 521 (2002).
16. D. J. Loes *et al.*, *Am. J. Neuroradiol.* **15**, 1761 (1994).
17. M. Cavazzana-Calvo *et al.*, *Science* **288**, 669 (2000).
18. S. Hacein-Bey-Abina *et al.*, *N. Engl. J. Med.* **346**, 1185 (2002).
19. H. B. Gaspar *et al.*, *Lancet* **364**, 2181 (2004).
20. A. Aiuti *et al.*, *N. Engl. J. Med.* **360**, 447 (2009).
21. N. Uchida *et al.*, *Proc. Natl. Acad. Sci. U.S.A.* **95**, 11939 (1998).
22. W. Piacibello *et al.*, *Blood* **100**, 4391 (2002).
23. S. Hacein-Bey-Abina *et al.*, *Science* **302**, 415 (2003).
24. E. Montini *et al.*, *J. Clin. Invest.* **119**, 964 (2009).
25. M. De Palma *et al.*, *Blood* **105**, 2307 (2005).
26. E. Montini *et al.*, *Nat. Biotechnol.* **24**, 687 (2006).
27. N. Davoust, C. Vuallat, C. Androdias, S. Nataf, *Trends Immunol.* **29**, 227 (2008).
28. A. Biffi *et al.*, *J. Clin. Invest.* **116**, 3070 (2006).
29. We thank A. Salzman and R. Salzman for their continuous help and support in this project; the pediatricians and nurses of the Unité d'Endocrinologie et Neurologie Pédiatriques, Hôpital Saint-Vincent de Paul and the Unité d'Immunologie et d'Hématologie Pédiatriques, Hôpital Necker-Enfants Malades for patient care; A. Pujol and C. Sever Bermejo for patient referral; C. Adamsbaum for neuroimaging studies; F. Audat for cytapheresis; P. Lebon for HIV and VSV.G serologies; C. Lagresle-Peyrou for setting up the transduction protocol; P. Working and Cell Genesys staff for the lenti-MND-ALD vector; PeproTech for SCF, Flt-3, MGDF, and IL-3 cytokines; Takara Bio for the CH-296 fibronectin fragment; and E. Postaire and C. Sebastiani at INSERM. P.A. and N.C. were supported by grants from INSERM, European Leukodystrophy Association, Association Française contre les Myopathies, La Fondation de France, the STOP-ALD foundation, La Fondation Avenir, Etablissement Français des Greffes, Thermo Fisher Scientific, the 6th Framework European Economic Community (EEC) Programme (LSHM-CT2004-502987) and the Programme Hospitalier de Recherche Clinique (AOM 3043, French Health Ministry). S.H.-B.-A., L.D.-C., L.C., F.L., A.F., and M.C.-C. were supported by INSERM, Assistance Publique–Hôpitaux de Paris, Centre d'Investigation Clinique–Biotherapy, and Association Française contre les Myopathies. C.V.K. and M.S. were supported by grants from the Deutsche Forschungsgemeinschaft (SPP 1230), the German Ministry of Education and Research (TREATID), the Helmholtz Association, and the 6th Framework EEC Programme (CONSERT, CLINIGENE). P. Leboulch owns stock in Genetix Pharmaceuticals, and G. Veres, V. Kiermer, and D. Mittelstaedt were formerly employed at Cell Genesys. This gene therapy trial was approved by AFSSAPS on 15 November 2005 and CCPPRB Paris-Cochin (local Institutional Review Board) on 7 September 2004. Informed consent was obtained from the parents of the patients after the nature and possible consequences of the studies were explained.

Supporting Online Material
www.sciencemag.org/cgi/content/full/326/5954/818/DC1
Materials and Methods
SOM Text
Figs. S1 to S5
Tables S1 and S2
References

22 January 2009; accepted 4 September 2009
10.1126/science.1171242

REPORTS

Three-Color Entanglement

A. S. Coelho,[1] F. A. S. Barbosa,[1] K. N. Cassemiro,[2] A. S. Villar,[2,3] M. Martinelli,[1] P. Nussenzveig[1]*

Entanglement is an essential quantum resource for the acceleration of information processing as well as for sophisticated quantum communication protocols. Quantum information networks are expected to convey information from one place to another by using entangled light beams. We demonstrated the generation of entanglement among three bright beams of light, all of different wavelengths (532.251, 1062.102, and 1066.915 nanometers). We also observed disentanglement for finite channel losses, the continuous variable counterpart to entanglement sudden death.

Since Schrödinger defined entanglement as "the characteristic trait of quantum mechanics" (*1*), much study has been devoted to its understanding. Possible applications to information tasks such as storage, computation, and communications have generated a large amount of research (*2*). Quantum computing is expected to be more efficient than its classical counterpart, and there are quantum algorithms (*3*) that greatly surpass the best classical ones. Quantum communications can, in principle, provide absolute security (*4*). Nevertheless, many technological challenges remain, because the quantum resources are fragile and undergo decoherence from their inevitable interactions with the surrounding environment (*5*). Furthermore, many fundamental issues regarding the nature and dynamics of entanglement remain to be understood (*6*).

A variety of physical systems are currently under investigation to perform the envisioned information tasks (*7*–*12*). Because each one has its advantages and disadvantages, it is likely that several of them will be combined to perform reliable quantum information tasks. Light, in view of its high speed and weak interaction with the environment, is a strong candidate to convey quantum information by using quantum teleportation (*13*, *14*). To connect such different physical systems (typically lacking a joint resonance) at the nodes of a quantum network (*15*), however, different frequencies of light will be necessary. For two such beams, entanglement has already been demonstrated, ranging from small frequency differences (*16*, *17*) up to one frequency being twice the other (*18*). It is important to go beyond just two beams for multimode networks. Our demonstration used three field modes with different wavelengths.

Our system is an optical parametric oscillator (OPO), which consists of a nonlinear optical crystal inside a cavity, so that the fields are fed back into the system. Light that is incident on the crystal undergoes parametric down-conversion, a process whereby an incident photon is converted into a pair of longer-wavelength photons, fulfilling energy conservation $\omega_0 = \omega_1 + \omega_2$, where the ω_i (i = 0, 1, 2) values are the angular frequencies of the incident light and of the two generated photons, respectively. Momentum is also conserved, corresponding to the phase-matching condition. Owing to the cavity feedback, down-converted photons can be emitted in occupied field modes, a process known as stimulated emission, with increasing probability as the number of photons in the mode grows, thus providing gain. When the pump laser power is increased, the gain overcomes the losses and the system oscillates. Above this oscillation threshold, tripartite entanglement has been predicted (*19*). Down-converted photons are produced in pairs, yielding strong intensity correlations among the twin beams. To produce twin photons, a pump photon must be annihilated; thus, anticorrelations are expected between the reflected pump intensity and the sum of twin beams' intensities. The frequency constraint translates into a constraint for the phase variations (or fluctuations) of the three fields. The twins' phase fluctuations should be anticorrelated, and their sum should be correlated to the pump's phase fluctuations. One of the criteria for analyzing tripartite entanglement (*20*) is written directly in terms of these correlations, as sums of variances V involving the three fields.

$$V_0 = \Delta^2\left(\frac{p_1 - p_2}{\sqrt{2}}\right) + \Delta^2\left(\frac{q_1 + q_2}{\sqrt{2}} - \alpha_0 q_0\right) \geq 2$$
$$V_1 = \Delta^2\left(\frac{p_0 + p_1}{\sqrt{2}}\right) + \Delta^2\left(\frac{q_0 - q_1}{\sqrt{2}} - \alpha_2 q_2\right) \geq 2$$
$$V_2 = \Delta^2\left(\frac{p_0 + p_2}{\sqrt{2}}\right) + \Delta^2\left(\frac{q_0 - q_2}{\sqrt{2}} - \alpha_1 q_1\right) \geq 2 \quad (1)$$

It suffices to violate two of these inequalities to demonstrate tripartite entanglement. The p_i (i = 0, 1, 2) represent the amplitude quadratures of the fields, the q_i (i = 0, 1, 2) stand for their phase quadratures, and the α_i (i = 0, 1, 2) values are free parameters, chosen to maximally violate the inequalities. Phase and amplitude

[1]Instituto de Física, Universidade de São Paulo, Post Office Box 66318, São Paulo, SP 05314-970, Brazil. [2]Max Planck Institute for the Science of Light, Günther-Scharowsky-Strasse 1/Bau 24, 91058 Erlangen, Germany. [3]University of Erlangen-Nuremberg, Staudtstrasse 7/B2, 91058 Erlangen, Germany.

*To whom correspondence should be addressed. E-mail: nussen@if.usp.br

quadratures of each field do not commute, leading to a minimum uncertainty product, which characterizes the standard quantum limit (SQL). Variances in Eq. 1 are normalized to the SQL.

Above the oscillation threshold, bright, narrowband, and frequency-tunable twin beams are emitted by the OPO. Their quadrature fluctuations are measured by reflecting them off nearly resonant empty analysis cavities (*21*) before detection on high–quantum efficiency photodiodes (Fig. 1). Any quadrature of any given field can be measured by scanning the resonance frequency of the respective analysis cavity. In this way, the full three-field covariance matrix of the system, with terms of the form $<\delta X_i(\Omega)\delta X_j(-\Omega)>$ and $<\delta X_i(\Omega)\delta Y_j(-\Omega)>$ (where X and Y represent the field amplitude and phase quadratures; $i, j = 0, 1, 2$; and Ω is the analysis frequency), is directly measured (*22*). Thermal phonons that are present in the nonlinear crystal generate excess phase noise and hinder the quantum correlations, as recently described (*23*). Thus, we cooled the crystal to –23°C.

For Gaussian states, the complete information is available from the mean values (first-order moments) and the covariance matrix (second-order moments), of which only the latter is relevant for entanglement properties. By inspecting higher-order moments (up to 10) from the measured photocurrents, we verified that within the experimental precision, the three-field state from the above-threshold OPO is indeed Gaussian. We can thus test the entanglement using a necessary and sufficient criterion for Gaussian states: the positivity under partial transposition (*24*, *25*). If one party is separable from the rest, the full density matrix remains positive under partial transposition with respect to that party. Partial transposition for Gaussian states is equivalent to inverting the sign of the quadrature of one of the fields (*24*). The positivity is checked by evaluating the symplectic eigenvalues of the partially transposed matrix. The state is separable if and only if all the symplectic eigenvalues are greater than or equal to 1. This criterion is necessary and sufficient for all $1 \times N$ decompositions of Gaussian states (*25*), where $N + 1$ is the total number of entangled modes. In the tripartite scenario, the three possible 1×2 partitions have to be tested.

To demonstrate the full three-field inseparability (Fig. 2), we characterized the OPO for several values of the pump power relative to the threshold power ($\sigma = P/P_{th}$). For each value of σ, the covariance matrix was directly measured, and the smallest symplectic eigenvalue under partial transposition for each field was evaluated, as well as the standard deviations of the eigenvalues (*21*). Full inseparability was demonstrated for σ ranging from 1.1 to 1.6 and for crystal temperatures below –10°C. In terms of the inequalities of Eq. 1, which provide only a sufficient criterion, entanglement was also verified: $V_0 = 1.35 \pm 0.02$, $V_1 = 1.93 \pm 0.02$, and $V_2 = 1.93 \pm 0.02$ for $\sigma = 1.24$. This represents the direct generation of continuous-variable entanglement between more than two subsystems, and we took advantage of this approach by entangling fields of different wavelengths. Continuous-variable multipartite entanglement is classified in terms of full or partial inseparability (*26*). The phonon-induced phase noise in the OPO enables transitions from full inseparability to partial inseparability (the pump field becomes separable) just by tuning a single parameter, the crystal temperature.

Because losses are a concern in communications systems, it is important to assess the robustness of the generated tripartite entanglement. We investigated the dependence of the symplectic eigenvalues on linear losses imposed on the twin beams by placing variable attenuators immediately in front of the photodetectors (we verified that pump beam losses had little effect). As expected, noise terms in the covariance matrix linearly approach the SQL and correlations tend to zero, as losses increase (*21*). This is also an important verification that the detection system is working properly. Although a squeezed state remains squeezed under finite linear losses, we found that tripartite entanglement behaves differently: We observed disentanglement of the

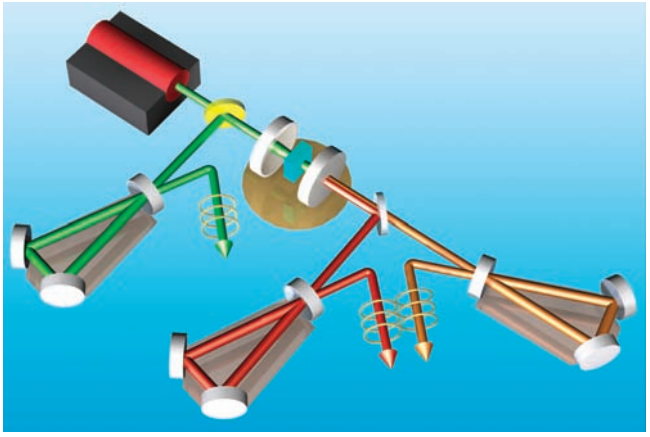

Fig. 1. The OPO (blue, center) is pumped by a coherent light source, producing three light fields of different wavelengths (green, red, and orange arrows). Entanglement verification is realized by using one analysis cavity for each beam to access all entries of the full covariance matrix. The golden rings illustrate the tripartite entanglement among the optical fields.

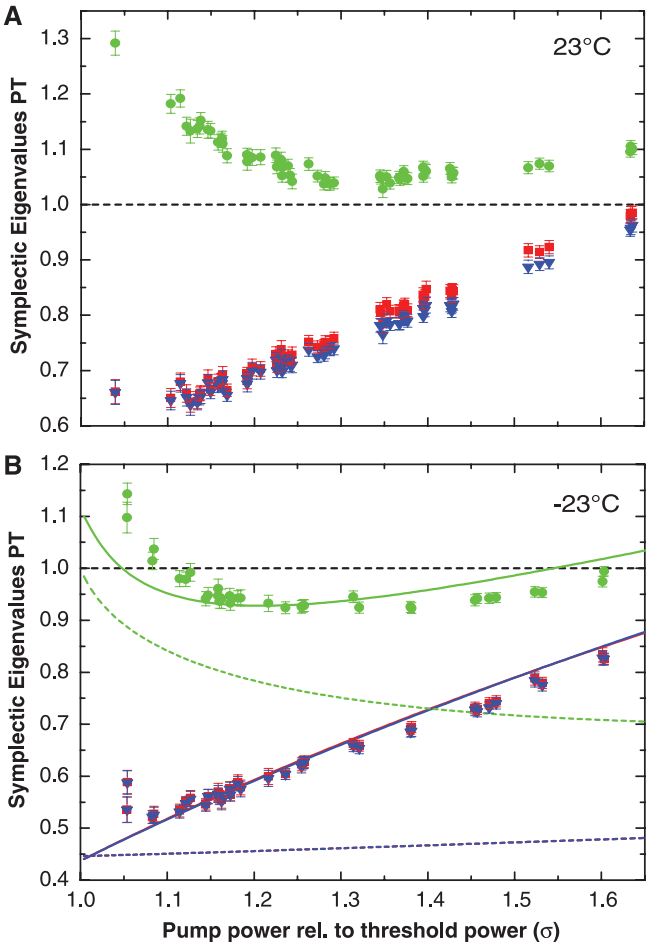

Fig. 2. Symplectic eigenvalues, extracted from the measured covariance matrices, are plotted as functions of $\sigma = P/P_{th}$. Three eigenvalues are plotted, each corresponding to partial transposition with respect to one of the beams. (**A**) Measurements made at +23°C. We observe that at room temperature, ν_0 (transposition of the pump, green circles) is greater than 1, whereas ν_1 (transposition of signal, red squares) and ν_2 (transposition of idler, blue triangles) are smaller than 1 for a large range of σ values. Thus, at room temperature only bipartite entanglement between the twin beams exists. (**B**) At –23°C, we also observed ν_0 drop below 1, demonstrating the full inseparability of the three fields. The dashed lines indicate the usual theoretical prediction without taking into account the phonon noise. By taking into account the phonon noise (*23*), we obtain the solid lines, which agree well with the data. Error bars are standard deviations (*21*).

pump field from the twins for finite losses (Fig. 3). This effect is reminiscent of so-called entanglement sudden death (*6*, *27*), which is observed in discrete-variable systems and predicted to occur in continuous-variable systems as well (*28*, *29*). For a pair of entangled qubits, each interacting with an independent environment, even though single-qubit coherence decays exponentially, entanglement can be lost at a finite time. Likewise, even though squeezing of individual beams tends only asymptotically to the SQL as a function of losses, we already observed disentanglement for finite losses. This could be harmful for applications to quantum communications, such as in information networks. On the other hand, it is not present for all values of σ, as can be seen in Fig. 3; this is an important result for our system. The robustness of entanglement with respect to channel losses depends on σ, indicating that the entangled states are not of the same nature, even though they are always Gaussian. The phonon noise present in the entangled state that exits the OPO cavity certainly plays a role in this process. The theory neglecting this noise does not predict disentanglement.

The tripartite entangled state demonstrated here presents a fundamental feature—disentanglement

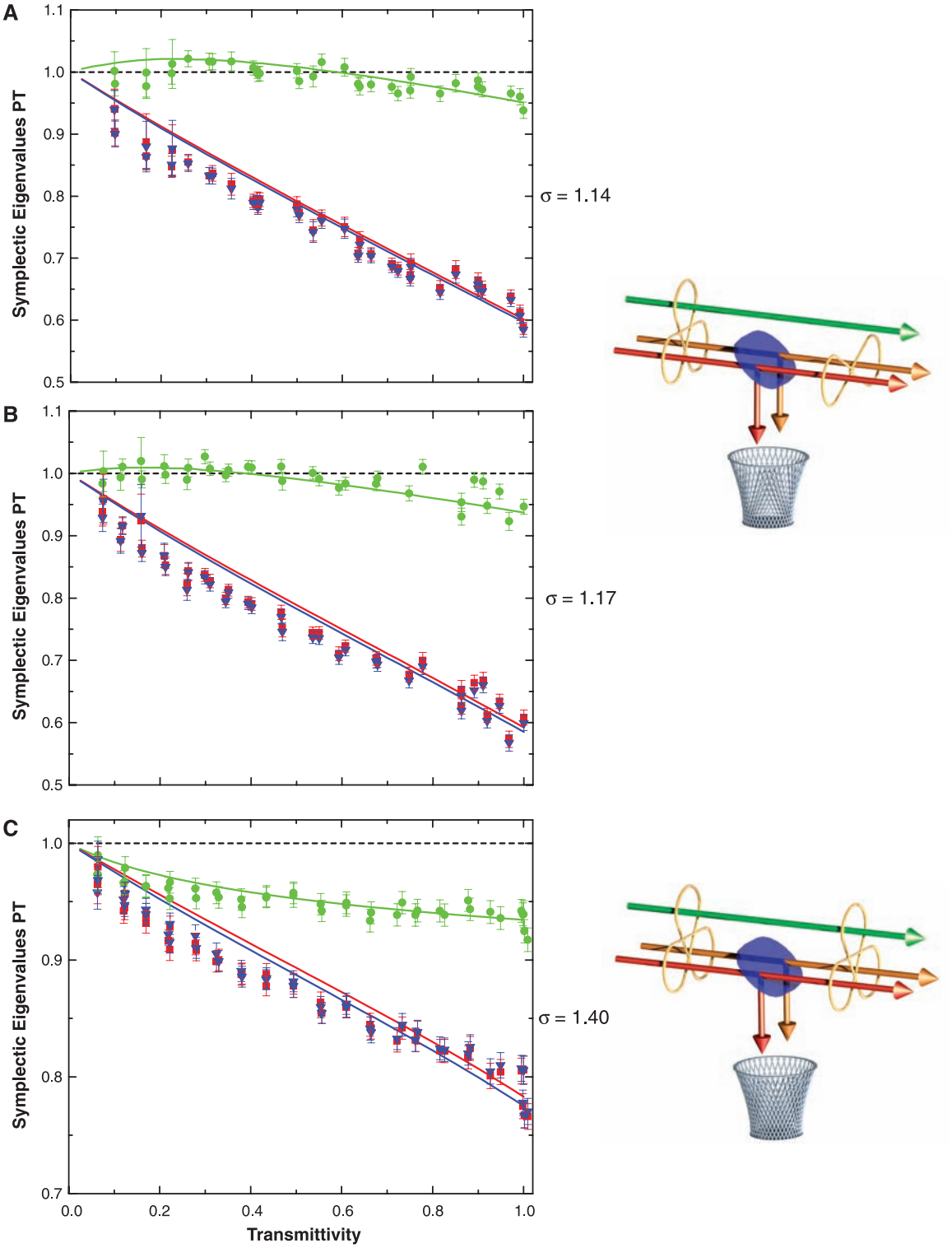

Fig. 3. Investigation of disentanglement for finite losses. Color conventions are the same as in Fig. 2. In (**A**) (σ = 1.14) and (**B**) (σ = 1.17), we observe that the pump beam becomes separable from the twins for finite losses (transmittance near 0.6 and 0.4, respectively); on the right-hand side, the situation is sketched. Because of the variable linear losses imposed on the twin beams (beam-splitter losses), entanglement of the pump beam is lost, as indicated by the golden rings. In (**C**) (σ = 1.40), there is no disentanglement for finite losses and the entanglement signature is monotonically reduced, yet all three fields remain inseparable until total loss, as sketched on the right-hand side. Data were obtained at −10°C. The solid curves were extracted from the covariance matrices that were obtained with no attenuation by calculating the effect of losses on each of their elements (*21*).

for finite linear losses—that should be observable in other continuous-variable systems as well. This serves as a reminder that much is still unknown about the nature and dynamics of quantum entanglement. The relatively small violations of the entanglement criteria found here can be improved by better OPO cavity optics and by further cooling of the nonlinear crystal. Another possibility that is currently under consideration is to change the wavelengths. The OPO pump field can be at 780 nm, so as to interact resonantly with Rb atoms, generating output fields at wavelengths close to 1560 nm. Quantum information stored in an atomic sample can thus be transferred to a wavelength that is suitable for propagation in low-loss optical fibers. Future quantum information networks may connect systems of different natures by multicolored entangled light.

References and Notes

1. E. Schrödinger, *Proc. Camb. Philos. Soc.* **31**, 555 (1935).
2. M. A. Nielsen, I. L. Chuang, *Quantum Computation and Quantum Information* (Cambridge Univ. Press, Cambridge, 2000).
3. P. W. Shor, *SIAM J. Comput.* **26**, 1484 (1997).
4. V. Scarani *et al.*, *Rev. Mod. Phys.*, **81**, 1301 (2009).
5. W. H. Zurek, *Nat. Phys.* **5**, 181 (2009).
6. T. Yu, J. H. Eberly, *Science* **323**, 598 (2009).
7. S. Deleglise *et al.*, *Nature* **455**, 510 (2008).
8. R. Blatt, D. Wineland, *Nature* **453**, 1008 (2008).
9. I. Bloch, *Nature* **453**, 1016 (2008).
10. J. Clarke, F. K. Wilhelm, *Nature* **453**, 1031 (2008).
11. R. Hanson, D. D. Awschalom, *Nature* **453**, 1043 (2008).
12. T. Aoki *et al.*, *Nat. Phys.* **5**, 541 (2009).
13. C. H. Bennett *et al.*, *Phys. Rev. Lett.* **70**, 1895 (1993).
14. A. Furusawa *et al.*, *Science* **282**, 706 (1998).
15. H. J. Kimble, *Nature* **453**, 1023 (2008).
16. C. Schori, J. L. Sørensen, E. S. Polzik, *Phys. Rev. A* **66**, 033802 (2002).
17. A. S. Villar, L. S. Cruz, K. N. Cassemiro, M. Martinelli, P. Nussenzveig, *Phys. Rev. Lett.* **95**, 243603 (2005).
18. N. B. Grosse *et al.*, *Phys. Rev. Lett.* **100**, 243601 (2008).
19. A. S. Villar, M. Martinelli, C. Fabre, P. Nussenzveig, *Phys. Rev. Lett.* **97**, 140504 (2006).
20. P. van Loock, A. Furusawa, *Phys. Rev. A* **67**, 052315 (2003).
21. See the supporting material available on *Science* Online.
22. K. N. Cassemiro, A. S. Villar, M. Martinelli, P. Nussenzveig, *Opt. Express* **15**, 18236 (2007).
23. J. E. S. César *et al.*, *Phys. Rev. A* **79**, 063816 (2009).
24. R. Simon, *Phys. Rev. Lett.* **84**, 2726 (2000).
25. R. F. Werner, M. M. Wolf, *Phys. Rev. Lett.* **86**, 3658 (2001).
26. G. Giedke, B. Kraus, M. Lewenstein, J. I. Cirac, *Phys. Rev. A* **64**, 052303 (2001).
27. M. P. Almeida *et al.*, *Science* **316**, 579 (2007).
28. C. H. Chou, T. Yu, B. L. Hu, *Phys. Rev. E* **77**, 011112 (2008).
29. J. P. Paz, A. J. Roncaglia, *Phys. Rev. Lett.* **100**, 220401 (2008).

30. We thank P. van Loock, M. Wolf, and S. Walborn for discussions and H. M. Nussenzveig, W. P. Schleich, and R. W. Boyd for comments on the manuscript. This work was funded by the Brazilian agencies Conselho Nacional de Desenvolvimento Científico e Tecnológico (CNPq), Coordenação de Aperfeiçoamento de Pessoal de Nível Superior (CAPES), and Fundação de Amparo à Pesquisa do Estado de São Paulo (FAPESP). It was performed as part of the Brazilian National Institute of Science and Technology for Quantum Information. K.N.C. and A.S.V. acknowledge support from the Alexander von Humboldt Foundation.

Supporting Online Material
www.sciencemag.org/cgi/content/full/1178683/DC1
Materials and Methods
Fig. S1
References

6 July 2009; accepted 26 August 2009
Published online 17 September 2009;
10.1126/science.1178683
Include this information when citing this paper.

Electronic Structure Controls Reactivity of Size-Selected Pd Clusters Adsorbed on TiO_2 Surfaces

William E. Kaden, Tianpin Wu, William A. Kunkel, Scott L. Anderson*

The catalytic activity of metal clusters of different sizes adsorbed on oxide surfaces can be explored systematically by using model catalysts. We studied the temperature-programmed reaction of CO with O_2 catalyzed by Pd clusters (Pd_n, for n = 1, 2, 4, 7, 10, 16, 20, and 25) that were size-selected in the gas phase and deposited on rutile TiO_2(110). X-ray photoemission spectroscopy revealed that the Pd 3d binding energy varied nonmonotonically with cluster size and that the changes correlated with strong size variations in CO oxidation activity. Taking final-state effects into account, low activity was correlated with higher-than-expected Pd 3d binding energy, which is attributed to a particularly stable valence electronic structure; electron transfer from the TiO_2 support to the Pd clusters also occurs. Ion scattering shows that small clusters form single-layer islands on the surface and that formation of a second layer begins to occur for clusters larger than Pd_{10}.

Heterogeneous catalysts often consist of small metal clusters, adsorbed on metal oxides. Because these clusters can vary widely in size, it can be difficult to sort out the extent to which changes in reactivity with cluster size predicted by theory (*1*–*3*) are caused by variations in electronic structure or in geometric effects (the number and type of reactive sites). During the past decade, model catalysts consisting of small mass-selected clusters (one to 30 atoms) deposited on oxide surfaces have been used to demonstrate that catalytic activity can depend strongly on cluster size (*4*–*9*). However, the systematic interpretation of size trends has been limited by the lack of experimental probes of sample structure. Here, we present an example in which reactivity is clearly correlated with the electronic structure of the supported metal: in this case, CO oxidation over planar Pd_n/TiO_2 (110) model catalysts, with n = 1, 2, 4, 7, 10, 16, 20, and 25. The changes in electronic structure are determined by both inherent size effects and by cluster-bonding to the oxide support.

The small cluster size range is where the largest effects of cluster size are expected, but recent work has demonstrated that such small clusters can dominate catalytic activity, even when most of the catalytic metal is present in the form of much larger particles (*10*, *11*). CO oxidation has been studied extensively over Pd/metal-oxide (*12*, *13*) and single-crystal surfaces (*14*), both because it is relatively simple and because it is important in pollution remediation.

The experimental protocol is detailed in (*15*). Briefly, Pd/TiO_2(110) samples were prepared and studied by the deposition of mass-selected Pd_n^+ on clean, vacuum-annealed rutile TiO_2(110) at an energy of 1 eV per atom. The TiO_2(110) support is commonly used in model catalyst studies and has well-characterized properties (*16*–*21*). The support is conductive enough to neutralize the initial ion charge, and the 1 eV-per-atom energy previously has been shown to result in the landing of intact clusters (that is, the sample structure is determined by the chemical interaction of the clusters with the support, not impact energy) (*22*, *23*). All samples contained the same total Pd concentration (1.53×10^{14} atoms per cm^2 = 0.1 monolayer equivalent), with the only difference being cluster size. Deposition times were 10 to 30 min with a background pressure of 1.5×10^{-10} torr. X-ray photoemission spectroscopy (XPS) was used both to verify the Pd coverage on the samples and to probe the Pd electronic structure. The as-deposited Pd 3d XPS as a function of cluster size is shown in Fig. 1A. The vertical lines indicate the binding energies (BEs) (the energy difference between the initial and final states of the photoemission process) observed for bulk Pd, which are consistent with reported values (*24*). The shift in $3d_{5/2}$ BE, relative to bulk Pd, as a function of cluster size is shown in Fig. 1B.

Initial state effects, also known as chemical shifts, reflect changes in the electronic structure of the sample. For example, if bonding to the support transferred an electron to the Pd clusters, the Pd BE would shift to lower energy, and if bonding to the support transferred an electron from the Pd clusters, the Pd BE would shift to higher energy. Quantum confinement effects and

Department of Chemistry, University of Utah, 315 South 1400 East, Room 2020, Salt Lake City, UT 84112-0850, USA.

*To whom correspondence should be addressed. E-mail: anderson@chem.utah.edu

Claro que uma última verificação nos resultados da matriz de covariância fazia-se necessária. Tomou-se a saída do OPO, e mediu-se a variância para diferentes atenuações do feixe. Como sabemos, a variância deve ser reduzida, linearmente, para a de um estado coerente. Efetivamente, os termos diagonais foram a 1, e os fora da diagonal principal a zero, linearmente com a atenuação. A surpresa ocorreu quando, sobre a matriz atenuada, aplicamos o teste Simon-PPT. A curiosidade foi plenamente recompensada: a assinatura de emaranhamento cruzou o limite para o estado separável em perdas finitas. Espantados, concluímos que havíamos observado a transição de um estado emaranhado para separável em sua interação como o ambiente. Era portanto um efeito semelhante à morte súbita de emaranhamento observada em variáveis discretas [15, 16].

Seria isto uma peculiaridade de estados emaranhados tripartite? O que poderia ocorrer para o caso bipartite? Seria ele necessariamente robusto, devido ao caráter mais restritivo da desigualdade de Duan? O OPO revelou-se agora a fonte de uma nova linha de estudos sobre a robustez de emaranhamento para variáveis contínuas.

Capítulo 5

Morte Súbita de Emaranhamento

O último artigo apresentado configura um fechamento do trabalho de caracterização e demonstração do OPO como fonte de estados não-clássicos do campo. A surpresa final ficou por conta do desemaranhamento do mesmo.

O emaranhamento gerado pela interação entre dois sistemas que são posteriormente separados pode acabar se extinguindo com o passar do tempo. A causa disto é que cada um destes subsistemas irá interagir posteriormente com o ambiente, ou com outros elementos, e nesse process parte da informação será transferida para eles. Neste caso, temos um aumento da complexidade do problema, e não podemos mais resumi-lo ao emaranhamento de duas partes. Se a interação for com um reservatório sem memória, a informação sera perdida. É a perda da informação que dará origem à morte súbita do emaranhamento.

Para podermos dizer que o emaranhamento foi perdido, precisamos de critérios de emaranhamento que sejam necessários e suficientes para apontar a existência de um estado emaranhado, traçando claramente o limite entre estes e os estados separáveis. Para variáveis discretas, a medida da "concurrence" em sistemas de dois "qubits" [53] é um testemunho de emaranhamento que satisfaz este critério. Já para sistemas mais complexos, envolvendo mais de duas partições ou mais de dois níveis discretos, faltam critérios conclusivos para assegurar o desemaranhamento do sistema.

No regime de variáveis contínuas, a situação é ainda mais complexa. No entanto, para o subespaço dos sistemas gaussianos, o critério de Simon-PPT [51] satisfaz esta condição para bipartições do tipo $1 \times N$. Estes estados gaussianos são completamente caracterizados pela matriz de covariância, portanto uma vez que esta é medida, toda a informação sobre o sistema está disponível. O critério de Simon permite extrair a informação sobre o emaranhamento.

Nossa atenção para a morte súbita foi despertada na medida do emaranhamento tripartite, ao verificar que para perdas finitas nos modos sinal e complementar, a testemunha de emaranhamento do bombeio cruzava o limite de separabilidade (figura 5.1).

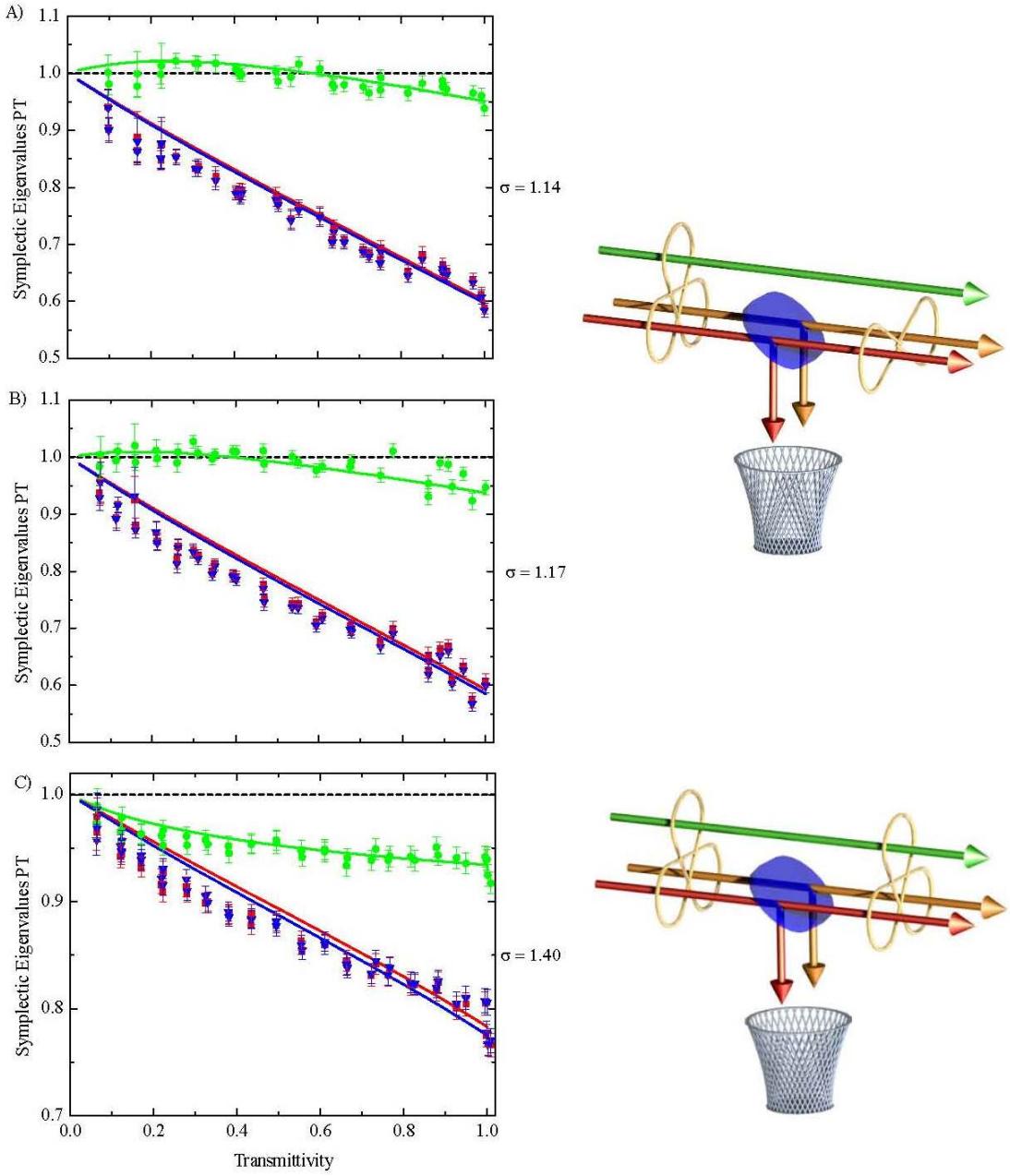

Figura 5.1: Variação do menor autovalor simplético da matriz de ruído após transposição parcial de cada campo, calculado para diferentes transmissões no divisor de feixe colocado diante dos modos sinal e complementar, para diferentes potências de bombeio, normalizadas pelo limiar de oscilação do OPO. nos dois primeiros casos, vemos a perda de emaranhamento para atenuações finitas nos campos.

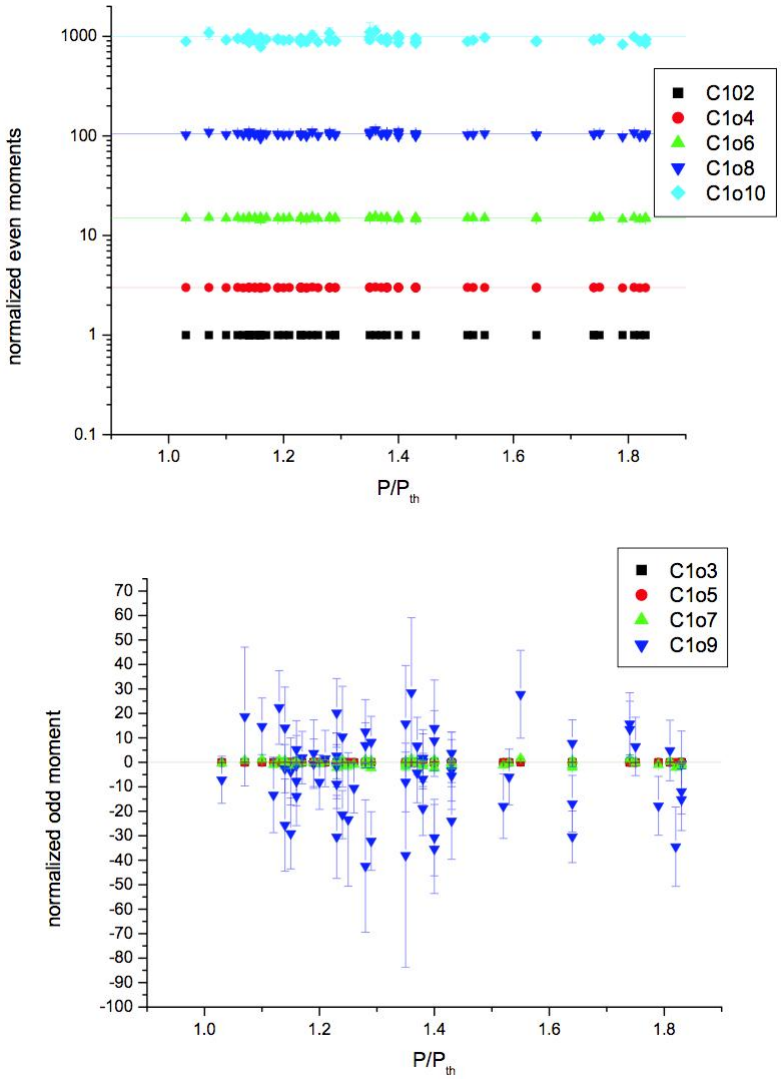

Figura 5.2: Momentos normalizados pela variância para o modo sinal $(\Delta^i \hat{p}_1/(\Delta^2 \hat{p}_1)^{i/2})$, em função do bombeio normalizado. Acima: momentos pares. Abaixo: momentos ímpares. Nota-se que eles evoluem conforme esperado para uma distribuição gaussiana.

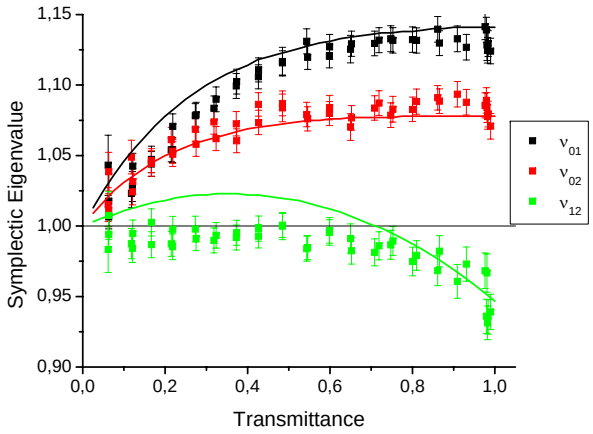

Figura 5.3: Teste de Simon para emaranhamento bipartite, para diferentes atenuações do campo, para o bombeio 40% acima do limiar de oscilação.

No entanto, só poderíamos dizer com certeza que o estado é separável se ele pudesse ser completamente descrito por sua matriz de covariância. Fizemos, portanto, testes sobre a gaussianidade do estado, levantando os momentos de ordem superior.

Realizamos portanto diversos testes. Todos os momentos de autocorrelação das flutuações de ordem ímpar e par, entre 0 e 10, foram compatíveis com uma distribuição gaussiana, seguindo a relação $\Delta^i \hat{p}_1 = (i-1)\Delta^2 \hat{p}_1 \times \Delta^{(i-2)} \hat{p}_1$, partindo de uma média nula. Além disso, todas as correlações de terceira ordem envolvendo qualquer combinação dos três campos foram nulas. Sem encontrar nenhuma evidência de desvio do comportamento gaussiano, consideramos que para todos os propósitos práticos verificamos a morte súbita do emaranhamento tripartite no OPO acima do limiar. Resultados semelhantes aos mostrados na figura 5.2 para o modo sinal foram igualmente obtidos para os modos bombeio e complementar, permitindo extender a eles estas conclusões.

Se caracterizamos portanto que o estado é gaussiano, o critério de Simon é necessário e suficiente, e temos portanto que o emaranhamento dos feixes gerados pelo OPO desaparece, em certos casos, para atenuações finitas. Qual seria, no entanto, a origem desta morte súbita de emaranhamento. Pensávamos, a princípio, que fosse algo ligado à natureza tripartite dos campos, e que para sistemas bipartite, o emaranhamento permaneceria. Tal sentimento vinha do conceito que o critério de Duan [42] fosse uma condição necessária e suficiente para o emaranhamento bipartite. Na realidade, veremos que não é o caso.

Nas condições da medida mostrada na figura 5.1c, foi feito o teste do emaranhamento com as matrizes de covariância reduzidas para dois modos dos campos. O resultado, apresentado na figura 5.3, é compatível com campos bombeio e sinal, ou bombeio e complementar, separáveis. O emaranhamento ocorre apenas no caso tripartite. No entanto, para o par sinal-complementar, vemos que o emaranhamento, inicialmente presente, acaba desaparecendo para uma transmitância da ordem de 75 %. É curioso notar, no entanto, que o emaranhamento tripartite continua presente.

Quais seriam então as condições necessárias para que um estado emaranhado permaneça emaranhado em sua interação com o ambiente? Um trabalho ainda não publicado, realizado pelo estudante de doutorado Felippe Alexandre da Silva Barbosa, e pelo pós-doutorando Alencar José de Faria, mostrou que tais condições podem ser obtidas a partir do critério de Simon.

Considere um sistema bipartite, completamente descrito pela matriz de covariância da forma

$$V = \begin{pmatrix} A_1 & C \\ C^T & A_2 \end{pmatrix}. \tag{5.1}$$

onde as matrizes A_i envolvem as variâncias de um subsistema, e a matriz C, as correlações entre as variáveis conjugadas de cada subsistema. O critério de Simon pode então ser expresso em termos dos determinantes destas matrizes, que nos fornecem um testemunho do emaranhamento.

$$W_{ppt} = 1 + \det V + 2 \det C - \sum_{i=1,2} \det A_j. \tag{5.2}$$

Se $W_{ppt} < 0$, o sistema está emaranhado. Para sistemas gaussianos, $W_{ppt} \geq 0$ implica em separabilidade. Considerando que fazemos a atenuação em um ou dois campos, levando à interação deles com um reservatório a 0 K, podemos reescrever W_{ppt} em função da transmitância T_i dos canais de comunicação

$$W'_{ppt}(T_1, T_2) = T_1 T_2 \left[T_1 T_2 \Gamma_{22} + T_2 \Gamma_{12} + T_1 \Gamma_{21} + \Gamma_{11} \right]. \tag{5.3}$$

Note que teremos termos com dependência quadrática para as duas perdas, e um com dependência linear em T_1 e T_2. Se atenuarmos o campo até o limite próximo de sua extinção (fazendo $T_i \to 0$), sinal do termo dominate Γ_{11} vai determinar se o emaranhamento permanece ou não. Esta nova testemunha de emaranhamento vai nos dizer se o emaranhamento é robusto, ou sujeito à morte súbita por perdas.

$$W_{full} = \Gamma_{11} = (\mathrm{tr} A_1 - 2)(\mathrm{tr} A_2 - 2) - \mathrm{tr}(C^T C) + 2 \det C. \tag{5.4}$$

Note que $W_{full} < 0$ é uma testemunha de emaranhamento, implicando que $W_{ppt} < 0$. Vale lembrar aqui que um sistema separável não pode evoluir, mediante perdas, para um sistema emaranhado, portanto se ele se encontra emaranhado perto da extinção total ele era, a princípio, emaranhado. Por outro lado, se a matriz de covariância inicial tiver $W_{ppt} < 0$ e $W_{full} > 0$, o sistema é sujeito à morte súbita, tornando-se separável para perdas finitas.

Na figura 1 do próximo artigo vemos diferentes situações nas quais, a partir de um estado inicial emaranhado, podemos evoluir mediante perdas para estados separáveis. Existem, portanto, estados gaussianos emaranhados nos quais há desemaranhamento para perdas em ambos os campos, bem como situações nas quais as perdas em apenas um dos campos não são suficientes para destruir o emaranhamento. A necessidade de estados robustos é particularmente interessante no caso de empregarmos os campos gerados para implementar um protocolo de comunicação quântica baseado no emaranhamento (criptografia ou teletransporte).

Disentanglement in bipartite continuous-variable systems

F. A. S. Barbosa,[1] A. J. de Faria,[2] A. S. Coelho,[1] K. N. Cassemiro,[1,3] A. S. Villar,[1,3,4] P. Nussenzveig,[1] and M. Martinelli[1,*]

[1]*Instituto de Física, Universidade de São Paulo, P.O. Box 66318, 05315-970 São Paulo, Brazil*

[2]*Instituto de Ciência e Tecnologia, Universidade Federal de Alfenas, 37715-400 Poços de Caldas, MG, Brazil*

[3]*Max Planck Institute for the Science of Light, DE-91058 Erlangen, Germany*

[4]*Lehrstuhl fuer Optik, Universitaet Erlangen-Nuernberg, DE-91058 Erlangen, Germany*

(Received 21 September 2011; published 28 November 2011)

Entanglement in bipartite continuous-variable systems is investigated in the presence of partial losses such as those introduced by a realistic quantum communication channel, e.g., by propagation in an optical fiber. We find that entanglement can vanish completely for partial losses, in a situation reminiscent of so-called entanglement sudden death. Even states with extreme squeezing may become separable after propagation in lossy channels. Having in mind the potential applications of such entangled light beams to optical communications, we investigate the conditions under which entanglement can survive for all partial losses. Different loss scenarios are examined, and we derive criteria to test the robustness of entangled states. These criteria are necessary and sufficient for Gaussian states. Our study provides a framework to investigate the robustness of continuous-variable entanglement in more complex multipartite systems.

DOI: 10.1103/PhysRevA.84.052330 PACS number(s): 03.67.Bg, 03.67.Pp, 42.50.Xa, 42.50.Dv

I. INTRODUCTION

The dynamics of open quantum systems leads, in general, to a degradation of key quantum features such as coherence and entanglement. Since entanglement is considered to be an important resource for applications in quantum information, its degradation may seriously hinder the envisioned protocols. Careful analyses of environment-induced loss of entanglement are thus important steps in quantum information science. In the discrete-variable scenario, studies of 2-qubit systems have shown that entanglement can be completely lost after a finite time of interaction with the environment, an effect now mostly known as entanglement sudden death (ESD) [1,2]. Quantum information can also be conveyed, stored, and processed by continuous-variable (CV) systems. Bright beams of light can be described by means of CV field quadratures and are natural conveyors of quantum information. Unavoidable transmission loss is the fiercest enemy for quantum communications. It has recently been observed that losses may lead to complete disentanglement in Gaussian CV systems [3,4]. This phenomenon is a partial-loss analog of the finite-time disentanglement observed in qubit systems.

The simplest CV systems one can consider are those described by Gaussian statistics. Gaussian states are indeed well studied [5] and fairly well characterized. For instance, there exist necessary and sufficient criteria for Gaussian-state entanglement of up to $1 \times N$ systems (in which one subsystem is collectively entangled to N other subsystems) [6,7]. In spite of all this knowledge, the sensitivity of entanglement to the interaction with the environment is still not completely mapped. As experimentally observed by Coelho *et al.* [3] and by Barbosa *et al.* [4], some Gaussian states become separable for partial losses, while others remain entangled. What distinguishes one class of states from the other? Are there only two classes of such states? Is it sufficient to produce states with a large degree of squeezing in order to avoid disentanglement? Is there any strategy involving local operations to protect states against disentanglement?

In this paper, we extend the treatment of Ref. [4] and provide answers to some of these questions. We theoretically analyze the conditions leading to CV disentanglement in the simplest case of bipartite systems. In the framework of open-system dynamics, the effect of a lossy channel (without any added noise) is equivalent to the interaction with a reservoir at zero temperature. The property of entanglement resilience to losses will be referred to as "robustness." Entanglement robustness is assessed by entanglement criteria previously derived by other authors. For general CV states, these criteria provide sufficient conditions for the robustness of bipartite systems. Necessary and sufficient entanglement criteria for Gaussian states lead to necessary and sufficient conditions for entanglement robustness upon propagation in lossy channels. Entanglement of CV Gaussian states may be created by a number of different strategies such as, for instance, passive operations on initially squeezed states [8]. We shall not discuss these in detail here, but take for granted initially entangled states.

A thorough investigation reveals the possibility of distinct entanglement dynamics as losses are imposed on the subsystems. We consider realistic scenarios, as depicted in Fig. 1. A bipartite entangled state is the quantum resource of interest. It can be distributed to two parties who wish to communicate, as in Fig. 1(a), in a scenario that we refer to as a dual-channel communication scheme. Another possibility would be that one of the parties holds the quantum-state generator and only one mode needs to propagate through a lossy quantum channel, as in Fig. 1(b). We refer to this situation as a single-channel scheme. One could surmise that, in principle, it is equivalent to concentrate losses in a single channel or split them among two channels. If our channels are optical fibers, losses increase exponentially with the propagation distance. Thus, one could think that propagation in a single fiber over a certain distance would have the same effect as propagation of both modes, each in one fiber, over half the distance (which would result in the same overall losses). This is not correct:

*mmartine@if.usp.br

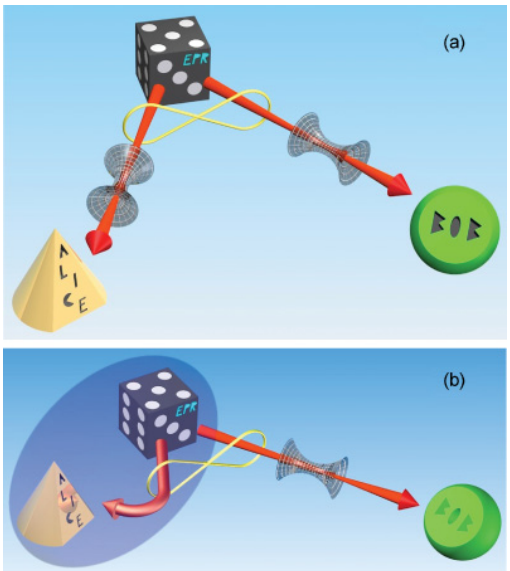

FIG. 1. (Color online) (a) *Dual-channel losses*: An entangled quantum state is distributed to two parties, Alice and Bob, over two lossy quantum channels. (b) *Single-channel losses*: Alice holds the quantum-state generator and only distributes one entangled mode to Bob over a single lossy quantum channel.

for certain states, one could propagate one of the modes over an infinite distance in a single lossy channel without losing entanglement, whereas entanglement would disappear after a finite propagation distance if both modes were to suffer losses.

These different scenarios lead to the introduction of a formal classification, consisting of three robustness classes. On one extreme, the entanglement of *fully robust* states vanishes only for total attenuation of either beam. On the opposite extreme, *fragile states* become separable for partial attenuations on either beam or a combination of both. An intermediate class of *partially robust* states shows either robustness or fragility, depending on the way losses are introduced. Thus, imposing losses on one field may be less harmful in a quantum communication system than distributing both beams over two lossy channels. Furthermore, we show that even states with very strong squeezing [e.g., amplitude difference squeezing, as in twin beams produced by an above-threshold optical parametric oscillator (OPO)] can disentangle for partial losses. A moderate excess noise, commonly encountered in existing experiments, suffices for this. In addition, one could speculate that pure states would necessarily be robust. We provide an example of a pure state that disentangles for partial losses as well.

The paper is organized as follows. In Sec. II, we establish notation and the basic reservoir model (the environment). In Sec. III, a sufficient criterion to determine the robustness of the entangled state is demonstrated. In Sec. IV, we extend the robustness criterion, resulting in a necessary and sufficient robustness condition for all Gaussian bipartite states. The different classes of entanglement robustness against losses in each channel are defined in Sec. V. In Sec. VI, we examine particular quantum states commonly treated in the literature. A final Sec. VII is focused on the main physical results and implications of our findings.

II. ENTANGLEMENT AND ESD IN LOSSY GAUSSIAN CHANNELS

The quantum properties of Gaussian states are completely characterized by the second-order moments of the appropriate observables. The choice of observables depends on the system under consideration. In the case of the electromagnetic field, a complete description can be given in terms of orthogonal field quadratures. We will consider the amplitude and phase quadratures, respectively, written as $\hat{p}_j = (\hat{a}_j^\dagger + \hat{a}_j)$ and $\hat{q}_j = i(\hat{a}_j^\dagger - \hat{a}_j)$ in terms of the field annihilation $\hat{a}_j$ and creation $\hat{a}_j^\dagger$ operators. The indices $j = 1,2$ stand for the two field modes of our bipartite system. The quadrature operators obey the commutation relation $[\hat{p}_j,\hat{q}_j] = 2i$, from which we obtain an uncertainty product lower bound of one. The standard quantum limit (SQL) is thus equal to one, representing the noise power present in the quadrature fluctuations of a coherent state.

It is useful to organize the second-order moments in the form of a 4×4 covariance matrix V. Its entries are the averages of the symmetric products of quadrature fluctuation operators

$$V = \tfrac{1}{2}\langle \delta\hat{\xi}\delta\hat{\xi}^T + (\delta\hat{\xi}\delta\hat{\xi}^T)^T \rangle , \tag{1}$$

where $\hat{\xi} = (\hat{q}_1,\hat{p}_1,\hat{q}_2,\hat{p}_2)^T$ is the column vector of quadrature operators, and $\delta\hat{\xi} = \hat{\xi} - \langle\hat{\xi}\rangle$ are the fluctuation operators with zero average. Similar notation will be valid for the individual quadratures, e.g., $\delta\hat{p}_1$. The noise power is proportional to the variance of the fluctuation, denoted for a given quadrature by (e.g.) $\Delta^2\hat{p}_1 = \langle(\delta\hat{p}_1)^2\rangle$. The Heisenberg uncertainty relation can be expressed as [6,9]

$$\begin{gathered} V + i\Omega \geqslant 0, \\ \Omega = \begin{bmatrix} J & 0 \\ 0 & J \end{bmatrix} \quad \text{and} \quad J = \begin{bmatrix} 0 & 1 \\ -1 & 0 \end{bmatrix}. \end{gathered} \tag{2}$$

The covariance matrix can be divided in three 2×2 submatrices, from which two (A_j) represent the reduced covariance matrices of the individual subsystems and one (C) expresses the correlations between the subsystems

$$V = \begin{pmatrix} A_1 & C \\ C^T & A_2 \end{pmatrix}. \tag{3}$$

The correlations originate from both classical and quantum backgrounds, and can not be directly associated to entanglement without considering the properties of each subsystem. As we will see, the occurrence of ESD is related to the presence of uncorrelated noise in the system, normally in the form of unbalanced or insufficient correlations between different subsystems or quadratures.

For bipartite Gaussian states, there exist necessary and sufficient entanglement criteria [6,10]. These criteria are the basis for our assessment of entanglement robustness.

First, we need to adopt a model for the quantum channel. Here, we consider the realistic case of a lossy bosonic channel, equivalent to the attenuation of light by random scattering. Losses are modeled by independent beam splitters placed in the beam paths. Each beam-splitter transformation combines one field mode with the vacuum field. In the absence of added noise, it can be associated to a reservoir at zero temperature.

A Gaussian attenuation channel transforms the field operators according to [11,12]

$$\hat{a}_j \longrightarrow \hat{a}'_j = \sqrt{T_j}\,\hat{a}_j + \sqrt{1-T_j}\,\hat{a}_j^{(E)}, \tag{4}$$

where T_j is the beam-splitter transmittance and $\hat{a}_j^{(E)}$ is the annihilation operator from the environment. It acts on the covariance matrix as

$$V' = \mathcal{L}(V) = L(V-I)L + I, \tag{5}$$

where $L = \mathrm{diag}(\sqrt{T_1},\sqrt{T_1},\sqrt{T_2},\sqrt{T_2})$ is the loss matrix and I is the 4×4 identity matrix.

The question we address here regards the behavior of entanglement as the covariance matrix undergoes the transformation of Eq. (5).

III. DUAN ENTANGLEMENT CRITERION AND ROBUSTNESS

We direct our attention, in a first moment, to the entanglement criterion presented in Ref. [10], here referred to as the Duan criterion. According to them, a sufficient condition for the existence of entanglement is obtained by fulfilling the inequality

$$W_D = \Delta^2\hat{u} + \Delta^2\hat{v} - \left(a^2 + \frac{1}{a^2}\right) < 0, \tag{6}$$

where

$$\hat{u} = \frac{1}{\sqrt{2}}\left(|a|\hat{p}_1 - \frac{1}{a}\hat{p}_2\right) \text{ and } \hat{v} = \frac{1}{\sqrt{2}}\left(|a|\hat{q}_1 + \frac{1}{a}\hat{q}_2\right). \tag{7}$$

The $\hat{p}_i$ and $\hat{q}_i$ are quadrature operators, obeying the commutation relations stated above, and a is an arbitrary real nonzero number. The quadrature combinations $\hat{u}$ and $\hat{v}$ are collective operators corresponding to the original example of Einstein, Podolsky, and Rosen (EPR) [13]. As such, they are called EPR-type collective operators.

The quantity W_D can be viewed as an entanglement witness. We shall use the symbol W for witnesses in general. The presence of a given property is signaled by a negative value of the corresponding witness. As a merely sufficient criterion, no statement can be made if $W_D \geqslant 0$: the state could be either separable or entangled. Nevertheless, the witness W_D is compelling from a practical point of view because it does not require full knowledge of the covariance matrix, simplifying the detection of entanglement in experiments. The downside is its limited detection ability.

For $a = 1$, entanglement can be detected by a balanced beam-splitter transformation of the input fields followed by a measurement of squeezing in the two output fields [14,15]. Alternatively, one can measure the quadrature variances $\Delta^2\hat{p}_i$ and $\Delta^2\hat{q}_i$ of each field and the cross correlations $c_p = \langle\delta\hat{p}_1\,\delta\hat{p}_2\rangle$ and $c_q = \langle\delta\hat{q}_1\,\delta\hat{q}_2\rangle$. The optimum choice for the parameter a that minimizes W_D is $a^2 = \sqrt{\sigma_2/\sigma_1}$, where the σ_j are given by

$$\sigma_j = \Delta^2\hat{p}_j + \Delta^2\hat{q}_j - 2 = \mathrm{tr}A_j - 2. \tag{8}$$

The sign indeterminacy in a is solved by taking into account the signs of the quadrature correlations. With these considerations, one arrives at the minimized form of the Duan criterion

$$W_M = \sigma_1\sigma_2 - (c_p - c_q)^2 < 0. \tag{9}$$

Equation (9) provides the first insight into the robustness of bipartite states. The crucial fact to be observed is that the sign of W_M is conserved by attenuations. In fact, using Eq. (5), the correlations transform as $c'_p = \sqrt{T_1T_2}\,c_p$ and $c'_q = \sqrt{T_1T_2}\,c_q$, while $\sigma'_j = T_j\sigma_j$. The attenuation operation factorizes in the entanglement witness

$$W'_M = T_1T_2W_M. \tag{10}$$

Therefore, an initially entangled state satisfying Eq. (9) will not disentangle under partial losses. This fact was experimentally verified by Bowen *et al.* [16].

Entangled states satisfying the Duan criterion do not disentangle for partial losses imposed on any mode: they are *fully robust*. Among them lie the two-mode squeezed states, a large class of states for which both EPR-type observables are squeezed [15,17,18].

Since W_M is only a sufficient witness, the existence of robust states for which $W_M \geqslant 0$ can not be excluded. Below, we demonstrate a necessary and sufficient criterion for robustness of Gaussian states, effectively determining the boundary between robust and fragile states.

IV. ENTANGLEMENT ROBUSTNESS: GENERAL CONDITIONS

In order to obtain clear-cut conditions for the robustness of entanglement, we must employ a necessary and sufficient entanglement criterion. By analyzing whether the subsystems remain entangled or become separable upon attenuation, we will classify all bipartite Gaussian states.

A. PPT criterion

We find a convenient separability criterion in the requirement of positivity under partial transposition (PPT) of the density matrix for separable states [19,20]. An entangled state, on the other hand, will necessarily lead to a negative partially transposed density matrix, which is nonphysical.

The partial transposition (PT) of the density operator is equivalent in the level of the Wigner function to the operation of time reversal applied to a single subsystem. On the covariance matrix level, time reversal is obtained by changing the sign of the momentum (for harmonic oscillators), or the sign of the phase quadrature of one mode (for electromagnetic fields), in this manner affecting the sign of its correlations [6].

Physical validity is assessed using Eq. (2). The uncertainty relation can be recast into a more explicit form by expressing it in terms of the determinants of the covariance matrix and its submatrices as

$$1 + \det V - 2\det C - \sum_{i=1,2}\det A_j \geqslant 0. \tag{11}$$

The PT operation modifies the sign of $\det C$, resulting in the following condition for entanglement [6]:

$$W_{\rm PPT} = 1 + \det V + 2\det C - \sum_{i=1,2} \det A_j < 0. \quad (12)$$

Since all separable states fulfill $W_{\rm PPT} \geqslant 0$, $W_{\rm PPT}$ is a sufficient entanglement witness. For Gaussian states, it is a necessary witness as well, and the equation $W_{\rm PPT} = 0$ traces a clear boundary in the space of bipartite Gaussian states, setting apart the subspaces of separable and entangled states.

It is convenient to recall here that the purities of Gaussian states are directly related to the determinant of the covariance matrices [21]

$$\mu = (\det V)^{-\frac{1}{2}}, \quad (13)$$

$$\mu_j = (\det A_j)^{-\frac{1}{2}}, \quad (14)$$

so that the entanglement witness of Eq. (12) involves the total purity of the systems, the purity of each subsystem, and the shared correlations.

B. Covariance matrix under attenuation

By applying the witness of Eq. (12) to the attenuated covariance matrix of Eq. (5), one obtains

$$W'_{\rm PPT}(T_1,T_2) = 1 + \det V' + 2\det C' - \sum_{j=1,2} \det(A'_i), \quad (15)$$

from which $W'_{\rm PPT}(T_1 = 1,\ T_2 = 1) = W_{\rm PPT}$. From Eq. (5), it follows that the individual submatrices transform as $C' = \sqrt{T_1T_2}C$ and $A'_j = T_j(A_j - I) + I$ under attenuations. The bilinear dependence of Eq. (9) on T_1 and T_2, which led to a constant sign of the witness, is not expected here and robustness is not a general feature of bipartite entangled states.

In the Appendix, we derive an explicit transmittance-dependent form of $W'_{\rm PPT}(T_1,T_2)$. We can factor out a term T_1T_2, which can not change the sign of $W_{\rm PPT}$. It assumes the form

$$W'_{\rm PPT}(T_1,T_2) = T_1T_2W_R(T_1,T_2). \quad (16)$$

The reduced witness W_R preserves the sign of $W'_{\rm PPT}$ (except for $T_1 = T_2 = 0$, for which we know both modes are in their vacuum states and $W'_{\rm PPT} = 0$), maintaining only the relevant dependence on T_1 and T_2. It reads as

$$W_R(T_1,T_2) = T_1T_2\Gamma_{22} + T_2\Gamma_{12} + T_1\Gamma_{21} + \Gamma_{11}. \quad (17)$$

The expressions for the coefficients Γ_{ij} in terms of the covariance matrix entries are given in the Appendix. We note that they are regarded as constants here, independent of T_1 and T_2.

The different dynamics of entanglement under losses appear in the witnesses $W'_{\rm PPT}$ and W_R. Figure 2 depicts four entangled states (three of them fragile) plus a separable state

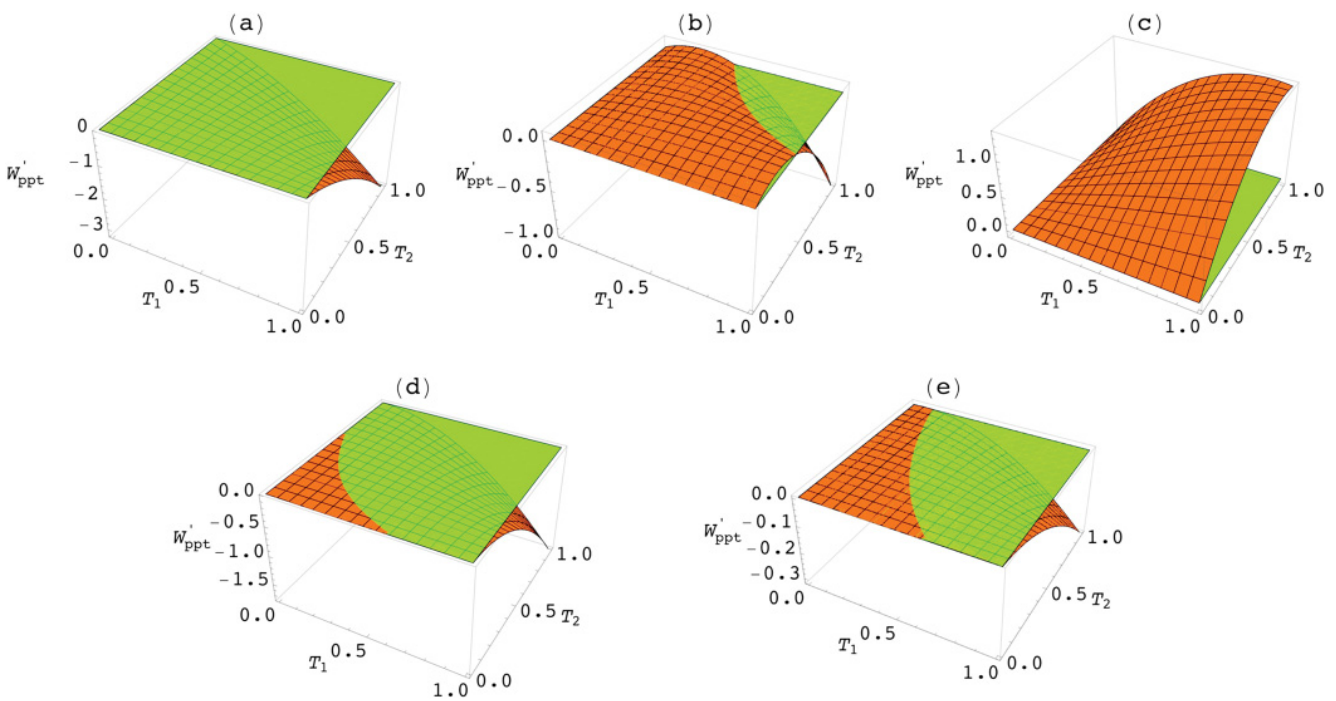

FIG. 2. (Color online) Possible behaviors of the PPT entanglement witness $W'_{\rm PPT}$ under attenuation, as a function of the transmittances T_1 and T_2. (a) Fully robust entanglement. (b) Fragility for any combination of beam attenuations. (c) Separable state. (d) Single-channel partial robustness: either mode, i.e., the state is robust for any individual attenuation, but not for a combination of attenuations, such as equal attenuations. (e) Single-channel partial robustness: specific mode, i.e., the state is robust when one mode is attenuated but presents ESD upon attenuation of the other mode.

under attenuation. The plots show $W'_{\rm PPT}(T_1,T_2)$ based on the covariance matrix

$$V = \begin{bmatrix} \Delta^2 q_1 & 0 & c_q & 0 \\ 0 & \Delta^2 p_1 & 0 & c_p \\ c_q & 0 & \Delta^2 q_2 & 0 \\ 0 & c_p & 0 & \Delta^2 p_2 \end{bmatrix}, \tag{18}$$

constructed from diagonal submatrices. This simple form of V, observed in the experiments of Ref. [4], suffices to span all types of entanglement dynamics of Gaussian states.

The curves of Figs. 2(a)–2(d) were specifically obtained from

$$V = \begin{bmatrix} 2.55 & 0 & c_q & 0 \\ 0 & 1.80 & 0 & -1.26 \\ c_q & 0 & 2.55 & 0 \\ 0 & -1.26 & 0 & 1.80 \end{bmatrix}. \tag{19}$$

As the correlation c_q is varied, different types of entanglement dynamics are observed. Modifying this parameter while keeping constant the other entries of the covariance matrix is equivalent to adding uncorrelated noise to the system (for instance, classical phonon noise dependent on the temperature of the nonlinear crystal [4,22]). In Fig. 2(a) ($c_q = 1.275$), a state violating the Duan criterion is *fully robust*, as expected. Disentanglement does not occur for finite losses imposed on any of the fields. In Fig. 2(b), the choice $c_q = 0.893$ characterizes a state for which ESD occurs for partial attenuation in a single channel (mode) or in both channels. This represents the most fragile class of states. In Fig. 2(c) ($c_q = 0.3825$), the initial state is separable and it naturally remains separable throughout the whole region of attenuations.

A more subtle entanglement dynamics appears in Fig. 2(d) ($c_q = 1.033$). The state is robust against any single-channel attenuation but may become separable if both modes are attenuated. Such a state would suffice as a resource for quantum communications involving single-channel losses.

If we consider a more general covariance matrix, with asymmetric modes, the system may be robust against losses on one mode, but not on the other. This is observed in Fig. 2(e), where $W'_{\rm PPT}$ is calculated for the covariance matrix

$$V = \begin{bmatrix} 2.55 & 0 & 0.653 & 0 \\ 0 & 1.80 & 0 & -0.797 \\ 0.653 & 0 & 1.62 & 0 \\ 0 & -0.797 & 0 & 1.32 \end{bmatrix}. \tag{20}$$

This particular covariance matrix is obtained from Eq. (19), with $c_q = 1.033$, by imposing the attenuation $T_2 = 0.40$. Before this attenuation, the state was partially robust, as in Fig. 2(d). It remains robust against losses on mode 2, but now disentanglement with respect to losses solely on mode 1 may occur. This illustrates the fact that the new states produced upon attenuation become more fragile. Since attenuation is a Gaussian operation, states can not become more robust upon attenuation [23,24].

C. Full robustness

We show here that fully robust states can be directly identified from the covariance matrix. In order to obtain the necessary condition, we note from Eq. (17) that the entanglement dynamics close to complete attenuation is dominated by Γ_{11}. Thus, an initially entangled state $W_R(T_1 = 1, T_2 = 1) < 0$ with $\Gamma_{11} > 0$ must become separable for sufficiently large attenuation, from which we derive the witness

$$W_{\rm full} = \Gamma_{11} = \sigma_1\sigma_2 - {\rm tr}(C^T C) + 2\det C. \tag{21}$$

$W_{\rm full} \leqslant 0$, provided $W_{\rm PPT} < 0$, supplies a simple, direct, and general condition for testing the entanglement robustness of bipartite Gaussian states.

The robustness can not depend on the choice of local measurement basis for each mode since, as discussed in the Appendix, local rotations commute with the operation of losses. In other words, local passive operations, such as rotations and phase shifts, do not change the robustness. By using local rotations to diagonalize the correlation matrix C, we obtain

$$W^{(D)}_{\rm full} = \sigma_1\sigma_2 - (c_p - c_q)^2 \leqslant 0, \tag{22}$$

which coincides with W_M of Eq. (9). Thus, the Duan criterion in the simple form of Eq. (9) is a particular case of Eq. (21) when the correlation submatrix is diagonal. For Gaussian states given by covariance matrices with diagonal correlation submatrix, W_M is a necessary and sufficient witness for robust entanglement, but only sufficient otherwise.

D. Partial robustness

As seen in Fig. 2, there exist states that can be robust against single-channel losses, yet disentangle for finite losses split among two channels. Similar to the procedure in the previous section, we will define witnesses capable of identifying partial robustness.

Let us consider the case $T_2 = 1$ for definiteness. The attenuated witness of Eq. (17) becomes

$$W_R(T_1,T_2 = 1) = (W_{\rm PPT} - W_1)T_1 + W_1, \tag{23}$$

where

$$W_1 = W_{\rm full} + \Gamma_{21} \tag{24}$$

(see Appendix for the expression of Γ_{21}). The analysis of W_1 follows the same lines used in the case of fully robust states, with the simplification that the witness depends linearly on the attenuation. Thus, there is only one possible path cutting the plane $W_R(T_1,T_2 = 1) = 0$. The fraction of transmitted light for which ESD occurs is

$$T_1^c = \frac{W_1}{W_1 - W_{\rm PPT}}. \tag{25}$$

From $W_{\rm PPT} < 0$, it follows that $0 < W_1 < W_1 - W_{\rm PPT}$ to assure that T_1^c exists as a meaningful physical quantity ($0 < T_1^c < 1$) whenever $W_1 > 0$.

Therefore, an entangled state satisfying $W_1 \leqslant 0$ is robust against losses in channel 1, and W_1 is the witness for this type of robustness. The corresponding analysis regarding attenuations on the subsystem 2 yields the witness

$$W_2 = W_{\rm full} + \Gamma_{12}, \tag{26}$$

with the same properties of W_1. A relation analogous to Eq. (25) holds for T_2^c. Both witnesses are invariant under local rotations, as expected.

V. ROBUSTNESS CLASSES

Based on the different dynamics of entanglement of Fig. 2, we propose a classification of bipartite entangled states according to their resilience to losses. We take guidance in the sign of the reduced witness $W_R(T_1,T_2)$, which is a hyperbolic paraboloid surface. The contour defined by the condition $W_R(T_1,T_2) = 0$ provides a complete description of the entanglement dynamics in terms of Γ_{ij}. As depicted in Fig. 2, there are three relevant situations. Bipartite entangled Gaussian states can be assigned to the following different classes:

(i) *Fully robust states* remain entangled for any partial attenuation: $W_R(T_1,T_2) < 0, \forall T_{1,2}$.

(ii) *Partially robust states: (a) symmetric:* remain entangled against losses on a single mode, but may disentangle for combinations of partial attenuations on both modes: $W_R(T_1,T_2 = 1) < 0, \forall T_1$, and $W_R(T_1 = 1,T_2) < 0, \forall T_2$. *(b) asymmetric*: remain entangled against losses on a specific mode, but may disentangle for partial losses on the other mode: either $W_R(T_1,T_2 = 1) < 0, \forall T_1$, or $W_R(T_1 = 1,T_2) < 0, \forall T_2$.

(iii) *Fragile states* disentangle for partial attenuation on any mode or combinations of partial attenuations on both modes.

For a complete classification of all bipartite Gaussian states, one should include the separable states.

With the witnesses previously defined, we have necessary criteria to assess the robustness of all bipartite Gaussian states. A state will be robust with respect to losses imposed on subsystem 1 if

$$W_1 \leqslant 0. \tag{27}$$

Likewise, robustness to losses on subsystem 2 is given by

$$W_2 \leqslant 0. \tag{28}$$

States will be partially robust if at least one of W_1 or W_2 is negative or even if both are negative simultaneously (partially robust, symmetric). Only if $W_R(T_1,T_2) < 0, \forall T_{1,2}$ will we have full robustness.

As mentioned above, this classification is of practical interest. Several quantum communication protocols using continuous variables can be realized by one of the parties (Alice) locally producing the entangled state and sending only one mode to a remote location. The other party (Bob) then performs operations on his part of the state, according to instructions sent by Alice through a classical channel. The success of these communication schemes strongly depends on the losses that the subsystem of Bob may undergo, which could be detected by an eavesdropper (Eve). In this situation, Alice must produce entangled states that are at least partially robust in order to avoid problems with signal degradation. It may not be necessary for her to produce fully robust states: partially robust entangled states may suffice for successful quantum communication protocols.

VI. PARTICULAR CASES

In the preceding analysis, we have found precise conditions to determine whether or not bipartite Gaussian entangled states are robust against losses. Given the practical interest of such states as resources for quantum communication protocols, we examine here particular Gaussian states that fall within the classification scheme proposed above. One might think that it should suffice to generate pure states with a large amount of squeezing in order to have robust entanglement. We begin by providing a specific example of a pure strongly squeezed state, which is only partially robust. We then examine different forms of the covariance matrix in order to map out the different possibilities.

A. Pure and highly squeezed states with only partial robustness

In most experiments, Gaussian bipartite entanglement is witnessed by a violation of the simplified Duan inequality of Eq. (6). Typically, this is done by combining highly squeezed individual modes on a beam splitter. This method allows the creation of arbitrarily strong entanglement in the sense that quantum information protocols such as teleportation could, in principle, be realized with perfect fidelity in the limit of an EPR state.

If such a state is contaminated by uncorrelated classical noise (e.g., from Brillouin scattering in an optical fiber [25]), it may then become subject to disentanglement from losses. Even states that are pure may be subject to disentanglement in a dual-channel scenario. We present below the covariance matrix for a pure state with these characteristics:

$$V = \begin{pmatrix} 52.5 & 0 & -47.5 & 0 \\ 0 & 0.105 & 0 & 0.095 \\ -47.5 & 0 & 52.5 & 0 \\ 0 & 0.095 & 0 & 0.105 \end{pmatrix}. \tag{29}$$

This state has a very small symplectic eigenvalue, indicating very strong entanglement [26]. As can be observed in Fig. 3, the state is partially robust: losses on any single channel do not lead to disentanglement, while ESD will occur for combined losses in both channels.

Let us now examine different symmetries of the covariance matrix and their implications on the entanglement dynamics.

B. Symmetric modes and quadratures: Fully robust states

We begin by examining completely symmetric modes, for which $\Delta^2\hat{p}_1 = \Delta^2\hat{q}_1 = \Delta^2\hat{p}_2 = \Delta^2\hat{q}_2 = s$ and $\langle\delta\hat{p}_1\delta\hat{p}_2\rangle = \langle\delta\hat{q}_1\delta\hat{q}_2\rangle = c$, and $\langle\delta\hat{p}_j\delta\hat{q}_{j'}\rangle = 0$. The covariance matrix has the form

$$V = \begin{pmatrix} s & 0 & c & 0 \\ 0 & s & 0 & -c \\ c & 0 & s & 0 \\ 0 & -c & 0 & s \end{pmatrix}. \tag{30}$$

Such states can be generated, for instance, by the interference of (symmetric) squeezed states on a balanced beam splitter (entangled squeezed states) [15,17]. In this case, one has $s = \nu\cosh 2r$ and $c = \nu\sinh 2r$, where r is the squeezing parameter and $\nu \geqslant 1$ accounts for an eventual thermal

mixedness, representing a correlated classical noise between the systems.

Entanglement and robustness witnesses are thus

$$W_{\rm PPT} = (s^2 - c^2 + 1)^2 - 4s^2 \tag{31}$$

and

$$W_{\rm full} = 4[(s-1)^2 - c^2] = 4(s^2 - c^2 + 1 - 2s), \tag{32}$$

from which one directly sees that $W_{\rm PPT} < 0$ and $W_{\rm full} < 0$ lead to the same condition ($s - 1 - |c| < 0$). Therefore, entangled states with symmetry between the two modes and the two quadratures are fully robust. The lack of ESD in these systems indicates that strong symmetries lead to entanglement robustness, even when classical noise is present, as long as it is correlated.

The highly symmetric covariance matrices of Eq. (30) are a particular case of the standard form II of Ref. [10]. For these, the Duan criterion is equivalent to the PPT criterion, which then entails full robustness for all entangled states with covariance matrices in standard form II. Moreover, since any state can be brought to standard form II by local squeezing and quadrature rotations without changing its entanglement [10], any fragile state can be made robust by suitable local unitary operations. The converse is also true: local squeezing can transform robust states into fragile ones without changing the entanglement. For instance, if one applies a gate that makes use of local squeezing to a given robust entangled state, it can become fragile and undergo disentanglement upon transmission. Local squeezing is one of the important steps in an implementation of a controlled-NOT (C-NOT) [or quantum nondemolition (QND)] gate with continuous variables [27].

C. Symmetric modes and asymmetric quadratures

More general covariance matrices are necessary in order to observe disentanglement. States that are symmetric on both modes but asymmetric on the quantum statistics of the quadratures have been recently observed to present ESD [4]. The system under investigation consisted of the twin light beams produced by an optical parametric oscillator, described by a covariance matrix of the form

$$V = \begin{pmatrix} \Delta^2 q & 0 & c_q & 0 \\ 0 & \Delta^2 p & 0 & c_p \\ c_q & 0 & \Delta^2 q & 0 \\ 0 & c_p & 0 & \Delta^2 p \end{pmatrix}. \tag{33}$$

The entanglement and robustness witnesses read as

$$W_{\rm PPT} = \left[(\Delta^2 p)^2 - c_p^2\right]\left[(\Delta^2 q)^2 - c_q^2\right] - 2\Delta^2 p\,\Delta^2 q + 2c_p c_q + 1 \tag{34}$$

and

$$W_{\rm full} = (\Delta^2 p + \Delta^2 q - 2)^2 - (c_q - c_p)^2. \tag{35}$$

In this situation, the subsystems have equal purities ($\mu_S = 1/\sqrt{\Delta^2 p \Delta^2 q}$). The quadrature variances and correlations are constrained by $(\Delta^2 p)^2 - c_p^2 \geqslant 0$ and $(\Delta^2 q)^2 - c_q^2 \geqslant 0$. We introduce the normalized correlations $\bar{C}_p = c_p/\Delta^2 p$ and $\bar{C}_q = c_q/\Delta^2 q$ for simplicity. They are bounded by $-1 \leqslant \bar{C}_j \leqslant 1$. These parameters suffice to describe any state with the form of Eq. (33).

In Fig. 4, the robustness condition is mapped in terms of the correlations for a fixed purity $\mu_S = 0.626$, showing the regions corresponding to different robustness classes. Fully robust state (a) falls within the **I** region in Fig. 4, while the separable state (c) is located in the **IV** region. Within the intermediate region, two different types of *fragile* states are present. State (d) is partially robust, lying close to the boundary to robust states. State (b) shows ESD for partial losses in general, lying close to the boundary to separable states.

Alternatively, following the treatment described in Ref. [4], the covariance matrix of Eq. (33) can be parametrized in terms of the physically familiar EPR-type operators

$$\hat{p}_\pm = \frac{1}{\sqrt{2}}(\hat{p}_1 \pm \hat{p}_2) \tag{36}$$

and

$$\hat{q}_\pm = \frac{1}{\sqrt{2}}(\hat{q}_1 \pm \hat{q}_2). \tag{37}$$

Entanglement can be directly observed from the product of squeezed variances of the proper pair of EPR operators $(\hat{p}_-,\hat{q}_+)$ or $(\hat{p}_+,\hat{q}_-)$. Additionally, the entanglement and robustness criteria of symmetric two-mode systems of Eqs. (34) and (35) can be written in the simpler forms

$$W_{\rm PPT} = W_{\rm prod}\overline{W}_{\rm prod}, \tag{38}$$

$$W_{\rm full} = W_{\rm sum}\overline{W}_{\rm sum}, \tag{39}$$

where

$$W_{\rm sum} = \Delta^2\hat{p}_- + \Delta^2\hat{q}_+ - 2,$$
$$\overline{W}_{\rm sum} = \Delta^2\hat{p}_+ + \Delta^2\hat{q}_- - 2,$$
$$W_{\rm prod} = \Delta^2\hat{p}_-\Delta^2\hat{q}_+ - 1,$$
$$\overline{W}_{\rm prod} = \Delta^2\hat{p}_+\Delta^2\hat{q}_- - 1.$$

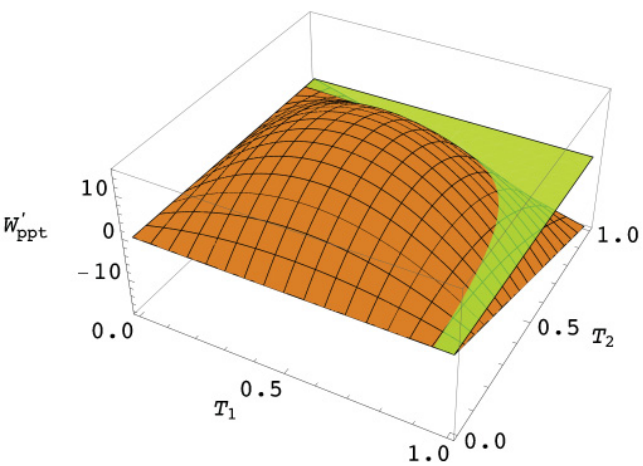

FIG. 3. (Color online) Entanglement as a function of losses for the covariance matrix given by Eq. (29). Disentanglement may occur only for combined losses on both modes. In this example, the symplectic eigenvalue [6] is only 0.22 for the initial state.

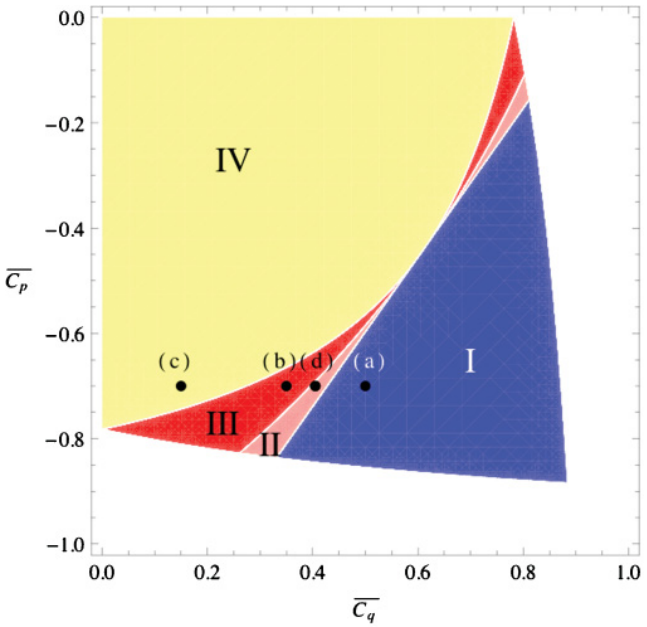

FIG. 4. (Color online) The space of states with covariance matrices of the form of Eq. (33) is plotted as a function of the normalized correlations $\bar{C}_p$ and $\bar{C}_q$. Separable states lie in the region **IV**; fully robust states are comprised within the region **I**; partially robust states are in the region **II**, and fragile states are in the region **III**. Points outside of these regions do not correspond to physical states. Here, we use $\Delta^2 p = 1.80$ and $\Delta^2 q = 2.55$. The points included represent the states in Figs. 2(a)–2(d).

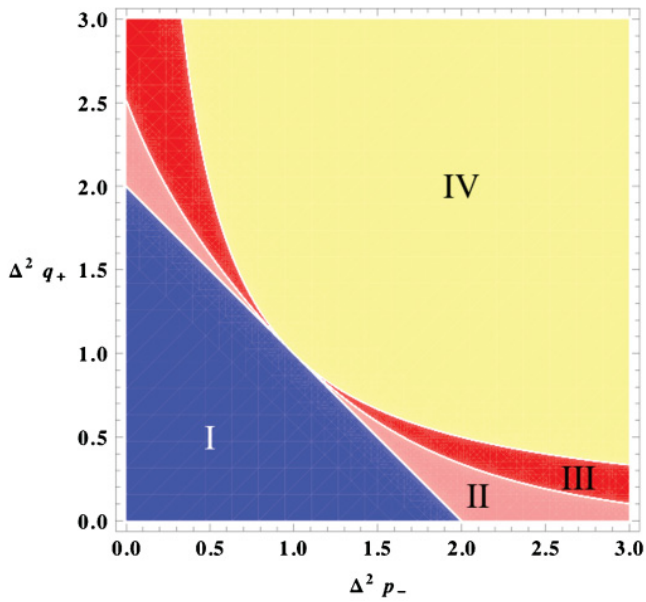

FIG. 5. (Color online) The space of symmetric two-mode states is plotted as a function of the EPR variances $\Delta^2\hat{q}_+$ and $\Delta^2\hat{p}_-$, normalized to the standard quantum limit (SQL). Separable states lie in the region **IV**; fully robust entangled states are within the region **I**; partially robust states are in the region **II**, and fragile states are in the region **III**. The partial purities are $\mu_- = 0.7267$ and $\mu_+ = 0.4529$.

The distinction between robust and partially robust entanglement is clearly illustrated with symmetric modes. Considering attenuation solely on mode 1 (entirely equivalent to attenuation on mode 2, given the symmetry), the condition for partial robustness of Eq. (27) yields

$$W_1 = W_{\text{sum}}\overline{W}_{\text{prod}} + W_{\text{prod}}\overline{W}_{\text{sum}}. \tag{40}$$

The condition $W_1 = 0$ defines the border between partial robustness and fragility. Since a state must be initially entangled in order to disentangle, obviously,

$$W_{\text{full}} < 0 \Longrightarrow W_{\text{PPT}} < 0. \tag{41}$$

Given the commutation relations between $\hat{p}$ and $\hat{q}$, W_{prod} and $\overline{W}_{\text{prod}}$ (or W_{sum} and $\overline{W}_{\text{sum}}$) can not be simultaneously negative. In this context, the condition of Eq. (41) can be restated as

$$W_{\text{sum}} < 0 \Longrightarrow W_{\text{prod}} < 0 \tag{42}$$

or

$$\overline{W}_{\text{sum}} < 0 \Longrightarrow \overline{W}_{\text{prod}} < 0. \tag{43}$$

For $W_1 = 0$,

$$W_{\text{sum}}\overline{W}_{\text{prod}} = -W_{\text{prod}}\overline{W}_{\text{sum}}. \tag{44}$$

This equation holds only if $W_{\text{prod}} < 0$ and $W_{\text{sum}} > 0$ (or $\overline{W}_{\text{prod}} < 0$ and $\overline{W}_{\text{sum}} > 0$). Thus, $W_1 = 0$ lies between the curves $W_{\text{PPT}} = 0$ and $W_{\text{full}} = 0$.

A plot of the state space in terms of these EPR variables is presented in Fig. 5. Fixed values for the partial purities $\mu_+ = 1/\sqrt{\Delta^2\hat{p}_+\Delta^2\hat{q}_+}$ and $\mu_- = 1/\sqrt{\Delta^2\hat{p}_-\Delta^2\hat{q}_-}$ are assumed, so that we can write the entanglement and robustness conditions in terms of $\Delta^2\hat{p}_-$ and $\Delta^2\hat{q}_+$. The observation of ESD reported in Ref. [4] was obtained for partially robust states lying in the region delimited by the conditions $W_{\text{sum}} > 0$ and $W_1 < 0$.

D. System in standard form I

The last case we consider is a covariance matrix in the standard form I [6,10]. It represents two different modes with symmetric quadratures

$$V = \begin{pmatrix} s & 0 & c_q & 0 \\ 0 & s & 0 & c_p \\ c_q & 0 & t & 0 \\ 0 & c_p & 0 & t \end{pmatrix}. \tag{45}$$

The entanglement and full robustness witnesses read as

$$W_{\text{PPT}} = \left(st - c_q^2\right)\left(st - c_p^2\right) - s^2 - t^2 + 2c_q c_p + 1 \tag{46}$$

and

$$W_{\text{full}} = 4(s-1)(t-1) - (c_q - c_p)^2. \tag{47}$$

The subsystems have purities $\mu_1 = s^{-1}$ and $\mu_2 = t^{-1}$. We define the normalized correlations $\bar{c}_j = c_j/\sqrt{st} = c_j\sqrt{\mu_1\mu_2}$ as before.

A covariance matrix in standard form I also presents ESD for certain parameters, spanning all three classes of states described above. Owing to the symmetry in the covariance matrix, ESD in such a system does not occur for symmetric correlations $\bar{c}_q = -\bar{c}_p$ independently of the purities μ_1 and μ_2.

VII. CONCLUSION

We have addressed in this paper the issue of entanglement in the open-system dynamics of continuous-variable (CV) systems. Entanglement is a crucial albeit fragile resource for quantum information protocols. Understanding its behavior in open systems is very important for future practical applications.

Our analysis is carried out for the simplest possible situation in the CV setting: bipartite Gaussian states under linear losses. The general study undertaken here was motivated by the experimental results presented in [3,4].

Starting from necessary and sufficient entanglement criteria, we derived necessary and sufficient *robustness* criteria, which enable us to classify these states with respect to their entanglement resilience under losses. Having in mind realistic communications scenarios, we present a robustness classification: states may be fully robust, partially robust, or fragile. For instance, if one generates an entangled state for which only one mode will propagate in a lossy quantum channel (single-channel losses), the conditions derived for partially robust states apply. Such partial robustness would be the minimum resource required for single-channel robust quantum communications.

On the other extreme, EPR states, for which quantum correlations appear in collective operators of both quadratures, are the best desirable quantum resource. Their entanglement is resilient to any combination of losses acting on both modes, only disappearing when the state suffers total loss. However, a rather likely deviation from such states could already be catastrophic for entanglement: if a moderate amount of uncorrelated noise (e.g., thermal noise) is introduced in the EPR-type collective operators for one quadrature, even when the other quadrature remains untouched and is perfectly squeezed, entanglement can be lost for partial attenuation. This offers a clue to the main ingredients leading to ESD in bipartite Gaussian states. An appealing example is given by the OPO operating above threshold. The usual theoretical analysis leads to symmetric modes, with asymmetric quadratures, but no uncorrelated classical noise. Thus, the OPO is predicted to generate fully robust entangled states. However, uncorrelated thermal noise originating in the nonlinear crystal couples into the two modes [22], leading to ESD [4].

We have also found that such noise does not necessarily have to imply mixedness. Even for pure states, the lack of correlation between modes increases the state's fragility. Robustness is thus achieved not only for high levels of entanglement between CV systems, but also symmetry in the form of quantum correlations is desirable. This point was illustrated by our study of mathematical examples of Gaussian states, for which symmetry implied robustness in spite of mixedness. We also point out that robustness can be obtained, in principle, for any entangled state by local unitary operations, such as squeezing and quadrature rotations. However, these operations are not always simple to implement in an experiment.

As an outlook, we should keep in mind that scalability is one of the main goals in quantum information research at present. As larger and more complex systems are envisioned for the implementation of useful protocols, higher orders of entanglement will be required. Disentanglement for partial losses was experimentally observed in the context of a tripartite system [3]. An understanding of entanglement resilience for higher-order systems will be important. The methods and analyses developed here constitute the starting point for such investigations.

ACKNOWLEDGMENTS

This work was supported by the Conselho Nacional de Desenvolvimento Científico e Tecnológico (CNPq) and the Fundação de Amparo à Pesquisa do Estado São Paulo (FAPESP). K.N.C. and A.S.V. acknowledge support from the AvH Foundation.

APPENDIX: ATTENUATED WITNESS

We would like to obtain an explicit expression for $W'_{\rm PPT}(T_1,T_2)$ in terms of the physical parameters of the bipartite system (variances and correlations). We note that the procedure can not be directly realized by first bringing V' (or V) to a standard form and then applying the attenuation, since local symplectic operations $S \in \mathrm{Sp}(2,\Re) \oplus \mathrm{Sp}(2,\Re)$ normally do not commute with the attenuation operation $\mathcal{L}(SVS^T) \neq S\mathcal{L}(V)S^T$ [12,28]. Consequently, invariant quantities under global and local symplectic transformations are not necessarily conserved by attenuations, such as the global and local purities. On the other hand, $S\mathcal{L}(V)S^T = \mathcal{L}(SVS^T)$ is satisfied only if $SS^T = I$, i.e., S must be a local phase space rotation $S \in \mathrm{SO}(2,\Re) \oplus \mathrm{SO}(2,\Re)$. Therefore, a criterion for entanglement robustness should depend solely on local rotational invariants.

We derive the explicit behavior of the witness $W'_{\rm PPT}$ under attenuation. Writing the PPT separability criterion in terms of the symplectic invariants [6], we obtain

$$W_{\rm PPT} = 1 + \det V + 2\det C - \sum_{j=1,2} \det A_j, \tag{A1}$$

$$\det V = \det A_1 \det A_2 + \det C^2 - \Lambda_4, \tag{A2}$$

$$\Lambda_4 = \mathrm{tr}(A_1 J C J A_2 J C^T J). \tag{A3}$$

After attenuation, the matrices A_1, A_2, and C become

$$C' = \sqrt{T_1 T_2}\, C, \tag{A4}$$

$$A'_i = T_i(A_i - I) + I. \tag{A5}$$

To derive Eq. (17), we express the symplectic invariants in terms of quantities presenting similar behavior. Two such quantities are obtained from Eqs. (5) and (A4):

$$\det(V' - I) = T_1^2 T_2^2 \det(V - I), \tag{A6}$$

$$\det C' = T_1 T_2 \det C. \tag{A7}$$

For any 2×2 matrix M, the following expressions are valid:

$$\det(M - I) = \det M - \mathrm{tr} M + 1, \tag{A8}$$

$$\mathrm{tr}(M - I) = \mathrm{tr}(M) - 2, \tag{A9}$$

and one obtains

$$\varpi'_j - \sigma'_j = T_j^2(\varpi_j - \sigma_j), \tag{A10}$$

$$\sigma'_j = T_j \sigma_j, \tag{A11}$$

where $\sigma_i = \mathrm{tr}A_i - 2$, and $\varpi_i = \det A_i - 1$ is the deviation from a pure state (impurity), which is zero for a pure state and positive for any mixed state.

By applying Eq. (A8) to $\det(V - I)$, we find quantities that scale polynomially on the beam attenuations:

$$\det V = \det(V - I) + \eta, \tag{A12}$$

$$\begin{aligned}\eta &= \sigma_1(\varpi_2 - \sigma_2) + \sigma_2(\varpi_1 - \sigma_1) + \sigma_1\sigma_2 \\ &\quad + \det(A_1) + \det(A_2) + \Lambda_1 + \Lambda_2 - \Lambda_C - 1,\end{aligned} \tag{A13}$$

$$\begin{aligned}\Lambda_1 &= \mathrm{tr}[C^T J(A_1 - I)JC], \\ \Lambda_2 &= \mathrm{tr}[CJ(A_2 - I)JC^T], \\ \Lambda_C &= \mathrm{tr}(C^T C),\end{aligned} \tag{A14}$$

where the last three quantities scale as

$$\Lambda_1' = T_1^2 T_2 \Lambda_1, \quad \Lambda_2' = T_1 T_2^2 \Lambda_2, \tag{A15}$$

$$\Lambda_C' = T_1 T_2 \Lambda_C. \tag{A16}$$

By substituting Eq. (A12) in (A1) and applying the attenuation operation, we arrive at

$$\begin{aligned}W'_{\mathrm{PPT}}(T_1, T_2) &= \sum_{i,j=1,2} T_1^i T_2^j \Gamma_{ij}, \\ \Gamma_{22} &= \det(V - I) = \det(V) - \eta, \\ \Gamma_{12} &= \sigma_1(\varpi_2 - \sigma_2) + \Lambda_2, \\ \Gamma_{21} &= \sigma_2(\varpi_1 - \sigma_1) + \Lambda_1, \\ \Gamma_{11} &= \sigma_1\sigma_2 - \Lambda_C + 2\det(C),\end{aligned} \tag{A17}$$

The function W'_{PPT} describes the dynamics of all bipartite Gaussian states under losses.

[1] T. Yu and J. H. Eberly, Science **323**, 598 (2009), and references therein.
[2] M. P. Almeida, F. de Melo, M. Hor-Meyll, A. Salles, S. P. Walborn, P. H. Souto Ribeiro, and L. Davidovich, Science **316**, 579 (2007).
[3] A. S. Coelho, F. A. S. Barbosa, K. N. Cassemiro, A. S. Villar, M. Martinelli, and P. Nussenzveig, Science **326**, 823 (2009).
[4] F. A. S. Barbosa, A. S. Coelho, A. J. de Faria, K. N. Cassemiro, A. S. Villar, P. Nussenzveig, and M. Martinelli, Nat. Photon. **4**, 858 (2010).
[5] S. L. Braunstein and P. van Loock, Rev. Mod. Phys. **77**, 513 (2005).
[6] R. Simon, Phys. Rev. Lett. **84**, 2726 (2000).
[7] R. F. Werner and M. M. Wolf, Phys. Rev. Lett. **86**, 3658 (2001).
[8] M. M. Wolf, J. Eisert, and M. B. Plenio, Phys. Rev. Lett. **90**, 047904 (2003).
[9] R. Simon, N. Mukunda, and B. Dutta, Phys. Rev. A **49**, 1567 (1994).
[10] Lu-Ming Duan, G. Giedke, J. I. Cirac, and P. Zoller, Phys. Rev. Lett. **84**, 2722 (2000).
[11] A. S. Holevo and R. F. Werner, Phys. Rev. A **63**, 032312 (2001).
[12] J. Eisert and M. M. Wolf, in *Quantum Information with Continuous Variables of Atoms and Light*, edited by N. J. Cerf, G. Leuchs, and E. S. Polzik (Imperial College Press, London, 2007), pp. 23–42.
[13] A. Einstein, B. Podolsky, and N. Rosen, Phys. Rev. **47**, 777 (1935).
[14] N. Bohr, Phys. Rev. **48**, 696 (1935).
[15] Ch. Silberhorn, P. K. Lam, O. Weiss, F. Konig, N. Korolkova, and G. Leuchs, Phys. Rev. Lett. **86**, 4267 (2001).
[16] W. P. Bowen, R. Schnabel, P. K. Lam, and T. C. Ralph, Phys. Rev. Lett. **90**, 043601 (2003).
[17] A. Furusawa *et al.*, Science **23**, 706 (1998).
[18] A. S. Villar, L. S. Cruz, K. N. Cassemiro, M. Martinelli, and P. Nussenzveig, Phys. Rev. Lett. **95**, 243603 (2005).
[19] A. Peres, Phys. Rev. Lett. **77**, 1413 (1996).
[20] M. Horodecki, P. Horodecki, and R. Horodecki, Phys. Lett. A **223**, 1 (1996).
[21] S. L. Braunstein and P. van Loock, Rev. Mod. Phys. **77**, 513 (2005).
[22] J. E. S. César, A. S. Coelho, K. N. Cassemiro, A. S. Villar, M. Lassen, P. Nussenzveig, and M. Martinelli, Phys. Rev. A **79**, 063816 (2009).
[23] J. Eisert, S. Scheel, and M. B. Plenio, Phys. Rev. Lett. **89**, 137903 (2002).
[24] G. Giedke and J. I. Cirac, Phys. Rev. A **66**, 032316 (2002).
[25] D. Elser, U. L. Andersen, A. Korn, O. Glöckl, S. Lorenz, Ch. Marquardt, and G. Leuchs, Phys. Rev. Lett. **97**, 133901 (2006).
[26] G. Vidal and R. F. Werner, Phys. Rev. A **65**, 032314 (2002).
[27] J. I. Yoshikawa, Y. Miwa, A. Huck, U. L. Andersen, P. van Loock, and A. Furusawa, Phys. Rev. Lett. **101**, 250501 (2008).
[28] Arvind, B. Dutta, N. Mukunda, and R. Simon, Pramana **45**, 471 (1995).

A pureza de um estado gaussiano, como mostrado na ref [54], pode ser obtida a partir do determinante da matriz de covariância: $trace[\hat{\rho}^2] = 1/\sqrt{det(V)}$. Vemos que o critério de emaranhamento (5.2) envolve tanto a pureza global, quanto a pureza de cada subsistema, além da informação comum a ambos, representada por $det(C)$. Dependendo da situação, mesmo estados emaranhados puros podem evoluir para estados separáveis mediante perdas, conforme a eq. (5.4). Neste caso, o balanceamento da informação entre as quadraturas do campo será também importante para que o estado seja robusto. Note que o critério de robustez (5.4), para estados com matriz C diagonal, fica reduzido a

$$W_{full}^{(D)} = (\mathrm{tr}A_1 - 2)(\mathrm{tr}A_2 - 2) - (c_p - c_q)^2 \leq 0, \tag{5.5}$$

envolvendo os traços das matrizes dos subsistemas, e da matriz C após a transposição parcial (o que implica na troca de sinal de uma das correlações de quadratura). Evidentemente que estados emaranhados, puros e simétricos serão robustos contra perdas. Estados com forte assimetria entre as quadraturas podem, porém estar sujeitos à morte súbita, ainda que sejam puros em sua origem (fig. 5.4).

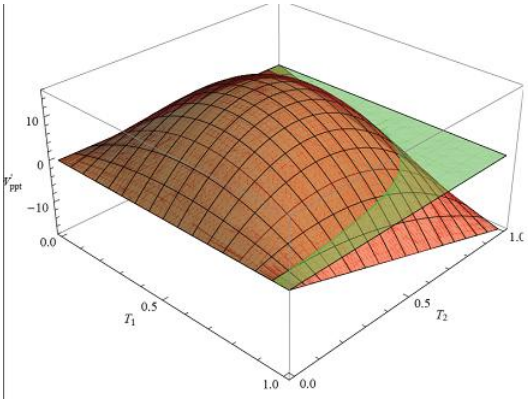

$$V = \begin{bmatrix} 0.105 & 0 & 0.095 & 0 \\ 0 & 52.5 & 0 & -47.5 \\ 0.095 & 0 & 0.105 & 0 \\ 0 & -47.5 & 0 & 52.5 \end{bmatrix}$$

Figura 5.4: Evolução da testemunha de emaranhamento de Simon para um estado puro, mediante perdas em cada modo.

Realizamos por este período uma série de medidas com diferentes estados emaranhados bipartite gerado pelo OPO. Os feixes sinal e complementar apresentam ruídos semelhantes, balanceados entre si. Porém, a razão entre a variância da quadratura fase pela variância da amplitude pode ser modificada de acordo com a potência de bombeio, conforme vimos anteriormente [13]. Usando então o bombeio como parâmetro de controle, pudemos variar o estado de saída do OPO de um estado robusto, para um estado sujeito à morte súbita, e atingir ao final um estado separável.

LETTERS
PUBLISHED ONLINE: 17 OCTOBER 2010 | DOI: 10.1038/NPHOTON.2010.222

nature photonics

Robustness of bipartite Gaussian entangled beams propagating in lossy channels

F. A. S. Barbosa[1], A. S. Coelho[1], A. J. de Faria[1], K. N. Cassemiro[2], A. S. Villar[2,3], P. Nussenzveig[1] and M. Martinelli[1]*

Subtle quantum properties offer exciting new prospects in optical communications. For example, quantum entanglement enables the secure exchange of cryptographic keys[1] and the distribution of quantum information by teleportation[2,3]. Entangled bright beams of light are increasingly appealing for such tasks, because they enable the use of well-established classical communications techniques[4]. However, quantum resources are fragile and are subject to decoherence by interaction with the environment. The unavoidable losses in the communication channel can lead to a complete destruction of entanglement[5–8], limiting the application of these states to quantum-communication protocols. We investigate the conditions under which this phenomenon takes place for the simplest case of two light beams, and analyse characteristics of states which are robust against losses. Our study sheds new light on the intriguing properties of quantum entanglement and how they may be harnessed for future applications.

Quantum entanglement is a counterintuitive feature that was first introduced by Einstein, Podolsky and Rosen (EPR)[9] and discussed by Schrödinger[10] in 1935. As well as its philosophical implications and fundamental character, it is increasingly important in proposals to boost the processing power of computers and to make communications more secure. Bright beams of light can be described in terms of physical observables (the amplitude and phase quadratures) analogous to the position and momentum of a particle as in the original EPR conundrum. These continuous variables may be entangled and then used for quantum key distribution or for quantum teleportation. Among all the quantum states, an important class is the one presenting Gaussian statistics, which have been extensively investigated both theoretically and experimentally.

In the realm of quantum optics, squeezed states of light are an excellent example of non-classical Gaussian states. They have quadrature fluctuations smaller than the classical limit of a coherent state. It is well known that squeezing is degraded under channel losses, an unwelcome effect for communications. Squeezed states always remain squeezed for partial losses, linearly approaching the classical limit for complete attenuation[11]. Recently, the effect of channel losses was analysed for entanglement in continuous variables[8]. Similar to observations in two-qubit systems[5–7], entanglement can behave differently from the properties of each individual system: it can vanish completely even for partial losses. To understand and devise ways of controlling this effect in practical applications, we investigate the simplest and most fundamental situation of two entangled Gaussian beams. We pinpoint conditions leading to bipartite disentanglement and trace a boundary for those entangled states that are robust against channel losses.

We begin by describing our source of entangled light, an optical parametric oscillator (OPO) operating above threshold. In this system, the nonlinear process of parametric downconversion is stimulated, generating gain of the twin beams. As gain overcomes losses, the system oscillates and outputs bright twin beams of light, with classical coherence resembling that of a laser. The twin beams are entangled in their quadrature amplitude and phase components[12,13]. This can be understood from the perspective of energy conservation: on the one hand, photons are created in pairs, implying strong intensity correlations; on the other hand, the sum of their optical frequencies (thus their phase fluctuations) has to equal the pump frequency, leading to phase anticorrelations. However, this simple picture is somewhat upset by the existence of phonon noise in the crystal, which degrades the phase quantum correlations and therefore hinders entanglement[14]. Control over the effects of this noise enables the investigation of quantum-state entanglement robustness.

The states produced by the OPO can be a physical realization of an EPR-type state; that is, the (normalized) amplitude difference ($\hat{p}_-$) and the phase sum ($\hat{q}_+$) of the light beams show squeezing. Such states violate a simple inequality, derived by Duan and colleagues[15],

$$\Delta^2\hat{p}_- + \Delta^2\hat{q}_+ \geq 2 \qquad (1)$$

where the quadrature variance of a coherent state, the standard quantum limit (SQL), is unity. Violation of this inequality is sufficient for entanglement. We will refer to it henceforth as the 'Duan inequality'. It is very convenient to check experimentally, for it only requires measurements of joint amplitude and phase correlations of both fields. However, it is not a necessary criterion in this form; that is, fulfilment of equation (1) does not imply separability.

It is straightforward to check that two-mode squeezed states and, more generally, states that violate the Duan inequality are robust entangled states. By evenly attenuating two such light beams by the amount $1-T$ (T is the fraction of light detected), the sum of variances transforms as

$$\Delta^2\hat{p}_{-,T} + \Delta^2\hat{q}_{+,T} = T(\Delta^2\hat{p}_- + \Delta^2\hat{q}_+) + 2(1-T) \qquad (2)$$

where $\Delta^2\hat{p}_{-,T}$ and $\Delta^2\hat{q}_{+,T}$ are the new values of the EPR pair variances after attenuation. Once violated, equation (1) will remain below 2 for all values $T > 0$ (ref. 16). In the case of uneven attenuations, a state initially violating the inequality could fulfil it for a finite attenuation. However, it could be brought back to violation by attenuating the second beam, according to equation (2). Because attenuation is a Gaussian operation and, as such, cannot increase the amount of entanglement[17,18], it must be concluded that entanglement was already present, although not detected by

[1]Instituto de Física, Universidade de São Paulo, Caixa Postal 66318, 05315-970 São Paulo, SP, Brazil, [2]Max Planck Institute for the Science of Light, Günther-Scharowsky-straβe 1/Bau 24, 91058 Erlangen, Germany, [3]University of Erlangen-Nuremberg, Staudtstraβe 7/B2, 91058 Erlangen, Germany.
*e-mail: mmartine@if.usp.br

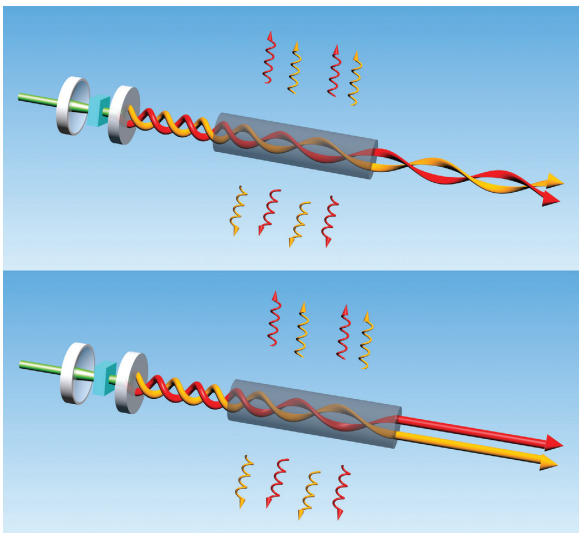

Figure 1 | Pictorial view of the process. An entangled state of two light beams in transmission through a lossy channel. At the output, the state may remain entangled (shown intertwined, above) or become disentangled (below).

the restrictive form of the Duan inequality. This demonstrates the robustness of such entangled states. In fact, one can derive strict conditions that all entangled Gaussian states robust against arbitrary attenuations on both fields must fulfil[19].

To experimentally address the issue of disentanglement, we need a necessary and sufficient entanglement criterion. For bipartite Gaussian states, the positivity under partial transposition (PPT) fulfils this requirement[20]. Quantum properties of Gaussian states are completely characterized by their second-order moments (variances and covariances), which can be conveniently organized in the form of a covariance matrix. The PPT criterion can be stated in terms of the smallest symplectic eigenvalue of the covariance matrix corresponding to the partially transposed state: if smaller than one, the matrix represents an entangled state; otherwise, a separable state[20]. To apply the PPT test, we completely reconstruct the covariance matrix. Our study is thus conceptually simple: we generate twin light beams from the OPO, perform a complete set of quadrature measurements and test the covariance matrix obtained for entanglement. We then subject one of the beams to a controlled attenuation, simulating propagation losses in a quantum channel, and repeat the procedure. For each attenuation the symplectic eigenvalue reveals whether the beams remain entangled. The situation is illustrated in Fig. 1.

We concentrate here on an interesting and practical situation. If the source of the entangled beams lies with one of the parties that wish to establish secure communication, only one beam has to be sent over a lossy channel. States that could disentangle for partial losses on both beams may in fact remain entangled until total loss on a single beam, reducing the demands on the preparation of the quantum state[19]. In the following, we consider a particularity of our twin beams that does not affect the essential physics but greatly simplifies the mathematical treatment. We assume a symmetric state upon exchange of the two beams and that no cross-quadrature (amplitude-phase) correlations exist. Then, states subject to disentanglement fulfil the following inequality (see Supplementary Information):

$$W_{\mathrm{prod}}\overline{W}_{\mathrm{sum}} + \overline{W}_{\mathrm{prod}}W_{\mathrm{sum}} > 0 \qquad (3)$$

Here we define $W_{\mathrm{sum}} \equiv \Delta^2\hat{p}_- + \Delta^2\hat{q}_+ - 2, \overline{W}_{\mathrm{sum}} \equiv \Delta^2\hat{p}_+ + \Delta^2\hat{q}_- - 2$ and $W_{\mathrm{prod}} \equiv \Delta^2\hat{p}_-\Delta^2\hat{q}_+ - 1, \overline{W}_{\mathrm{prod}} \equiv \Delta^2\hat{p}_+\Delta^2\hat{q}_- - 1$. The sign of W_{prod} determines whether the state is entangled ($W_{\mathrm{prod}} < 0$) or separable ($W_{\mathrm{prod}} \geq 0$). The different sets of possible states are shown in Fig. 2 as a function of $\Delta^2\hat{p}_-$ and $\Delta^2\hat{q}_+$, the squeezed variances of the twin beams. Entangled states subject to disentanglement (green) lie in the region between the robust states (yellow) and the separable states (blue). The boundary of robust states depends on the overall purity. Two limiting situations can be recognized. For pure states, partial-loss disentanglement never occurs. For highly mixed states, robustness is restricted to states violating the Duan inequality (region to the left of the dashed line). Because one always deals with mixed states in an experiment, it becomes important to consider the exact boundary of equation (3) to assess robustness. One should be aware that in the more general case when both fields are subject to losses, even pure states may disentangle[19].

We generate either robust entanglement or disentangling states by operating the OPO under different conditions. By varying the pump power, we control the amount of classical phonon noise coupled to the quantum phase noise. For pump power very close to the OPO threshold, the twin beams violate the Duan inequality and their entanglement is robust against channel losses. As it is pumped with more power, the phase sum noise increases. The amplitude difference noise is insensitive to the pump power ($\Delta^2\hat{p}_- \approx 0.55$) (ref. 21). We also checked that states experimentally produced are Gaussian by measuring higher than second-order moments. Details of the experiment can be found in the Supplementary Information and references therein. The symplectic eigenvalues are shown in Fig. 3 as a function of the single-channel losses. The different plots correspond to several values of the pump power, and therefore to the different initial quantum states indicated in Fig. 2 (red dots). The solid lines represent the expected theoretical behaviour. We find good agreement.

The sensitivity of entanglement to the interaction with the environment requires careful understanding because of its implications for quantum information tasks. We have presented the experimental

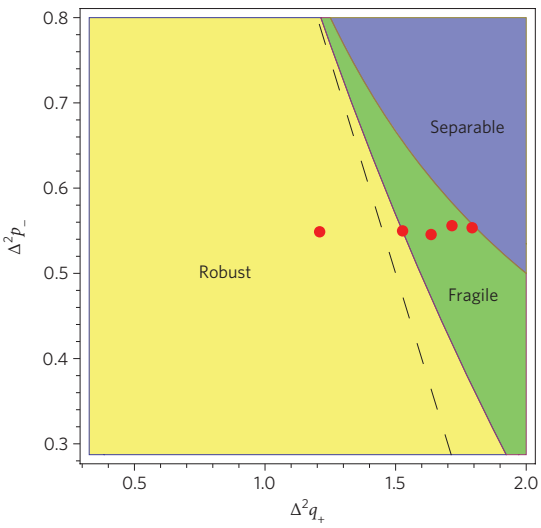

Figure 2 | Space of states. The state space is plotted as a function of the operator variances $\hat{p}_-$ and $\hat{q}_+$. Separable states lie in the blue region. Robust entangled states lie within the yellow region (including those states violating the Duan inequality, region to the left of the dashed line). Fragile states, subject to disentanglement in a lossy channel, are in the green region. The red dots indicate the initial states produced in our experiment (Fig. 3), along a line of approximately constant $\Delta^2 p_- \approx 0.55$. Increasing values of $\Delta^2 q_+$ were obtained by varying the pump power from 1.20 to 1.43 times the threshold power. In this plot we keep fixed values for $\Delta^2 p_+ = 3.06$ and $\Delta^2 q = 3.48$, which correspond to typical experimental parameters in our set-up.

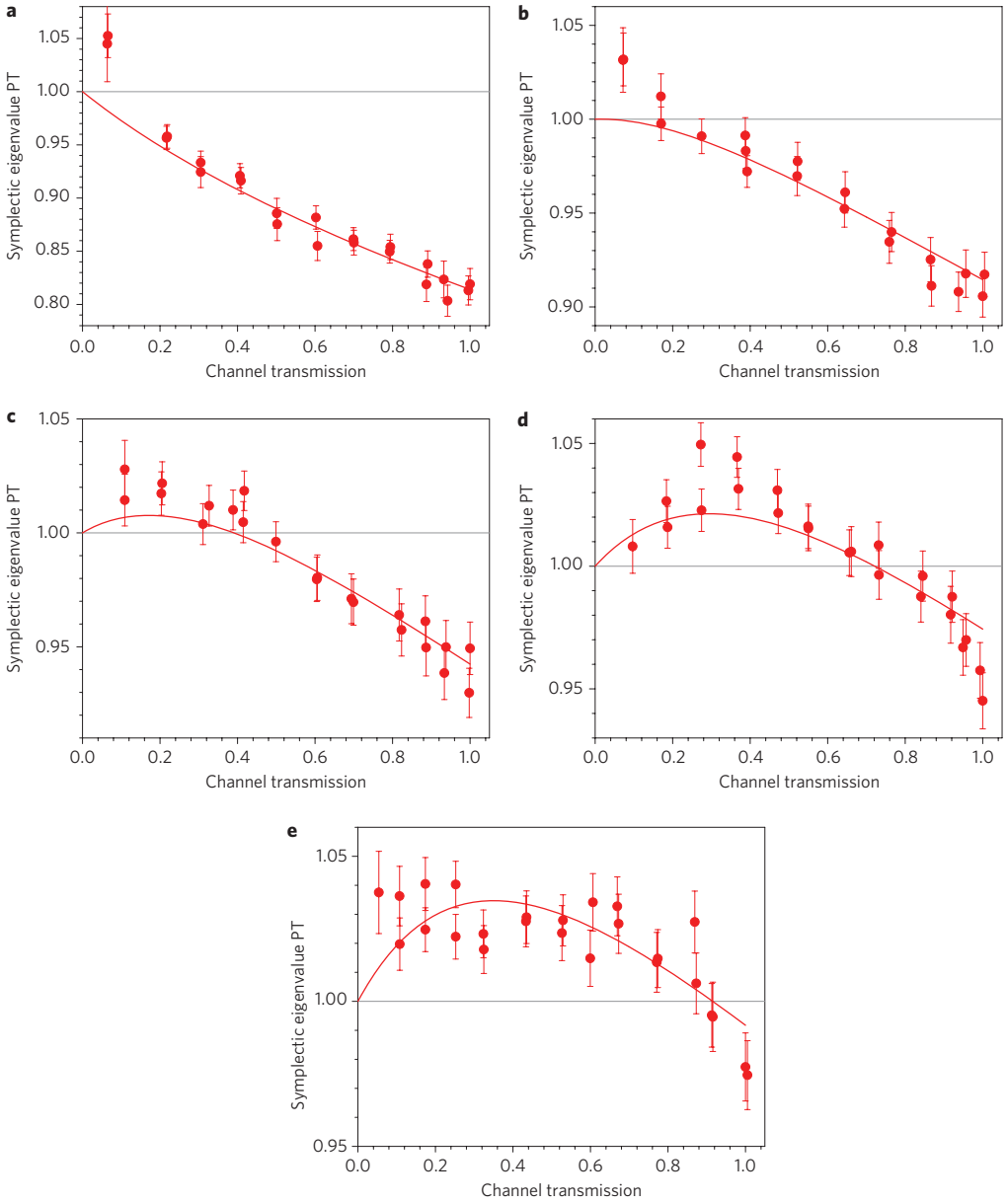

Figure 3 | Entanglement data. Symplectic eigenvalues after partial transposition (PT) as a function of the quantum channel transmission, for different values of pump power relative to the threshold power ($\sigma = P/P_{th}$). **a–e**, As pump power increases ($\sigma = 1.20$, 1.30, 1.35, 1.38 and 1.43 from **a** to **e**, respectively), we observe, in sequence, robust entangled states, states that undergo disentanglement and, finally, a weakly entangled state. Solid lines correspond to the theoretical dependence of the states on losses. Good agreement is observed. Error bars correspond to two standard deviations of the symplectic eigenvalue, as detailed in the Supplementary Information.

observation of partial-loss disentanglement in a bipartite continuous-variable system, which can harm the potential applications to quantum optical communications. In spite of the possibility of its occurrence, we could clearly draw the boundaries of those entangled states that are robust against channel losses. This boundary can be enlarged in certain communication schemes, decreasing the demands on the amounts of entanglement and state purity. Understanding the simplest situations should help us to deal with more complex settings involving a larger number of entangled parties. Given that a 'bright future for quantum communications' can be foreseen[4], we have investigated here conditions for its robustness against losses in the quantum channel.

Received 24 March 2010; accepted 23 August 2010; published online 17 October 2010

References

1. Scarani, V. *et al.* The security of practical quantum key distribution. *Rev. Mod. Phys.* **81,** 1301–1350 (2008).
2. Furusawa A. *et al.* Unconditional quantum teleportation. *Science* **282,** 706–709 (1998).
3. Kimble, H. J. The quantum internet. *Nature* **453,** 1023–1030 (2008).
4. Ralph, T. C. & Lam, P. K. A bright future for quantum communications. *Nature Photon.* **3,** 671–673 (2009).
5. Yu, T. & Eberly, J. H. Sudden death of entanglement. *Science* **323,** 598–601 (2009).
6. Almeida, M. P. *et al.* Environment-induced sudden death of entanglement. *Science* **316,** 579–582 (2007).
7. Yu, T. & Eberly, J. H. Quantum open system theory: bipartite aspects. *Phys. Rev. Lett.* **97,** 140403 (2006).
8. Coelho, A. S. *et al.* Three-color entanglement, *Science* **326,** 823–826 (2009).
9. Einstein, A., Podolsky, B. & Rosen, N. Can quantum-mechanical description of physical reality be considered complete? *Phys. Rev.* **47,** 777–780 (1935).

10. Schrödinger, E. Discussion of probability relations between separated systems. *Proc. Camb. Philos. Soc.* **31,** 555–563 (1935).
11. Bachor, H. A. & Ralph, T. C. *A Guide to Experiments in Quantum Optics* 2nd edn (Wiley-VCH, 2004).
12. Reid, M. D. & Drummond, P. D. Quantum correlations of phase in nondegenerate parametric oscillation. *Phys. Rev. Lett.* **60,** 2731–2733 (1988).
13. Villar, A. S., Cruz, L. S., Cassemiro, K. N., Martinelli, M. & Nussenzveig, P. Generation of bright two-color continuous variable entanglement. *Phys. Rev. Lett.* **95,** 243603 (2005).
14. César, J. E. S. *et al.* Extra phase noise from thermal fluctuations in nonlinear optical crystals. *Phys. Rev. A* **79,** 063816 (2009)
15. Duan, L. M., Giedke, G., Cirac, J. I. & Zoller, P. Inseparability criterion for continuous variable systems. *Phys. Rev. Lett.* **84,** 2722–2725 (2000).
16. Bowen, W. P., Schnabel, R., Lam, P. K. & Ralph, T. C. Experimental investigation of criteria for continuous variable entanglement. *Phys. Rev. Lett.* **90,** 043601 (2003).
17. Eisert, J., Scheel, S. & Plenio, M. B. Distilling Gaussian states with Gaussian operations is impossible. *Phys. Rev. Lett.* **89,** 137903 (2002).
18. Giedke, G. & Cirac, J. I. Characterization of Gaussian operations and distillation of Gaussian states. *Phys. Rev. A* **66,** 032316 (2002).
19. Barbosa, F. A. S. *et al.* Early stage disentanglement in bipartite continuous-variable systems. Preprint at http://arXiv:1009.4255v1 (2010).
20. Simon, R. Peres–Horodecki separability criterion for continuous variable systems. *Phys. Rev. Lett.* **84,** 2726–2729 (2000).
21. Villar, A. S. *et al.* Entanglement in the above-threshold optical parametric oscillator. *J. Opt. Soc. Am. B* **24,** 249–256 (2007).

Acknowledgements

This work was funded by the Brazilian agencies Conselho Nacional de Desenvolvimento Científico e Tecnológico (CNPq), Coordenação de Aperfeiçoamento de Pessoal de Nível Superior (CAPES), and Fundação de Amparo à Pesquisa do Estado de São Paulo (FAPESP). It was performed as part of the Brazilian National Institute of Science and Technology for Quantum Information. K.N.C. and A.S.V. acknowledge support from the Alexander von Humboldt Foundation. We thank D. Elser for assistance in an earlier stage of the experiment.

Author contributions

F.A.S.B. and A.S.C. performed the experiments and participated in data analysis, discussions and writing the manuscript. A.J.F., K.N.C. and A.S.V. participated in data analysis, discussions and writing the manuscript. P.N. and M.M. were responsible for general planning and participated in data analysis, discussions and writing the manuscript.

Additional information

The authors declare no competing financial interests. Supplementary information accompanies this paper at www.nature.com/naturephotonics. Reprints and permission information is available online at http://npg.nature.com/reprintsandpermissions/. Correspondence and requests for materials should be addressed to M.M.

nature photonics

SUPPLEMENTARY INFORMATION

DOI: 10.1038/NPHOTON.2010.222

Robustness of bipartite Gaussian entangled beams propagating in lossy channels

Supplementary Information

F. A. S. Barbosa[1], A. S. Coelho[1], A. J. de Faria[1], K. N. Cassemiro[2], A. S. Villar[2,3], P. Nussenzveig[1], and M. Martinelli[11]

[11] *Instituto de Física, Universidade de São Paulo, Caixa Postal 66318, 05315-970 São Paulo, SP, Brazil.*

[2] *Max Planck Institute for the Science of Light, Günther-Scharowsky-str. 1 / Bau 24, 91058 Erlangen, Germany.*

[3] *University of Erlangen-Nuremberg, Staudtstr. 7/B2, 91058 Erlangen, Germany.*

(Dated: August 17, 2010)

DISENTANGLEMENT CRITERION: Gaussian states are fully described by the covariance matrix V, given by the second-order moments:

$$V_{\alpha\beta} = \langle \{\hat{\xi}_\alpha, \hat{\xi}_\beta\}\rangle = \langle \frac{\hat{\xi}_\alpha\hat{\xi}_\beta + \hat{\xi}_\beta\hat{\xi}_\alpha}{2}\rangle, \quad \alpha = 1,2,3,4. \tag{1}$$

The vector $\hat{\xi} = (\hat{q}_1\,\hat{p}_1\,\hat{q}_2\,\hat{p}_2)$ contains the Hermitian canonical operators of the electromagnetic field: the phase $\hat{q}$ and amplitude $\hat{p}$ quadratures. They are written in terms of the annihilation and creation operators as $\hat{q}_j = (\hat{a}_j^\dagger + \hat{a}_j)$ and $\hat{p}_j = i(\hat{a}_j^\dagger - \hat{a}_j)$ $(j = 1,2)$, fulfilling the commutation relation $[\hat{q}_j, \hat{p}_j] = 2i$. With this choice of normalization, the variances of the quadratures of a coherent state (the standard quantum level, or SQL) are unity. For bipartite states, the covariance matrix assumes the form

$$V = \begin{bmatrix} A & C \\ C^T & B \end{bmatrix}, \tag{2}$$

where A, B, and C are 2×2 matrices. Following the definition of Eq. 1, A and B are the covariance matrices of the individual beams and C contains the bipartite correlations. In our treatment, we assume no correlations between different quadratures ($\langle \hat{p}_j\,\hat{q}_{j'}\rangle = 0$) and symmetric fields ($A = B$). These simplifying assumptions do not restrict the understanding of the phenomenon and correspond within an excellent approximation to our experimental situation.

The smallest sympletic eigenvalue ν resulting from the partial transposition of V reads [1],

$$\nu = \sqrt{\frac{\Delta' - \sqrt{\Delta'^2 - 4\Gamma}}{2}}\,, \tag{3}$$

with Δ' and Γ defined as

$$\begin{aligned} \Delta' &= \det A + \det B - 2\det C\,, \\ \Gamma &= \det V\,. \end{aligned} \tag{4}$$

The PPT criterion states that the bipartite system is entangled if and only if $\nu < 1$.

We model the effect of losses by a beam splitter with variable transmission $T = t^2$ placed on the path of one beam. The covariance matrix V_T of the lossy system is related to the original covariance matrix by

$$V_T = L(V - I)L + I, \tag{5}$$

where $L = \mathrm{diag}(t, t, 1, 1)$ represents the losses and I is the identity matrix.

To find the boundary between the robust states and those subject to disentanglement, we calculate the smallest symplectic eigenvalue ν_T of the partially transposed V_T as a function of the attenuation. Robust states will have $\nu_T < 0, \forall T$, while states that disentangle will cross the line $\nu_T = 1$ for some value of $0 < T < 1$. From Eq. (3), the condition $\nu_T = 1$ is equivalent to

$$\Delta'_T - \Gamma_T - 1 = 0\,, \tag{6}$$

which contains essentially all the required information to assess the robustness of the state against losses. A state is robust if no $0 < T < 1$ exists that satisfies Eq. 6.

DOI: 10.1038/NPHOTON.2010.222

In the case of symmetric beams without amplitude-phase correlations, a convenient and simple expression for the robustness against losses can be found by parametrizing the covariance matrix in terms of collective operators of the bipartite system,

$$\hat{q}_{\pm} = \frac{1}{\sqrt{2}}(\hat{q}_1 \pm \hat{q}_2), \qquad \hat{p}_{\pm} = \frac{1}{\sqrt{2}}(\hat{p}_1 \pm \hat{p}_2), \tag{7}$$

then the smallest symplectic eigenvalue is simply $\nu_T = \min\{\Delta^2\hat{p}_{+,T} \times \Delta^2\hat{q}_{-,T}; \Delta^2\hat{p}_{-,T} \times \Delta^2\hat{q}_{+,T}\}$. The attenuation at which ν_T crosses unity is given explicitly by

$$T_{\mathrm{D}} = \frac{W_{prod}\overline{W}_{sum} + \overline{W}_{prod}W_{sum}}{-2W_{prod}\overline{W}_{prod} + W_{prod}\overline{W}_{sum} + \overline{W}_{prod}W_{sum}} \ . \tag{8}$$

where W_{sum}, W_{prod} $\overline{W}_{sum}$, and $\overline{W}_{prod}$ are defined in the main text. Disentanglement occurs if $0 < T_D < 1$. It can be shown that the denominator is strictly positive if the initial state violates the PPT criterion. Then the numerator alone defines the robustness boundary for attenuation of one beam, as presented in the main text.

SETUP The entangled beams are generated by a triply resonant type-II OPO pumped by a frequency-doubled diode-pumped Nd:YAG laser (Innolight Diabolo) at 532 nm, filtered with a mode cleaning cavity to ensure that pump fluctuations are reduced to standard quantum limit (SQL) for frequencies above 20 MHz. The OPO consists of a non-linear crystal inside a linear Fabry-Perot cavity. Reflectivity for the input coupler (IC) is 70% for the pump (highly reflective for the downconverted beams) and 96% for the output coupler (OC) around 1064 nm (highly reflective for the pump field). The crystal is a bulk high gray-tracking resistant potassium titanyl phosphate (HGTR-KTP, by Raicol Crystals) with length $\ell = 12mm$, and antireflective coating for both wavelengths. Owing to the excess noise added by thermal phonons of the crystal in the phase quadrature [2], its temperature is kept at $-10°C$ and a vacuum chamber is built around the OPO, in order to avoid moisture on the crystal surfaces. Output beams have orthogonal polarizations and are separated by a polarizing beam splitter (PBS). Each of the twin beams is reflected off an empty optical cavity before being measured, in order to perform a self-homodyne detection [3]. Synchronous scan of the cavities allows access to each beam's covariance matrix and to the correlations between equal quadratures of both beams. By scanning only one cavity, cross-quadrature correlations are accessed. After passing through the cavities, each beam is divided in a 50/50 beam splitter and the fluctuations are independently measured in a balanced detection scheme [4].

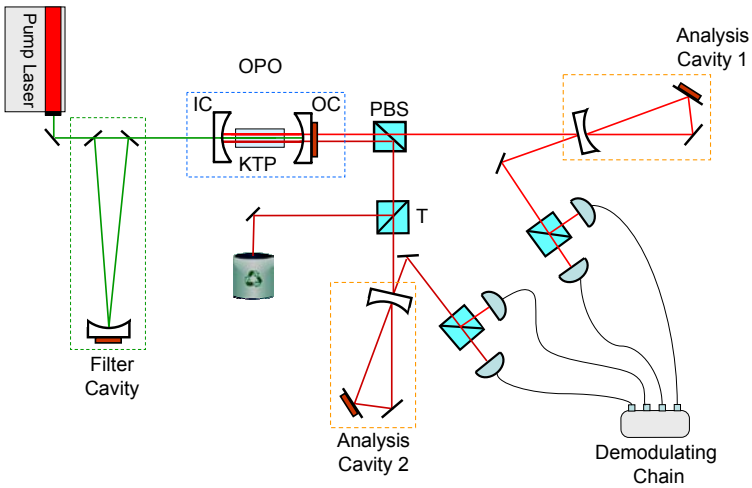

FIG. 1: **Setup for the measurement of entanglement in the Optical Parametric Oscillator. Variable attenuation T is inserted in the beam path of one of the output beams.**

The variance of the photocurrents' subtraction corresponds to a homodyne measurement of vacuum fluctuations and yields the standard quantum limit (SQL). The variance of the sum of the photocurrents gives the intensity noise of the incoming beam. In order to obtain quadrature variances and correlations normalized by the shot noise, we extract their ratio with respect to the noise of the photocurrents subtraction. Electronic noise is measured beforehand, and its value is constantly checked during the measurement. Its contribution to the measured variances is subtracted and it is typically one order of magnitude smaller than the measured noise in the presence of light. Fluctuations at 21 MHz are measured by mixing the photocurrent with a sinusoidal signal at this frequency and low-pass filtering the beat note with a 600 kHz bandwidth. Each acquisition corresponds to 450000 points and variances and correlations of these fluctuations are calculated by taking groups of 1000 points, resulting in a curve of 450 points acquired for different detunings of the analysis cavities. The parameters of a least squares fit in this curve are the covariance matrix entries, obtained with an uncertainty of 1.4% of the SQL. The fluctuation statistics are Gaussian within the experimental error [5]. This is verified by testing skewness and kurtosis. The two beams present very similar statistics and all cross-quadrature correlations are null within the experimental error.

DATA ANALYSIS We obtain the sympletic eigenvalue resulting from the partial transposition of each measured covariance matrix. To assess the error bar in ν, we perform Monte Carlo simulations. From the reconstructed matrix and the error bars in its entries, ten thousand matrices are randomly picked within the uncertainty region of each entry, giving a well-behaved distribution (smooth and single-peaked) of symplectic eigenvalues. The value and uncertainty in ν are given, respectively, by the mean value and standard deviation of such distribution.

[1] Serafini, A., Detecting entanglement by symplectic uncertainty relations, *J. Opt. Soc. Am. B* **24**, 347 (2007).
[2] César, J. E. S., Coelho, A. S., Cassemiro, K. N., Villar, A. S., Lassen, M., Nussenzveig, P. & Martinelli, M. Extra phase noise from thermal fluctuations in nonlinear optical crystals, *Phys. Rev. A* **79**, 063816 (2009).
[3] Villar, A. S. The conversion of phase to amplitude fluctuations of a light beam by an optical cavity, *Am. J. Phys.* **76**, 922 (2008).
[4] H. A. Bachor, T. C. Ralph, A Guide to Experiments in Quantum Optics (Wiley-VCH, ed. 2, 2004).
[5] Coelho, A. S., Barbosa, F. A. S., Cassemiro, K. N., Villar, A. S., Nussenzveig, P. & Martinelli, M. *in preparation.*

Estes dois artigos colocam os limites necessários para a geração de estados emaranhados úteis para protocolos de comunicação quântica, e permitem determinar com segurança os campos a serem usados para a realização de processos de teletransporte. Isto permite usar o OPO como ferramenta, tendo ele uma vez completamente caracterizado.

Aparentemente, sabemos agora tudo no OPO, exceto por um pequeno detalhe. Quando estudamos o comportamento do emaranhamento tripartite, foi observado que o OPO, mesmo em condição inicial, apresenta uma matriz de ruído cujo determinante era, aparentemente, superior a um, o que implica em uma pureza não unitária [55]. Ora, processos unitários devem conservar pureza, e conforme descrito na literatura, para sistemas gaussianos a pureza é igual ao inverso da raiz do determinate da matriz de covariância. Falta ainda algo a aprender sobre o OPO?

Capítulo 6

O futuro do emaranhamento

Vimos nos quatro capítulos anteriores a evolução do Oscilador Paramétrico Ótico como fonte de estados emaranhados em sistemas de variáveis contínuas. Se ele era já bem conhecido abaixo do limiar de oscilação, como fonte de estados comprimidos [17], e se estes estados foram sempre combinados usados em sistemas de informação quântica, como teletransporte com estados bipartite [37], "quantum dense coding" com estados tripartite [47, 48] ou com mais modos, gerando cachos de estados ("cluster states") [56]. Estas técnicas estão baseadas na realização de medidas de quadraturas por homodinagem e interferência para geração de campos emaranhados. O seu conjunto apresenta, portanto, a limitação evidente de poder operar apenas em uma frequência.

A manipulação de informação quântica deve contar, eventualmente, com diferentes sistemas, operando em diferentes frequências. Em variáveis discretas, a geração de fótons gêmeos por conversão paramétrica descendente é naturalmente multimodo, e permite empregar tal facilidade, possibilitando o acoplamento de "qubits" espectralmente distintos.

Podemos fazer algo semelhante para variáveis contínuas. Vale lembrar que nos processos com variáveis discretas temos geralmente um caráter intrinsecamente probabilístico na geração do emaranhamento, enquanto que para variáveis contínuas este é gerado de forma determinística. Isto representa uma vantagem para estes sistemas. Porém, como vimos acima, os processos até hoje contam apenas com técnicas interferométricas de geração e medida.

Desde 2004 demonstramos a viabilidade de geração de campos emaranhados em cores distintas, sejam sistemas bipartite, sejam sistemas tripartite. Verificamos as condições de robustez do emaranhamento bipartite na interação com o meio. Desenvolvemos técnicas de medida do campo que dispensam a interferência com campos de referência, usando o próprio campo médio como oscilador (realmente) local. O próximo passo é combinar estas possibilidades para gerar o teletransporte entre diferentes cores do espectro eletromagnético.

6.1 Teletransporte no espectro eletromagnético

No teletransporte de um estado quântico, o estado de um sistema é medido em uma primeira estação (A, ou Alice), e o resultado é enviado à segunda estação (B ou Bob), que irá tentar produzir um estado com a máxima fidelidade ao estado original. No entanto, no processo de medida em variáveis discretas, projetamos o sistema em um auto-estado escolhido pela nossa base onde fazemos a medida [57]. Para variáveis contínuas, medimos as flutuações de operadores conjugados, o que é sempre limitado pela incerteza de nossa medida. Deste modo temos sempre um limitação da informação disponível, reduzindo a fidelidade do estado recriado remotamente [37].

Podemos entender isso pelo fato de Alice obter efetivamente uma informação na aniquilação do sistema durante o processo de medida. Porém, o uso de estados emaranhados permite que, neste processo, a informação fique oculta ao interferirmos o estado a ser medido com um dos subsistemas do par emaranhado, e realizarmos a medida sobre o resultado desta combinação[1]. A informação clássica transmitida de Alice para Bob contém tanto a informação do estado a ser teletransportado quanto do subsistema do par emaranhado. Na estação remota, Bob recebe esta informação e o outro subsistema do par emaranhado. Usando a informação clássica recebida, ele tem condição de recuperar o estado aniquilado por Alice. A fidelidade deste processo é tanto maior quanto maior for o emaranhamento do par empregado.

Tal processo foi empregado com sucesso em sistemas de variáveis discretas [57] e em sistemas de variáveis contínuas [37]. Enquanto que o estado de polarização é transportado no primeira caso, no segundo são as flutuações do campo que são transferidas de uma estação à outra. No caso de variáveis contínuas, temos nas implementações realizadas sempre uma limitação no modo do estado gerado. Por produzir o emaranhamento a partir da combinação de dois estados comprimidos em um divisor de feixe, temos na saída de nossa fonte de estados EPR estados emaranhados de mesma frequência. O estado a ser transportado e o estado final terão, consequentemente, a mesma frequência. Em uma visão "naive" do problema, um bom sistema de teletransporte deveria ser semelhante a um jogo de espelhos, que enviasse o estado de Alice para Bob!

Em nosso laboratório, o projeto dos estudantes Antônio Sales Coelho e Paula Sampaio Meirelles é empregar o estado emaranhado produzido pelo OPO, com cores distintas, para realizar o teletransporte entre regiões diferentes do espectro eletromagnético. O estado quântico de um dado sistema, em uma dada cor, será aniquilado, e o estado será recriado agora em uma cor diferente.

A primeira estação (Alice) recebe um dos feixes produzidos pelo controle do sistema (Charlie), e faz a interferência em um divisor de feixe 50/50. As saídas são medidas, escolhendo duas quadraturas ortogonais do campo, portanto duas observáveis conjugadas, como as associadas à amplitude e fase. Esta informação é enviada para Bob por um canal clássico. Charlie envia a Bob o outro feixe do OPO, em uma cor distinta, além de

[1] O ocultamento da informação pode ser entendido pelo ao fato que no caso emaranhado, as flutuações do subsistema são maiores que as do estado coerente, e tanto maiores quanto maior o emaranhamento.

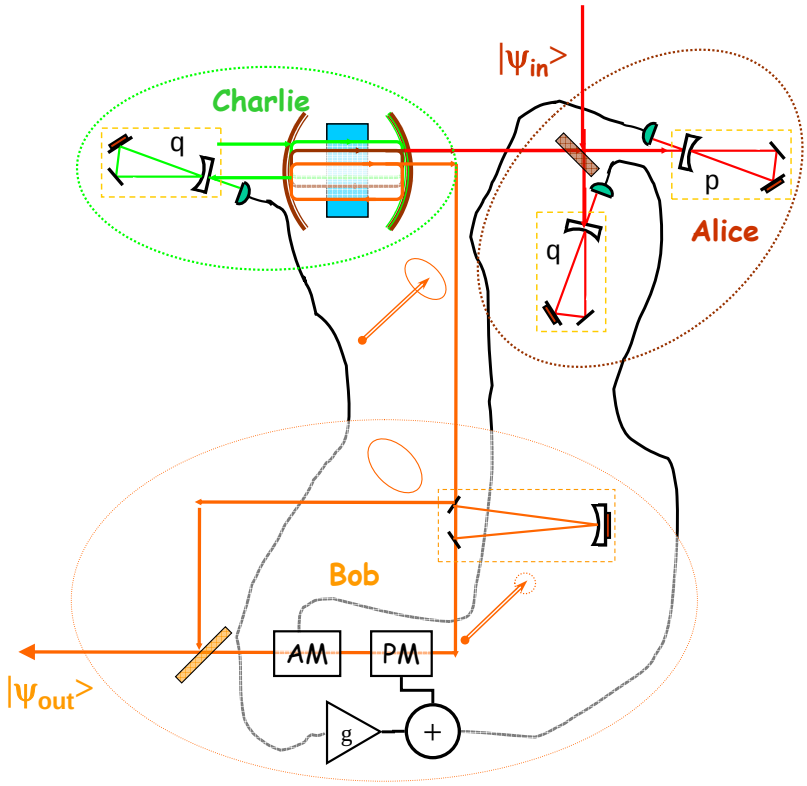

Figura 6.1: Implementação para teletransporte quântica empregando um OPO para produzir o emaranhamento entre Alice e Bob.

sua medida do campo de bombeio.

Bob tem agora um dos pares emaranhados, e a informação clássica da medida enviada por Alice e Charlie. Falta-lhe, no entanto, uma fonte de campo clássico que ele deve empregar para modular o campo e adicionar as flutuações do par emaranhado. Ele pode tomar parte do campo recebido para estabilizar em frequência um oscilador local (injetando um laser,por exempo), e fazer o procedimento realizado por Kimble *et al.* [37]. Porém, uma forma simples e direta é usar a portadora do campo emaranhado do OPO. Uma cavidade de filtro permite refletir as flutuações do campo do feixe recebido, que estão correlacionadas quanticamente com as flutuações do feixe recebido por Alice, separando-as da portadora central que é transmitida pela cavidade. Sobre esta, será adicionado o vácuo refletido pela cavidade na porta de saída, gerando um estado coerente. Ele pode agora modular este campo empregando a informação recebida pelo canal clássico, e empregando um divisor de feixe, sobrepor as flutuações sobre o campo modulado. Ajustando corretamente as intensidades envolvidas e as modulações, teremos na saída da estação B o estado recebido pela estação A, porém agora em uma frequência diferente.

Para a realização deste sistema de emaranhamento, e a primeira demonstração do teletransporte incondicional entre diferentes regiões do espectro eletromagnético, precisamos atualizar a instrumentação do laboratório. Tal medida permitirá que os resultados obtidos pelo nosso grupo, além do ponto de vista qualitativo, passem a ter destaque no ponto de vista quantitativo. Para a realização de teletransporte, o nível de compressão de 3 dB que alcançamos não é mais suficiente, e precisamos de pelo menos 6 dB para obter resultados comparáveis aos demais existentes na literatura. Isto se dará através de várias adaptações:

- **Aumento da compressão de ruído** Inicialmente, devemos aumentar o nível de compressão de ruído obtido no OPO, o que deve ser obtido pela redução de perdas espúrias intracavidade, comparadas ao acoplamento pelos espelhos da cavidade. Para isso, precisamos melhores espelhos para a montagem da cavidade, e cristais com menores perdas através do tratamento anti-refletor de suas superfícies. Para tanto, iremos adquirir espelhos com refletância de 5% em 1064 nm e 99,99% em 532 nm para a saída dos feixes no infravermelho, e espelhos de entrada de refletância de 15% no verde e 99,99% no infravermelho. Para o cristal, iremos realizar a deposição de tratamento anti-refletor que permita reduzir a reflexão espúria para menos de 0,1 % por face.

- **Controle do ruído espúrio** Como vimos [13], o espalhamento da potência intracavidade é uma fonte extra de ruído. Por isso, trabalhar com feixes intensos, mas limitados a poucos mW, será interessante. O controle do ruído no OPO se dá por duas formas, portanto: redução da potência, através de redução de perdas e aumento da não-linearidade, e resfriamento do cristal. Vamos realizar a montagem do OPO em vácuo, com controle de temperatura, permitindo chegar a -50°C, e empregar cristais PPKTP, onde a condição de inversão periódica de domínio (periodically poling) aumenta a não-linearidade efetiva do cristal. Com isso o limiar de oscilação é reduzido, contribuindo igualmente para a redução do excesso de ruído.

- **Mudança na cavidade**
  Para estender o sistema de emaranhamento ao caso tripartite, incluindo o campo de bombeio no processamento do sinal, é conveniente que o feixe refletido seja detectado diretamente. Neste caso, o sistema atual, empregando um isolador ótico, impõe perdas importantes na deteção, limitando a sua eficiência. O uso de um OPO em anel elimina estas perdas. Neste caso, esperamos uma redução da largura de banda da cavidade, devido ao maior tempo de voo, o que leva a medidas em uma faixa de frequência menor. Isto demanda modificações no sistema de deteção e na faixa de frequência de trabalho das cavidades auxiliares do sistema.

- **Sistema de deteção**
  Quanto à parte de medida, dispomos de detetores eficientes na faixa de 1064 nm, porém detetores melhores para o visível precisam ser adquiridos, e atualmente os melhores em 532 nm são da Hamamatsu. Quanto à eletrônica, precisamos expandir as instalações do laboratório, o que implica na aquisição de componentes específicos. Necessitamos de amplificadores para os detetores com excelente ganho na faixa de alta frequência (1 a 30 MHz) e ruído extremamente baixo. Para a medida deste sinal eletrônico precisamos ainda de circuitos demoduladores para compatibilizar o sinal de alta frequência com a faixa de aquisição da carta analógico digital.

A área de informação quântica mantém um interesse revigorado pelas diversas possibilidades de manipulação de informação. Diversos meios se apresentam como candidatos para o armazenamento quântico de informação, sejam átomos, íons, pontos quânticos, etc. Por outro, a transmissão desta informação se faz por meio do campo eletromagnético. Atualmente, não há claramente um sistema vitorioso para a realização do processamento quântico de informação. O nosso sistema é proposto como uma ferramenta interessante para, através do teletransporte, fazer o acoplamento direto entre diferentes componentes ("hardwares") cobrindo uma barreira intrínseca de sua comunicação direta - o fato de diferentes sistemas operarem em diferentes faixas de energia, portanto diferentes comprimentos de onda.

Atualmente, o OPO é a única ferramenta que possibilita esta manipulação de informação, posto que os demais sistemas emaranhados empregam ou variáveis discretas, o que implica em teletransporte condicional, ou sistemas degenerados em frequência no regime de variáveis contínuas, que permitem o teletransporte incondicional. A experiência aqui proposta não irá conectar diretamente outros sistemas quânticos, mas prestará como demonstração de princípio da realização deste teletransporte. Futuramente, poderemos realizar novos experimentos com OPO´s bombeados por lasers de Ti:Safira, permitindo a manipulação de feixes emaranhados em ressonância com átomos de rubídio, uma das linha de estudo em nosso laboratório.

Apêndice A

Descrição do Oscilador Paramétrico Ótico

A invenção do laser possibilitou a geração de campos eletromagnéticos intensos no espectro ótico (então no visível e infravermelho). Esta revolução colocou à disposição campos intensos, gerados em cavidades óticas, com elevadas potências de saída, gerando feixes espectralmente estreitos, com modos espaciais bem definidos, possibilitando sua manipulação espacial, com alta focalização com perdas praticamente nulas, além de uma elevada coerência de tais campos.

Graças a esta ferramenta foi possível investigar as propriedades óticas da luz, para além do limite linear. Tais efeitos não lineares já eram conhecidos quando acoplava-se, pela não linearidade do meio, o campo ótico a campos elétricos ou magnéticos de baixa frequência (do ponto de vista do campo ótico, pode-se dizer quase-estáticos) [1]. Mas somente com a intensidade gerada por um feixe do tipo laser tornou-se possível empregar a resposta não-linear do meio para acoplar diretamente campos no domínio ótico.

Com isto, houve a possibilidade direta da geração do segundo harmônico a partir de uma frequência fundamental, fenômeno conhecido também por conversão ascendente, e a conversão de um campo de bombeio em dois campos com frequências inferiores (conversão paramétrica descendente), que estão na origem do funcionamento do Oscilador Paramétrico Ótico e da Geração de Segundo Harmônico.

Para aplicações em Ótica Quântica, estamos interessados em ter feixes estáveis, coerentes, capazes de gerar, sob demanda, campos emaranhados ou comprimidos para aplicações de espectroscopia sensível [58], teletransporte [37], interferometria [59] ou metrologia [60]. Estamos portanto interessados em situações estáveis de funcionamento do OPO, fora das condições biestáveis [61] ou de regime caótico ou pulsado [62]. Ainda que possamos esperar fenômenos interessantes nesses regimes de operação, as técnicas de medida tem favorecido, até o momento, o funcionamento em condições de operação onde aproximações lineares dos processos são válidas.

Para estudar o OPO, precisamos levar em conta a dinâmica no interior da cavidade, dentro da Eletrodinâmica Quântica. Situações de cavidade extremamente bem isolada permitem os estudos fundamentais desta teoria, no domínio da Eletrodinâmica Quântica de Cavidades (Cavity QED). Um belíssimo exemplo de tal sistema pode ser visto nos artigos do grupo de Serge Haroche (ENS), onde temos o estudo do estado da cavidade (na faixa de micro-ondas) através de átomos-sonda (*e. g.* [63]). Outros sistemas permitem ainda o estudo através da transmitância da cavidade para campos em regime clássico, no domínio ótico (*e. g.* [64, 65]).

No nosso caso, estamos em um regime onde podemos considerar que a interação da cavidade com o mundo externo é relativamente forte. Temos portanto uma interação entre os modos da cavidade, um campo de alimentação da mesma, e as perdas desta para o resto do universo. Neste caso, um único modo da cavidade pode ser descrito pela Hamiltoniana em um referencial de campo girante

$$\hat{H}_i = \hbar\Delta_i \hat{a}_i^\dagger \hat{a}_i + i\hbar(\epsilon_i \hat{a}_i^\dagger - \epsilon_i^* \hat{a}_i) + \hat{a}_i \hat{\Gamma}_i^\dagger + \hat{a}_i^\dagger \hat{\Gamma}_i = \hat{H}_{Li} + \hat{H}_{Di} + \hat{H}_{Ri} \tag{A.1}$$

O primeiro termo ($\hat{H}_{Li} = \hbar\Delta_i \hat{a}_i^\dagger \hat{a}_i$) corresponde à evolução do campo dentro da cavidade, relativa à situação de exata ressonância, em função da dessintonia $\Delta_i = \omega_i - \omega_r$ entre o campo e a ressonância da cavidade . Do segundo termo, $\hat{H}_{Di} = i\hbar(\epsilon_i \hat{a}_i^\dagger - \epsilon_i^* \hat{a}_i)$, podemos ver que surge um operador deslocamento sobre o campo, na evolução do sistema, produzido pela injeção de um campo externo E_i na cavidade. Por fim temos dois termos envolvendo a troca de fótons com o reservatório térmico ($\hat{H}_{Ri}$), sobre o qual atuam os operadores de criação e aniquilação $\Gamma_i^\dagger$ e Γ_i.

Para obtermos a hamiltoniana do OPO, incluímos um acoplamento não linear entre três modos distintos do campo

$$\hat{V} = i\hbar \left(\kappa \hat{a}_0 \hat{a}_1^\dagger \hat{a}_2^\dagger - \kappa^* \hat{a}_0^\dagger \hat{a}_1 \hat{a}_2 \right) \tag{A.2}$$

de forma que a hamiltoniana total do sistema será dada pela hamiltoniana de cada modo ressonante, mais o termo de interação não linear

$$\hat{H} = \hat{H}_0 + \hat{H}_1 + \hat{H}_2 + \hat{V}. \tag{A.3}$$

Usando o formalismo da equação mestra, podemos substituir a interação com o reservatório $\hat{H}_R$, considerado markoviano, por operadores de Lindblad [66, 67] na equação de evolução do sistema. Com isto, a equação de evolução para o operador densidade do campo intracavidade será dada por

$$i\hbar \frac{\partial \hat{\rho}}{\partial t} = \left[\hat{H}_{L0} + \hat{H}_{D0} + \hat{H}_{L1} + \hat{H}_{D1} + \hat{H}_{L2} + \hat{H}_{D2} + \hat{V}, \hat{\rho} \right] + i\hbar(L_0 + L_1 + L_2)\hat{\rho} \tag{A.4}$$

sendo os operadores de Lindblad $L_i\hat{\rho} = \gamma_i(2\hat{a}_i \hat{\rho} \hat{a}_i^\dagger - \hat{a}_i^\dagger \hat{a}_i \hat{\rho} - \hat{\rho} \hat{a}_i^\dagger \hat{a}_i)$, onde γ_i são as taxas de amortecimento da cavidade.

Uma forma de lidar com a equação mestra é buscar uma descrição alternativa do sistema, substituindo o operador densidade por uma representação do operador. Neste caso, ao substituir os operadores do campo eletromagnético por variáveis complexas, e

o operador densidade por uma "quase-distribuição" de probabilidade $\wp$ (que é função do tempo e das variáveis conjugadas do campo) podemos lidar com o problema classicamente, através da solução de uma equação diferencial para a representação, e a partir desta calcular as grandezas de interesse. A questão do ordenamento dos operadores é resolvida, assim ao se estabelecer, pela representação, uma "regra de uso" do cálculo dos observáveis expressos em termos dos operadores de criação e aniquilação. O objetivo, para o OPO, é chegar a uma equação de Fokker-Planck

$$\frac{\partial \wp(\vec{X},t)}{\partial t} = \left[-\sum_i \frac{\partial}{\partial x_i} A_i(\vec{X},t) + \frac{1}{2}\sum_{ij} \frac{\partial}{\partial x_i}\frac{\partial}{\partial x_j} D_{ij}(\vec{X},t) \right] \wp(\vec{X},t) \tag{A.5}$$

onde temos um vetor de arrasto do campo $\vec{A}(\vec{X},t)$, permitindo o cálculo do valor estacionário do mesmo (se houver), e um termo de difusão $\mathbb{D}(\vec{X},t) = \mathbb{B}(\vec{X},t)\mathbb{B}^T(\vec{X},t)$, responsável pela dispersão do valor médio, ou seja, pela flutuação associada ao mesmo.

Diferentes equações podem ser obtidas para diferentes representações, tais como a P de Glauber-Sudarshan, a representação de Wigner, e a Q de Husimi. É curioso notar que a contribuição dos comutadores das hamiltonianas da cavidade serão iguais para os três campos.

$$\left[\hat{H}_{Li},\hat{\rho}\right] \to \hbar\Delta_i \left(\frac{\partial}{\partial \alpha_i}\alpha_i - \frac{\partial}{\partial \alpha_i^*}\alpha_i^* \right) \wp \tag{A.6}$$

$$\left[\hat{H}_{Di},\hat{\rho}\right] \to \hbar \left(\frac{\partial}{\partial \alpha_i}\epsilon_i + \frac{\partial}{\partial \alpha_i^*}\epsilon_i^* \right) \wp. \tag{A.7}$$

No entanto, para o comutador do termo de interação e para os operadores de Lindblad, a situação muda.

$$\hat{L}_i\hat{\rho} \to i\hbar\gamma_i \left(\frac{\partial}{\partial \alpha_i}\alpha_i + \frac{\partial}{\partial \alpha_i^*}\alpha_i^* \right) \wp + O_{Li}(2)\wp \tag{A.8}$$

$$\begin{aligned} \left[\hat{V},\hat{\rho}\right] \to\ & i\hbar \left(\kappa \frac{\partial}{\partial \alpha_2^*}\alpha_0^*\alpha_1 + \kappa^* \frac{\partial}{\partial \alpha_2}\alpha_0\alpha_1^* \right) \wp \\ & + i\hbar \left(\kappa \frac{\partial}{\partial \alpha_1^*}\alpha_0^*\alpha_2 + \kappa^* \frac{\partial}{\partial \alpha_1}\alpha_0\alpha_2^* \right) \wp \\ & - i\hbar \left(\kappa \frac{\partial}{\partial \alpha_0}\alpha_1\alpha_2 + \kappa^* \frac{\partial}{\partial \alpha_0^*}\alpha_1^*\alpha_2^* \right) \wp \\ & O_V(2)\wp + O_V(3)\wp. \end{aligned} \tag{A.9}$$

Note que os termos envolvendo as derivadas de primeira ordem permanecem idênticos para as três representações. Isto é consistente com a ideia que tais termos estão associados com a evolução dos valores médios do campo em uma equação de Langevin, como veremos a seguir. O acoplamento entre os campos dará origem a termos de ganho e atenuação das amplitudes, adicionais aos termos de alimentação externa por um campo injetado na cavidade ϵ_i, e o termo de atenuação originado no operador de Lindblad.

Já para os termos de ordem superior, vemos as diferenças de tratamento de cada representação. Para a representação P, as derivadas de ordem 2 no operador de Lindblad

são nulas - não há processo difusivo oriundo destes termos. Este termo virá, porém, da contribuição da interação entre os campos

$$O_V(2)P = i\hbar\gamma_i \left(\kappa \frac{\partial^2}{\partial\alpha_1\partial\alpha_2}\alpha_0 + \kappa^* \frac{\partial^2}{\partial\alpha_1^*\partial\alpha_2^*}\alpha_0^* \right) P \tag{A.10}$$

a qual, dependendo do valor da fase de α_0, pode ser negativo. Uma difusão negativa implica em um problema não solúvel para a equação de Fokker-Planck: na evolução temporal, a difusão leva o sistema à uma singularidade. Portanto, a equação pode ser empregada abaixo do limiar, mas acima ela apresenta séria dificuldades na sua solução. Por outro lado, os termos de terceira ordem estão ausentes.

Já na representação Q de Husimi, ainda que o comutador com a interação dos campos dê os mesmos operadores diferenciais, a equação de Lindblad resulta em um termo de difusão positivo adicional ao termo anterior

$$O_{Li}(2)Q = i2\hbar\gamma_i \left(\frac{\partial^2}{\partial\alpha_i\partial\alpha_i} + \frac{\partial^2}{\partial\alpha_i^*\partial\alpha_i^*} \right) Q \tag{A.11}$$

presente nos três campos, garantindo a existência de uma resposta não-divergente.

Por outro lado, a representação de Wigner não apresenta termo de difusão para o operador de acoplamento ($O_V(2) = 0$), apenas no termo de Lindblad, sendo este igual à metade do termo equivalente na representação de Husimi

$$O_{Li}(2)W = i\hbar\gamma_i \left(\frac{\partial^2}{\partial\alpha_i\partial\alpha_i} + \frac{\partial^2}{\partial\alpha_i^*\partial\alpha_i^*} \right) W \tag{A.12}$$

este termo de flutuação ligado à transmitância do espelho tem uma interpretação fácil: trata do acoplamento das flutuações do campo externo (incluindo o vácuo) ao campo interno da cavidade. O único problema nesta representação é a existência de termos de terceira ordem na interação dos campos

$$O_V(3)W = -i\frac{\hbar}{4} \left(\kappa \frac{\partial^3}{\partial\alpha_0^*\partial\alpha_1\partial\alpha_2} + \kappa^* \frac{\partial^3}{\partial\alpha_0\partial\alpha_1^*\partial\alpha_2^*} \right) W. \tag{A.13}$$

Este termo é normalmente desprezado no tratamento, sendo assumido como muito pequeno. O resultado dele será alterar a gaussiana esperada como resposta da solução linearizada. Não será porém a única aproximação feita .

Podemos associar uma equação diferencial estocástica de Langevin à equação de Fokker-Planck (A.5) [67],

$$\frac{d\vec{X}}{dt} = \vec{A}(\vec{X}, t) + \mathbb{B}(\vec{X}, t)\vec{X}^{in}(t) \tag{A.14}$$

onde os termos de flutuação estocástica tem média zero e são responsáveis pela difusão ($\langle X_i^{in}(t)X_j^{in}(t')\rangle = \delta_{ij}\delta(t-t')$). Resolvemos a equação de Langevin começando pela determinação dos valores médios dos campos no regime estacionário

$$\langle \vec{A}(\vec{X}, t)\rangle \simeq \vec{A}(\langle \vec{X}\rangle, t) = 0 \tag{A.15}$$

Feito isso, podemos passar para uma mudança de variáveis no sistema, calculando a resposta em termos deste valor médio e de uma flutuação estocástica adicional

$$\delta\vec{X} = \vec{X} - \langle\vec{X}\rangle \tag{A.16}$$

A solução desta equação implica em uma aproximação linear em torno do valor médio, desprezando os termos de ordem quadrática e acima nas flutuações.

$$\mathbb{A}\delta\vec{X} \simeq \vec{A}(\vec{X},t) - \langle\vec{A}(\vec{X},t)\rangle. \tag{A.17}$$

A validade desta aproximação deve ser tratada corretamente. Lembre-se que assumimos que

- $\vec{A}(\vec{X},t)$ pode ser substituído por $\vec{A}(\vec{X})$
- os termos de flutuação de ordem superior a um podem ser desprezados, o que é valido se $\langle\delta x_i\delta x_j\rangle \ll (\langle x_i\rangle, \langle x_i\rangle)$, ou $\langle\delta x_i\delta x_j\rangle \ll (\Delta x_i, \Delta x_j)$, *i. e.*, os termos de flutuação cruzados são muito menores, em média, que as variâncias dos termos correspondentes.

Se estas condições forem satisfeitas, e se

- $\mathbb{B}(\vec{X},t) \simeq \mathbb{B}(\langle\vec{X}\rangle) = \mathbb{B}$, *i.e.*, descartamos correlações cruzadas entre as flutuações de entrada responsáveis pela difusão e as flutuações do próprio campo,
- as aproximações responsáveis pela equação mestra são válidas,
- a equação diferencial da representação da matriz densidade contém derivadas de primeira e segunda ordem apenas, ou seja, é uma equação de Fokker-Planck.

Chegamos a uma forma simples para resolver as flutuações intracavidade

$$\frac{d\delta\vec{X}(t)}{dt} = \mathbb{A}\delta\vec{X}(t) + \mathbb{B}\vec{X}^{in}(t). \tag{A.18}$$

No caso mais comum, o acoplamento entre OPO e meio externo é feito através de perdas pequenas, com cavidades bem fechadas e espelhos com elevada reflexão. É a transmissão pelo espelho de saída que irá nos fornecer informações sobre a evolução do sistema. Neste caso, emprega-se o formalismo de entrada e saída, que relaciona os operadores analisados (medidos pelo sistema de deteção) com os operadores de entrada do OPO [68]. O acoplamento do campo interno para a saída é dado pela matriz de difusão $\mathbb{B}$, e a reflexão é tratada como unitária

$$\delta\vec{X}^{out}(t) = \mathbb{B}\delta\vec{X}(t) - \mathbb{I}\vec{X}^{in}(t) \tag{A.19}$$

onde $\mathbb{I}$ é a matriz identidade.

Para um ruído de entrada gaussiano, a evolução intracavidade não mudará este perfil. A descrição da distribuição gaussiana será completamente determinada pela matriz de covariância

$$\mathbb{V}_i = \langle \delta\vec{X}(t)\delta\vec{X}^T(t)\rangle. \tag{A.20}$$

Para o campo de saída teremos

$$\mathbb{V} = \langle \delta\vec{X}^{out}(t)\delta[\vec{X}^{out}(t)]^T\rangle, \tag{A.21}$$

Sendo que esta matriz pode ser vista como a matriz de correlação entre dois tempos distintos, com um intervalo τ tendendo a zero.

$$\mathbb{V}(t, t+\tau) = \mathbb{V}(\tau) = \langle \delta\vec{X}^{out}(t)[\delta\vec{X}^{out}(t+\tau)]^T\rangle \tag{A.22}$$

O cálculo das covariâncias pelas equações (A.18) e (A.19) pode ser relativamente complicado, em consequência de uma derivada temporal sobre um sinal de ruído. No entanto, a solução é simples ao passarmos para o domínio espectral. A transformada de Fourier da flutuação é dada por

$$\vec{X}(\Omega) = \frac{1}{\sqrt{2\pi}}\int_{-\infty}^{\infty} \delta\vec{X}(t)exp(-i\Omega t)dt. \tag{A.23}$$

onde, por simplicidade, abandonamos o δ no domínio espectral. Devemos no entanto lembrar que estes são também termos flutuantes, ainda que lentamente variados.

Teremos portanto, partindo da eq. (A.18)

$$-i\Omega\vec{X}(\Omega) = \mathbb{A}\vec{X}(\Omega) + \mathbb{B}\vec{X}^{in}(\Omega). \tag{A.24}$$

O campo intracavidade é linearmente ligado às flutuações do campo de entrada

$$\vec{X}(\Omega) = \left[-(\mathbb{A} + i\Omega\mathbb{I})^{-1}\mathbb{B}\right]\vec{X}^{in}(\Omega). \tag{A.25}$$

e o mesmo ocorre para o campo de saída

$$\vec{X}^{out}(\Omega) = -\left[\mathbb{B}(\mathbb{A} + i\Omega\mathbb{I})^{-1}\mathbb{B} + \mathbb{I}\right]\vec{X}^{in}(\Omega). \tag{A.26}$$

A matriz espectral será dada por

$$\mathbb{S}(\Omega) = \langle \vec{X}^{out}(\Omega)[\vec{X}^{out}(-\Omega)]^T\rangle. \tag{A.27}$$

A partir da matriz espectral, podemos calcular a matriz de correlação, usando a transformada de Fourier

$$\mathbb{V}(\tau) = \frac{1}{\sqrt{2\pi}}\int_{-\infty}^{\infty} S(\Omega)\exp(i\Omega\tau)d\Omega. \tag{A.28}$$

Algumas consequências importantes devem ser ressaltadas. Como a matriz $\mathbb{V}(\tau)$ é real, teremos propriedades de simetria na matriz espectral: $\mathbb{S}^*(\Omega) = \mathbb{S}(-\Omega) = \mathbb{S}^T(\Omega)$. Uma consequência importante é que esta matriz é necessariamente hermitiana. Isto implica em termos diagonais reais, e os termos fora da diagonal principal são conjugados ($S_{ij} = S_{ij}^*$) porém não necessariamente reais!

Apêndice B

Critérios de Emaranhamento em Variáveis Contínuas

Podemos colocar o início da discussão sobre o conceito de emaranhamento nos artigos de Einstein, Podolski e Rosen [5], e na resposta de Niels Bohr [69] em 1935. O questionamento posto envolvia o aparente conflito na Mecânica Quântica, entre o conceito que da função de onda temos toda informação possível sobre o estado de um sistema, e suas implicações quanto à realização de medidas. No caso, é proposta uma função de onda para duas partículas que interagiram em um dado instante de tempo

$$\Psi(x_1, x_2) = \int exp\left[i\frac{2\pi}{\hbar}(x_1 - x_2 + L)p\right] dp \tag{B.1}$$

que equivale, no formalismo da função de Wigner, a uma equação do tipo

$$W(x_1, p_1, x_2, p_2) = \delta(x_1 - x_2 + L)\delta(p_1 + p_2). \tag{B.2}$$

O argumento apresentado por Einstein *et al.* é de que, dependendo da escolha da observável medida no subsistema 1 (posição ou momento), temos o subsistema 2 em um auto-estado de posição, ou em um auto-estado de momento. Ora, como não há interação entre as partículas após o instante inicial, que aja sobre a partícula 2 mudando o seu estado, e a partícula 2 não pode estar simultaneamente em um auto-estado de posição *e* momento, limitada pelas relações de incerteza, a informação deveria estar presente anteriormente no sistema, possivelmente em variáveis não contempladas pelo formalismo da mecânica quântica, que seria, então, incompleta.

Bohr descarta esta visão, ao mostrar que o estado proposto continua satisfazendo as relações de incerteza. Aponta que neste caso temos um auto-estado da diferença de posições, e da soma dos momentos. A determinação encontra-se apenas na medida conjunta. Isto significa que, ao fazer uma medida em uma quadratura de um subsistema, sabemos de antemão o resultado da medida da mesma observável no segundo subsistema. Permanecemos, no entanto, na completa ignorância da variável conjugada. Ao repetir a medida para um conjunto de estados, temos uma distribuição enorme no conjunto de valores possíveis desta grandeza, e uma igual distribuição para os resultados possíveis da

grandeza no segundo subsistema. Porém, a forte correlação garante que a combinação das variáveis se mantém constante. A discussão, no entanto, não descarta uma possível teoria de variáveis ocultas.

A discussão sobre a existência de uma teoria de variáveis ocultas permanece no campo filosófico até a década de 60, quando John Bell traduz o emaranhamento para um par de sistemas discretos de dois níveis [1], e mostra que qualquer teoria de variáveis ocultas deveria satisfazer uma certa inequação, para uma séria de medidas combinadas realizadas. Esta inequação pode ser violada, no entanto, pela teoria quântica [71]. Medidas posteriores com fótons gêmeos permitiram confirmar as predições da mecânica quântica, e limitar as condições possíveis para a validade de uma teoria de variáveis ocultas.

No entanto, voltando aos estados propostos por Einstein *et al.*, vemos que a primeira descrição do emaranhamento ocorre em um sistema de variáveis contínuas. Ainda que o estado proposto possa aceitar uma interpretação estatística, posto que sua função de Wigner é positiva, ele será extremamente útil para a realização de experimentos em Informação Quântica, em especial no domínio da Ótica. Usando as quadraturas do campo eletromagnético como variáveis conjugadas, podemos criar estados *emaranhados*, ou estados que permitem a realização de teletransporte ou criptografia batendo os limites impostos por estados clássicos do campo (tomando como estados clássicos aqueles com função P de Glauber-Sudarshan analíticas).

Para variáveis contínuas, vários critérios de emaranhamento foram formulados desde então. Discutiremos aqui alguns deles, suas motivações históricas, e suas limitações, selecionando aqueles aplicados aos testes de emaranhamento realizados no corpo desta tese.

B.1 Critério EPR

Proposto para variáveis contínuas do campo [20], este critério baseia-se na ideia que, dados dois campos, ao fazermos a medida de uma das variáveis conjugadas do primeiro, podemos atuar na medida do segundo, seja ajustando o ganho g do amplificador após a medida, seja modulando o campo antes da fotodeteção, seja por uma operação de deslocamento (com a ajuda de um divisor de feixe, um campo intenso, e um modulador de fase e amplitude) (fig. B.1).

A variância inferida após a otimização do parâmetro g, baseada nos momentos de segunda ordem das grandezas dos dois campos, pode neste caso apresentar uma incerteza inferior àquela de um estado coerente, tomada como limite clássico-quântico:

$$\Delta^2\hat{X}_1^{inf}(\theta_1) = \Delta^2(\hat{X}_1(\theta_1) - g\hat{X}_2(\theta_2)) = \Delta^2\hat{X}_1(\theta_1) - \frac{\langle\hat{X}_1(\theta_1)\hat{X}_2(\theta_2)\rangle^2}{\Delta^2\hat{X}_2(\theta_2)} \tag{B.3}$$

[1] Aqui vale lembrar que em 1935, Schrödinger havia proposto, no paradoxo do gato[70], um estado emaranhado entre o gato (vivo/morto) e um estado atômico (excitado/fundamental).

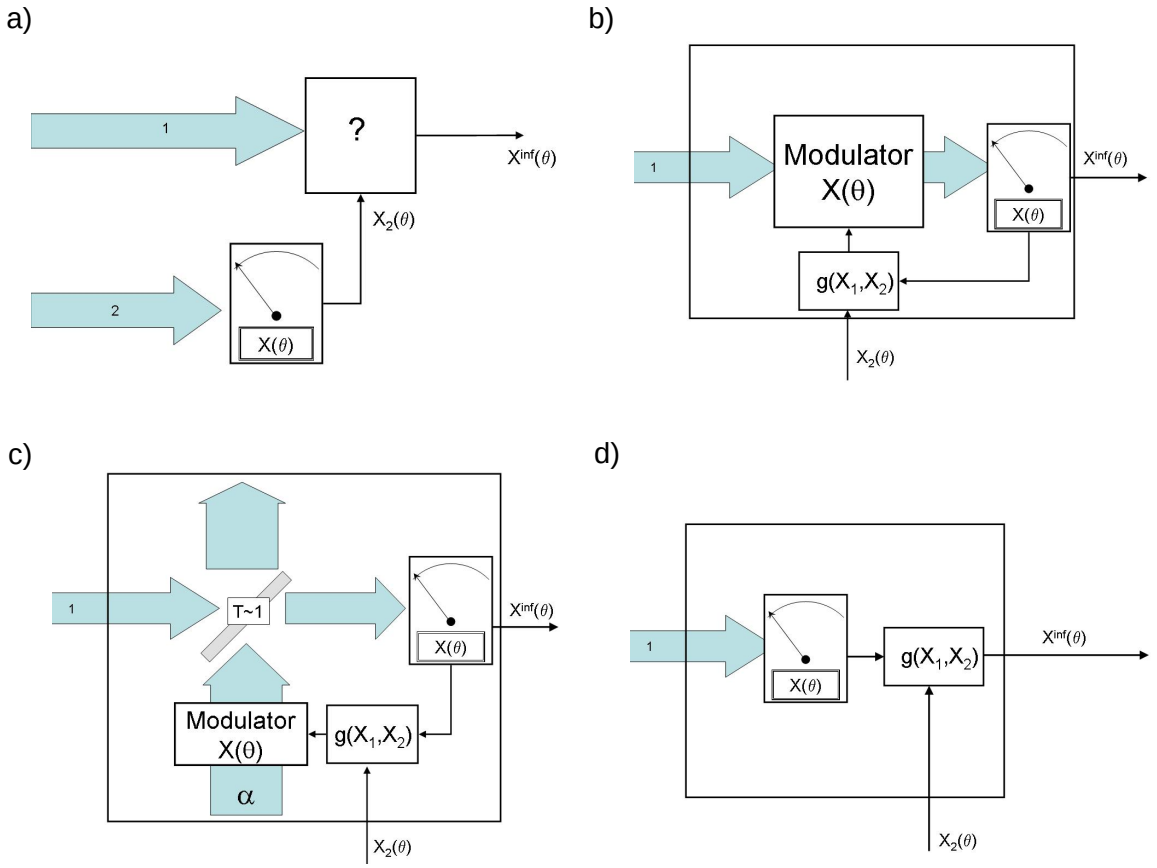

Figura B.1: Critério EPR, proposto em [20]. Em (a), a medida da quadratura do campo 2 é empregada para modular a resposta no campo 1, e sua consequente medida. A modulação pode se dar diretamente através de um atuador que modula a fase ou amplitude do campo (b), através da aplicação de um operador deslocamento cm um divisor de feixe de alta transmissão e um campo intenso (c) ou diretamente sobre o ganho da eletrônica de deteção (d), o que também pode ser feito *a posteriori* sobre a tabela de dados obtidos.

Se esta variância inferida for, portanto, inferior à unidade, considera-se que esta correlação $\langle \hat{X}_1(\theta_1)\hat{X}_2(\theta_2)\rangle$ tem caráter "quântico".

O emaranhamento ocorreria para uma violação aparente do princípio da incerteza. Este prevê que as variâncias dos observáveis conjugados deve satisfazer uma relação como

$$\Delta^2\hat{X}_1(\theta_1)\Delta^2\hat{X}_1(\theta_1+\pi/2) \geq 1, \tag{B.4}$$

porém, usando as variáveis inferidas, a inequação

$$\Delta^2\hat{X}_1^{inf}(\theta_1)\Delta^2\hat{X}_1^{inf}(\theta_1+\pi/2) \geq 1 \tag{B.5}$$

pode ser violada. Esta violação aparente do princípio da incerteza vem do fato de estarmos fazendo uma medida combinada sobre dois campos, e portanto obtendo informação de forma "seletiva". Neste caso, mostra-se que os estados estão emaranhados por esta violação.

O problema deste critério é que, dependendo da forma como fazemos a medida (medida em 1 e atuação em 2 ou vice-versa), podemos ter ou não um testemunho de emaranhamento. Além disso, estados longe de um limite de mínima incerteza, ainda que reconhecidamente emaranhados, não serão identificados por este critério. Veremos que existem formas mais seletivas de identificar os estados emaranhados em variáveis contínuas.

B.2 Critério DGCZ

O critério proposto por Duan *et al.*[42] busca testar o emaranhamento na descrição feita por Peres [52] e Horodecki *et al.* [72] para variáveis discretas. No caso, eles mostram que, em um sistema de dois qubits, ou um qubit e um qutrit, um estado é considerado separável se sua matriz densidade pode ser descrita por uma mistura estatística de produtos de matrizes densidade de cada subsistema, com pesos $p_i \geq 0$, ou seja, se existe

$$\hat{\rho}_{12} = \sum p_i \hat{\rho}_{i1} \otimes \hat{\rho}_{i2}. \tag{B.6}$$

Estados bipartite que não podem ser descritos desta forma são considerados emaranhados.

Baseados neste critério, mostra-se que um condição necessária para a separabilidade pode ser verificada com a ajuda de variáveis combinadas envolvendo os dois sistemas, semelhantes às propostas por Einstein *et al.*[5], e portanto chamadas de variáveis EPR,

$$\Delta^2\hat{u} + \Delta^2\hat{v} \geq a^2 + \frac{1}{a^2}, \qquad \text{onde} \qquad \hat{u} = a\hat{x}_1 + \frac{1}{a}\hat{x}_2 \qquad \text{e} \qquad \hat{v} = a\hat{p}_1 - \frac{1}{a}\hat{p}_2 \tag{B.7}$$

onde $\hat{x}_i$ e $\hat{p}_i$ são variáveis conjugadas do sistema i, e a é um peso considerado na medida da variável EPR, colocando a contribuição de cada campo separadamente.

Note que para $a = 1$, as variáveis EPR são proporcionais a uma transformação de divisor de feixe. Ou seja, neste caso a violação da desigualdade de Duan implica na deteção de compressão de ruído (*squeezing*) após a interferência em um divisor balanceado. Por traduzir emaranhamento em *squeezing*, este critério tornou-se muito popular entre os experimentais, sendo usado em diversas ocasiões, como pode ser visto no artigo de revisão por van Loock e Braunstein [73].

A limitação neste caso é que a violação deste critério de separabilidade é uma condição apenas suficiente para demonstrar emaranhamento. No entanto, a condição não é necessária e suficiente, nem mesmo para estados gaussianos (definidos completamente pela matriz de covariâncias), exceto para uma forma de matriz muito específica empregada no artigo, obtida a partir de transformações (compressões e rotações) da matriz de covariância inicial.

B.3 Critério Simon-PPT

Os dois critérios anteriores são conceitualmente simples, envolvendo *squeezing* ou variâncias inferidas, estas familiares às medidas QND (Quantum Non Demolition Measurement). No entanto, não são seletivos, pois se a violação implica em uma condição suficiente para emaranhamento, ela não é necessária. Para isso, há um critério mais útil, baseado na transposição parcial da matriz densidade, proposta por Peres [52]. Se um estado pode ser descrito por uma matriz da forma de eq. (B.6), então ao fazer uma transposição parcial, manipulando os elementos de matriz do primeiro subsistema, o resultado será uma matriz ainda válida fisicamente,

$$\hat{\sigma}_{12} = \sum p_i \hat{\rho}_{i1}^{PT} \otimes \hat{\rho}_{i2}. \tag{B.8}$$

No entanto, para um estado emaranhado, a matriz resultante vai carecer de significado físico. Ou seja, terá autovalores negativos.

Ao levar a transposição parcial para o caso de variáveis contínuas, usando a descrição da função de Wigner, vemos que a transposição parcial corresponde à troca de sinal em uma das quadraturas na representação [51]. Ou seja, para dois subsistemas, a transposta parcial corresponde, na função de Wigner, à transformação

$$W(x_1, p_1, x_2, p_2) \to W(x_1, p_1, x_2, -p_2). \tag{B.9}$$

O teste passa a ser a verificação se a função de Wigner resultante corresponde a um estado físico. Uma forma de ver isso é empregar os momentos de segunda ordem. Tomando a matriz de covariância, podemos ver se a matriz resultante da transposição parcial continua válida, ou seja, se satisfaz o princípio da incerteza.

Neste caso, dada a relação de incerteza na forma matricial

$$\mathbb{V} + i\mathbf{\Omega} > 0 \tag{B.10}$$

onde

$$\mathbf{\Omega} = diag(\mathbb{J}, \mathbb{J}) \qquad \text{and} \qquad \mathbb{J} = \begin{bmatrix} 0 & 1 \\ -1 & 0 \end{bmatrix} \tag{B.11}$$

A transposição parcial irá transformar a matriz de covariância

$$\widetilde{\mathbb{V}} = \Lambda \mathbb{V} \Lambda \qquad \text{com} \qquad \Lambda = diag(1, 1, 1, -1). \tag{B.12}$$

Uma condição necessária para a separabilidade será

$$\widetilde{\mathbb{V}} + i\mathbf{\Omega} > 0 \qquad \text{ou de forma equivalente,} \qquad \mathbb{V} + i\widetilde{\mathbf{\Omega}} > 0. \tag{B.13}$$

Neste caso, para estados gaussianos, sendo que a função de Wigner é completamente determinada pela matriz de covariância (a menos de uma operação de translação), o critério se torna necessário e suficiente. Se o estado não for gaussiano, torna-se mais difícil determinar se o estado é separável, posto que momentos de ordem superior podem ainda revelar o emaranhamento [74].

Existem várias formas de verificar o critério de Simon (B.13). Por exemplo, podemos construir uma inequação semelhante à obtida por Duan [42]. Podemos ainda calcular os autovalores simpléticos, e verificar se algum deles é inferior a 1, ou seja, se a matriz diagonal abaixo tem autovalores superiores a 1 (critério usado nos nossos testes de emaranhamento tripartite),

$$-(\widetilde{\mathbf{\Omega}}\mathbb{V})^2 > \mathbb{I} \tag{B.14}$$

Ou ainda empregar os chamados invariantes simpléticos da matriz $\mathbb{V}$. Dada a matriz de covariância

$$\mathbb{V} = \begin{bmatrix} \mathbb{A}_i & \mathbb{C}_{ij} \\ \mathbb{C}_{ij}^T & \mathbb{A}_j \end{bmatrix}, \tag{B.15}$$

podemos colocar a condição necessária para separabilidade na forma

$$1 + \det \mathbb{V}_{ij} + 2 \det \mathbb{C}_{ij} - \det \mathbb{A}_i - \det \mathbb{A}_j > 0. \tag{B.16}$$

A violação desta implica no emaranhamento dos estados.

A vantagem do critério Simon, ou Simon-PPT, é que este é necessário e suficiente para estados gaussianos. Claro está que o custo disso é ter o conhecimento completo da matriz de covariâncias. Por uma questão de completeza, vale lembrar ainda o critério proposto por Mancini [75], mais seletivo que o DGCZ, porém inferior ao Simon-PPT

O critério de Simon resolve, dentro das limitações da gaussianidade, o problema do emaranhamento bipartite. Mas e no caso de sistemas envolvendo mais modos? Podemos empregar extensões destes métodos para verificar o emaranhamento. Veremos a seguir duas condições para o emaranhamento tripartite.

B.4 Emaranhamento Tripartite

O primeiro critério, derivado por van Loock e Furusawa [9], se aplica a sistemas tripartite. No caso, eles chegam a uma relação semelhante às propostas por Duan *et al.*[42] para o caso bipartite. Ou seja, definem um par de variáveis

$$\hat{u} = h_1\hat{x}_1 + h_2\hat{x}_2 + h_3\hat{x}_3 \qquad \text{e} \qquad \hat{v} = g_1\hat{p}_1 + g_2\hat{p}_2 + g_3\hat{p}_3 \tag{B.17}$$

e demonstram uma condição necessária para a separabilidade, ainda que parcial, depende da otimização de uma função f dos pesos empregados nas variáveis acima:

$$\Delta^2\hat{u} + \Delta^2\hat{v} \geq f(h_1, h_2, h_3, g_1, g_2, g_3). \tag{B.18}$$

A inconveniência desta técnica é que, como a DGCZ, não é necessária e suficiente.

Por outro lado, foi demonstrado [76] que pelo menos para o caso tripartite, o emaranhamento pode ser testado através de partições 1×2 pela técnica da transposta parcial. Isto permite aplicar a transposição a cada um dos modos do campo por vez, e verificar a separabilidade de cada um deles.

Bibliografia

[1] A. Yariv, *Quantum Electronics*, John Wiley & Sons, third edition ed., 1988.

[2] M. D. Reid and P. D. Drummond, *Quantum correlations of phase in nondegenerate parametric oscillation*, Phys. Rev. Lett. **60**, 2731 (1988);

[3] M. D. Reid and P. D. Drummond *Correlations in nondegenerate parametric oscillation: Squeezing in the presence of phase diffusion*, Phys. Rev. A **40**, 4493 (1989).

[4] M. D. Reid and P. D. Drummond *Correlations in nondegenerate parametric oscillation 2: below threshold results*, Phys. Rev. A **41**, 3930 (1990).

[5] A. Einstein, B. Podolsky, and N. Rosen, *Can Quantum-Mechanical Description of Physical Reality Be Considered Complete?* Phys. Rev. **47**, 777 (1935).

[6] Z. Y. Ou, S. F. Pereira, H. J. Kimble, and K. C. Peng, *Realization of the Einstein-Podolsky-Rosen paradox for continuous variables*, Phys. Rev. Lett. **68**, 3663–3666 (1992);
Z. Y. Ou, S. F. Pereira and H. J. Kimble, *Realization of the Einstein-Podolsky-Rosen paradox for continuous variables in nondegenerate parametric amplification*, Applied Physics B: Lasers and Optics **55**, 265 (1992).

[7] A. S. Villar, L. S. Cruz, K. N. Cassemiro, M. Martinelli, and P. Nussenzveig, *Generation of Bright Two-Color Continuous Variable Entanglement*, Phys. Rev. Lett. **95,** 243603 (2005).

[8] A. S. Villar, K. N. Cassemiro, K. Dechoum, A. Z. Khoury, M. Martinelli, P. Nussenzveig, *Entanglement in the above-threshold optical parametric oscillator*, J. Opt. Soc. Am. B, **24**, 249 (2007).

[9] P. van Loock and A. Furusawa, *Detecting genuine multipartite continuous-variable entanglement*, Phys. Rev. A **67,** 052315 (2003).

[10] A. S. Villar, M. Martinelli, C. Fabre, and P. Nussenzveig, *Direct Production of Tripartite Pump-Signal-Idler Entanglement in the Above-Threshold Optical Parametric Oscillator*, Phys. Rev. Lett. **97**, 140504 (2006).

[11] K. N. Cassemiro, A. S. Villar, M. Martinelli, P. Nussenzveig, *The quest for three-color entanglement: experimental investigation of new multipartite quantum correlations*, Optics Express, **15**, 18236 (2007).

[12] K. N. Cassemiro, A. S. Villar, P. Valente, M. Martinelli, P. Nussenzveig, *Experimental observation of three-color optical quantum correlations*, Optics Letters, **32**,695 (2007).

[13] J. E. S. César, A. S. Coelho, K. N. Cassemiro, A. S. Villar, M. Lassen, P. Nussenzveig, M. Martinelli, *Extra phase noise from thermal fluctuations in nonlinear optical crystals*, Phys. Rev. A **79**, 063816 (2009).

[14] A. S. Coelho, F. A. S. Barbosa, K. N. Cassemiro, A. S. Villar, M. Martinelli, and P. Nussenzveig, *Three-Color Entanglement*, Science **326**, 823 (2009).

[15] T. Yu and J. H. Eberly *Sudden Death of Entanglement*, Science **323**, 598 (2009), e referências lá citadas.

[16] M. P. Almeida, F. de Melo, M. Hor-Meyll, A. Salles, S. P. Walborn, P. H. Souto Ribeiro, and L. Davidovich *Environment-Induced Sudden Death of Entanglement*, Science **316**, 579 (2007).

[17] L. A. Wu, H. J. Kimble, J. L. Hall, and H. F. Wu, *Generation of squeezed states by parametric down conversion*, Phys. Rev. Lett., **57**, 2520 (1986).

[18] S. Reynaud, C. Fabre, and E. Giacobino, *Quantum fluctuations in a 2-mode parametric oscillator*, J. Opt. Soc. Am. **B 4**, 1520 (1987).

[19] A. Heidmann, R. J. Horowicz, S. Reynaud, E. Giacobino, C. Fabre, and G. Camy, *Observation of quantum noise reduction on twin laser beams*, Phys. Rev. Lett., **59**, 255 (1987).

[20] M. D. Reid, *Demonstration of the Einstein-Podolsky-Rosen paradox using nondegenerate parametric amplification*, Phys. Rev. A, **40**, 913 (1989).

[21] C. Schori, J. L. Sørensen, E. S. Polzik *Narrow-band frequency tunable light source of continuous quadrature entanglement* Phys. Rev. A, **66**, 033802 (2002).

[22] M. Martinelli, C. L. Garrido, P. H. S. Ribeiro, and P. Nussenzveig, *Classical and quantum properties of optical parametric oscillators*, Brazilian J. Phys., **4**, 597 (2001).

[23] E. J. Mason and N. C. Wong, *Observation of two distinct phase states in a self-phase-locked type II phase-matched optical parametric oscillator*, Opt. Letters **23**, 1733–1735, (1998);
C. Fabre, E. J. Mason, and N. C. Wong, *Theoretical analysis of self-phase-locking in a type II phase-matched optical parametric oscillator*, Opt. Comm., **170**, 299 (1999).

[24] Sheng Feng and Olivier Pfister *Stable nondegenerate optical parametric oscillation at degenerate frequencies in Na:KTP*, J. Opt. B: Quantum Semiclass. Opt. **5**, 262 (2003).

[25] A. L. Schawlow, C. H. Townes, *Infrared and Optical Masers*, Phys. REv. **112**, 1940-1949 (1958).

[26] T. -C. Zhang, J. P. Poizat, P. Grelu, J. -F. Roch, P. Grangier, F. Marin, A. Bramati, V. Jost, M. D. Levenson and E. Giacobino, *Quantum noise of free-running and externally-stabilized laser diodes*, Quantum Semiclass. Opt. **7**, 601 (1995)

[27] M. D. Levenson, R. M. Shelby, and S. H. Perlmutter, *Squeezing of classical noise by nondegenerate four-wave mixing in an optical fiber*, Opt. Letters, **10**, 514 (1985); M. D. Levenson, R. M. Shelby, M. D. Reid, D. F. Walls and A. Aspect, *Generation and detection of squeezed states of light by nondegenerate 4-wave mixing in an optical fiber*, Phys. Rev. A 32, 1550 (1985).

[28] Alessandro de Souza Villar, *Estudo de emaranhamento no oscilador paramétrico ótico não-degenerado acima do limiar*, Dissertação de Mestrado, IFUSP (2004)

[29] K. S. Zhang, T. Coudreau, M. Martinelli, A. Maitre, C. Fabre *Generation of bright squeezed light at 1.06 mu m using cascaded nonlinearities in a triply resonant cw periodically-poled lithium niobate optical parametric oscillator*, Phys. Rev. A, **64**, 033815 (2001).

[30] P. Galatola, L. A. Lugiato, M. G. Porreca, P. Tombesi, G. Leuchs, *System control by variation of the squeezing phase*, Opt. Comm. **85**, 95 (1991).

[31] A.S. Villar, M. Martinelli, and P. Nussenzveig, *Testing the entanglement of intense beams produced by a non-degenerate optical parametric oscillator*, Opt. Comm. **242**, 551 (2004).

[32] J. P. Fève, B. Boulanger, and G. Marnier, *Repetition rate dependence of gray-tracking in $KTiOPO_4$ during second-harmonic generation at 532 nm*, Appl. Phys. Lett., **70**, 277 (1997).

[33] W. P. Bowen, R. Schnabel, P. K. Lam, T. C. Ralph *Experimental characterization of continuous-variable entanglement*, Phys. Rev. A **69**, 012304 (2004).

[34] Jietai Jing, Sheng Feng, Russell Bloomer, and Olivier Pfister *Experimental continuous-variable entanglement from a phase-difference-locked optical parametric oscillator*, Phys. Rev. A **74**, 041804(R) (2006)

[35] G. Keller, V. D'Auria, N. Treps, T. Coudreau, J. Laurat, C. Fabre, *Experimental demonstration of frequency-degenerate bright EPR beams with a self-phase-locked OPO*, Opt. Express **16**, 9351 (2008).

[36] X. L. Su, A. H. Tan, X. J. Jia, Q. Pan, C. D. Xie, K. C. Peng, *Experimental demonstration of quantum entanglement between frequency-nondegenerate optical twin beams*, Opt. Lett. **31**, 1133 (2006).

[37] A. Furusawa, J. L. Sorensen, S. L. Braunstein, C. A. Fuchs, H. J. Kimble, and E. S. Polzik, *Unconditional quantum teleportation*, Science, **282**, 706 (1998).

[38] C. Silberhorn, N. Korolkova, G. Leuchs, *Quantum key distribution with bright entangled beams*, Phys. Rev. Lett. **88**, 167902 (2002).

[39] K. Dechoum, P. D. Drummond, S. Chaturvedi, M. D. Reid, *Critical fluctuations and entanglement in the nondegenerate parametric oscillator*, Phys. Rev. A **70**, 053807 (2004).

[40] B. Coutinho dos Santos, K. Dechoum, A. Z. Khoury, L. F. da Silva, and M. K. Olsen, *Quantum analysis of the nondegenerate optical parametric oscillator with injected signal*, Phys. Rev. A **72**, 033820 (2005).

[41] V. D'Auria, A. Chiummo, M. De Laurentis, A. Porzio, S. Solimeno, M. Paris, *Tomographic characterization of OPO sources close to threshold*, Optics Express **13**, 948 (2005).

[42] Lu-Ming Duan, G. Giedke, J. I. Cirac and P. Zoller, *Inseparability criterion for continuous variable systems*, Phys. Rev. Lett. **84**, 2722 (2000).

[43] Dong Wang, Yana Shang, Zhihui Yan, Wenzhe Wang, Xiaojun Jia, Changde Xie and Kunchi Peng *Experimental investigation about the influence of pump phase noise on phase-correlation of output optical fields from a non-degenerate parametric oscillator*, European Phys. Lett. **82**, 24003 (2008).
Dong Wang, Yana Shang, Xiaojun Jia, Changde Xie and Kunchi Peng *Dependence of quantum correlations of twin beams on the pump finesse of an optical parametric oscillator*, J. Phys. B: At. Mol. Opt. Phys. **41**, 035502 (2008).

[44] G. D. Boyd and D. A. Kleinman, *Parametric interaction of focused gaussian light beams*, J. Appl. Phys, **39**, 3597–3639 (1968).

[45] N. B. Grosse, S. Assad, M. Mehmet, R. Schnabel, T. Symul, P. K. Lam, *Observation of entanglement between two light beams spanning an octave in optical frequency*, Phys. Rev. Lett. **100**, 243601 (2008).

[46] K. Goda, K. McKenzie, E. E. Mikhailov, P. K. Lam, D. E. McClelland, and N. Mavalvala *Photothermal fluctuations as a fundamental limit to low-frequency squeezing in a degenerate optical parametric oscillator*, Phys. Rev. A **72**, 043819 (2005).

[47] H. Yonezawa, T. Aoki and A.Furusawa, *Demonstration of a quantum teleportation network for continuous variables*, Nature **91**, 080404 (2003).
T. Aoki, N. Takei, H. Yonezawa, K. Wakui, T. Hiraoka, A.Furusawa and P. van Loock, *Experimental creation of a fully inseparable tripartite continuous-variable state*, Phys. Rev. Lett. **431**, 430 (2004).

[48] J. Jing, J. Zhang, Ying Yan, F. Zhao, C. Xie and K. Peng, *Experimental demonstration of tripartite entanglement and controlled dense coding for continuous variables*, Phys. Rev. Lett. **90**, 167903 (2003).

[49] Juan Guo, Hongxin Zou, Zehui Zhai, Junxiang Zhang, and Jiangrui Gao, *Generation of continuous-variable tripartite entanglement using cascaded nonlinearities*, Phys. Rev. A **71**, 034305 (2005)

[50] Antônio Sales Oliveira Coelho, *Emaranhamento tripartite no oscilador paramétrico ótico*, dissertação de mestrado, IFUSP (2009)

[51] R. Simon, *Peres-Horodecki separability criterion for continuous variable systems*, Phys. Rev. Lett. **84**, 2726 (2000).

[52] A. Peres, *Separability Criterion for Density Matrices*, Phys. Rev. Lett. **77**, 1413 (1996).

[53] Scott Hill and William K. Wootters, *Entanglement of a Pair of Quantum Bits*, Phys. Rev. Lett. **78**, 5022 (1997)

[54] G. Adesso, A. Serafini and F. Illuminati, *Extremal entanglement and mixedness in continuous variable systems*, Phys. Rev. A **70**, 022318 (2004).

[55] T. Golubeva, Yu. Golubev, C. Fabre, and N. Treps, *Quantum state of an injected TROPO above threshold: purity, Glauber function and photon number distribution*, Eur. Phys. J. D **46**, 179 (2008).

[56] M. Yukawa, Ryuji Ukai, P. van Loock, A. Furusawa, *Experimental generation of four-mode continuous-variable cluster states*, Phys. Rev. A **78**, 012301 (2008).

[57] D. Bouwmeester, J. -W. Pan, K. Mattle, M. Eibl, H. Weinfurter, A. Zeilinger, *Experimental quantum teleportation* Nature **390**, 575 (1997)

[58] P. H. S. Ribeiro, C. Schwob, A. Maître, and C. Fabre, *Sub-shot-noise high-sensitivity spectroscopy with optical parametric oscillator twin beams*, Opt. Letters, **22**, 1893 (1997).

[59] K. Goda, O. Miyakawa, E. E. Mikhailov, S. Saraf, R. Adhikari, K. McKenzie, R. Ward, S. Vass, A. J. Weinstein, N. Mavalvala, *A quantum-enhanced prototype gravitational-wave detector*, Nature Physics **4**, 472 (2008).

[60] B. Lamine, C. Fabre, N. Treps, *Quantum improvement of time transfer between remote clocks*, Phys. Rev. Lett. **101**, 123601 (2008).

[61] C. Richy, K. I. Petsas, E. Giacobino, and C. Fabre, *Observation of bistability and delayed bifurcation in a triply resonant optical parametric oscillator*, J. Opt. Soc. Am. **B 12**, 456 (1995).

[62] L. Lugiato, C. Oldano, C. Fabre, E. Giacobino, and R. J. Horowicz, *Bistability, self-pulsing and chaos in optical parametric oscillators*, Nuovo Cimento **10**, 959 (1988).

[63] A. Rauschenbeutel, G. Nogues, S. Osnaghi, P. Bertet, M. Brune, J. M. Raimond, S. Haroche, *Coherent operation of a tunable quantum phase gate in cavity QED*, Phys. Rev. Lett. **83**, 5166 (1999).

[64] L. M. Duan, A. Kuzmich, H. J. Kimble, *Cavity QED and quantum-information processing with "hot" trapped atoms*, Phys. Rev. A **67**, 032305 (2003).

[65] W. P. Smith, J. E. Reiner, L. A. Orozco, S. Kuhr, H. M. Wiseman, *Capture and release of a conditional state of a cavity QED system by quantum feedback*, Phys. Rev. Lett. **89**, 133601 (2002).

[66] D. Walls and G. J. Milburn, *Quantum Optics*, Berlin Heidelberg: Springer-Verlag (1994).

[67] C. W. Gardiner and P. Zoller, *Quantum Noise: A Handbook of Markovian and Non-Markovian Quantum Stochastic Methods with Applications to Quantum Optics* (Springer Series in Synergetics)
C. W. Gardiner, *Handbook of stochastic methods for physics, chemistry and the material sciences*. Springer Series in Synergetics, Berlin: Springer (1983).

[68] B. Yurke, *Use of cavities in squeezed-state generation*, Phys. Rev. A **29**, 408 (1984); J. M. Courty and S. Reynaud, *Generalized linear input-output theory for quantum fluctuations*, Phys. Rev. A **46**, 2766 (1992).

[69] N. Bohr, *Can Quantum-Mechanical Description of Physical Reality be Considered Complete?*, Phys. Rev. **48**, 696 (1935).

[70] E. Schrodinger, *Discussion of probability relations between separated systems*, Proc. Cambridge Philosophical Society **31**, 555 (1935).

[71] J. S. Bell, *Speakable and Unspeakable in Quantum Mechanics*, Cambridge University Press (1988).

[72] M. Horodecki, P. Horodecki, and R. Horodecki, *Separability of mixed states: necessary and sufficient conditions*, Phys. Lett. A **223**, 1 (1996).

[73] S. L. Braunstein and P. van Loock, *Quantum information with continuous variables*, Rev. Mod. Phys. **77**, 513 (2005).

[74] E. Shchukin and W. Vogel, *Inseparability Criteria for Continuous Bipartite Quantum States*, Phys. Rev. Lett. **95**, 230502 (2005).

[75] V. Giovannetti, S. Mancini, D. Vitali, and P. Tombesi, *Characterizing the entanglement of bipartite quantum systems*, Phys. Rev. A **67**, 022320 (2003).

[76] R. F. Werner, M. M. Wolf, *Bound Entangled Gaussian States*, Phys. Rev. Lett. **86**, 3658 (2001).